CONTROLLED MODIFICATION OF SILOXANE OR HYDROCARBON INTERFACES USING ORGANOSILANES

CONTROLLED MODIFICATION OF SILOXANE OR HYDROCARBON INTERFACES USING ORGANOSILANES

By

JIANFENG ZHANG, M. Eng.

A Thesis

Submitted to the School of Graduate Studies

In Partial Fulfillment of the Requirements for the Degree of

Doctor of Philosophy

Doctor of Philosophy (2015), McMaster University (Chemistry), Hamilton, Ontario

TITLE:

Controlled Modification of Siloxane or Hydrocarbon Interfaces Using Organosilanes

AUTHOR: Jianfeng Zhang,

M. Eng. (Beijing University of Chemical Technology)

SUPERVISOR: Dr. Michael A. Brook

NUMBER OF PAGES: xxxi, 218

ABSTRACT

Surfaces/interfaces are considered as one of the key factors that determine performance, and ultimately the application, of materials. In many cases, surface/interface modifications are required for desired properties, such as adhesion and wettability. Organosilanes have been widely used to alter surface/interfacial properties for many materials including metals, glass, and polymers, etc. However, controllable processes for surface/interfacial modification are desired.

This thesis aims to explore controllable paths for surface/interfacial modifications on siloxane or hydrocarbon-based materials using organosilanes. Further understanding about the methodologies for quantification of functional groups located at surfaces/interfaces is also within the scope of this thesis.

In this thesis, a comprehensive study of PDMS surface modification using thioalkylsilane coupling agents is described. An equilibrium silanization allowed the introduction of thiols on silicone elastomer surfaces under control and without damaging the surface. Two different titration methods for testing thiols in solution were developed and improved for quantification of thiol groups located at air-solid interfaces. The thiol-functionalized silicone could be further modified with maleic anhydride and/or with a variety of polymers and surfactants in a single step or two steps. A long term, stable hydrophilic surface was obtained after these modifications.

In this thesis, the modification of hydrocarbon-based materials is also described. A method based on the Piers-Rubinsztajn reaction was used to convert lignin into value-added chemicals, including monomeric/oligomeric aromatics and lignin composites. For the hard wood lignin, reduction of the ether bonds and silylation with hydrosilanes led to nearly complete fragmentation. The monomeric/oligomeric aromatics decomposed from hard wood lignin are easy to process as demonstrated by their excellent solubility in various solvents. Alternatively, softwood, which does not have an ideal structure for fragmentation, is effectively employed as "green filler" in silicones for lignin-based elastomer/foams. The partial (interfacial) reduction of hydrosilanes at lignin interfaces results in covalent linkage sbetween lignin and siloxane network, improving the interfacial miscibility. The softwood lignin, thus plays dual roles as a crosslinking and reinforcing agent. Formulations were readily developed to prepare silicone foams/elastomers by controlling processing parameters and methods. Lignin-based silicone elastomers could be obtained with additional solvent and casting in an open mold; lignin-based silicone foams could be molded in a volume-confined mold after extrusion.

ACKNOWLEDGEMENTS

First and foremost I would like to express my heartfelt gratitude to my supervisor Dr. Michael A. Brook. It is my honor to pursue a Ph.D. under his supervision. He has not only taught me how excellent research is performed, but also fired up my eagerness to explore the unknown. I definitely would not to be who I am today without his guidance, support and encouragement. Thank you for providing me with so many opportunities, which allow me to grow. Not only that, he has also taught me lessons about Canadian cultures and lifestyles. Thank you for explaining me the menu every time in restaurants.

The Brook research group members always supported me both professionally and personally. I would like to give my heartfelt thanks to Dan Chen for his help and guidance over the years. I would also like to express my gratitude to all the other group members for their help and cooperation. Thanks to all the group members for giving me a feeling of home in the lab.

I would like to express my sincere gratitude to my committee members: Dr. Adronov and Dr. Pelton, for their guidance and advice on my projects. I am also grateful to Dr. Etienne Fleury (INSA de Lyon, France) for his guidance and help during my visit to do research in France. I would like to particularly thank Dr. Kornic, Dr. Green, Megan Fair, Sujan Fernando, Greg Bahun, Jeff Landry, and Christine Cosgrove in Department of Chemistry, and Elizabeth Takacs in Department of Chemical Engineering for their

training and help. I would also like to thank the “Sentinel” and FIBRE networks for providing me financial support and opportunities to communicate with colleague nationally and internationally.

感谢我的父母，你们给予我生命，哺育和教导我成长；感谢你们在我人生的每个阶段的对我所有决定的尊重，支持，和鼓舞；你们的无疆大爱是我能奋起逐梦的信心和支柱。我也要感谢所有的家人和朋友，你们的支持和鼓励无一不是我前进的动力。

Lastly, I would like to dedicate my thesis to my lovely wife, Huiying Li for her patience, support, understanding, and love. I love you more than words can say.

TABLE OF CONTENT

ABSTRACT IV

ACKNOWLEDGEMENTS VI

TABLE OF CONTENT VIII

LIST OF SCHEMES XIII

LIST OF FIGURES XVII

LIST OF TABLES XXVIII

LIST OF ABBREVIATIONS AND SYMBOLS XXXI

CHAPTER 1: INTRODUCTION 1

1.1 SURFACES AND INTERFACES 1

1.2 SURFACE MODIFICATION OF SILICONE ELASTOMER 2

1.2.1 Silicone elastomer 2

1.2.2 Hydrophobic recovery – a challenge for PDMS surface modification 3

1.2.3 Modification without changing -Si-O- bonds 4

1.2.4 Modification with cleavage or rearrangement of -Si-O- bonds 9

1.2.5 Objective 14

1.3 INTERFACIAL/SURFACE MODIFICATION OF LIGNIN 16

1.3.1 Lignocellulosic biomass 16

1.3.2 Chemical structure of lignin 18

1.3.3 Depolymerization/degradation of lignin: toward the bio-refinery chemicals 21

1.3.4 Interfacial modification of lignin: toward the bio-composite materials 27

1.3.5 Objectives of the controlled depolymerization and modification of lignin using organosilanes 34

1.4 REFERENCES 36

CHAPTER 2: FACILE FUNCTIONALIZATION OF PDMS ELASTOMER SURFACES USING THIOL-ENE CLICK CHEMISTRY§ 44

2.1 ABSTRACT 44

2.2 INTRODUCTION 45

2.3 EXPERIMENTAL SECTION 48

2.3.1 Materials 48
2.3.2 Characterization 49
2.3.3 Preparation of PDMS elastomers 51
2.3.4 Base-catalyzed equilibrium of silicone elastomers PDMS-SH 51
2.3.5 Quantification of thiols on the PDMS elastomer surface 52
2.3.6 Monitoring the partition of thiols between the surface and the bulk 53
2.3.7 Modification of thiol-functionalized surfaces 54
2.3.8 Modification of the anhydride surfaces 56

2.4 RESULTS AND DISCUSSION 57

2.4.1 Introduction of thiols to the PDMS elastomer surface PDMS-SH 57
2.4.2 The distribution of thiol groups within PDMS-SH 60
2.4.3 Susceptibility of the thiol surface to reversion 67
2.4.4 Modification of the thiol-rich surface 68
2.4.5 Wettability and Reversion 70

2.5 CONCLUSION 76

2.6 ACKNOWLEDGEMENTS 77

2.7 REFERENCES 77

CHAPTER 3: REDUCTIVE DEGRADATION OF LIGNIN AND MODEL COMPOUNDS BY HYDROSILANES§ 81

3.1 ABSTRACT 81

3.2 INTRODUCTION 82

3.3 EXPERIMENTAL 86

3.3.1 Materials 86

3.3.2 Methods 87

3.3.3 Reduction of lignin model compounds 88

3.3.4 Reduction of lignins 90

3.4 RESULTS AND DISCUSSION 93

3.5 CONCLUSIONS 105

3.6 ACKNOWLEDGEMENTS 106

3.7 REFERENCES 106

CHAPTER 4: UTILIZATION OF SOFTWOOD LIGNIN AS BOTH CROSSLINKER AND REINFORCING AGENT IN SILICONE ELASTOMERS[§] 110

4.1 ABSTRACT 110

4.2 INTRODUCTION 111

4.3 EXPERIMENTAL SECTION 115

4.3.1 Materials 115

4.3.2 Quantitation of reactive surface functional groups on lignin particles 116

4.3.3 Control Experiments 117

4.3.4 Fabrication of lignin crosslinked/reinforced silicone elastomers 118

4.3.5 Characterization 120

4.4 RESULTS AND DISCUSSION 120

4.5 CONCLUSIONS 136

4.6 ACKNOWLEDGEMENTS 137

4.7 REFERENCES 137

CHAPTER 5: FOAMED LIGNIN-SILICONE BIO-COMPOSITES BY EXTRUSION THEN COMPRESSION MOLDING[§] 141

5.1 ABSTRACT 141

5.2 INTRODUCTION 142

5.3 EXPERIMENTAL SECTION 146

5.3.1 Materials 146

5.3.2 Lignin-silicone foam fabrication - optimization of conditions and formulations 146

5.3.3 Hydrolysis of Si-H groups remaining after cure 150

5.3.4 Characterization 151

5.4 RESULTS AND DISCUSSION 152

5.4.1 Optimal foam structures 152

5.4.2 Chemistry at the lignin-silicone interface 153

5.4.3 Optimization of formulations and processing conditions for lignin-silicone foam 154

5.4.4 Mechanical properties of lignin-silicone foams 163

5.5 CONCLUSIONS 168

5.6 ACKNOWLEDGEMENTS 169

5.7 REFERENCES 169

CHAPTER 6: GENERAL CONCLUSIONS 175

CHAPTER 7: APPENDIX 179

7.1 SUPPORTING INFORMATION FOR CHAPTER 2: FACILE FUNCTIONALIZATION OF PDMS ELASTOMER SURFACES USING THIOL-ENE CLICK CHEMISTRY 179

7.1.1 DTDP titration: calibration curve and sample calculation for surface concentration of thiol 179

7.1.2 Iodine titration: calibration curve and sample calculation for surface concentration of thiol 181

7.2 SUPPORTING INFORMATION FOR CHAPTER 3: REDUCTIVE DEGRADATION OF LIGNIN AND MODEL COMPOUNDS BY HYDROSILANES 187

7.3 SUPPORTING INFORMATION FOR CHAPTER 4: UTILIZATION OF SOFTWOOD LIGNIN AS BOTH CROSSLINKER AND REINFORCING AGENT IN SILICONE ELASTOMERS 200

7.3.1 Equipment associated with titration of the lignin surface 200

7.3.2 Chemistry associated with titration of the lignin surface 200

7.3.3 Solvent resistance 204

7.4 SUPPORTING INFORMATION FOR CHAPTER 5: FOAMED LIGNIN-SILICONE BIO-COMPOSITES BY EXTRUSION THEN COMPRESSION MOLDING 206

7.5 REFERENCES 217

LIST OF SCHEMES

CHAPTER 1: Introduction

Scheme 1.1 The chemical structure for silicones, and the common pendent groups. 2

Scheme 1.2 Hydrophobic recovery of silicone surface.....4

Scheme 1.3 Modification of silicone surface without altering the –Si-O- bond via physical adsorption, blending, and polymerization from surface adsorbing/blending reactive reagents. 6

Scheme 1.4 The dynamic cleavage and re-association of -SiO- bonds under acid (A) or basic (B) conditions. 10

Scheme 1.5 Modification of silicone surfaces through cleavage or rearrangement of -SiO- bonds: silanization via acid or base catalysis (A), UV, plasma, or corona activation (B). 11

Scheme 1.6 Thiol-ene click reaction (A), and its application on surface modifications (B) "grafting to" and (C) "grafting from". 15

Scheme 1.7 A) The three basic building units for lignin: p-hydroxylphenyl-, coniferyl-, and sinapylpropane.(Heitner et al., 2010) B) The typical linkages of lignin.(Zakzeski et al., 2010) C). The typical structures of hardwood lignin and softwood lignin, respectively.(Evtuguin et al., 1998) 20

Scheme 1.8 The main methods for lignin depolymerization. 22

Scheme 1.9 The reduction β-O-4 and 4-O-5 using Ni based catalyst; (A) selective reduction: a) Ni@SiC,(Zaheer et al., 2014) b) $Ni(COD)_2$ or (CH_2TMEDA),(Sergeev et al., 2012, Sergeev and Hartwig, 2011) c) $Ni(COD)_2/PCy_3$,(Tobisu et al., 2011) and Ni/C;(Song et al., 2013) and (B) non-selective reduction: e) NiAu,(Zhang et al., 2014a) f) NiM (M = Ru, Rh, and Pd),(Zhang et al., 2014b) g)Ni/SiO_2,(He et al., 2014, He et al., 2012) and $Ni(COD)_2$.(Sergeev et al., 2012) 26

Scheme 1.10 The cleavage of aryl ether bonds using (A) photo-,(Nguyen et al., 2013) or (B) electro- chemical reduction.(Wu and Huang, 2014).....27

Scheme 1.11 The effective reactions for lignin grafting/modification, integrating lignin into other polymeric matrixes. 29

Scheme 1.12 Using the lignin as the phenol substitution in phenol resin (A) directly without pre-modification, (B) after phenolation, (C) via Mannich reaction.....34

CHAPTER 2: Facile functionalization of PDMS elastomer surfaces using thiol-ene click chemistry

Scheme 2.1 Schematic illustration of the process to introduce thiols onto PDMS elastomer surfaces. (A) reactions at silicone; (B) reactions at MTS; and (C) metathesis at the elastomer interface. 58

CHAPTER 3: Reductive degradation of lignin and model compounds by hydrosilanes

Scheme 3.1 The three basic building units for lignin and some representative linkages found in lignin. 84

Scheme 3.2 Facile reduction of organofunctional groups using hydrosilanes catalyzed by $B(C_6F_5)_3$. 86

Scheme 3.3 Reaction of model lignin compounds with PMDS in presence of $B(C_6F_5)_3$. .94

Scheme 3.4 Staged reduction of 3-hydroxy-4-methoxybenzyl alcohol. The relative reactivity order: phenol > primary alcohol > methoxybenzene > aliphatic silyl ether >> aromatic silyl ether. 96

CHAPTER 4: Utilization of softwood lignin as both crosslinker and reinforcing agent in silicone elastomers

Scheme 4.1 The typical linkages in lignin molecules that are backbone cleavable (red) and partly degradable (black) under Piers-Rubinsztajn conditions 112

Scheme 4.2 Reaction scheme: A: Piers-Rubinsztajn process for elastomer formation; B: Replacement of alkoxysilane by lignin for both crosslinking and physical reinforcement. 115

CHAPTER 5: Foamed lignin-silicone bio-composites by extrusion then compression molding

Scheme 5.1 (A) Typical reactions at phenolic linkages in lignin. (B) The chemical structures hydride-terminated PDMS (H-PMDS-H) and poly(hydromethylsiloxane) (PHMS). 145

Scheme 5.2 Illustration of the extrusion and compression molding process. The inset images show the cross-section and assembled views of micro-scale twin-extruder. 148

Scheme 5.3 The chemistry at lignin interface: silylation and crosslinking during the compression molding processing. 154

LIST OF FIGURES

CHAPTER 2: Facile functionalization of PDMS elastomer surfaces using thiol-ene click chemistry

Figure 2.1 SEM images of elastomer surfaces resulting from different KOH concentrations (w/v), (A) 1% KOH, no cracking, (B) 2.5 % KOH, starts cracking, (C) 5% KOH, cracked. 59

Figure 2.2 Cross-sectional EDX for the elastomer treated for different reaction times. (A/B) EDX spot location on the cross-section of a treated elastomer. (C) Intensity of sulfur in the elastomer cross-section after 6 hours treatment. (D) Sulfur concentrations as a function of reaction time. All the EDX measurements were performed using the same accelerating voltage and collection time. 62

Figure 2.3 Fluorescence microscopy images of the thiol-functionalized PDMS elastomer dyed with *N*-(5-fluoresceinyl)maleimide. The experimental conditions for surface equilibration: reaction time = 6 hours, KOH concentration = 1%, MTS concentration = 10%, and reaction temperature = 50 °C. (A) The top view of the thiol-functionalized surface labeled with *N*-(5-fluoresceinyl) maleimide. (B) Cross-sectional view of the fluorescently labeled, thiol-functionalized PDMS elastomer. The inset is an LSCM (laser scanning confocal microscopy) image obtained by the "z stack" mode (obtaining cross sectional images of planes at various depths (z)

within the sample, scale bar = 50 μm). (C) The EDX spectrum of the thiol surface, labeled with **AuNP**. The signals for Au and sulfur were both detected. (D) The EDX spectrum collected at the middle of the elastomer after labeling with AuNP. No signal for either Au or sulfur was detected. The photos show that after labeling the thiol-functionalized elastomer was tinted pink (right inset), while the control remained uncolored (unmodified elastomer, left). 64

Figure 2.4 Quantitative analysis of thiol groups: (A) determination of thiol groups on the interface of PDMS elastomer by DTDP titration, (B) determination of thiol groups in the surface layer by iodine titration. 66

Figure 2.5 A: The change of thiol surface concentration over time, and the rearrangement in DCM. The surface and interfacial concentration were monitored by iodine and DTDP titration, respectively. B: Cross-sectional image of fluorescence labeling the maleic anhydride-modified surface with rhodamine 123. 68

Figure 2.6 Surface modification of thiol-silicones: Surface thiol-ene reactions with A: ACR A008-UP, B: *N*-(5-fluoresceinyl)maleimide, and C: maleic anhydride, followed in the latter case by ring-opening of the surface anhydride with D: M-PEG, E: chitosan or F: rhodamine 123. 69

CHAPTER 3: Reductive degradation of lignin and model compounds by hydrosilanes

Figure 3.1 ^{1}H-NMR of guaiacylglycerol-beta-guaiacyl ether and its silylated products (solvent $CDCl_3$). 97

Figure 3.2 (A) Schematic illustration of possible structure changes to lignin during reduction and de-silylation. (B) ^{13}C-NMR of (a) hardwood lignin, (b) reduced and silylated hardwood lignin fragments (in DMSO d_6). (C) Reduction with three different catalyst concentrations showing increasing reduction/silylation (c 2.0% $B(C_6F_5)_3$, d 5.8%; e 10.2%, samples were run in $CDCl_3$).....102

Figure 4.3 The FT-IR spectra of hardwood lignin and its reduced/degraded products: (A) residual/isolated product. Soluble products collected from the (B) third, (C) second, and (D) first reduction processes; and (E) unmodified hardwood lignin (yellow OH groups, red Si-O, blue Ph-O/C-O, green Si-O and Si-CH3).....104

CHAPTER 4: Utilization of softwood lignin as both crosslinker and reinforcing agent in silicone elastomers

Figure 4.1 Gas production (red) and equivalents of hydride used (blue) as a function of lignin content in the solvent. Images A-C are the microscopic images of lignin dispersions at different solid/liquid ratios: A: dispersion of lignin at low content (5 mg/g), evenly distribution of particles; B dispersion of lignin with higher content (50mg/g), formation of clusters; C highly agglomerated lignin particles at concentrated dispersion (200 mg/g).....123

Figure 4.2 Elimination of bubble defects by solvent: A no added solvent, B with D_5 127

Figure 4.3 A schematic illustration of lignin crosslinked silicone networks at different lignin contents. A: low lignin content (0.5 to 16%); B: optimized content range (27

to 57%); and, C: excess content (60 to 71%). Images D-H show the changes in elastomer appearance with different lignin contents.....128

Figure 4.4 Cross-sectional images (D-F are the higher magnification images of A-C) of lignin/silicone elastomers of different lignin content: 16% A, D; 41% B, E; 68% C, F, respectively. 131

Figure 4.5 Structure evolution of silicone foam/elastomer with: A: increasing lignin content, and, B: co-crosslinker content.....133

CHAPTER 5: Foamed lignin-silicone bio-composites by extrusion then compression molding

Figure 5.1 Illustrations of lignin-silicone foam structures, and their resultant mechanical properties: tensile modulus increases with crosslinking density, while the elongation-at-break are depended on both crosslinking density and uniformity of foams. Type A structures are foams either with large trapped (A1) or collapsed voids (A2, closer to an elastomer than a foam); Type A1 foams are easy to break with extension of bending due to the large defects. Type B structures are foams with uniform morphology; these foams are flexible with tunable toughness. Types C are foams with excessive crosslinking density and fewer voids; Type C1 foams are tough, while Type C2 were brittle. 153

Figure 5.2 The reprehensive DMA curves of lignin-silicone (F-9). 164

CHAPTER 7: Appendix

Figure 7.1 Calibration curve for DTDP titration, the eight data points at each concentration were triplicates each from three different DTDP stock solutions. Abs = 0.0068 [SH] + 2.4313.....180

Figure 7.2 Calibration curve for iodine titration, Abs = 0.0012 [I_2](Gandubert and Lennox, 2005) – 0.0387. 181

Figure 7.3 The sandwich structure of elastomer labeled with rhodamine (PDMS-S-MA-RH).....182

Figure 7.4 Transparency of PDMS elastomer after surface treatment with different base concentrations. 182

Figure 7.5 AFM and 3D plotted profilometry images for surface roughness characterization. (A) and (C) were measured from unmodified PDMS elastomer surfaces. (B) and (D) are the measurements of PDMS elastomer surfaces treated in 1% of KOH and 10% of MTS at 50 °C for 6 h. (E) 3D plotted profilometry images for surface modified with Silmer ACR. The image Rq for (A) to (E) were 4.09 nm, 4.80nm, 10.92 nm, 27.66 nm, and 20.0 nm, respectively. 183

Figure 7.6 The EDX spectra obtained from different regions on the cross-section of the silicone elastomer.....184

Figure 7.7 The ATR-FTIR spectra for PDMS surfaces modified with ACR-A008 UP (PDMS-S-ACR-A008UP), maleic anhydride (PDMS-S-MA), PEG (PDMS-S-MA-PEG), and chitosan (PEG-S-CH).....184

Figure 7.8 The Raman spectra of unmodified **PDMS**, thiol-functionalized **PDMS-SH**, and maleic anhydride modified **PDMS-S-MA**. 185

Figure 7.9 Fluorescence microscopy images of the thiol-functionalized PDMS elastomer (stored in ~2 °C refrigerator, sealed and soaked in methanol for more than 4 months), dyed with *N*-(5-fluoresceinyl) maleimide. 185

Figure 7.10 The ATR-FTIR spectrum for PDMS-SH surface (used within 2 weeks and over 4 month after base-catalyzed equilibrium treatment) modified with ACR-A008 UP 186

Figure 7.11 Model structures of (A) hardwood lignin, and (B) softwood lignin. 187

Figure 7.12 ^{1}H-NMR spectrum of 2-phenoxy-1-phenylethanol and its reduced products ($CDCl_3$ solvent). 187

Figure 7.13 ^{1}H-NMR spectrum of 1-phenyl-2-propanol (A), its silylated product (B), and mixture of silylated and fully reduced products (C) ($CDCl_3$ solvent). The silyl ether is a stable intermediate product and rather difficult to completely reduce. The spectra (C) was obtained without removing toluene (solvent) and PMDS (reagent), because the boiling point were very close to the fully reduced product (n-propylbenzene). 188

Figure 7.14 ^{1}H-NMR spectrum of 3-phenyl-1-propanol (A), its silylated (B) and fully reduced (C) products ($CDCl_3$ solvent). 188

Figure 7.15 1H-NMR spectrum of benzyl phenyl ether and its reduced products ($CDCl_3$ solvent). 189

Figure 7.16 ^{1}H-NMR spectrum of intermediate products form staged reduction of 3-hydroxy-4-methoxybenzyl alcohol ($CDCl_3$ solvent). The relative reactivity order was found: phenol > primary alcohol > methoxyl > silylether 190

Figure 7.17 ^{1}H-NMR and ^{13}C-NMR spectrum before ((A) and (C)) and after ((B) and (D)) treating diphenyl ether with PMDS and $B(C6F5)_3$. The identical spectra before and after the reaction indicated no reaction occurred during this process. 191

Figure 7.18 (A) ^{1}H-NMR spectrum of sinapyl alcohol and its reduced products ($CDCl_3$ solvent). (B) GC/MS spectrum for reduced products of sinapyl alcohol. 192

Figure 7.19 GC/MS spectrum for reduced products of guaiacylglycerol-beta-guaiacyl ether. The identified main peaks were highlighted with color masks: peaks highlighted by red and blue masks were the two reduced products. The chemical structures and MS spectra of these two products were also highlighted with corresponding color masks. The other two peaks do not correspond to structures of guaiacylglycerol-beta-guaiacyl ether or its reduced products.....193

Figure 7.20 ^{1}H-NMR spectrum of guaiacylglycerol-beta-guaiacyl ether and its reduced products ($CDCl_3$ solvent). 194

Figure 7.21 General process for the reduction/degradation of softwood/hardwood lignin, and purification of residual/isolated and reduced lignin products. 195

Figure 7.22 Process for degradation of hardwood lignin using increasing amounts of catalyst. 195

Figure 7.23 Virtually no change in turbidity was noted before and after sonicating softwood lignin with PMDS and $B(C6F5)_3$ in a 50 °C water bath for 3 hours. The percentage of soluble lignin was failed to obtain due to the weight gain of residual. 196

Figure 7.24 The visible difference of hardwood reduction/degradation with different catalyst concentrations. Turbidity decreases dramatically as the residual undissoved lignin drops from 73.4% (26.6% solubilization) to 4.4% (95.6% solubilization).The solubilization percentage is defined as (1 - Final insoluble weight/starting insoluble weight) x 100%. 196

Figure 7.25 The ^{1}H-NMR and ^{13}C-NMR spectra of softwood lignin (A) and (C), and the soluble and products (B) and (D) after reduction by Et_3SiH. The solvent for (A) and (C) was DMSO, and for the more soluble products (B) and (D) was $CDCl_3$. 197

Figure 7.26 A: Calibration curve using PEO standards B: GPC chromatogram of unmodified hardwood lignin in DMF containing 50 mmol LiBr. C: GPC chromatogram of silylated hardwood lignin in DMF containing 50 mmol LiBr, after treatment with TBAF to remove silyl groups. 198

Figure 7.27 ^{13}C-NMR spectra for TBAF (solvent DMSO). 199

Figure 7.28 The water displacement method for gas production measurement. 200

Figure 7.29 The molar ratio of reactive surface functional group to gaseous by-product (5 equiv./4 equiv.). 200

Figure 7.30 The DRIFT-IR spectrum for lignin particles titrated with different concentration in solvent. (A) and (B) The intensity of "Si-H" peak dropped with the increasing of lignin content in solvent (mg lignin/g solvent). 201

Figure 7.31 Images of bubble lignin/silicone elastomers made without solvent, right image is the cross-section of elastomer. 203

Figure 7.32 Swelling the lignin-C/R-elastomer with different solvent. The diameter ratios before and after swelling are list sequently: 1.32, 1.14, 1.00, 1.12, 1.00, 1.29, 1.41, 1.23, and 1.24 (left is the elastomer swell in solvent, right is control). 205

Figure 7.33 TGA thermograms of LE-41B (red), lignin (blue), and silicone (black) under air atmosphere 205

Figure 7.34 A gas volume meter was used to measure volume of gas produced during the reaction in solvent during preliminary optimizations and hydrolysis studies.....206

Figure 7.35 Testing the conversion of "Si-H" in lignin-silicone foam. Before reaction, the sliced lignin-silicone foam layers were dispersed in KOH/BuOH; the foam lost its integrity (fell apart to give a suspension) after treatment. 207

Figure 7.36 Kinetics studies for PHMS conversion % under different conditions and formulations: (A) mixing order: mixing order A led to longer induction times. The inset graph is the expanded range showing different induction times; (B) catalyst loading: conversion% increased, while induction time decreased, with increased catalyst loading; (C) temperature: higher temperature led to faster reaction rates and

greater conversion% of PHMS. (D) PHMS content had no impact on induction time. 208

Figure 7.37 Gelation or crosslinking of foam precursors blocked the extruder channels. 209

Figure 7.38 Cross-sectional images of lignin-silicone foams prepared from formulations with different catalyst loading: (A) F-1, BCF = 300 ppm, (B) F-2, BCF = 1000 ppm, (C) F-3, BCF = 1350 ppm, and (D) F-4, BCF = 2050 ppm. 209

Figure 7.39 Images of lignin-silicone composite foams made with different catalyst content. (A) BCF = 300 ppm, curing for 180 min; (B) BCF = 1000 ppm, curing time = 5 min. 210

Figure 7.40 Cross-sectional images of lignin-silicone foam sprepared from formulations with varying lignin content: (A) F-8, 15 % of lignin, (B) F-9, 25% lignin, (C) F-4, 41% lignin, and (D) F-10, 55% lignin. 210

Figure 7.41 Cross-sectional images of lignin-silicone foams prepared from formulations with varying PHMS content: (A) F-5, 4 % of PHMS, (B) F-4, 8 % of PHMS, (C) F-6, 16 % of PHMS, and (D) F-7, 24 % of PHMS.....211

Figure 7.42 Cross-sectional images of lignin-silicone foams prepared from formulations with different molecular weight H-PDMS-H: (A) F-11, DMS-H25 (Mw = 6000 g/mol), (B) F-4, DMS-H31 (Mw = 28000 g/mol), and (C) F-13, Mixture of DMS-H25/31/41 (containing 26% H25, 48% H31, and 26% H41, H-41: Mw = 62700 g/mol). 211

Figure 7.43 Attempts to make lignin-silicone foams using DMS-H41 (F-12) failed due to the high intrinsic viscosity of DMS-H41. The precursor is semi-cured, and could not be processed in extruder.....212

Figure 7.44 Cross-sectional images of lignin-silicone foams (formulation F-4) molded under different temperatures: (A) 60, (B) 90, and (C) 120°C.....212

Figure 7.45 Preparation samples for ATR-IR characterization: how signal changes of "Si-H" groups in the foam were tracked. 212

Figure 7.46 ATR-FTIR spectra for lignin-silicone foams made under different conditions and formulations: (A) different catalyst loading (from 300 to 2050 ppm), cured at 90 °C for 180 min, (B) foams in mold with different holding times (from 5 to 180 min), cured with 1350 ppm catalyst at 90 °C. The expanded spectra ranged from 2100 to 2250 cm^{-1} to track the intensity change of the "Si-H" signal. 213

Figure 7.47 NMR spectrum of the cyclohexane extract from lignin-silicone foam, and the proton ratios ("Si-H"/"Si-CH_3") of samples obtained with different conditions and formulations. 214

Figure 7.48 TGA of lignin-silicone foams (purple: 41% lignin in foam, red: 55% lignin in foam), lignin (black), and silicone (blue) under an air atmosphere. 216

LIST OF TABLES

CHAPTER 1: Introduction

Table 1.1 Approximate abundance of building blocks in lignin from different sources.(Heitner et al., 2010) 19

Table 1.2 Approximate abundance (%) of different chemical linkages in hardwood and softwood lignin.(Zakzeski et al., 2010) 19

CHAPTER 2: Facile functionalization of PDMS elastomer surfaces using thiol-ene click chemistry

Table 2.1 The effect of experimental conditions on resulting surface density of thiols 61

Table 2.2 The contact angle of modified PDMS 71

CHAPTER 3: Reductive degradation of lignin and model compounds by hydrosilanes

Table 3.1 Molecular weight profile[a] of lignin before and after reduction. 88

Table 3.2 The reaction conditions and yields of model compounds.....89

Table 3.3 The reaction conditions for degradation of hard- and softwood lignin. 91

CHAPTER 4: Utilization of softwood lignin as both crosslinker and reinforcing agent in silicone elastomers

Table 4.1 Use of lignin as crosslinker/reinforcement in silicone elastomers.....119

Table 4.2 The reactivity of lignin particles and silicone hydride with different chemical structures (lignin content = 50 mg/g). 126

Table 4.3 Mechanical performance of lignin/silicone elastomers, the impact of lignin content, co-crosslinker content, and silicone molecular weight. 130

Table 4.4 The mechanical performance of lignin/silicone elastomers after treatment at higher temperatures and selected organic solvents 135

CHAPTER 5: Foamed lignin-silicone bio-composites by extrusion then compression molding

Table 5.1 Parameters used to optimize extrusion and molding conditions, and formulations for lignin-silicone foam. 149

Table 5.2 The weight formation (%) of lignin-silicone foams after extraction with cyclohexane 161

Table 5.3 The conversion ratio of Si-H in lignin-silicone foam after post-curing at higher temperature, and their mechanical performance 163

Table 5.4 The tensile test for lignin-silicone foams 166

CHAPTER 7: Appendix

Table 7.1 Assignments of ^{13}C-NMR signals for lignin (β-O-4 related)(Hawkes et al., 1993, Wen et al., 2013) 198

Table 7.2 Example formulation of lignin (SKL from Weyerhaeuser, 40.9%) as crosslinker/reinforcement in silicone elastomer. a co-crosslinker (HMS-992) was

used for keeping the chemical stoichiometry of hydride to surface functional group of lignin close to 1:1. 203

Table 7.3 The hydride content of hydride functionalized silicone with different chemical structures 204

Table 7.4 Solvent resistance of lignin-C/R-elastomer to organic solvents and water 204

Table 7.5 Preliminarily optimizations for extrusion and molding conditions of different formulations. 207

Table 7.6 The degree of conversion of "Si-H" in lignin-silicone foams, tested by hydrolysis in solution 215

Table 7.7 The mechanical properties of lignin-silicone foams characterized using DMA 217

LIST OF ABBREVIATIONS AND SYMBOLS

AFM	Atomic force microscopy
AIBN	Azobisisobutyronitrile
ATR	Attenuated total reflectance
ATRP	Atom transfer radical polymerization
AuNP	Gold nanoparticles
BCF	Tris(pentafluorophenyl)borane
DCM	Dichloromethane
DRIFTS	Diffuse reflectance infrared Fourier transform spectroscopy
DTDP	4,4'-dithiodipyridine
E'	Storage modulus
E"	Loss modulus
EDX	Energy-dispersive X-ray spectroscopy
GC-MS	Gas chromatography–mass spectrometry
GPC	Gel permeation chromatography
IgG	Immunoglobulin G
IPN	Interpenetrating polymer network
Mn	Number average molecular weight
Mw	Weight average molecular weight
NMR	Nuclear magnetic resonance
PEO	Poly(ethylene oxide)
PEG	Poly(ethylene glycol)
PDMS	Polydimethylsiloxane
PHMS	Poly(hydromethylsiloxane)
PMDS	Pentamethyldisiloxane
PPO	Poly(phenylene oxide)
SEM	Scanning electron microscope
SKL	Softwood Kraft lignin
TBAF	Tetrabutylammonium fluoride trihydrate
Tg	Glass-transition temperature
TGA	Thermogravimetric analysis
THF	Tetrahydrofuran
UV	Ultraviolet
XPS	X-ray photoelectron spectroscopy

CHAPTER 1: Introduction

1.1 Surfaces and Interfaces

The terms “surface” or “interface” generally refers to the common boundary between two immiscible phases. Surface is specifically used to describe the boundary between condensed and gaseous phases or a vacuum, while interface is mainly used to describe the boundary of two condensed phases.(Myers, 1991) The surface or interface, chemically, only has a thickness of about a few layers of atoms; the surface/interface exhibits completely different chemical and physical properties when compared to the bulk phase.(Lüth, 2001) Surfaces and interfaces play key roles in many applications, such as heterogeneous catalysis, semiconductor electronics, and medical- and bio-materials to name only a few. For polymers, the properties of the surface/interface, such as wettability, friction, adhesion, and biocompatibility, often determine the performance and applications rather than the bulk material.(Somorjai and Li, 2010)

In most cases, an application requires the maintenance of bulk performance of polymeric materials, while altering the surface/interfacial properties.(Mittal et al., 1997) Examples can be easily found in our daily life, including: coatings for scratch resistant surfaces,(Hwang et al., 2003) interfacial treatment to provide better compatibility of heterogeneous phases in polymer blends or composites,(Pukánszky, 2005) as well as the surface treatment of devices for improving biocompatibility.(Ikada, 1994) The

importance of surface and interface modifications is increasing, especially for controllable modification and modification for bio-renewable materials.(Thakur and Singha, 2015) Thus, the focus of this thesis is on developing methodologies to permit controllable surface/interface modifications on both synthetic and natural polymeric matrices including siloxanes and hydrocarbon base materials.

1.2 Surface modification of silicone elastomer

1.2.1 Silicone elastomer

Silicones are polymers that consist of -Si-O- repeating units as the backbone, with various pendent groups, such as methyl, ethyl, or phenyl (Scheme 1.1).(Shit and Shah, 2013) Silicones have found widespread application in various fields, due to their advantages, including optical transparency, flexibility, bio-inertness, and ease of fabrication, etc. The silicone is also distinct for the very high hydrophobicity that originates from its chemical structure.(Brook, 1999) The hydrophobic feature facilitates its use in applications like coatings or sealants; however, applications in microfluidics or biomaterials may be impeded by hydrophobicity.(Wong and Ho, 2009)

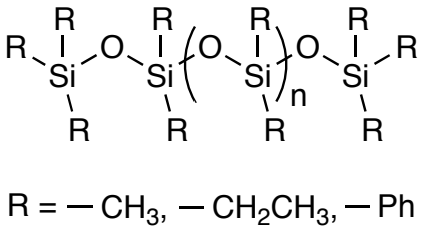

Scheme 1.1 The chemical structure for silicones, and the common pendent groups.

Polydimethylsiloxane (PDMS) is one of the most commonly used silicones. The PDMS elastomer has very low surface free energy (~ 22 mN m^{-1} and high water contact angles, near from 110 to 120°).(Owen and Dvornic, 2012) In the past few decades, a number of modification methods have been developed to create hydrophilic PDMS surfaces. (Wong and Ho, 2009, García et al., 2005) The methodologies can be classified into the following two types: in one type of procedure, the modification involved altering the chemical structure of siloxanes at the interface; in other cases, the modification generally involved a cleavage and rearrangement of -Si-O- bonds. The methodology described in this thesis falls in the latter category.

1.2.2 Hydrophobic recovery – a challenge for PDMS surface modification

The silicone chain is very flexible, due to the large Si-O-Si bond angle (145°) and low bending forces.(Brook, 1999) The methyl groups in silicones typically present at air interfaces, as locating hydrophobic groups there is thermodynamically advantageous. Once a silicone surface has been disrupted, silicone chains can migrate to the air interface if the system is above the Tg (-123 °C). Hydrophobic recovery – the ability of silicone polymers that have been hydrophilically modified to return to a hydrophobic state – is mainly attributed to: a) the re-arrangement of polar and non-polar functional groups/polymers (e.g., methyl groups can be exchanged for hydroxyl or hydrophilic polymers) at an interface, or, b) the migration of free low molecular weight/network pendent silicone polymer chains to the surface, as shown in Scheme 1.2. The re-arrangement and migration processes are spontaneous as they result in improved free

energy configurations.(Bacharouche et al., 2013) The modification of silicone involves, therefore, not the simple functionalization of the interface because of the mobility of silicone monomer units: maintaining coating agents/polymers on silicone surfaces, in the face of hydrophobic recovery, is a challenge. A brief review follows on the most commonly used methods to alter PDMS surfaces from hydrophobic to hydrophilic.

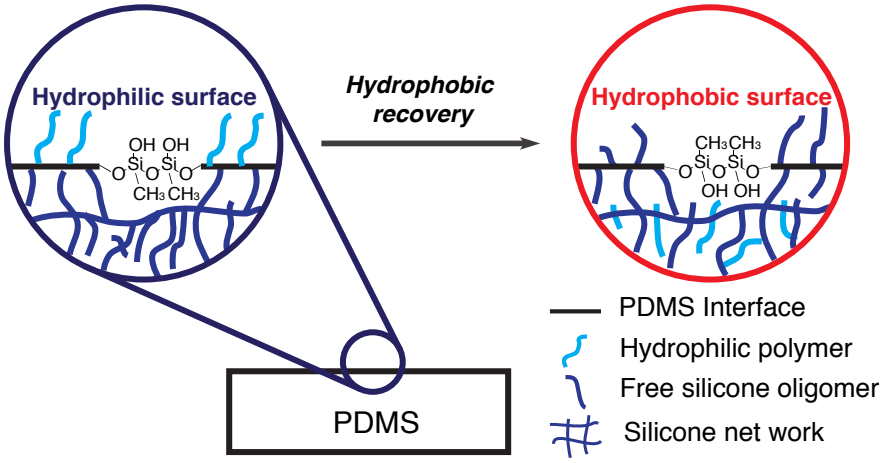

Scheme 1.2 Hydrophobic recovery of silicone surface.

1.2.3 Modification without changing -Si-O- bonds

As shown in Scheme 1.1, the chemical modification of PDMS surfaces is challenging due to the lack of reactive functional groups that can act as tethering sites:(Roth et al., 2008) the hydrophobic surface predominantly attracts other hydrophobic materials. Therefore, several methods based on this interaction were developed to modify PDMS surfaces, with the aim to alter the surface properties towards becoming more hydrophilic without changing the chemical structures of siloxanes at the interface. The

general procedure involves physical adsorption or blending of amphiphilic or reactive hydrophobic agents with PDMS, and maybe further polymerization from the surface adsorbing/blending reactive groups, as shown in Scheme 1.3.

Coating the silicone surface with a layer of amphiphilic reagent is the most simple and easy method to change surface characteristics, such as surfactants, block polymers, or proteins.(García et al., 2005, Yu and Han, 2006, Wang et al., 2007) Amphiphilic proteins are ideal for coating PDMS surfaces, especially for biomaterial applications. The amphiphilic proteins are physically deposited on silicone surface, without cleavage or association of chemical bonds. Hydrophobin, an amphiphilic fungal protein, prefers to self-assemble and form a membrane at a hydrophobic-hydrophilic interface. Taking advantage of these properties hydrophobin was used for PDMS surface modification. After coating the PDMS surface with hydrophobin, the water contact angle was reduced from 124 to 51°.(Wang et al., 2007) The interaction between the hydrophobin and silicone surface was strong enough to permit the subsequent grafting of a layer of chicken IgG and fluorescent anti-chicken IgG. The resulting amphiphilic protein-modified surface demonstrated resistance to "hydrophobic recovery" for a long period in air – 20 days.(Wang et al., 2007)

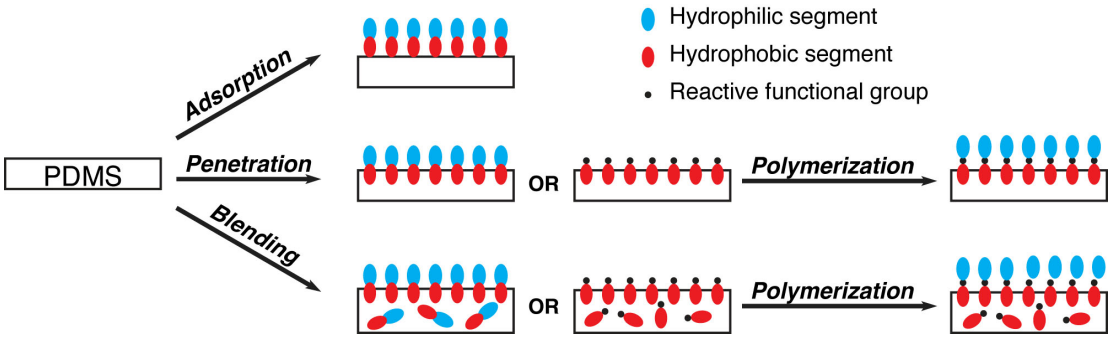

Scheme 1.3 Modification of silicone surface without altering the –Si-O- bond via physical adsorption, blending, and polymerization from surface adsorbing/blending reactive reagents.

Alternatively, an amphiphilic block polymer (PEO-b-PDMS) could be employed for surface modification and introduced to the surface through a swelling-deswelling process.(Yu and Han, 2006) In a good solvent for silicone – chloroform – the hydrophobic segments of the block polymer diffused into the silicone body, driven by van der Waals forces and hydrophobic interactions, while the hydrophilic segments were left at the interface. After removing the solvent, the hydrophobic segments were trapped at the interface, resulting in a coating of PEO on the PDMS surface. The hydrophilicity was found to increase proportionally to the density of hydrophilic segments on the surface, lowering the water contact angle down to 56°.(Yu and Han, 2006) However, other surfactants could also be used for surface modification of PDMS device, which had been reviewed comprehensively.(García et al., 2005)

The two methods discussed above were based on utilization of weak interactions between silicone and hydrophobic agents. Tugulu et al. developed an ingenious method to create an IPN (interpenetrating polymer network) with reactive groups at interface of silicones.(Tugulu and Klok, 2009) The IPN was produced by first condensing 4-(chloromethylphenyl)trichlorosilane on the silicone, where it penetrated the interface. Following hydrolysis and condensation, the interpenetrated phenyl silicone and dimethylsilicone networks led to an interface that was surface functionalized with benzyl chloride residues. However, the siloxane network of the matrix is not affecting during the formation of secondary network. This surface could be used for initiating the polymerization of hydrophilic polymer (poly(poly(ethylene glycol)methacrylate)) via ATRP (atom-transfer radical-polymerization). Thus, a hydrophilic coating was immobilized on PDMS surface, indirectly, through the entanglement of silane and siloxane networks. After modification, the advancing contact angle was reduced from 104 to 60°.(Tugulu and Klok, 2009) This method will also change the properties of the surface due to an increase in the crosslinking density caused by IPN at the interface. Alternatively, a simple and effective method was developed by Hu et al.(Hu et al., 2004b, Hu et al., 2004a) The modification was achieved first by the physical adsorption of a radical polymerization initiator at the silicone surface. Because the radicals generated from the initiator were reactive enough to cleave the C-H of silicon-methyl groups, the methylene radicals ($SiCH_2^{\bullet}$) could act as surface initiators to graft hydrophilic polymers to the PDMS surface.(Schneider et al., 2011) Due to the versatility of a radical initiator to

facilitate the polymerization of different monomers, the silicone surface could be easily tailored by polymerizing monomers with different characteristics, including both charged or neutral moieties.(Ebara et al., 2007, Hu et al., 2004b)

The surface modification of silicone can be also achieved by blending silicones with hydrophilic polymers. Similar to the swelling-deswelling induced modification discussed above,(Yu and Han, 2006) Wu et al. reported a straightforward method that involved simply blending two commercial products, Pluronic (PEO-PPO-PEO triblock polymer) and a two component PDMS elastomer kit (RT601 A and B, Pt cured silicone elastomer, Wacker Chemie).(Wu and Hjort, 2009) After curing the mixture, the hydrophilic segments of Pluronic in the matrix were "pulled out" to the interface by exposing the surface to water. Although minor amounts of PEO-PPO-PEO were lost during extraction, such a modified surface demonstrated satisfactory resistance to nonspecific protein adsorption and hydrophilicity with contact angles dropping down to 63°.(Wu and Hjort, 2009)

As an alternative, the hydrophilic polymer could be covalently trapped in a silicone. For example, triethoxysilylpropyl-functionalized PEO was synthesized and used as crosslinker for silicone network fabrication. The PEO chains were encouraged to migrate to the surface by soaking in water after the elastomer cured.(Chen et al., 2004) Because the no chemical bond was cleavage or re-associated, PEO rearranged onto surface, showing with conformation change only. Although these methods can alter the surface properties, the bulk properties also changed due to the presence of immiscible

components or polymer segments. Therefore, blending the silicones with more miscible reagents and then covalently bonding with the hydrophilic polymers is a better method for surface modification of elastomers, while still retaining the properties of bulk PDMS. In one example, vinyl-functionalized polymerization initiators were dispersed in a silicone matrix (Sylgard 184) at the molecular level, and were covalently bonded to the silicone network via hydrosilylation with curing; then, polymerization of hydrophilic monomers (e.g., vinyl acetate, oligo(ethylene glycol)methyl methacrylate, or *N*-vinylpyrrolidone, etc.) was triggered from the initiators located at the interface, permanently modifying the surface with hydrophilic polymers.(Xiong et al., 2015, Wu et al., 2007)

Although modifying silicone surfaces via physical adsorption or blending is simple and effective, drawbacks also exist, including the weak interactions between the coating and matrix, and changes in the bulk properties that often occur.

1.2.4 Modification with cleavage or rearrangement of -Si-O- bonds

The bond strength of -SiO- is significantly greater than that of -CC- (477 to 549 vs 334 kJ mol^{-1}).(Brook, 1999) Not surprisingly, therefore, silicone-based polymers demonstrate remarkable thermal and extreme environmental resistance, particularly when compared with organic polymers. However, due to a partial ionic characteristic of the bond, the -SiO- bond is unstable to acidic/basic conditions, as manifested by dynamic cleavage or re-association of Si and O bonding – a redistribution or metathesis – as shown in Scheme 1.4.

Both acidic and basic catalysts can depolymerize silicone surfaces: the bulk of PDMS elastomers can also be efficiently degraded in the presence of a good solvent for silicones. However, controlled surface etching could only be obtained with poor solvents for PDMS. A systematic study was carried out by Brook's lab, who examined the competition between cleavage and re-association of silicon-oxygen bonds under acidic (triflic acid) or basic (tetrabutylammonium fluoride and KOH) conditions.(Brook et al., 2011)

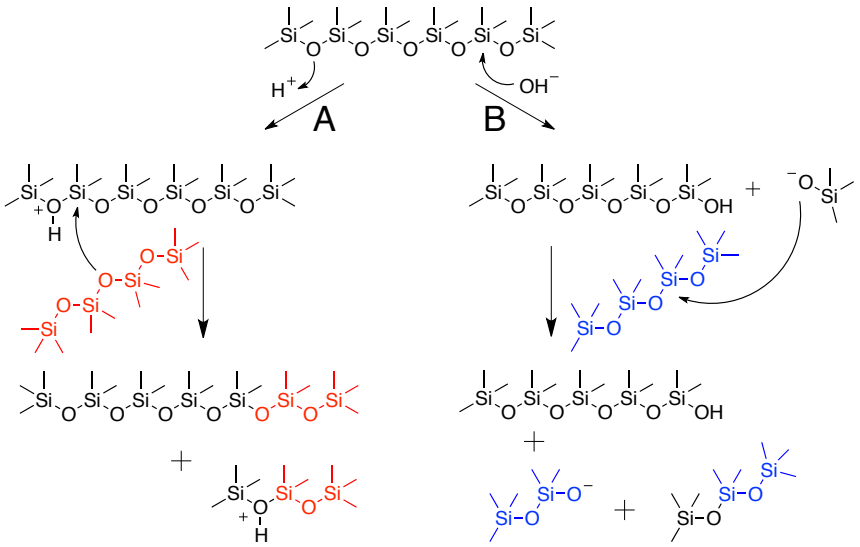

Scheme 1.4 The dynamic cleavage and re-association of -SiO- bonds under acid (A) or basic (B) conditions.

Several methods based on this unique feature of siloxanes have been developed for the modification of silicone surfaces. As shown in Scheme 1.5, silane-coupling reagents with a reactive functional group are readily able to anchor on PDMS surfaces through the

re-association of Si and O bond under either acid/base or high-energy irradiation conditions.

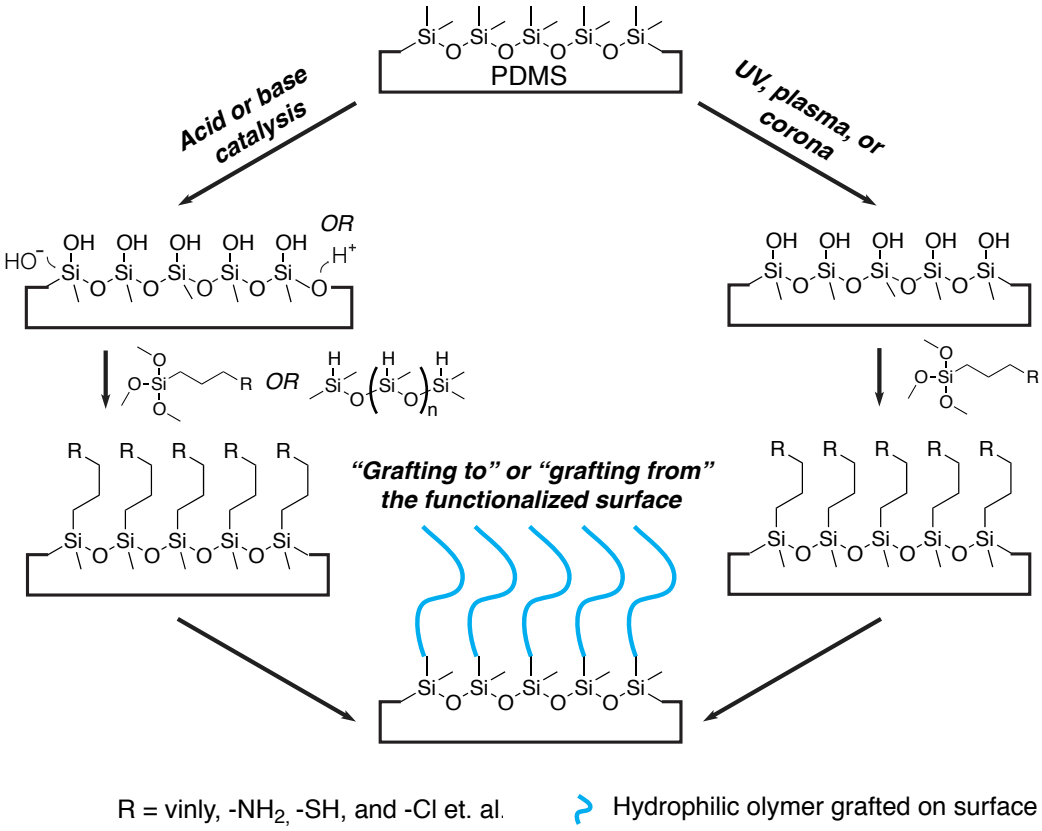

Scheme 1.5 Modification of silicone surfaces through cleavage or rearrangement of -SiO- bonds: silanization via acid or base catalysis (A), UV, plasma, or corona activation (B).

In addition to dynamic -SiO- bond redistribution at interfaces, PDMS surfaces could be functionalized by involving silane-coupling agents in these processes. For example, silane-coupling agents could be immobilized onto a silicone surface that was treated under oxidative acidic conditions (Scheme 1.5A). Mixtures of HCl/H_2O_2 or

H_2SO_4/H_2O_2 are the two most commonly used systems for silicone surface activation.(Sui et al., 2006, Xu et al., 2003, Yang et al., 2010) A similar result was obtained using a basic catalyst: NaOH was used to replace the acid/oxidant mixture for silanization of the surface using a coupling agent.(Slentz et al., 2001) However, a longer reaction period was required for basic solution treatment, increasing from ~30 minutes with acid to 24 hours with base.(Slentz et al., 2001, Yang et al., 2010) Although the PDMS surface was modified effectively using this protocol, it is difficult to keep the process under control, and avoid damaging the silicone network structure at both the interface and in the bulk due to the aggressive conditions. A basic catalyst is ideal for surface silanization because it promotes efficient monomer equilibration of siloxane chains.(Brook, 1999) But an acidic catalyst can have more practical utility as, unlike base, it can introduce functional "Si-H" groups to PDMS surfaces.(Chen et al., 2005, Brook et al., 2011) Note that the silane-coupled surface can be further modified by grafting hydrophilic polymers or bio-molecules to it covalently,(Sui et al., 2006) which is distinct from the physical interactions discussed above.(Wang et al., 2007)

The silicone surface can also be activated via treatment with coronas, plasma, or ultraviolet (UV).(Wong and Ho, 2009) Within a few minutes of treatment under high-energy irradiation, the PDMS surface was converted from hydrophobic to hydrophilic. The pendent methyl groups on silicone backbone were converted to hydroxyl groups (silanols) by oxidation (Scheme 1.5), which conveys hydrophilic characteristics to the surface;(Bodas and Khan-Malek, 2007) a silica-like layer was formed with the further

condensation of silanols.(Hillborg et al., 2000) Similar results were obtained for surfaces treated with UV light or coronas.(Hillborg and Gedde, 1998, Oláh et al., 2005) The hydrophilicity resulting from all these treatments were temporary due to the recovery of hydrophobic siloxane units at the interface (see above),(Bodas and Khan-Malek, 2007, Ginn and Steinbock, 2003) however, the incorporation of hydrophilic polymers can significantly retard the recovery during treatment. Bodas et al. initiated the polymerization of 2-hydroxyethyl methacrylate from the plasma-treated PDMS surface; the hydrophilicity was retained for about 10 days (contact angle increased from 7 to 44°).(Bodas and Khan-Malek, 2006)

Similar to the silanization achieved by acid or base treatments, silane-coupling agents could be immobilized on PDMS surface following high-energy treatments. (Xiao et al., 2002, Keefe et al., 2012, Yeh et al., 2014) The condensation between trimethoxyalkylsilanes (where the alkyl group can also be a functional group) and interfacial hydroxyl groups functionalizes the PDMS surface with various reactive groups.(Plueddemann, 1982) For example, an initiator for ATRP was immobilized to PDMS surface after UV/ozone activation; the hydrophilicity of the surface was significantly improved after radical grafting a layer of polyacrylamide to the surface.(Xiao et al., 2002) A stable long-term hydrophilic coating could be achieved by polymerizing the zwitterionic monomer carboxybetaine methacrylate from the surface. The modified surface demonstrated excellent non-fouling properties to serum, with a stable period for a month in air or more than two months in an aqueous

environment.(Keefe et al., 2012) This modification might even be simplified to a one-step process by silanizing a layer of zwitterionic silane (sulfobetaine silane), offering even more stable hydrophilic surface and repelling properties to bio-assays such as lipid, protein and bacteria.(Yeh et al., 2014)

Generally, surface modification, involving cleavage and re-association of an -Si-O- bond, results in a more stable coating due to covalent bonding, compared with physical adsorption. The PDMS surface functionalized after silanization provides a versatile stage for further modification with other hydrophilic agents. However, the vigorous reaction conditions (strong acid or base, or high-energy irradiation) may cause significant and irreversible damage (cracking or depolymerized oligomer) to the PDMS surfaces. Recently, click chemistry, especially thiol-ene reaction, has been widely used for surface modification due to it mild reaction condition and high efficiency.(Hoyle and Bowman, 2010) It is promising to involve this chemistry on PDMS surface modification, avoiding the damage described above.

1.2.5 Objective

Several methods have been developed, chemically or physically, for PDMS surface modification.(Wong and Ho, 2009) The problems associated with modification (e.g., surface cracking, hydrophobic recovery) have not been complete solved yet.(Bacharouche et al., 2013) The thiol-ene click reaction was considered to be an effective method for controllable and selective surface modification.(Kade et al., 2010, Hoyle and Bowman,

2010, Jonkheijm et al., 2008) It should be a promising tool for PDMS surface modification via grafting polymer from/to, as well as photo patterning on, PDMS surface.

Thiol-ene click chemistry is unique for being an efficient and simple reaction without yielding by-product (Scheme 1.6). This chemistry was introduced for surface modification due to its efficiency and ability of photo patterning. Generally, a thiol-functionalized surface could be modified via approaches named as "grafted to" and "grafted from" (Scheme 1.6),(Hoyle and Bowman, 2010) initiated either by thermal or photo radicals.

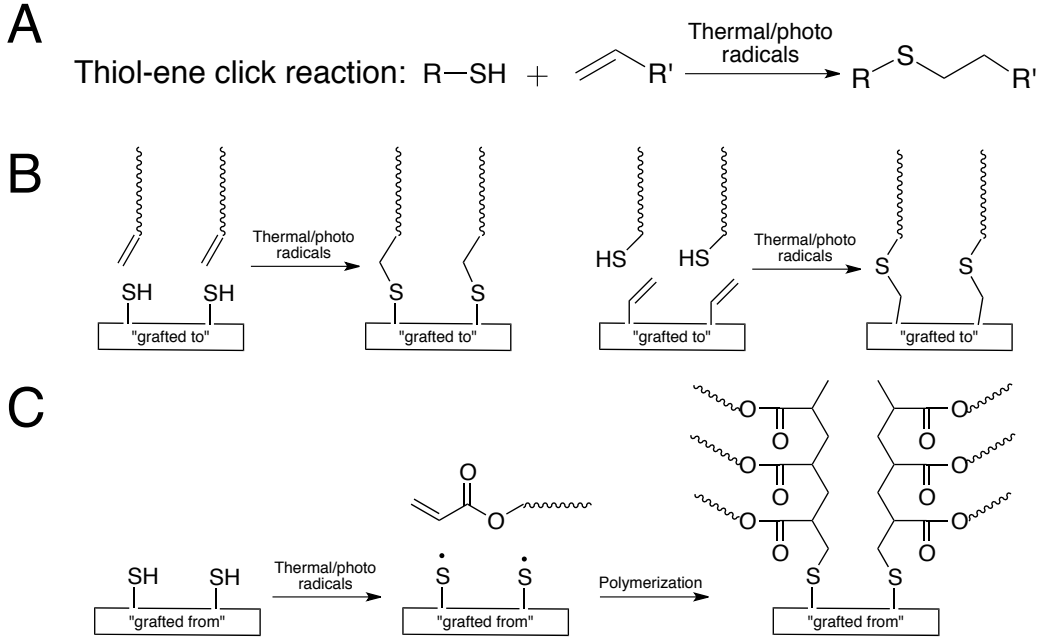

Scheme 1.6 Thiol-ene click reaction (A), and its application on surface modifications (B) "grafting to" and (C) "grafting from".

The objective of the research described in this thesis is to develop a controllable method that can functionalize PDMS surfaces with reactive thiol groups under mild conditions that will not damage the surface. In Chapter 2, base-catalyzed etching/equilibration surface treatment is used to controllably introduce thiols on PDMS surfaces. Further modification for improve hydrophilicity was performed on the thiol-functionalized PDMS surface using thiol-ene click chemistry. The hydrophobic recovery at the interface was also examined via tracking the location and migration of thiols on the surface.

The objective described above focusses on the modification at air-solid interface of siloxane-based materials. The miscibility of organosilanes with targeted polymeric matrix facilitates the modifications. However, it is also interesting to study modifications at solid-solid interface of siloxanes and hydrocarbons using organosilanes. Lignin, a natural occurred polymer, was chosen as an example for modification using hydrosilanes.

1.3 Interfacial/surface modification of lignin

1.3.1 Lignocellulosic biomass

Rising environmental challenges and global resource shortages have reinvigorated the search for (bio)renewable materials, including polymers, to partly or completely replace materials derived from petroleum resources.(Saxena et al., 2009) During the past few decades, a number of renewable polymers have been studied and introduced commercially for industrial applications(Kardas et al., 2013, Ojijo and Sinha Ray, 2013)

because of their advantages, that include: low cost, biodegradability, biocompatibility, and excellent mechanical performance (e.g., nano-crystalline cellulose, bamboo fibers),(Salas et al., 2014, Abdul Khalil et al., 2012) etc.(Thakur et al., 2014) However, there are still many challenges remaining in the transition from petroleum-based to sustainable bio-based industry.(Serrano-Ruiz et al., 2011, Xu et al., 2014)

The plant-derived polymers lignocellulose, comprising cellulose, hemicellulose, and lignin, are becoming a focus of interest for academics and industrial scientists alike.(Balat, 2011, Ruppert et al., 2012, Zakzeski et al., 2010, Pandey and Kim, 2011, Thakur et al., 2014) Cellulose is the most abundant fraction in plants, which can be either decomposed for biofuels,(Balat, 2011) extracted for to be used as reinforcement agents at the nano-scale (or micro-scale),(Moon et al., 2011) or modified for bio-medical applications.(Van Vlierberghe et al., 2011) Hemicellulose and lignin exist in plants as the glue that integrates the celluloses in cell wall.(Doherty et al., 2011) Hemicellulose, which has a similar chemical structure to cellulose, could be used for producing biofuel or other chemical intermediates.(Ruppert et al., 2012) However, lignin, comprising more than 25% in the lignocellulose, is the most underutilized fraction. Although several methods have been developed for converting lignin into value-added products, such as producing for monomeric chemicals,(Zakzeski et al., 2010, Pandey and Kim, 2011) or bio-composites,(Thakur et al., 2014) the majority of lignin is currently used as a low-value fuel. Due to its complex and highly branched polymeric network, the processing of lignin is extremely difficult.(Gosselink et al., 2004)

1.3.2 Chemical structure of lignin

Lignin is an irregular and amorphous polymer with a three-dimensional network structure and extremely high molecular weight, derived from three phenylpropanoid monomers: *p*-hydroxylphenyl propane, guaiacyl propane (G), and sinapyl propane (S), as shown in Scheme 1.7A.(Heitner et al., 2010, Thakur et al., 2014) Depending on the source (e.g., softwood, hardwood, or grass), the structure of the lignin varies with ratios of those basic building units (Table 1.1).(Heitner et al., 2010) The lignin derived from grass and softwood contains more guaiacyl units, while hardwood lignin consists of guaiacyl and sinapyl units in approximately equal proportions. Due to the high reactivity of the 5-position, G units are more highly condensed than S units during polymerization.(Santos et al., 2012, Zakzeski et al., 2010) Therefore, softwood lignin has a highly branched and crosslinked structure; by contrast, the structure of hardwood lignin is more linear (Scheme 1.7C).(Evtuguin et al., 1998, Zakzeski et al., 2010) The phenylpropanoid units in lignin are connected mainly by β-O-4 linkages (~50% or more),(Chakar and Ragauskas, 2004) together with other linkages like 5-5, β-5, 4-O-5, and 5-5, etc. (Table 1.2, Scheme 1.7B).(Zakzeski et al., 2010, Heitner et al., 2010) As noted above, these chemical structures are resistant to efficient degradation using commercially viable processes. Thus, value-added products derived from lignin are extremely limited.(Thakur et al., 2014) Also, the method used for lignin production significantly impacts on the depolymerization efficiency and structure of fragmented product.(Bruijnincx and Weckhuysen, 2014)

Table 1.1 Approximate abundance of building blocks in lignin from different sources.(Heitner et al., 2010)

	Guaiacyl propane	Sinapyl propane	p-Hydroxylphenyl propane
Grass lignin	70%	25%	5%
Softwood lignin	95%	1%	4%
Hardwood lignin	~50%	~50%	~2%

Table 1.2 Approximate abundance (%) of different chemical linkages in hardwood and softwood lignin.(Zakzeski et al., 2010)

	β-O-4	5-5	β-5	4-O-5	β-1	β-β
Hardwood	55-50	19-27	9-12	4-7	7-9	2-6
Softwood	60-62	3-9	3-11	9	1-7	3-12

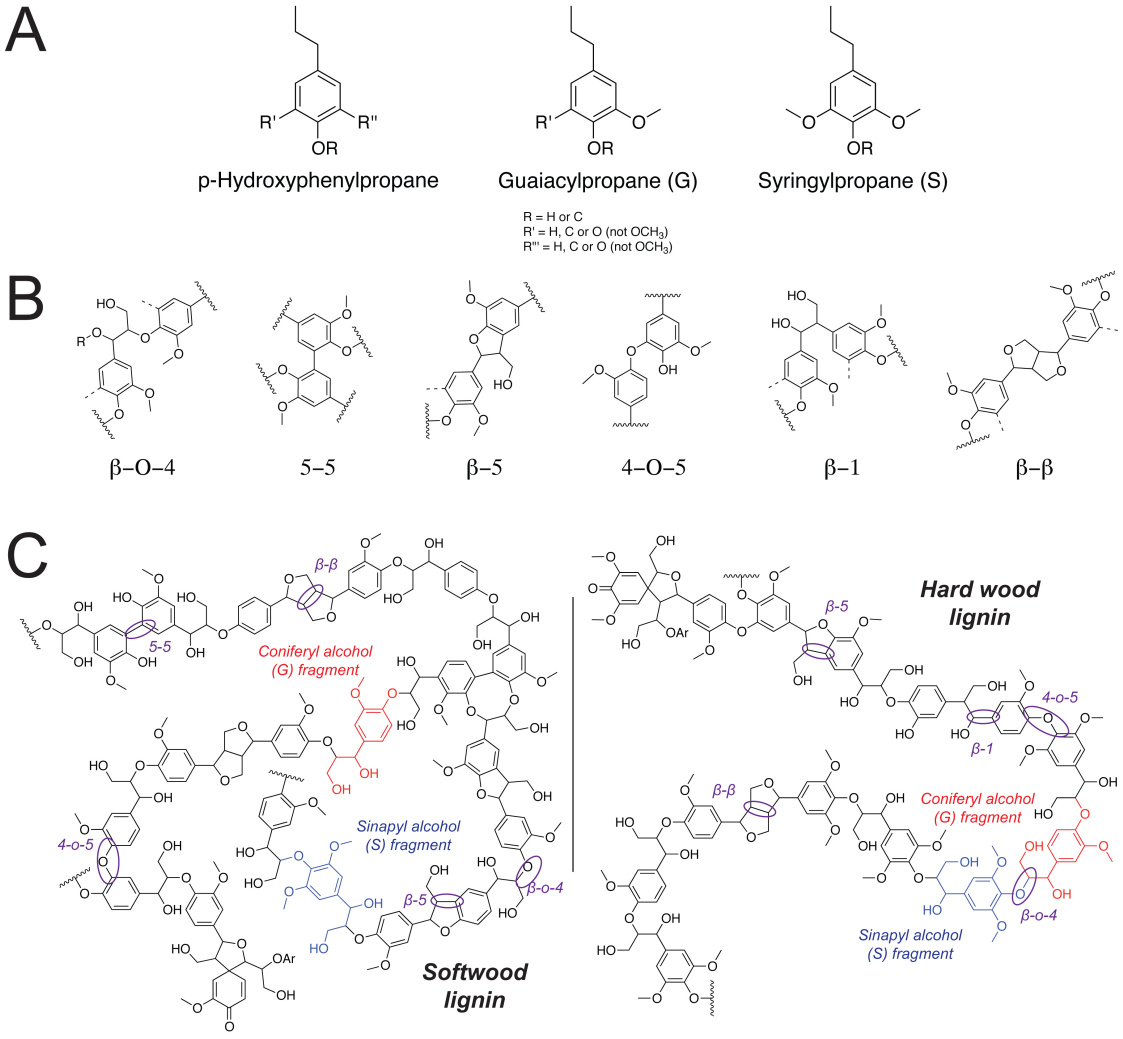

Scheme 1.7 A) The three basic building units for lignin: p-hydroxylphenyl-, coniferyl-, and sinapylpropane.(Heitner et al., 2010) B) The typical linkages of lignin.(Zakzeski et al., 2010) C). The typical structures of hardwood lignin and softwood lignin, respectively.(Evtuguin et al., 1998)

1.3.3 Depolymerization/degradation of lignin: toward the bio-refinery chemicals

In the natural environment, lignin is biodegraded using enzymatic and microbial processes and recycled as a carbon resource over long time periods.(Perez et al., 2002) While lignin can also be cracked chemically into phenolic monomers, harsh conditions are generally required.(Xu et al., 2014, Zakzeski et al., 2010) Many studies have focused on the depolymerization of model compounds. However, the results with model systems frequently do not translate to the polymer itself.(Zakzeski et al., 2010) Due to the complexity of lignin's chemical structure, success with model compound degradation/reduction does not guarantee an effective depolymerization process for actual lignin.(Bruijnincx and Weckhuysen, 2014, Zakzeski et al., 2010) Nevertheless, the model studies provide the insight into the reaction and better understanding for the mechanisms.

The depolymerization of lignin has been comprehensively reviewed in a number of recent published literatures;(Laurichesse and Avérous, 2014, Zakzeski et al., 2010, Xu et al., 2014, Azadi et al., 2013) however, in the scope of this thesis, the author will only briefly review the progress in the catalytic degradation of lignin.

Generally, lignin is chemically depolymerized via pyrolysis, oxidation or deoxygenation, as shown in Scheme 1.8.(Xu et al., 2014, Laurichesse and Avérous, 2014) For example, the pyrolysis of lignin produces hydrocarbons and aromatics at temperatures up to 900 °C.(Yang et al., 2007, Shen et al., 2010) However, the most interesting methods for lignin depolymerization are catalytic oxidation and deoxygenation due to the relative mild conditions and selectivity of cleavage of lignin bonds.(Zakzeski et al., 2010)

Successful depolymerization with high yields have been obtained in a few cases: Yan et al. achieved 42% conversion of lignin by using platinum as a catalyst,(Yan et al., 2008) even higher conversions were reported by using Ni-Mo or Cu-CrO (49-71%, and 70% of lignin, respectively).(Harris et al., 1938, Oasmaa et al., 1993) Nonetheless, challenges still remain for these strategies, including the efficiency, the cost of catalyst (especially for noble metals and considering the difficulties of catalyst recovery), the critical reaction conditions (mild conditions: low temperature, ambient/low pressure are desired), and more importantly, the controllability of the depolymerization, and the ability to purify the resulting products.(Zakzeski et al., 2010, Xu et al., 2014) We describe in more detail some selected examples.

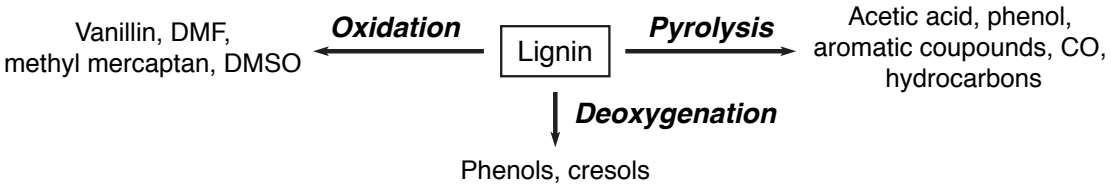

Scheme 1.8 The main methods for lignin depolymerization.

There are two major linkages in lignin polymers: C-O-C (e.g., Ar-O-C) and C-C-C. The β-O-4 linkage is the predominant ether linkage in lignin; but the presence of other linkages including 4-O-5, 5-5, β-5, and 5-5, although minor in concentration, explain why there are significant subtle differences in the fragmentation processes between different lignin types. Recently, several different catalysts have been developed to selectively

cleave the C-O-C bonds under mild conditions.(Feghali and Cantat, 2014, He et al., 2014, Tobisu et al., 2011)

Ni-based catalysts are the most developed for the cleavage of β-O-4 and 4-O-5 linkages. In the presence of hydrogen, the Ni-based catalyst can selectively cleave the C-O bond, as shown in Scheme 1.9A. Lignin model compounds were reduced from dimers into monomers, catalyzed by a soluble nickel carbene complex under mild conditions (1 bar hydrogen, 80 to 120 °C).(Sergeev and Hartwig, 2011) Later, a heterogeneous catalyst based on the nickel soluble catalyst was developed for the same reduction reaction . Such a heterogeneous catalyst requires no dative ligands and demonstrates high chemoselectivity, however, a high catalyst loading (typically 20 mol% of Ni) was essential for reduction.(Sergeev et al., 2012) Recently, it was found that loading the Ni catalyst on porous SiC composites can significantly improve the reaction efficiency.(Zaheer et al., 2014) The reduction reactions discussed above all involved high-pressure hydrogen gas as the hydride donor.(Zaheer et al., 2014, Sergeev et al., 2012) Hydrosilanes and aluminohydrides were used as alternative sources of hydrogen to avoid the concerns on pressure, and also for specific regioselectivity over the reduction of arenes.(Tobisu et al., 2011, Sergeev and Hartwig, 2011) Selective depolymerization by nickel catalysts was also tested on actual lignin samples. Birch wood-derived lignin was selectively degraded into propylguaiacol and propylsyringol with ~50% conversion.(Song et al., 2013) Reduction leads primarily to cleavage of aryl ether, but can also reduce arene groups to cyclohexanes (Scheme 1.9B). The heterogeneous nickel catalyst loses

selectivity in the absence of *t*-BuONa, resulting in significant amounts (more than 50%) of cyclohexanol, which is derived from phenols.(Sergeev et al., 2012) This non-selective reduction can be facilitated using Ni/SiO_2 in the aqueous phase.(He et al., 2012) A product mixture including phenol, cyclohexanol, cyclohexane, and reduced dimers were obtained under mild conditions (120 °C, and 6 bar hydrogen for a short periods - 50 minutes).(He et al., 2014, He et al., 2012) The reactivity of the Ni-based catalyst can be further improved via integration with noble metals to give a bimetallic catalyst (although the noble metal catalyst can facilitate the reduction of benzene rings).(Zhang et al., 2014a, Zhang et al., 2014b) Although both the Ni-based catalysts (with selectivity and non-selectivity) were effective for model compounds, poor conversion (14% in aqueous atmosphere, maximum 54% in alcoholic solution)(Zhang et al., 2014a, Song et al., 2013) was obtained when applying these catalysts to actual lignin depolymerization.

Although Ni-based catalysts have been well studied for both model compounds and lignin depolymerization, there are few drawbacks with these processes including unsatisfactory degrees of conversion, difficulty in catalyst recovery, rapid loss of reactivity, and the high cost of noble metals. Recently, several different methods including using low cost metallic systems or solid acid catalysts were explored for lignin depolymerization.(Ren et al., 2013, Deepa and Dhepe, 2014) Compared with nickel or noble metals, iron is considered to be an inexpensive reagent that has an interesting reactivity. Aryl C-O bonds (excluding phenol and aryl methyl ethers) were selectively cleaved in the presence of iron (III) acetylacetonates, ^{t}BuONa, and a hydrogen donor

($LiAlH_4$ or H_2). However, this catalyst is sensitive to moisture, which is unlikely to be very practical in depolymerizing actual lignin.(Ren et al., 2013) By contrast, a solid acid (SiO_2-Al_2O_3) was proved to be effective for actual lignin depolymerization with up to 60% of lignin degraded into monomers at 250 °C.(Deepa and Dhepe, 2014) Due to the high bond dissociation enthalpies of aryl ether linkages (218-314 kJ/mol),(He et al., 2014) the reductive cleavage of the ether bonds generally requires aggressive conditions (elevated temperature and pressure, and long treatment periods). It would be ideal and beneficial for industrial applications if the depolymerization could be performed at room temperature under atmosphere pressure. Nguyen et al. developed a two-step strategy for photochemical degradation of lignin, which involving a first step using (4-AcNH-TEMPO)$^+$ $^-BF_4$ for benzylic oxidation, and a secondary step using visible-light to cleave aryl ether bonds (C-O) catalyzed by $[Ir(ppy)_2(dtbbpy)]^+$ $^-PF_6$ (Scheme 1.10A).(Nguyen et al., 2013) However, impeded by the dark color of lignin (as it is a highly conjugated polymeric network), photochemical depolymerization was not efficient unless the entire solution was circulated in a flow reactor.(Nguyen et al., 2013) Alternatively, the aryl ether bonds could also be cleaved by electrolysis.(Wu and Huang, 2014) Wu et al. reduced the β-O-4 and 4-O-5 linkages in lignin model compounds in an undivided cell using sodium borohydride as the hydride donor (Scheme 1.10B). Although, overreduction of the aromatic rings was observed, this method for lignin depolymerization is encouraging given the relatively mild conditions used (room temperature, open air, 30 mA current).

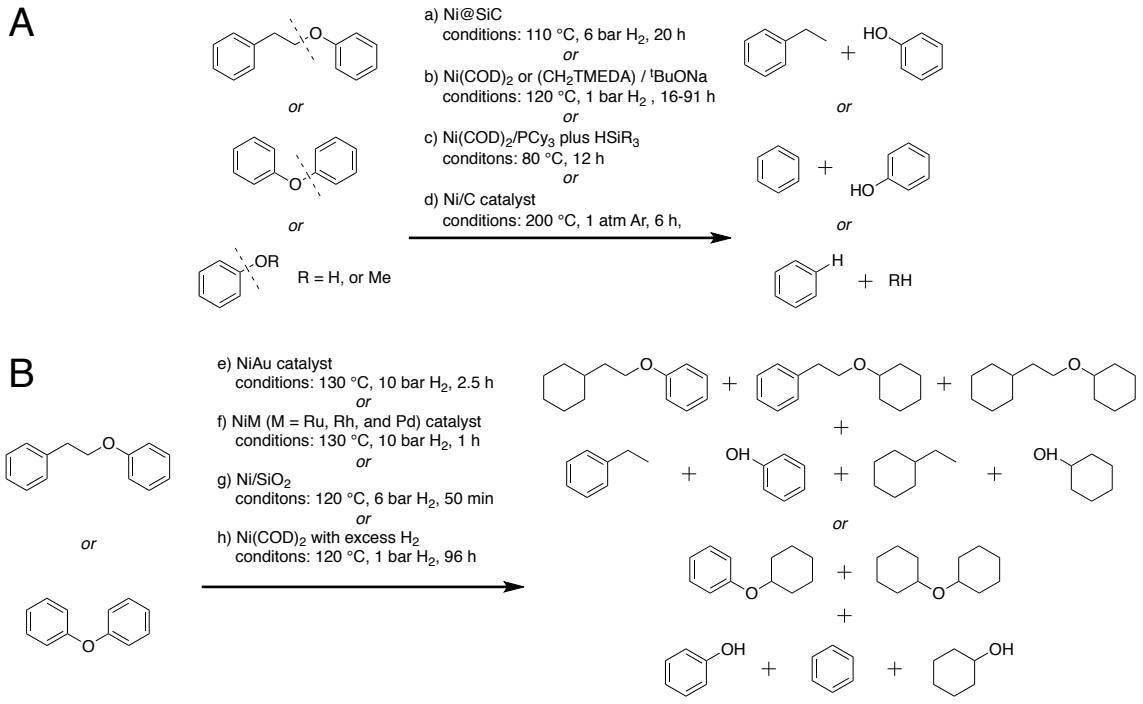

Scheme 1.9 The reduction β-O-4 and 4-O-5 using Ni based catalyst; (A) selective reduction: a) Ni@SiC,(Zaheer et al., 2014) b) $Ni(COD)_2$ or (CH_2TMEDA),(Sergeev et al., 2012, Sergeev and Hartwig, 2011) c) $Ni(COD)_2/PCy_3$,(Tobisu et al., 2011) and Ni/C;(Song et al., 2013) and (B) non-selective reduction: e) NiAu,(Zhang et al., 2014a) f) NiM (M = Ru, Rh, and Pd),(Zhang et al., 2014b) g)Ni/SiO_2,(He et al., 2014, He et al., 2012) and $Ni(COD)_2$.(Sergeev et al., 2012)

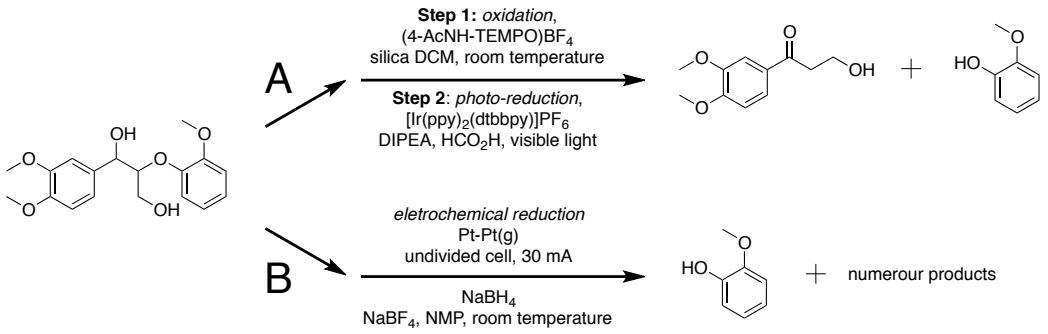

Scheme 1.10 The cleavage of aryl ether bonds using (A) photo-,(Nguyen et al., 2013) or (B) electro- chemical reduction.(Wu and Huang, 2014)

Research on lignin degradation has experienced explosive growth during the last few years.(Xu et al., 2014) Other than the strategies that have been reviewed above, various novel strategies, involving microwaves, ionic liquids, and supercritical fluids, etc., have emerged for the depolymerization of lignin.(Wang et al., 2013, Li et al., 2015) High degradation efficiency (fast depolymerization rate and complete conversion), mild conditions (low temperature and pressure), and low cost are always desirable for designing new routes to decompose lignin.

1.3.4 Interfacial modification of lignin: toward the bio-composite materials

Although the depolymerization of lignin can produce a variety of monomeric aromatic compounds, the extremely high cost and low efficiency of the processes used suggests that the 'biorefinery' with lignin as a feedstock is less practical for industrial production at the current time.(Xu et al., 2014) However, the lignin should be more readily used for practical applications as a component in composite materials. Such a

polymer based composite based on natural materials offers several advantages including biodegradability, antioxidant propertiese, relatively low cost.(Thakur et al., 2014)

Due to the complexity of its chemical structure, lignin demonstrates poor solubility in various solvents,(Laurichesse and Avérous, 2014) which made it difficult in incorporation with other materials. However, as a highly branched and high molecular weight aromatic network with an abundance of phenol and aryl ether functional groups, lignin surfaces should be able to effectively graft onto/incorporated with other polymers, showing improved miscibility at interface of lignin and polymer matrix. As shown in Scheme 1.11, lignin can be integrated into various resins to create bio-composites via etherification, esterification, urethanization, and/or phenolation.(Laurichesse and Avérous, 2014, Thakur et al., 2014) The reactions at the interface/surface play very important roles in the reinforcement of resins by lignin.(Thielemans et al., 2002, Thakur et al., 2014) The achievements on the preparation of lignin-based bio-composites have been comprehensively reviewed in the literature.(Laurichesse and Avérous, 2014, Thakur et al., 2014) I summarize here the key aspects of recent progress on the interfacial modification of lignin to permit bio-composite formation.

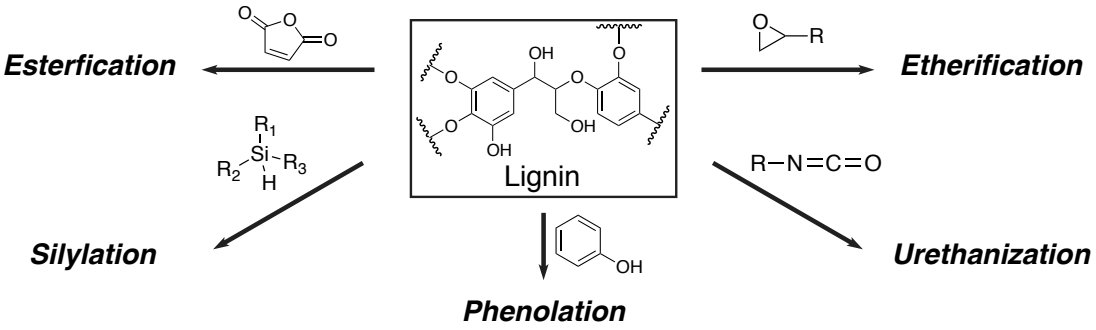

Scheme 1.11 The effective reactions for lignin grafting/modification, integrating lignin into other polymeric matrixes.

The availability of phenol functional groups in lignin allows its application, via etherification, in epoxy resins as a substitute for bisphenol-A. Lignin was formulated with the epoxide-terminated polymer poly(ethylene glycol) diglycidyl ether to create bio-based epoxy resins via a two-step procedure. The phenolic hydroxyl groups were first converted to phenolate and then etherified with epoxides. Although the phenol groups were not completely consumed even over a long curing periods, excess epoxide to lignin would cause stiff samples, which were failed for mechanical tests.(Delmas et al., 2013) Other than pre-treatment for phenolate, the etherification of the phenols can be achieved efficiently through reacting with dichlorohydrin PEG ($ClCH_2CH(OH)CH_2O(CH_2CH_2O)_nCH_2CH_2OCH_2CH(OH)CH_2Cl$).(Lin et al., 2014) The resultant copolymer, with lignin as the backbone and PEG as a branches, was shown to exhibit improved hydrophilic properties and better dispersibility than lignosulfonate or PEG.(Lin et al., 2014) The multi-functionality of the phenolic groups in lignin facilitated

its application in thermoset plastics; however, selective masking of the phenol is required to prepare lignin-based thermoplastics. Through methylation and oxypropylation, the phenolic groups could be capped to a controllable degree of derivatization,(Sadeghifar et al., 2012) thereby avoiding the crosslinking or hyperbranching of polymers that could occur in the case of growing/grafting from/to lignin.(Argyropoulos et al., 2013) Benefitting from this method, Argyropoulos et al. have prepared poly(arylene ether sulfone)/kraft lignin copolymers with uniform molecular structures that exhibited controllable mechanical and thermal properties.(Argyropoulos et al., 2013) The increasing ability to control lignin etherification demonstrates there will be a bright future in the use of lignin to replace other phenolic materials in polymer composites.

Compared with etherification, esterification of lignin is probably a more robust method considering the reagents' reactivity.(Laurichesse and Avérous, 2014) The hydroxyl groups in lignin can be esterified with acids, anhydrides, or acyl chlorides under mild conditions. The latter two reagents are more popular due to their higher reactivity. The surface of lignin can be easily functionalized with carboxylic acids or other functional groups like vinyl groups, or even polymer chains. Qin et al. esterified partially depolymerized softwood lignin with succinic anhydride and used it as a curing agent for epoxies.(Qin et al., 2013) The lignin was added in quantities up to 32.3% in the composite, which still had comparable properties to the epoxy resin prepared using commercial anhydride curing agent.(Qin et al., 2013, Liu et al., 2014)

Rather than use as a curing agent, lignin can be used as a building block for copolymerization. A lignin-based "bio-oil mimic" was obtained by esterifying lignin with methacrylic anhydride; these methacrylic-functionalized compounds can either self-polymerize or be copolymerized with styrene.(Stanzione et al., 2013) Interestingly, the polymerization can also be initiated from the surface of lignin. For example, the hydroxy group in lignin can initiate ring-opening polymerization of lactide.(Chung et al., 2013) A reversible addition-fragmentation chain-transfer polymerization can be also initiated from a lignin surface. Gupat et al. first grafted xanthates to lignin by esterifying the hydroxyl groups with acyl chloride; the xanthate-lignin was the used as an initiator to polymerize amphiphilic block polymers (e.g., lignin-PAA and PAm).(Gupta and Washburn, 2014) A lignin-based thermoplastic can be prepared from the esterification with synthetic polymers. Satio et al. synthesized a triblock polymer (lignin-polybutadiene-lignin) with the integration of both soft and hard polymer segments. The branched structures and toughness of lignin enhances the mechanical performance of lignin-based elastomers from liquid polybutadiene, showing a storage modulus of 8.2×10^7 Pa at -30 °C.(Saito et al., 2012) The esterification of hydroxyl groups in lignin not only alters the chemical reactivity of lignin, but also improves the interfacial miscibility with other polymer.

Similar to esterification, incorporating lignin in urethanes is another powerful method for lignin modification. This reaction has been well studied and explored for lignin-based polyurethane fabrications. The abundance of hydroxyl groups and the branched molecular structure allows the use of lignin either as building units for the

condensation polymerization, or as a cross-linker for polymeric networks.(Laurichesse and Avérous, 2014) Lignin can be used individually or in combination with diol (or polyol) monomers.(Xue et al., 2014, Yang et al., 2014) For example, a lignin-based polyurethane foam was prepared containing up to 37% of lignin.(Xue et al., 2014) With increasing lignin content, Yang et al. obtained a lignin-based xerogel with unique self-cleaning properties and super hydrophobicity, which was the result of micro- or nanoscale hierarchical porous structures.(Yang et al., 2014)

Lignin also can be used as crosslinker, which is similar to the application described above of succinic anhydride-modified lignin in epoxy resins but in this case no pre-modification is required. As an example, polybutadiene rubber was obtained by crosslinking isocyanate-functionalized polybutadiene with lignin.(Sarkar and Adhikari, 2001) However, the upper limit of lignin in the formulation was 3% for obtaining improved mechanical performance due to the presence of too many hydroxyl groups at higher concentrations. The selective masking of hydroxyl groups might help to increase lignin content in this composite.(Sarkar and Adhikari, 2001)

Phenolic resins are one of the earliest class of commercial synthetic resins, and are useful in many fields.(Board, 2002) Lignin, consisting of phenolic units, may be used directly as reactive fillers for phenol resin.(Effendi et al., 2008) Different to the two modifications reviewed above, phenolation is exceptional for different reactive functional spots (C-5 position of guaiacyl unit, as shown in Scheme 1.12A, rather than the hydroxyl groups). The lignin was employed as a substitute for phenol in the adhesives; the glue was

able to provide satisfactory performance with up to 50% of the phenolic resin replaced by lignin.(Klašnja and Kopitović, 1992) In addition to adding lignin directly, a phenolation on lignin was carried on to improve the reactivity of lignin during thermoset processing, and to improve the interfacial interaction between lignin and the polymer matrix (Scheme 1.12B). The phenolation was achieved by heating (to 70 °C) lignin and phenol in the presence of alcohols.(Effendi et al., 2008, Çetin and Özmen, 2002) The resultant resin had comparable performance to standard phenolic resin with up to 30% of phenol replaced by phenolated lignin.(Çetin and Özmen, 2002) However, such two-step processing requires extract effort and energy for the pre-modification step. More recently, the Du et al. developed a new method to prepare phenolic resins without phenolation. The C-5 position of the guaiacyl units could also be bonded directly to formaldehyde and participate subsequently in a Mannich reaction (Scheme 1.12C).(Du et al., 2014)

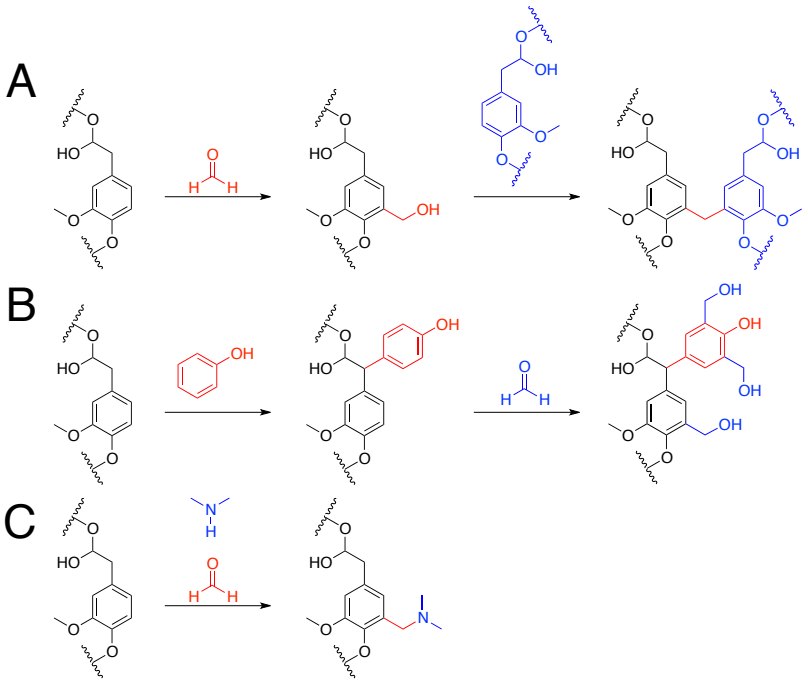

Scheme 1.12 Using the lignin as the phenol substitution in phenol resin (A) directly without pre-modification, (B) after phenolation, (C) via Mannich reaction.

1.3.5 Objectives of the controlled depolymerization and modification of lignin using organosilanes

Despite the fact that lignin is the second most abundant nature polymer in nature, its utilization is still on the very early stage without industrial scale production (except as a fuel). The prospect of a lignin-based industry, however, is promising provided that the efficiency of both its degradation and surface modification can be improved.

Neither the silylation of lignin nor organosilane-induced lignin depolymerization is well developed, especially the research using actual lignin samples rather than model

compounds.(Fedorov et al., 2013, Feghali and Cantat, 2014) Only a few papers could be found on lignin depolymerization involving hydrosilanes. Fedorov et al. found that triethylsilane (Et_3SiH) can selectively reduce the aryl ether (4-O-5), catalyzed by *t*-BuOK at 165 °C (for 20 h).(Fedorov et al., 2013) Later, Feghali et al. reported a method for aryl ether cleavage (β-O-4) using also triethylsilane, with catalysis by BCF (tris(pentafluorophenyl)borane).(Feghali and Cantat, 2014) The later method is more attractive due to the selectivity for the alkane aryl ether bond, and mild conditions used.

One of the research objectives was to develop strategies for $B(C_6F_5)_3$-catalyzed and hydrosilane-induced lignin depolymerization. In Chapter 3 the reduction of lignin model compounds containing β-O-4, α-O-4, hydroxyl, phenol, methyl phenolic ether, and 4-O-5 is described. Further research was undertaken to push this chemistry to decompose actual samples of softwood and hardwood lignin. The reactivity of hydrosilanes with different chemical structures was also examined.

Another objective of the research was to integrate lignin into polydimethylsiloxane matrices to give lignin-based silicone elastomers or foams. Importantly, the preparation of composites requires no pre-modification on lignin. Chapter 4 describes a method to prepare lignin-based elastomers using softwood lignin and hydride-functionalized silicones. The lignin plays dual roles as both crosslinker and reinforcing reagents in the composite. The properties of the elastomer are tunable via varying the lignin content and chemical structure of silicones used in formulation. The resistances to solvent and thermal aging of the lignin-silicone were also studied.

Visually, a foam is a material containing dispersed voids. They have been widely used in many fields for their low density, excellent thermal and electric insulation, etc. Silicone foams, featuring a unique chemical and physical stability, are ideal for applications like energy storage, hot gas filters, and thermal/electrical insulation/protection, etc.(Chruściel and Leśniak, 2011). In Chapter 5, the preparation of lignin-based silicone foams using extrusion and compression molding is described. In this thesis, we were particularly looking for closed cell foams with homogenous dispersed pore at macrocellular or microcellular scale. The impacts of formulations and processing conditions on foam structure and morphology were studied.

1.4 References

ABDUL KHALIL, H. P. S., BHAT, I. U. H., JAWAID, M., ZAIDON, A., HERMAWAN, D. & HADI, Y. S. 2012. Bamboo fibre reinforced biocomposites: A review. *Materials & Design,* 42**,** 353-368.

ARGYROPOULOS, D. S., SADEGHIFAR, H., CUI, C. & SEN, S. 2013. Synthesis and Characterization of Poly(arylene ether sulfone) Kraft Lignin Heat Stable Copolymers. *ACS Sustainable Chemistry & Engineering,* 2**,** 264-271.

AZADI, P., INDERWILDI, O. R., FARNOOD, R. & KING, D. A. 2013. Liquid fuels, hydrogen and chemicals from lignin: A critical review. *Renewable and Sustainable Energy Reviews,* 21**,** 506-523.

BACHAROUCHE, J., HAIDARA, H., KUNEMANN, P., VALLAT, M.-F. & ROUCOULES, V. 2013. Singularities in hydrophobic recovery of plasma treated polydimethylsiloxane surfaces under non-contaminant atmosphere. *Sensors and Actuators A: Physical,* 197**,** 25-29.

BALAT, M. 2011. Production of bioethanol from lignocellulosic materials via the biochemical pathway: A review. *Energy Conversion and Management,* 52**,** 858-875.

BOARD, N. 2002. *Modern Technology of Synthetic Resins & Their Applications*, Laurier Books, Limited.

BODAS, D. & KHAN-MALEK, C. 2006. Formation of more stable hydrophilic surfaces of PDMS by plasma and chemical treatments. *Microelectronic Engineering,* 83**,** 1277-1279.

BODAS, D. & KHAN-MALEK, C. 2007. Hydrophilization and hydrophobic recovery of PDMS by oxygen plasma and chemical treatment—An SEM investigation. *Sensors and Actuators B: Chemical,* 123**,** 368-373.

BROOK, M. A. 1999. *Silicon in Organic, Organometallic, and Polymer Chemistry*, Wiley.

BROOK, M. A., ZHAO, S., LIU, L. & CHEN, Y. 2011. Surface etching of silicone elastomers by depolymerization. *Canadian Journal of Chemistry,* 90**,** 153-160.

BRUIJNINCX, P. C. A. & WECKHUYSEN, B. M. 2014. Biomass conversion: Lignin up for break-down. *Nat Chem,* 6**,** 1035-1036.

ÇETIN, N. S. & ÖZMEN, N. 2002. Use of organosolv lignin in phenol–formaldehyde resins for particleboard production: I. Organosolv lignin modified resins. *International Journal of Adhesion and Adhesives,* 22**,** 477-480.

CHAKAR, F. S. & RAGAUSKAS, A. J. 2004. Review of current and future softwood kraft lignin process chemistry. *Industrial Crops and Products,* 20**,** 131-141.

CHEN, H., BROOK, M. A. & SHEARDOWN, H. 2004. Silicone elastomers for reduced protein adsorption. *Biomaterials,* 25**,** 2273-2282.

CHEN, H., ZHANG, Z., CHEN, Y., BROOK, M. A. & SHEARDOWN, H. 2005. Protein repellant silicone surfaces by covalent immobilization of poly(ethylene oxide). *Biomaterials,* 26**,** 2391-2399.

CHUNG, Y.-L., OLSSON, J. V., LI, R. J., FRANK, C. W., WAYMOUTH, R. M., BILLINGTON, S. L. & SATTELY, E. S. 2013. A Renewable Lignin–Lactide Copolymer and Application in Biobased Composites. *ACS Sustainable Chemistry & Engineering,* 1**,** 1231-1238.

DEEPA, A. K. & DHEPE, P. L. 2014. Lignin Depolymerization into Aromatic Monomers over Solid Acid Catalysts. *ACS Catalysis,* 5**,** 365-379.

DELMAS, G.-H., BENJELLOUN-MLAYAH, B., BIGOT, Y. L. & DELMAS, M. 2013. Biolignin™ based epoxy resins. *Journal of Applied Polymer Science,* 127**,** 1863-1872.

DOHERTY, W. O. S., MOUSAVIOUN, P. & FELLOWS, C. M. 2011. Value-adding to cellulosic ethanol: Lignin polymers. *Industrial Crops and Products,* 33**,** 259-276.

DU, X., LI, J. & LINDSTRÖM, M. E. 2014. Modification of industrial softwood kraft lignin using Mannich reaction with and without phenolation pretreatment. *Industrial Crops and Products,* 52**,** 729-735.

EBARA, M., HOFFMAN, J. M., STAYTON, P. S. & HOFFMAN, A. S. 2007. Surface modification of microfluidic channels by UV-mediated graft polymerization of non-fouling and 'smart' polymers. *Radiation Physics and Chemistry,* 76**,** 1409-1413.

EFFENDI, A., GERHAUSER, H. & BRIDGWATER, A. V. 2008. Production of renewable phenolic resins by thermochemical conversion of biomass: A review. *Renewable and Sustainable Energy Reviews,* 12**,** 2092-2116.

EVTUGUIN, D. V., PASCOAL NETO, C., ROCHA, J. & PEDROSA DE JESUS, J. D. 1998. Oxidative delignification in the presence of molybdovanadophosphate

heteropolyanions: mechanism and kinetic studies. *Applied Catalysis A: General,* 167**,** 123-139.

FEDOROV, A., TOUTOV, A. A., SWISHER, N. A. & GRUBBS, R. H. 2013. Lewis-base silane activation: from reductive cleavage of aryl ethers to selective ortho-silylation. *Chemical Science,* 4**,** 1640-1645.

FEGHALI, E. & CANTAT, T. 2014. Unprecedented organocatalytic reduction of lignin model compounds to phenols and primary alcohols using hydrosilanes. *Chemical Communications,* 50**,** 862-865.

GARCÍA, C. D., DRESSEN, B. M., HENDERSON, A. & HENRY, C. S. 2005. Comparison of surfactants for dynamic surface modification of poly(dimethylsiloxane) microchips. *ELECTROPHORESIS,* 26**,** 703-709.

GINN, B. T. & STEINBOCK, O. 2003. Polymer Surface Modification Using Microwave-Oven-Generated Plasma. *Langmuir,* 19**,** 8117-8118.

GOSSELINK, R. J. A., DE JONG, E., GURAN, B. & ABACHERLI, A. 2004. Co-ordination network for lignin - standardisation, production and applications adapted to market requirements (EUROLIGNIN). *Industrial Crops and Products,* 20**,** 121-129.

GUPTA, C. & WASHBURN, N. R. 2014. Polymer-Grafted Lignin Surfactants Prepared via Reversible Addition–Fragmentation Chain-Transfer Polymerization. *Langmuir,* 30**,** 9303-9312.

HARRIS, E. E., D'IANNI, J. & ADKINS, H. 1938. Reaction of Hardwood Lignin with Hydrogen. *Journal of the American Chemical Society,* 60**,** 1467-1470.

HE, J., ZHAO, C. & LERCHER, J. A. 2012. Ni-Catalyzed Cleavage of Aryl Ethers in the Aqueous Phase. *Journal of the American Chemical Society,* 134**,** 20768-20775.

HE, J., ZHAO, C., MEI, D. & LERCHER, J. A. 2014. Mechanisms of selective cleavage of C–O bonds in di-aryl ethers in aqueous phase. *Journal of Catalysis,* 309**,** 280-290.

HEITNER, C., DIMMEL, D. & SCHMIDT, J. A. 2010. *Lignin and Lignans: Advances in Chemistry*, Taylor & Francis.

HILLBORG, H., ANKNER, J. F., GEDDE, U. W., SMITH, G. D., YASUDA, H. K. & WIKSTRÖM, K. 2000. Crosslinked polydimethylsiloxane exposed to oxygen plasma studied by neutron reflectometry and other surface specific techniques. *Polymer,* 41**,** 6851-6863.

HILLBORG, H. & GEDDE, U. W. 1998. Hydrophobicity recovery of polydimethylsiloxane after exposure to corona discharges. *Polymer,* 39**,** 1991-1998.

HOYLE, C. E. & BOWMAN, C. N. 2010. Thiol–Ene Click Chemistry. *Angewandte Chemie International Edition,* 49**,** 1540-1573.

HU, S., REN, X., BACHMAN, M., SIMS, C. E., LI, G. P. & ALLBRITTON, N. L. 2004a. Surface-Directed, Graft Polymerization within Microfluidic Channels. *Analytical Chemistry,* 76**,** 1865-1870.

HU, S., REN, X., BACHMAN, M., SIMS, C. E., LI, G. P. & ALLBRITTON, N. L. 2004b. Tailoring the Surface Properties of Poly(dimethylsiloxane) Microfluidic Devices. *Langmuir,* 20**,** 5569-5574.

HWANG, D. K., MOON, J. H., SHUL, Y. G., JUNG, K. T., KIM, D. H. & LEE, D. W. 2003. Scratch Resistant and Transparent UV-Protective Coating on Polycarbonate. *Journal of Sol-Gel Science and Technology,* 26**,** 783-787.

IKADA, Y. 1994. Surface modification of polymers for medical applications. *Biomaterials,* 15**,** 725-736.

JONKHEIJM, P., WEINRICH, D., KÖHN, M., ENGELKAMP, H., CHRISTIANEN, P. C. M., KUHLMANN, J., MAAN, J. C., NÜSSE, D., SCHROEDER, H., WACKER, R., BREINBAUER, R., NIEMEYER, C. M. & WALDMANN, H. 2008. Photochemical Surface Patterning by the Thiol-Ene Reaction. *Angewandte Chemie,* 120**,** 4493-4496.

KADE, M. J., BURKE, D. J. & HAWKER, C. J. 2010. The power of thiol-ene chemistry. *Journal of Polymer Science Part A: Polymer Chemistry,* 48**,** 743-750.

KARDAS, I., STRUSZCZYK, M., KUCHARSKA, M., VAN DEN BROEK, L. M., VAN DAM, J. G. & CIECHAŃSKA, D. 2013. Chitin and Chitosan as Functional Biopolymers for Industrial Applications. *In:* NAVARD, P. (ed.) *The European Polysaccharide Network of Excellence (EPNOE)*. Springer Vienna.

KEEFE, A. J., BRAULT, N. D. & JIANG, S. 2012. Suppressing Surface Reconstruction of Superhydrophobic PDMS Using a Superhydrophilic Zwitterionic Polymer. *Biomacromolecules,* 13**,** 1683-1687.

KLAŠNJA, B. & KOPITOVIĆ, S. 1992. Lignin-Phenol-Formaldehyde resins as adhesives in the production of plywood. *Holz als Roh- und Werkstoff,* 50**,** 282-285.

LAURICHESSE, S. & AVÉROUS, L. 2014. Chemical modification of lignins: Towards biobased polymers. *Progress in Polymer Science,* 39**,** 1266-1290.

LI, H., QU, Y. & XU, J. 2015. Microwave-Assisted Conversion of Lignin. *In:* FANG, Z., SMITH, J. R. L. & QI, X. (eds.) *Production of Biofuels and Chemicals with Microwave.* Springer Netherlands.

LIN, X., ZHOU, M., WANG, S., LOU, H., YANG, D. & QIU, X. 2014. Synthesis, Structure, and Dispersion Property of a Novel Lignin-Based Polyoxyethylene Ether from Kraft Lignin and Poly(ethylene glycol). *ACS Sustainable Chemistry & Engineering,* 2**,** 1902-1909.

LIU, W., ZHOU, R., GOH, H. L. S., HUANG, S. & LU, X. 2014. From Waste to Functional Additive: Toughening Epoxy Resin with Lignin. *ACS Applied Materials & Interfaces,* 6**,** 5810-5817.

LÜTH, H. 2001. *Solid Surfaces, Interfaces and Thin Films*, Springer.

MITTAL, K. L., LEE, K. W. & CONFERENCE, S. P. E. T. 1997. *Polymer Surfaces and Interfaces: Characterization, Modification and Application*, Taylor & Francis.

MOON, R. J., MARTINI, A., NAIRN, J., SIMONSEN, J. & YOUNGBLOOD, J. 2011. Cellulose nanomaterials review: structure, properties and nanocomposites. *Chemical Society Reviews,* 40**,** 3941-3994.

MYERS, D. 1991. *Surfaces, Interfaces, and Colloids: Principles and Applications*, Wiley.

NGUYEN, J. D., MATSUURA, B. S. & STEPHENSON, C. R. J. 2013. A Photochemical Strategy for Lignin Degradation at Room Temperature. *Journal of the American Chemical Society,* 136**,** 1218-1221.

OASMAA, A., AL√¯©N, R. & MEIER, D. 1993. Catalytic hydrotreatment of some technical lignins. *Bioresource Technology,* 45**,** 189-194.

OJIJO, V. & SINHA RAY, S. 2013. Processing strategies in bionanocomposites. *Progress in Polymer Science,* 38**,** 1543-1589.

OLÁH, A., HILLBORG, H. & VANCSO, G. J. 2005. Hydrophobic recovery of UV/ozone treated poly(dimethylsiloxane): adhesion studies by contact mechanics and mechanism of surface modification. *Applied Surface Science,* 239**,** 410-423.

OWEN, M. & DVORNIC, P. 2012. General Introduction to Silicone Surfaces. *In:* OWEN, M. J. & DVORNIC, P. R. (eds.) *Silicone Surface Science.* Springer Netherlands.

PANDEY, M. P. & KIM, C. S. 2011. Lignin Depolymerization and Conversion: A Review of Thermochemical Methods. *Chemical Engineering & Technology,* 34**,** 29-41.

PEREZ, J., MUNOZ-DORADO, J., DE LA RUBIA, T. & MARTINEZ, J. 2002. Biodegradation and biological treatments of cellulose, hemicellulose and lignin: an overview. *International Microbiology,* 5**,** 53-63.

PLUEDDEMANN, E. P. 1982. *Silane Coupling Agents*, Springer.

PUKÁNSZKY, B. 2005. Interfaces and interphases in multicomponent materials: past, present, future. *European Polymer Journal,* 41**,** 645-662.

QIN, J., WOLOCTT, M. & ZHANG, J. 2013. Use of Polycarboxylic Acid Derived from Partially Depolymerized Lignin As a Curing Agent for Epoxy Application. *ACS Sustainable Chemistry & Engineering,* 2**,** 188-193.

REN, Y., YAN, M., WANG, J., ZHANG, Z. C. & YAO, K. 2013. Selective Reductive Cleavage of Inert Aryl C-O Bonds by an Iron Catalyst. *Angewandte Chemie International Edition,* 52**,** 12674-12678.

ROTH, J., ALBRECHT, V., NITSCHKE, M., BELLMANN, C., SIMON, F., ZSCHOCHE, S., MICHEL, S., LUHMANN, C., GRUNDKE, K. & VOIT, B. 2008. Surface Functionalization of Silicone Rubber for Permanent Adhesion Improvement. *Langmuir,* 24**,** 12603-12611.

RUPPERT, A. M., WEINBERG, K. & PALKOVITS, R. 2012. Hydrogenolysis Goes Bio: From Carbohydrates and Sugar Alcohols to Platform Chemicals. *Angewandte Chemie International Edition,* 51**,** 2564-2601.

SADEGHIFAR, H., CUI, C. & ARGYROPOULOS, D. S. 2012. Toward Thermoplastic Lignin Polymers. Part 1. Selective Masking of Phenolic Hydroxyl Groups in Kraft Lignins via Methylation and Oxypropylation Chemistries. *Industrial & Engineering Chemistry Research,* 51**,** 16713-16720.

SAITO, T., BROWN, R. H., HUNT, M. A., PICKEL, D. L., PICKEL, J. M., MESSMAN, J. M., BAKER, F. S., KELLER, M. & NASKAR, A. K. 2012. Turning renewable resources into value-added polymer: development of lignin-based thermoplastic. *Green Chemistry,* 14**,** 3295-3303.

SALAS, C., NYPELÖ, T., RODRIGUEZ-ABREU, C., CARRILLO, C. & ROJAS, O. J. 2014. Nanocellulose properties and applications in colloids and interfaces. *Current Opinion in Colloid & Interface Science,* 19**,** 383-396.

SANTOS, R. B., CAPANEMA, E. A., BALAKSHIN, M. Y., CHANG, H.-M. & JAMEEL, H. 2012. Lignin Structural Variation in Hardwood Species. *Journal of Agricultural and Food Chemistry,* 60**,** 4923-4930.

SARKAR, S. & ADHIKARI, B. 2001. Synthesis and characterization of lignin–HTPB copolyurethane. *European Polymer Journal,* 37**,** 1391-1401.

SAXENA, R. C., ADHIKARI, D. K. & GOYAL, H. B. 2009. Biomass-based energy fuel through biochemical routes: A review. *Renewable and Sustainable Energy Reviews,* 13**,** 167-178.

SCHNEIDER, M. H., TRAN, Y. & TABELING, P. 2011. Benzophenone Absorption and Diffusion in Poly(dimethylsiloxane) and Its Role in Graft Photo-polymerization for Surface Modification. *Langmuir,* 27**,** 1232-1240.

SERGEEV, A. G. & HARTWIG, J. F. 2011. Selective, Nickel-Catalyzed Hydrogenolysis of Aryl Ethers. *Science,* 332**,** 439-443.

SERGEEV, A. G., WEBB, J. D. & HARTWIG, J. F. 2012. A Heterogeneous Nickel Catalyst for the Hydrogenolysis of Aryl Ethers without Arene Hydrogenation. *Journal of the American Chemical Society,* 134**,** 20226-20229.

SERRANO-RUIZ, J. C., LUQUE, R. & SEPULVEDA-ESCRIBANO, A. 2011. Transformations of biomass-derived platform molecules: from high added-value chemicals to fuelsvia aqueous-phase processing. *Chemical Society Reviews,* 40**,** 5266-5281.

SHEN, D. K., GU, S., LUO, K. H., WANG, S. R. & FANG, M. X. 2010. The pyrolytic degradation of wood-derived lignin from pulping process. *Bioresource Technology,* 101**,** 6136-6146.

SHIT, S. & SHAH, P. 2013. A Review on Silicone Rubber. *National Academy Science Letters,* 36**,** 355-365.

SLENTZ, B. E., PENNER, N. A., LUGOWSKA, E. & REGNIER, F. 2001. Nanoliter capillary electrochromatography columns based on collocated monolithic support structures molded in poly(dimethyl siloxane). *ELECTROPHORESIS,* 22**,** 3736-3743.

SOMORJAI, G. A. & LI, Y. 2010. *Introduction to Surface Chemistry and Catalysis*, John Wiley & Sons.

SONG, Q., WANG, F., CAI, J., WANG, Y., ZHANG, J., YU, W. & XU, J. 2013. Lignin depolymerization (LDP) in alcohol over nickel-based catalysts via a fragmentation-hydrogenolysis process. *Energy & Environmental Science,* 6**,** 994-1007.

STANZIONE, J. F., GIANGIULIO, P. A., SADLER, J. M., LA SCALA, J. J. & WOOL, R. P. 2013. Lignin-Based Bio-Oil Mimic as Biobased Resin for Composite Applications. *ACS Sustainable Chemistry & Engineering,* 1**,** 419-426.

SUI, G., WANG, J., LEE, C.-C., LU, W., LEE, S. P., LEYTON, J. V., WU, A. M. & TSENG, H.-R. 2006. Solution-Phase Surface Modification in Intact Poly(dimethylsiloxane) Microfluidic Channels. *Analytical Chemistry,* 78**,** 5543-5551.

THAKUR, V. K. & SINGHA, A. S. 2015. *Surface Modification of Biopolymers*, Wiley.

THAKUR, V. K., THAKUR, M. K., RAGHAVAN, P. & KESSLER, M. R. 2014. Progress in Green Polymer Composites from Lignin for Multifunctional Applications: A Review. *ACS Sustainable Chemistry & Engineering,* 2**,** 1072-1092.

THIELEMANS, W., CAN, E., MORYE, S. S. & WOOL, R. P. 2002. Novel applications of lignin in composite materials. *Journal of Applied Polymer Science,* 83**,** 323-331.

TOBISU, M., YAMAKAWA, K., SHIMASAKI, T. & CHATANI, N. 2011. Nickel-catalyzed reductive cleavage of aryl-oxygen bonds in alkoxy- and pivaloxyarenes using hydrosilanes as a mild reducing agent. *Chemical Communications,* 47**,** 2946-2948.

TUGULU, S. & KLOK, H.-A. 2009. Surface Modification of Polydimethylsiloxane Substrates with Nonfouling Poly(Poly(ethylene glycol)methacrylate) Brushes. *Macromolecular Symposia,* 279**,** 103-109.

VAN VLIERBERGHE, S., DUBRUEL, P. & SCHACHT, E. 2011. Biopolymer-Based Hydrogels As Scaffolds for Tissue Engineering Applications: A Review. *Biomacromolecules,* 12**,** 1387-1408.

WANG, H., TUCKER, M. & JI, Y. 2013. Recent Development in Chemical Depolymerization of Lignin: A Review. *Journal of Applied Chemistry,* 2013**,** 9.

WANG, R., YANG, Y.-L., QIN, M., WANG, L.-K., YU, L., SHAO, B., QIAO, M.-Q., WANG, C. & FENG, X.-Z. 2007. Biocompatible Hydrophilic Modifications of Poly(dimethylsiloxane) Using Self-Assembled Hydrophobins. *Chemistry of Materials,* 19**,** 3227-3231.

WONG, I. & HO, C.-M. 2009. Surface molecular property modifications for poly(dimethylsiloxane) (PDMS) based microfluidic devices. *Microfluidics and Nanofluidics,* 7**,** 291-306.

WU, W.-B. & HUANG, J.-M. 2014. Electrochemical Cleavage of Aryl Ethers Promoted by Sodium Borohydride. *The Journal of Organic Chemistry,* 79**,** 10189-10195.

WU, Y., HUANG, Y. & MA, H. 2007. A Facile Method for Permanent and Functional Surface Modification of Poly(dimethylsiloxane). *Journal of the American Chemical Society,* 129**,** 7226-7227.

WU, Z. & HJORT, K. 2009. Surface modification of PDMS by gradient-induced migration of embedded Pluronic. *Lab on a Chip,* 9**,** 1500-1503.

XIAO, D., ZHANG, H. & WIRTH, M. 2002. Chemical Modification of the Surface of Poly(dimethylsiloxane) by Atom-Transfer Radical Polymerization of Acrylamide. *Langmuir,* 18**,** 9971-9976.

XIONG, X., WU, Z., PAN, J., XUE, L., XU, Y. & CHEN, H. 2015. A facile approach to modify poly(dimethylsiloxane) surfaces via visible light-induced grafting polymerization. *Journal of Materials Chemistry B,* 3**,** 629-634.

XU, C., ARANCON, R. A. D., LABIDI, J. & LUQUE, R. 2014. Lignin depolymerisation strategies: towards valuable chemicals and fuels. *Chemical Society Reviews,* 43**,** 7485-7500.

XU, C., TAYLOR, P., ERSOZ, M., FLETCHER, P. D. I. & PAUNOV, V. N. 2003. Microcontact printing of DNA-surfactant arrays on solid substrates. *Journal of Materials Chemistry,* 13**,** 3044-3048.

XUE, B.-L., WEN, J.-L. & SUN, R.-C. 2014. Lignin-Based Rigid Polyurethane Foam Reinforced with Pulp Fiber: Synthesis and Characterization. *ACS Sustainable Chemistry & Engineering,* 2**,** 1474-1480.

YAN, N., ZHAO, C., DYSON, P. J., WANG, C., LIU, L.-T. & KOU, Y. 2008. Selective Degradation of Wood Lignin over Noble-Metal Catalysts in a Two-Step Process. *ChemSusChem,* 1**,** 626-629.

YANG, H., YAN, R., CHEN, H., LEE, D. H. & ZHENG, C. 2007. Characteristics of hemicellulose, cellulose and lignin pyrolysis. *Fuel,* 86**,** 1781-1788.

YANG, L., LI, L., TU, Q., REN, L., ZHANG, Y., WANG, X., ZHANG, Z., LIU, W., XIN, L. & WANG, J. 2010. Photocatalyzed Surface Modification of Poly(dimethylsiloxane) with Polysaccharides and Assay of Their Protein Adsorption and Cytocompatibility. *Analytical Chemistry,* 82**,** 6430-6439.

YANG, Y., DENG, Y., TONG, Z. & WANG, C. 2014. Renewable Lignin-Based Xerogels with Self-Cleaning Properties and Superhydrophobicity. *ACS Sustainable Chemistry & Engineering,* 2**,** 1729-1733.

YEH, S.-B., CHEN, C.-S., CHEN, W.-Y. & HUANG, C.-J. 2014. Modification of Silicone Elastomer with Zwitterionic Silane for Durable Antifouling Properties. *Langmuir,* 30**,** 11386-11393.

YU, K. & HAN, Y. 2006. A stable PEO-tethered PDMS surface having controllable wetting property by a swelling-deswelling process. *Soft Matter,* 2**,** 705-709.

ZAHEER, M., HERMANNSDÖRFER, J., KRETSCHMER, W. P., MOTZ, G. & KEMPE, R. 2014. Robust Heterogeneous Nickel Catalysts with Tailored Porosity for the Selective Hydrogenolysis of Aryl Ethers. *ChemCatChem,* 6**,** 91-95.

ZAKZESKI, J., BRUIJNINCX, P. C. A., JONGERIUS, A. L. & WECKHUYSEN, B. M. 2010. The Catalytic Valorization of Lignin for the Production of Renewable Chemicals. *Chemical Reviews,* 110**,** 3552-3599.

ZHANG, J., ASAKURA, H., VAN RIJN, J., YANG, J., DUCHESNE, P., ZHANG, B., CHEN, X., ZHANG, P., SAEYS, M. & YAN, N. 2014a. Highly efficient, NiAu-catalyzed hydrogenolysis of lignin into phenolic chemicals. *Green Chemistry,* 16**,** 2432-2437.

ZHANG, J., TEO, J., CHEN, X., ASAKURA, H., TANAKA, T., TERAMURA, K. & YAN, N. 2014b. A Series of NiM (M = Ru, Rh, and Pd) Bimetallic Catalysts for Effective Lignin Hydrogenolysis in Water. *ACS Catalysis,* 4**,** 1574-1583.

CHAPTER 2: Facile functionalization of PDMS elastomer surfaces using thiol-ene click chemistry[§]

2.1 Abstract

A variety of methods have been developed for polydimethylsiloxane (PDMS) elastomer surface functionalization, particularly for the improvement of hydrophilicity. However, in addition to difficulties in avoiding undesired physical changes to the modified surface, including surface cracking, "hydrophobic recovery" frequently leads hydrophilically modified surfaces to completely return over time to their hydrophobic nature, with accompanying loss of accessible functional groups. Thiol-ene chemistry provides a mild and robust technology for synthetic elaboration. We demonstrate the introduction of thiol groups onto the PDMS surface via base-catalyzed equilibration of MTS ($(MeO)_3Si(CH_2)_3SH$). Thiols in the product elastomer were shown to be located primarily at the air interface using EDX, XPS and fluorescence labeling initially, and after extended periods of time: total thiol concentrations at the surface and in the bulk were established by complementary chemical titrations with DTDP (4,4'-dithiodipyridine) and iodine titrations in different solvents. The surface density of thiols was readily

---

[§] This chapter is reproduced from Jianfeng Zhang, Yang Chen, Michael A. Brook, in *Langmuir*, **2013**, 29, 12432-12442 with permission from American Chemical Society, 2013. Jianfeng Zhang designed the experimental procedure with assistance from Dr. Chen. Jianfeng Zhang performed all experiments, and wrote the majority of the manuscript with additions, edits and guidance provided by Dr. Brook.

controlled by reaction conditions: the rate of hydrophobic recovery, which led to incomplete loss of accessible functional groups, was determined. Thiol-ene click chemistry was then used to introduce a variety of hydrophilic moieties onto the surface including a silicone surfactant and maleic anhydride, respectively. In the latter case, molecular functionalization with both small (fluorescent labels) and polymeric nucleophiles (poly(ethylene glycol), chitosan) could be subsequently induced by simple ring-opening nucleophilic attack leading to permanently functional surfaces.

2.2 Introduction

Polydimethylsiloxane (PDMS) is a widely used polymeric material due to its beneficial characteristics, which include optical transparency, high flexibility, low biological activity, ease of fabrication, and so forth. The high hydrophobicity of silicones can be advantageous in many applications, but typically not those that involve linking to other materials: silicones can be very difficult to integrate with other substances because of their low surface energy. For such applications, silicone surface chemistry normally needs to be manipulated.

A number of methods have been developed to render PDMS surfaces hydrophilic and/or functional by the introduction of (polar) functional groups. One strategy employs high-energy treatments, such as a plasma,(He et al., 2003, Bae et al., 2007, Makamba et al., 2003) ultraviolet light,(Berdichevsky et al., 2004, Hu et al., 2002, Efimenko et al., 2002) or corona discharge to modify the surface.(Di Virgilio et al., 2011) Depending on

the conditions, functional groups, typically hydroxy groups, are introduced onto the PDMS surface. Alternatively, the surface can be modified by chemical treatment including etching or oxidization with reagents such as $H_2O/H_2O_2/HCl$ mixture,(Sui et al., 2006) or concentrated NaOH,(Hoek et al., 2010) KOH or tetrabutylammonium fluoride trihydrate (TBAF).(Brook et al., 2011) If other silicone species are present in solution during reactions of this type, it is possible to incorporate functional silicone monomers at the interface. For example, metathesis of a silicone elastomer surface with the functional polymer $Me_3SiO(MeHSiO)_nSiMe_3$ in the presence of triflic acid leads to surfaces rich in SiH groups.(Chen et al., 2006) In some cases, surface modification with these methods is accompanied by notable degradation of the surfaces as evidenced by increased opacity, increased roughness, or cracks.(Hui et al., 2005)

An alternative strategy to create hydrophilic silicones involves grafting hydrophilic polymers to the surface. For example, allyl-(Chen et al., 2006) or vinyl-terminated PEG can be attached to the silicon hydride-functionalized PDMS surfaces, described above, by hydrosilylation:(Chen et al., 2008) the PEG groups may additionally possess functional groups susceptible to substitution (tosylate)(Alauzun et al., 2009) or addition (activated esters, such as NHS (*N*-Hydroxysuccinimide))(Chen et al., 2006). It is also possible to polymerize from the surface. For example, methacrylate monomers functionalized with hydrophilic segments (PEG) or groups (amide) were polymerized from an elastomer surface using atom transfer radical polymerization (ATRP) after the initiator was bonded to an oxidized silicone surface.(Zhang et al., 2011, Xiao et al., 2002) Finally, rather than

oxidation alone, it is possible to use plasma to introduce PEG groups onto silicone surfaces: the resulting products have been applied to microfluidics fabrication and exploited for biological and pharmaceutical applications.(Demming et al., 2011, Mazutis et al., 2013)

Unlike most organic polymers, a key challenge with modified silicone elastomers is overcoming their ability to regenerate hydrophobic surfaces. As a consequence of very flexible polymer chains (low Tg) and very low surface energy even tethered silicone chains can migrate past the introduced hydrophilic groups to the air interface, where they are thermodynamically favored: migration of both tethered and free silicones buries the functional layer.(Morra et al., 1990, Hillborg et al., 2001, Kim et al., 2000, Hillborg and Gedde, 1998) Eventually, the surface loses hydrophilicity in a process coined "hydrophobic recovery" or "surface reversion."(Hillborg et al., 2004, Fritz and Owen, 1995) Permanently hydrophilic or functional silicones are difficult to make even when using the techniques described above.

Alcohols constitute a key functional group in organic chemistry and, as noted above, are very useful for surface modification. However, oxygen nucleophiles (alkoxides) initiate silicone depolymerization and oxygen radicals are difficult to both generate and control on surfaces. The sulfur analogue (thiols) by contrast, are better, less basic nucleophiles, and the radicals are easy to both generate and manipulate.(Hoyle and Bowman, 2010) Sulfur-based addition reactions can therefore proceed under either radical (generated either thermally or photochemically, termed thiol-ene click

reactions)(Hoyle et al., 2004) or anionic (thiol-Michael addition)(Li et al., 2010) conditions and are thus convenient alternatives to alcohol-derived reactions. Sulfur is also softer than oxygen, which opens the possibility of binding to soft metals such as gold. These features (simplicity, flexibility, and efficiency) make the thiol-ene reaction an ideal strategy for surface modification and for bulk polymerization, as elegantly shown in the synthesis of microfluidic channels.(Bounds et al., 2013) A variety of 'enes' including vinyl and acrylate have previously been grafted to thiol-functionalized surfaces under mild conditions.(Khire et al., 2007, Khire et al., 2008, Harant et al., 2006, Khire et al., 2006)

Since the surface modification of normal PDMS elastomers is limited by a lack of reactive functional groups, the introduction of thiol groups would provide broader latitude for surface modification. In this paper, we describe a method to introduce thiols onto the surface of PDMS elastomers and show that subsequent modification of the thiol-functionalized surface using thiol-ene processes leads to functional polar surfaces whose reactivity remains over extended periods of time.

2.3 Experimental Section

2.3.1 Materials

Sylgard184, a silicone elastomer kit, was purchased from Dow Corning (Midland, MI). (3-Mercaptopropyl)trimethoxysilane (MTS), KOH, maleic anhydride (MA), poly(ethylene glycol) methyl ether (Mw = 550 g/mol, 'PEG'), chitosan (Mw ~ 138,000

g/mol, 'CH'), 4,4'-dithiodipyridine (DTDP), *N*-(5-fluoresceinyl)maleimide, rhodamine 123, and iodine (I_2) were purchased from Sigma-Aldrich. An acrylate-terminated silicone surfactant (Silmer ACR A008-UP, Figure 2.6) was provided by Siltech Corporation. Solvents including methanol (MeOH), isopropanol (IPA), acetone, toluene, dichloromethane (DCM), and dimethyl sulfoxide (DMSO) were purchased from Caledon Laboratories and used as received.

2.3.2 Characterization

Energy-dispersive X-ray spectroscopy (EDX, JEOL 7000F) and X-ray photoelectron spectroscopy (XPS, Thermo Scientific Theta Probe XPS spectrometer) were used for surface elemental analysis: the data was analyzed with the software provided with the instruments. The samples for EDX characterization were coated before analysis with 10 nm of carbon. The parameters for all EDX characterization, including the accelerating voltage (15 kV) and collection period (300 s) were kept the same to facilitate comparison of samples. Take-off angles of 30°, 50°, and 70° were used for XPS characterization. ATR FT-IR (Thermo Nicolet 6700) was also used to characterize modification of the surfaces.

Thiol-modified surfaces were labeled with fluorescent dyes, and imaged with a fluorescence microscope (Olympus, BX51) or laser scanning confocal microscope (Zeiss, LSCM 510). The topography of the modified surface was examined using scanning electron microscopy (SEM, JEOL 7000F, 10 nm of copper coating was applied to the surface before measurement), atomic force microscopy (AFM, Veeco, Dimension ICON),

or a profilometer (WYKONT1100 optical profiler, Veeco). The AFM were undertaken using the ScanAsyst mode (resonance frequency = 90 kHz, spring constant = 0.4 N/m, and scanning frequency was 2 Hz). The contact force between the silicon tip and the samples was kept as low as possible. Phase shifting interferometry (PSI) mode was chosen for profilometer characterization (Mode: PSI, objective 5x, FOV 1.0x) as it allows one to characterize changes in a relatively smooth surface with height changes between two adjacent points of not more than approximately 160 nm.

The densities of thiol groups on and in PDMS elastomers were obtained by spectrophotometric measurements after chemical modification. A platereader (TECAN Safire) was used to measure the absorbance of the product 4-thiopyridone from 325 nm to 375 nm at 1 nm intervals during a DTDP titration.(Riener et al., 2002) A UV-vis spectrometer (Cary 50, Varian Inc.) was used to collect the absorbance changes of iodine solutions (scanning range from 450 nm to 550 nm at 180 nm/min). The UV-vis spectrometer was also used to study the transparency of the modified PDMS elastomer in the range from 300-800 nm.

The sessile drop water contact angles of modified surfaces were measured with a Ramé-Hart Model 100 goniometer. Milli-Q water with a constant volume (about 25 μl) was placed on the surface. Contact angle changes were recorded against time under room temperature.

2.3.3 Preparation of PDMS elastomers

The PDMS elastomer disk was prepared from the Dow Corning's Sylgard 184 elastomer kit. The two-part liquid components of the kit were mixed in a 10:1 ratio by weight following manufacturer's instructions. The mixture was mixed manually for 5 min. To cast the elastomer disk, the mixed liquid (5 g ± 0.05 g) was poured into a Petri dish (sterile 100 mm × 15 mm polystyrene Petri dish) that was then placed on a level surface for 12 h curing at room temperature, following by a 24 h post cure at 70 °C. The cured PDMS elastomer film (~ 0.5 mm thick) was peeled from the Petri dish and trimmed at the edge leaving a disk with a diameter of 7 cm.

2.3.4 Base-catalyzed equilibrium of silicone elastomers PDMS-SH

The introduction of thiols onto the PDMS elastomer surface was achieved by a base-catalyzed reaction with MTS at different concentrations. The concentration of MTS varied from 5% w/w to 20% w/w; the concentration of KOH varied from 1% w/w to 5% w/w. PDMS elastomer disks (with the diameter of about 7 cm x 0.5 mm thick) were soaked in the base/MTS solution (1 disk / 28 ml) during sonication (AQUASONIC, HT 50) for different periods (from 1 h to 6 h). The treatments were performed at two different temperatures (0 °C and 50 °C). The effects of the various parameters on the efficiency of thiol incorporation are reported in Table 2.1. After treatment, the PDMS elastomer was first rinsed with methanol (30 ml); then for further cleaning, the elastomer was soaked in larger amounts of methanol (300 ml) and sonicated for 5 min. The physically absorbed MTS and KOH were removed completely by extraction in fresh DCM (100 ml × 3, 3 h

each time). Finally, the elastomer disk was dried under nitrogen. From these large disks were cut disks of diameter 9.5 mm for use in subsequent modification studies.

2.3.5 Quantification of thiols on the PDMS elastomer surface

2.1.1.1 DTDP titration

DTDP has previously been demonstrated to be an efficient reagent to determine thiol concentrations. Following the literature procedure,(Riener et al., 2002, Egwim and Gruber, 2001) a calibration curve was first developed (Appendix, Figure 7.1). DTDP titration was employed in poor solvents for silicone to measure thiol surface concentrations on modified silicones.

Circular disks (diameter 9.5 mm and thickness about 0.5 mm) were punched from the thiol-modified elastomer. The disks were rinsed with methanol (30 ml), and dried under a flow of nitrogen for 5 min. During the titration, each of the disks was soaked separately in 3 ml of media (0.1% Et_3N in DMSO v/v) containing the DTDP reagent (150 µl of 4 mM in DMSO, 6×10^{-7} mmol). After shaking for 30 min, neat acetic acid was added (300 µl) and the absorbance at 347 nm was recorded. Sample calculations for the surface concentration of thiol are provided in the Appendix (Section 7.1.1).

2.1.1.2 Iodine titration

Iodometric titrations(Ciesielski and Zakrzewski, 2006) were also used to quantify the tethered thiols. Iodine in toluene solutions (2.14 mM, from 54.39 mg of iodine in 100 ml of toluene), a good solvent for silicones, were diluted to provide concentrations

varying from 0.096 to 0.496 mM. The absorbances of these standard solutions at 497 nm were read and plotted against concentration to give a calibration curve (Appendix, Figure 7.2).

To titrate the thiols in the PDMS elastomer, the disks of thiol-modified elastomer (diameter 9.5 mm and thickness about 0.5 mm) were incubated in 3 ml of iodine/toluene solution (about 0.2 mM) for 40 min (Table 2.1). The concentration change of the iodine solution, after removal of the elastomer, could be calculated from the calibration curve. It was necessary to compensate for the amount of iodine retained in the elastomer (about 10%), which was established by control experiments on virgin elastomers swollen with iodine solution (Appendix, Section 7.1.2).

2.3.6 Monitoring the partition of thiols between the surface and the bulk

The susceptibility of thiols to migrate from the surface into the bulk was monitored by the combination of DTDP and iodometric titrations. After exposing the elastomer to base-catalyzed silanization, the disks were separately titrated with DTDP (3 disks) and iodine (3 disks), respectively, following the procedures described previously. Another set of 24 disks was stored in methanol (100 ml) for titration afterwards. After 2 h, 4 h, and 6 h, respectively, another 18 disks were titrated with DTDP (3 disks × 3) and iodine (3 disks × 3). The remaining 6 disks were swelled in DCM for 2 h, and then titrated with DTDP (3 disks) and iodine (3 disks) after drying under nitrogen flow (5 min). The concentrations of thiol, obtained from both DTDP and iodine titrations, were plotted against time.

2.3.7 Modification of thiol-functionalized surfaces

2.1.1.3 Grafting gold nanoparticles to thiol-functionalized surface ***PDMS-S-Au***

Gold surfaces including nanoparticles (AuNPs) form a strong interaction with thiols. Therefore, AuNPs were used as an indicator for the presence of a thiol-functionalized surface. AuNP (with a diameter of about 5 nm) dispersions in toluene were prepared following literature procedures.(Gandubert and Lennox, 2005, Hill and Mirkin, 2006) Thiol-functionalized and unmodified PDMS disks, respectively, were soaked in 2 ml of AuNP solutions for 12 h. In order to remove the unanchored AuNPs, the disks were first sonicated in 10 ml of toluene, and then extracted by soaking in 10 ml of fresh toluene 3 times (12 h each time). The disks were left in a vacuum chamber until dried.

2.1.1.4 Grafting a silicone surfactant to the thiol-functionalized surfaces ***PDMS-S-ACR***

The silicone surfactant ACR-A008-UP (1 g, 10% w/v in THF) and AIBN (0.01 g, 0.061 mmol, 1% w/w to surfactant) were dissolved in THF (10 ml). Thiol-functionalized PDMS disks were incubated in the solution (6 disks in 10 ml of solution) for 36 h at 80 °C. The disks were soaked in 10 ml of fresh THF for 12 h after the grafting reaction: the soaking process was repeated in fresh solvent (3 repeats, each x 12 h). Before characterizing the surface with ATR-FTIR (Figure 2.6) and by contact angle (Table 2.2), the disks were dried under a flow of nitrogen.

2.1.1.5 Grafting maleic anhydride to the thiol-functionalized surface ***PDMS-S-MA***

The surface could alternatively be modified with maleic anhydride. The disks were soaked in maleic anhydride/THF solution (2 g maleic anhydride in 10 ml THF, 20% w/v; and 6 disks in 10 ml of solution) for 36 h at 80 °C. The disks were then washed in 10 ml of fresh and dry THF during the following 2 days (10 ml × 4, 12 h each time). After soaking, the disks were dried under a flow of nitrogen. ATR-FTIR characterization was carried out immediately after drying the disks. Contact angle measurements were performed after hydrolyzing the anhydride groups in a THF/water mixture (50/50 water to THF, 6 disks in 10 ml of solution).

2.1.1.6 Fluorescent labeling of the thiol modified surface ***PDMS-S-FL***

N-(5-Fluoresceinyl)maleimide (0.6 mg, 1.4×10-3 mmol) was dissolved in isopropanol (2 ml) to give a final concentration of 0.3 mg/ml (0.7 mM). The thiol-functionalized PDMS disk was split into 2-3 mm wide strips. The elastomer strips were incubated in the *N*-(5-fluoresceinyl)maleimide isopropanol solution for 3 days at room temperature. The elastomer strips were then soaked in fresh isopropanol over the following 4 days (solvent changed × 6 times (~12 soak), 20 ml each time). To follow changes in the surface vs the bulk elastomer concentrations, the disks were freeze fractured to expose a cross section that, together with the surface, was characterized with fluorescence microscopy and confocal laser scanning microscopy.

2.3.8 Modification of the anhydride surfaces

2.1.1.7 Fluorescent labeling of the anhydride-modified surface ***PDMS-S-MA-RH***

Following the previous procedure, the anhydride on the surface was labeled with rhodamine 123. The maleic anhydride-modified disk was split into strips (2-3 mm in width). The strips were incubated in rhodamine solution (0.05 mg, 1.31×10^{-4} mmol of rhodamine 123 in 10 ml of acetone) to give 0.005 mg/ml, 1.31×10^{-4} mM) for 36 h at room temperature. The strips were then soaked in 20 ml of fresh acetone 6 times during the following 4 days. The cross-section and surface of rhodamine-labeled strips (Appendix, Figure 7.3) were characterized with fluorescence microscopy and confocal laser scanning microscopy.

2.1.1.8 PEG grafted to the anhydride-modified ***PDMS-S-MA-PEG***

The anhydride-modified surface was also modified with PEG. Poly(ethylene glycol) methyl ether MW 550 was dissolved in DCM to give a 10% w/v solution in which the anhydride modified silicone disks were incubated (6 disks per 10 ml). After 12 h, the disks were extracted with fresh DCM (20 ml × 3, 12 h). The surfaces were characterized using ATR-FTIR (Figure 2.6) and sessile water drop contact angles (Table 2.2).

2.1.1.9 Chitosan grafted to the anhydride-modified ***PDMS-S-MA-CH***

The anhydride-modified surface was also modified with chitosan. Chitosan was dissolved in a mixture solvent (2% v/v of acetic acid in distilled water) to give a 5% w/v aqueous solution. Anhydride-functionalized disks were incubated in the aqueous solution

(10% w/v, 6 disks/10 ml) for 12 h. The disks were first washed in boiling distilled water (50 ml × 3, 5 minutes each time) in order to remove unanchored chitosan, and then washed with distilled water (soaking in 20 ml for 12 h). The surfaces were then characterized by ATR-FTIR (Figure 2.6) and sessile water drop contact angles (Table 2.2).

2.4 Results and Discussion

2.4.1 Introduction of thiols to the PDMS elastomer surface PDMS-SH

Although the surface of any silicone elastomer is susceptible to metathesis under basic conditions,(Brook et al., 2011) Sylgard 184 – a silicone commonly used for biomaterials applications, was chosen for surface modification. Silicone elastomer disks were made by combining the silicone base and the curing agent in a 10:1 ratio, mixing, pouring into a Petri dish and allowing cure for 36 h. The elastomer films were then cut into disks approximately 7 cm in diameter and 0.5 mm thick.

Under basic conditions, nucleophilic attack by OH^- will occur both at exposed PDMS polymer chains on the surface (Scheme 2.1A), and the alkoxysilane group on the coupling agent $(MeO)_3Si(CH_2)_3SH$ (MTS) (Scheme 2.1B). In both cases, silanolate ions (R_3SiO^-), which continue the equilibration process, form after the Si-O bond is cleaved. The silanolate ions undergo a cascade of nucleophilic reactions that can lead to oligomers of MTS,(Scott et al., 2010) depolymerization of PDMS(Brook et al., 2011) and, importantly for this process, metathesis reactions that lead to grafting of MTS in various forms to the silicone elastomer surface (Scheme 2.1C).

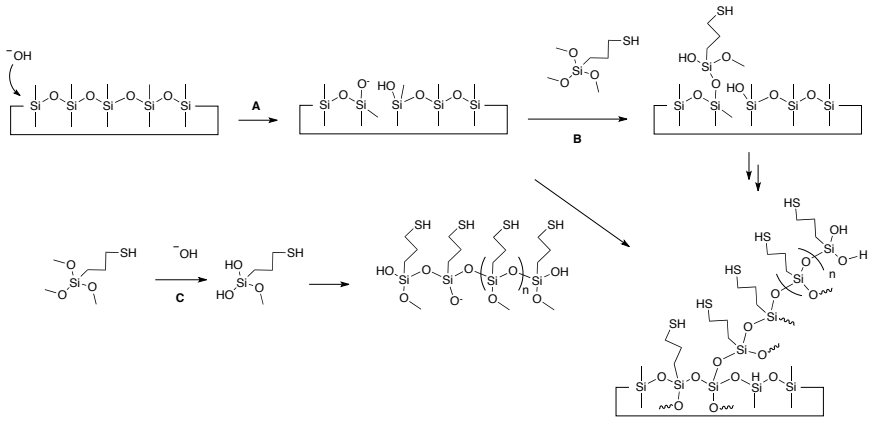

Scheme 2.1 Schematic illustration of the process to introduce thiols onto PDMS elastomer surfaces. (A) reactions at silicone; (B) reactions at MTS; and (C) metathesis at the elastomer interface.

A variety of experimental factors were examined to optimize control over the quantity of thiols that could be introduced to the surface, including: solvent; the effect of the MTS concentration; surface treatment time; and, temperature during the equilibrium equilibration process. Having surveyed a variety of solvents, methanol (a solvent in which silicones are not especially soluble) proved to be particularly effective to direct reaction mostly to the silicone surface (data not shown).(Brook et al., 2011)

2.1.1.10 Equilibration solution concentration (KOH)

Different KOH concentrations were examined to establish the efficiency of the process and the resulting physical changes in the elastomer, including surface morphology and transparency. As indicated in Table 2.1, the PDMS elastomers were treated with 1%, 2.5%, and 5% (w/v) of KOH in methanol, respectively, to give surfaces

with visibly different morphologies (Figure 2.1). It was found that surfaces started to exhibit cracks at base concentrations near or above 2.5 %, and the surface was completely crazed at higher base concentrations. However, the elastomer treated with 1% KOH in methanol exhibited neither obvious surface cracking nor changes in transparency (Appendix, Figure 7.4). The surface roughness determined by AFM for this sample showed almost no change during the etching process, increasing only from 4.09 nm to 4.80 nm over an area of 1 μm^2 (Appendix, Figure 7.5). Although the formation of a silsesquioxane layer at the surface could impact the hardness of the elastomer body, the layer was sufficiently thin that Shore hardness levels were indistinguishable from the starting elastomer (Shore OO of 90 - 95, or Shore A of 40 – 45).

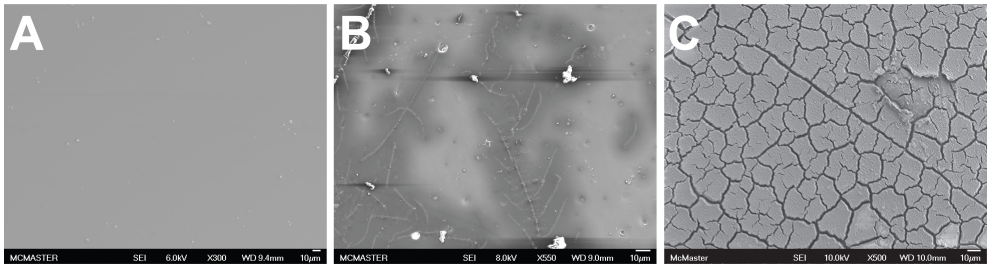

Figure 2.1 SEM images of elastomer surfaces resulting from different KOH concentrations (w/v), (A) 1% KOH, no cracking, (B) 2.5 % KOH, starts cracking, (C) 5% KOH, cracked.

2.1.1.11 MTS Concentration and Temperature

It was found that longer treatment times and higher treatment temperatures resulted in higher surface sulfur concentrations (see below). As shown in Table 2.1, the surface

concentration of thiol increased with increasing MTS concentration from 5-10% (w/v), but there was no additional change with MTS concentrations higher than 10%. As a comparison, the thiol surface concentrations increased significantly (more than 40%, Table 2.1) when increasing the MTS concentration from 5% and 10%.

2.4.2 The distribution of thiol groups within PDMS-SH

It was initially expected that, although most of the MTS would graft on the surface, some would partition into the elastomer body. A variety of techniques were therefore used to establish the location and quantity of thiols that became incorporated into the silicone, including EDX of cross-sections, labeling by fluorescent molecules and gold nanoparticles (AuNP), and XPS.

Table 2.1 The effect of experimental conditions on resulting surface density of thiols

Reaction conditions[a]	Treatment time (h)[a]	6	3	1	6	6	6	6	6
	Conc. of KOH (% w/v)	1	1	1	1	2.5	5	1	1
	Conc. of MTS (% w/v)	10	10	10	10	10	10	5	20
	Temperature (°C)	50	50	50	0	50	50	50	50
Atomic % sulfur (XPS)[c]		0.39	0.27	0.29	NM[e]	NM	NM	NM	NM
Iodine titration	[SH] nmol/cm^2	77	43	28	31	NM	NM	45	81
	SH molecules/nm^{2d}	463	259	168	186	NM	NM	271	488
	Error nmol/cm^{2b}	7	8	5	2	NM	NM	12	6
DTDP titration	[SH] surface nmol/cm^2	91	49	39	81	NM	NM	41	103
	SH molecules/nm^{2d}	548	295	235	488	NM	NM	247	620
	Error nmol/cm^2	21	23	18	11	NM	NM	12	22

[a] Each experiment involved 1 disk in 28 ml of equilibration solution. [b] Standard deviations, n = 3. [c] Take off angles = 30°. [d] SH molecules/nm^2 = [SH] nmol/cm^2 × 10^{-9} mol/nmol × 6.02 × 10^{23} molecules/mol / (10^7 nm/cm)^2. [e] NM not measured.

Cross sections of elastomers were examined using EDX. As shown in Figure 2.2, selected points across the cross section showed sulfur at low levels throughout the elastomer body, but in much higher intensity for sulfur near the external interface (Appendix, Figure 7.6). Note that the interaction volume for this technique means that the effective spot size is tens of microns in diameter. Thus, this technique demonstrates only that sulfur concentration decreases with distance from the external surface. Longer surface equilibration times were associated with deeper penetration of sulfur into the elastomer. In principle, in a poor solvent for silicones such as methanol, base-catalyzed equilibration should affect essentially only the surface layer of the elastomer.

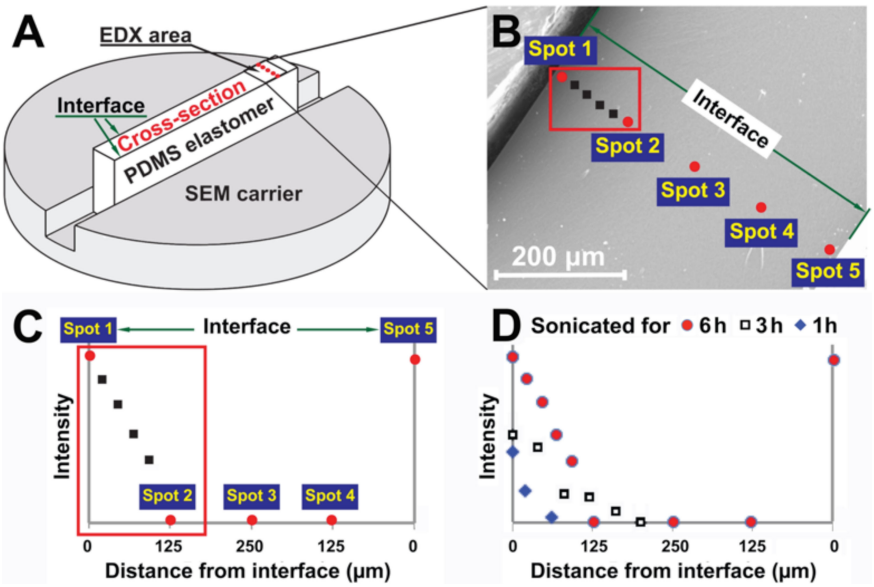

Figure 2.2 Cross-sectional EDX for the elastomer treated for different reaction times. (A/B) EDX spot location on the cross-section of a treated elastomer. (C) Intensity of sulfur in the elastomer cross-section after 6 hours treatment. (D) Sulfur concentrations as a function of reaction time. All the EDX measurements were performed using the same accelerating voltage and collection time.

To further refine the depth of the thiol-rich layer, labeling of the surface by fluorescent groups and gold nanoparticles was employed. The modified surfaces were fluorescently labeled with *N*-(5-fluoresceinyl)maleimide using a thiol-ene click reaction. The fluorescence was particularly strong on the external surface, and diminished with depth into the object and could not be observed beyond a depth of 5-10 µm (Figure 2.3). Compared with cross-sectional EDX, fluorescence labeling showed the thiol-rich layer to be more narrowly distributed near the air interface – 5-10 microns thick based on the

resolution of the z stack measurement. Chemofunctionalization of the silicone elastomer body with AuNP, which both efficiently bind to thiols and have exceptionally high extinction coefficients,(Demers et al., 2000) similarly showed a rich thiol (and gold) concentration on the silicone surface (Figure 2.3).

XPS characterization was employed to further refine the depth of the layer: the technique is sensitive to the topmost 10 nm at a 90° take off angle, and thinner layers at lower takeoff angles.(van der Heide, 2011) The XPS results indicated that the sulfur was located essentially at the air interface: 0.29 S atomic % (S_{2p}) at 30° take-off angle; 0.24 at 50°; and not detectable at 70° because the sulfur signal is overwhelmed by the dominant atoms C, O, Si. Taken in total, these EDX, fluorescence/AuNP labeling, and XPS data demonstrate that base-catalyzed equilibration between silicones and the MTS coupling agent preferentially introduces thiols onto a very thin external surface of the PDMS elastomers.

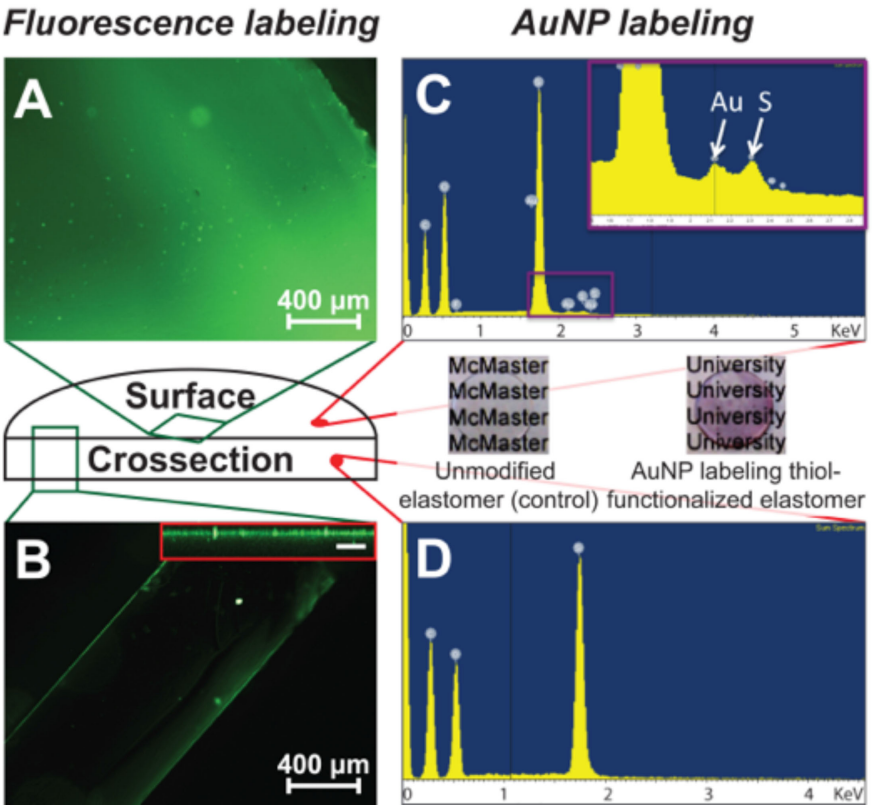

Figure 2.3 Fluorescence microscopy images of the thiol-functionalized PDMS elastomer dyed with *N*-(5-fluoresceinyl)maleimide. The experimental conditions for surface equilibration: reaction time = 6 hours, KOH concentration = 1%, MTS concentration = 10%, and reaction temperature = 50 °C. (A) The top view of the thiol-functionalized surface labeled with *N*-(5-fluoresceinyl) maleimide. (B) Cross-sectional view of the fluorescently labeled, thiol-functionalized PDMS elastomer. The inset is an LSCM (laser scanning confocal microscopy) image obtained by the "z stack" mode (obtaining cross sectional images of planes at various depths (z) within the sample, scale bar = 50 μm). (C) The EDX spectrum of the thiol surface, labeled with **AuNP**. The signals for Au and sulfur were both detected. (D) The EDX spectrum collected at the middle of the elastomer after

labeling with AuNP. No signal for either Au or sulfur was detected. The photos show that after labeling the thiol-functionalized elastomer was tinted pink (right inset), while the control remained uncolored (unmodified elastomer, left).

EDX, XPS and fluorescent labeling were very helpful in establishing the presence of surface thiols on modified silicone elastomers, but did not quantitate them. Although a variety of techniques can be employed to quantitate thiols, such as with Ellman's reagent,(Lafleur et al., 2013) we elected to use two complementary titration methods to provide a quantitative assessment of surface thiols: DTDP titration and iodine titration. As shown in Figure 2.4, both methods rely on the oxidation of free thiols to disulfides, however, because of solvent choice, one was used to quantitate the surface, while the other examined the entire elastomer bulk.

DMSO – an unfavorable solvent for PDMS – was used as the reaction medium for the DTDP titration. The reagent was therefore directed to react preferentially with the thiol groups on the surface (Figure 2.4A). The formation of 4-thiopyridone resulting from the thiol-disulfide exchange between thiol and DTDP can be following spectrophotometrically at ~347 nm. By contrast, the iodine oxidation, which could be followed by loss of intensity of the iodine absorbance at 497 nm, was undertaken in toluene, a solvent that effectively swells silicone elastomers. Thus, the two methods provide complementary information: the former measures primarily the surface thiols, while the latter can affect thiols throughout the silicone (Figure 2.4B).

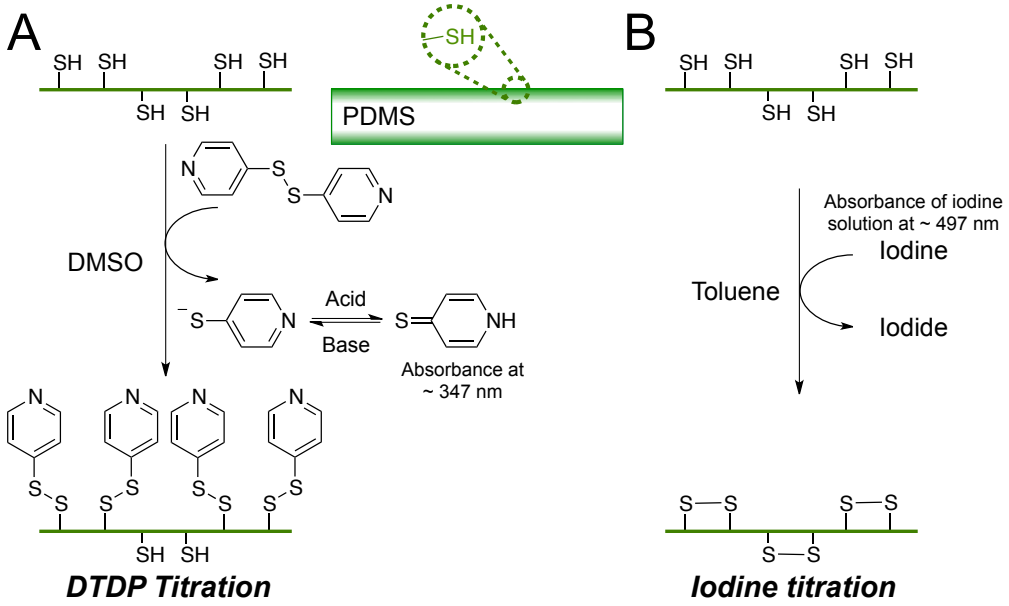

Figure 2.4 Quantitative analysis of thiol groups: (A) determination of thiol groups on the interface of PDMS elastomer by DTDP titration, (B) determination of thiol groups in the surface layer by iodine titration.

The incorporation of MTS, bearing three functional groups, in the elastomer will lead to increases in cross-link density at the reactive interface. The density of thiols could be controlled by straightforward manipulation of reaction conditions to give very high values of up to ~488 thiols/nm^2 (Table 2.1). Such high levels far exceed the functional group density of a monolayer, and are consistent with a three dimensional thiopropylsilsesquioxane network layer forming on the silicone elastomer.

2.4.3 Susceptibility of the thiol surface to reversion

Hydrophilically modified silicones undergo surface reversion; a process in which the hydrophiles become buried as more mobile, hydrophobic silicone chains migrate to the air interface. As noted above, the DTDP titration in DMSO preferentially reacts with thiols on the surface, while the iodine in toluene can react with thiols throughout the elastomer. By taking advantage of the different outcomes of these two titrations, it was possible to track changes in interfacial thiol concentration over time, and therefore to monitor the "hydrophobic recovery" of PDMS surface polymer chains: this process is an alternative to AFM force or contact angle measurements.(Meincken et al., 2005) As shown in Figure 2.5A, the interfacial concentration of thiols, obtained from DTDP titrations, decreased sharply by about 50% within 2 hours after surface treatment. The iodine titration, however, showed no net change of thiols in the elastomer. After 4 hours, the interfacial thiol concentration had dropped essentially to zero. However, a fraction of the thiols could be induced to return to the air interface by use of an appropriate solvent. For example, after a swelling/deswelling processing in dichloromethane (DCM), about 25% (~ 102 SH/nm^2) of the total thiols present became chemically accessible for titration by DTDP. As noted in the literature, the recovered thiols are more that sufficient to perform thiol-ene reactions to modify the surface as is further discussed below.(Lafleur et al., 2013, Jonkheijm et al., 2008)

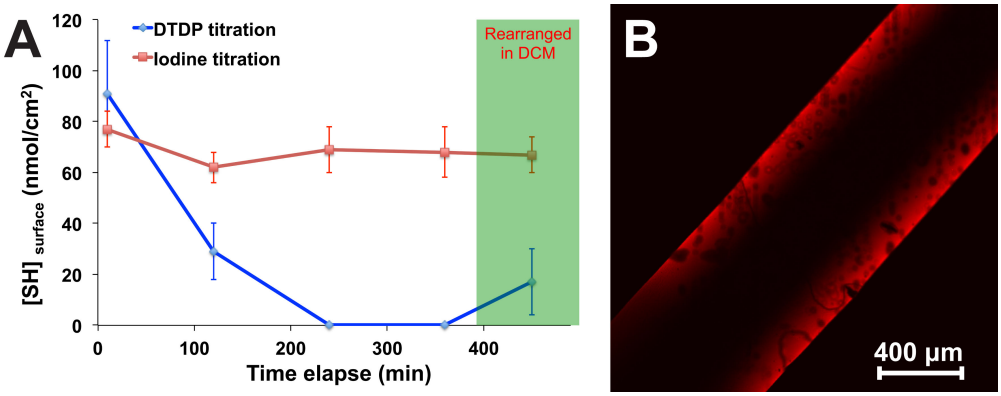

Figure 2.5 A: The change of thiol surface concentration over time, and the rearrangement in DCM. The surface and interfacial concentration were monitored by iodine and DTDP titration, respectively. B: Cross-sectional image of fluorescence labeling the maleic anhydride-modified surface with rhodamine 123.

2.4.4 Modification of the thiol-rich surface

Thiols are very versatile functional groups for further synthetic elaboration. To test the reactivity of the silicone surface-bound thiols, thiol-ene reactions initiated by AIBN(Campos et al., 2008) were attempted with maleic anhydride and, separately, with an acrylate-terminated silicone surfactant ACR (Figure 2.6). Surface modification was readily established by both spectroscopic and chemical analysis. Infrared data in both cases showed the presence of new carbonyl peaks at 1740 cm^{-1} for ACR and 1790 cm^{-1} for the anhydride (Appendix, Figure 7.7). Raman spectroscopy (Appendix, Figure 7.8) suggested about 20-25% of available thiols had been modified with maleic anhydride, a value that is consistent with the recovered thiol surface concentration after rearrangement in DCM.

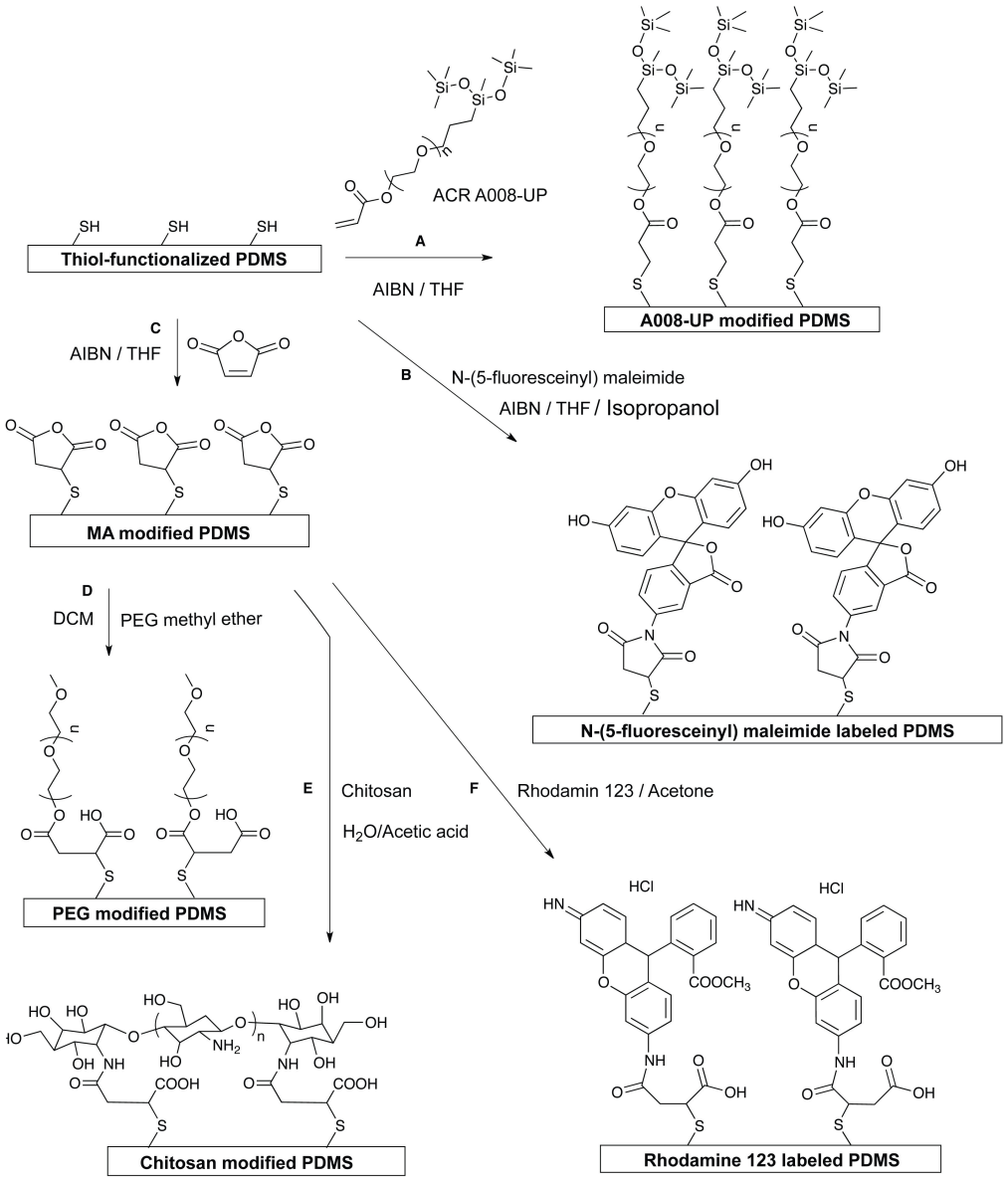

Figure 2.6 Surface modification of thiol-silicones: Surface thiol-ene reactions with A: ACR A008-UP, B: *N*-(5-fluoresceinyl)maleimide, and C: maleic anhydride, followed in the latter case by ring-opening of the surface anhydride with D: M-PEG, E: chitosan or F: rhodamine 123.

The presence of anhydride groups on the surface was confirmed by the subsequent reaction with rhodamine that led to a fluorescently labeled surface **PDMS-S-MA-RH** (Figure 2.5B). The red color was only found on the elastomer surfaces, as is clear from the sandwich structure observed when looking at the cross section of the elastomer (Appendix, Figure 7.3).

As confirmed by AT-FTIR (Appendix, Figure 7.7), the reactive anhydride-functionalized surface was readily further modified via ring-opening reaction with nucleophiles: PEG methyl ether (-OH) and chitosan ($-NH_2$) both readily reacted with the anhydride to give functional polymer surfaces (Figure 2.6). For the surface modified with PEG, the carbonyl peak of anhydride (1790 cm^{-1}) shifted to 1750 cm^{-1}, assigned to the carbonyl of ester; for the surface modified with chitosan, the carbonyl peak of anhydride (1790 cm^{-1}) split and shifted to peak at 1750 cm^{-1} and bands around 1660 cm^{-1}, assigned to -COOR and –CONHR, respectively.

2.4.5 Wettability and Reversion

The wettability of the thiol-modified surface changed subtly after grafting with ACR or maleic anhydride and then modification by PEG or chitosan. While unmodified PDMS elastomer surfaces exhibited high contact angles (sessile water drop) near 110°,(Hoek et al., 2010) all four modified surfaces were less hydrophobic, with **PDMS-S-ACR** surface showing a contact angle of ~74°, maleic anhydride-modified surface (after hydrolysis) **PDMS-S-MA** of ~84°, PEG-modified surface **PDMS-S-MA-PEG** 73°, and chitosan modified **PDMS-S-MA-CH** surface of 71° (Table 2.2) due to the presence of

hydrophilic functional groups (oligoether, carboxylic acid, amino-, hydroxyl groups), respectively.

At first view, although lower than pure silicones, the contact angles might appear rather higher than expected for a surface modified with 'hydrophilic' polymers: the alkane-rich thiopropyl-modified surface is expected to be hydrophobic. To provide some context, films of pure chitosan on glass exhibited a contact angle of 70° (138 kDa), similar to **PDMS-S-MA-CH**. In previous work, PEG-modified silicone surfaces prepared by hydrosilylation of PEG onto H-modified silicones had advancing contact angles of about 88°,(Chen et al., 2005) compared to the current process giving a surface **PDMS-S-MA-PEG** with contact angle 73°. Thus, the surface modification described above of silicones using thiols is comparably efficient.

Table 2.2 The contact angle of modified PDMS

	PDMS-S-ACR			PDMS-S-MAa			PDMS-S-MA-PEG			PDMS-S-MA-CH		
	New	Old		New	Old		New	Old		New	Old	
		Air[c]	H_2O[b]		Air[c]	H_2O[b]		Air[c]	H_2O[b]		Air[c]	H_2O[b]
Contact angle (°)	74	92	82	84	89	78	73	92	82	71	86	75
Error (°)[d]	4	3	1	6	3	5	2	1	3	7	5	3

[a] After hydrolysis to the dicarboxylic acid. [b] After equilibration in water for 3 days following storage of the elastomer in air for 6 months. [c] After storage of the elastomer in air for 6 months. [d] Standard deviations, n = 3.

In order to evaluate the availability of thiol groups on PDMS surface over extended time periods, both fluorescence labeling and modification with ACR-A008 UP were undertaken after the thiol-functionalized PDMS (**PDMS-SH**) had been stored in fridge (~2 °C, sealed and soaked in methanol) for more than 4 months. The aged surfaces were shown to contain reactive thiol groups that could be directly labeled by *N*-(5-fluoresceinyl)maleimide (Appendix, Figure 7.9). The efficiency of surface grafting could be enhanced by presoaking for 2 hours in a good solvent for silicones, as shown by grafting of ACR-A008 UP (Appendix, Figure 7.10). The approximately 25% recovery of functionality indicates the thiols remain proximal to the silicone elastomer surface, and provide sufficient functional tethers for grafting (see below). Note that, based on the absence of a change in Shore Hardness values (data not shown) before and after soaking and then drying, these swelling/shrinking processes do not affect the mechanical properties of the elastomer.

Reversion is a common feature of PDMS elastomers.(Hillborg et al., 2004, Fritz and Owen, 1995) Once surface reversion has occurred, it is generally difficult induce hydrophilic materials to migrate back to the interface. To be practical, therefore, functional surfaces must be modified immediately then stored in water, alcohol or other polar solvents. As just noted, the thiols themselves remain available for reaction after extended storage. In the case of the sulfur-linked materials, some hydrophobic recovery had occurred after 6 months: the wettability had changed to 92° for **PDMS-S-MA-ACR,** 89° for **PDMS-S-MA**, 92° for **PDMS-S-MA-PEG**, and 86° for **PDMS-S-MA-CH**.

However, the hydrophilicity could be reverted back partly (**PDMS-S-ACR** and **PDMS-S-MA-PEG**) or fully (**PDMS-S-ACR** and **PDMS-S-MA-CH**) after soaking in water for 3 days (Table 2.2). This ability to recovery hydrophilic character is much higher than is normally observed. It indicates the functional surfaces can be stored for extended periods of time, and then conveniently reconstituted and modified for their final use when desired.

The persistence of thiols at the MTS-modified silicone interface even after storage for extended periods of time, particularly after brief exposure to good solvents for silicones, could have a variety of origins. MTS, a trifunctional coupling agent, formed a three dimensional, highly reticulated network (Scheme 2.1), as shown by the high concentration of thiols measured at the interface. Such a dense layer will resist migration of PDMS chains from the elastomer body to the air interface. However, alone this should not be enough to account for the maintenance of surface functionality. We additionally ascribe it to the relative lack of polarity of the thiopropyl groups. Brennan et al., in a careful study of the utility of glass surfaces modified by MTS for surface polymerization, have shown that MTS-surfaces have relatively low surface energy.(Chen et al., 2011) The driving force for reversion is migration of lower surface energy of silicones, which are best accommodated at the air interface, from the elastomer body. The driving force for migration will be diminished when relatively nonpolar materials are already located at the air interface. We conclude that a combination of high cross-link density and low polarity accounts for the very low degree of reversion observed with these surfaces.

Depending on the specific reaction conditions, thiol densities of up to about 490 SH/nm^2 could be realized simply by controlling reaction conditions and time (Table 2.1). The relatively high densities, perhaps higher than necessary in some cases, are consistent with three-dimensional network structures presenting at the interface. These data compare favorably with alternative strategies for the preparation of thiolated surfaces. Jonkheijm et al.(Jonkheijm et al., 2008) demonstrated that densities of thiols of up to about 120 SH/nm^2) could be achieved by tethering of dendrimers onto silica, addition of a linker, immobilization of cystamine to the linker, and reduction of the disulfide-bond to liberate the thiols. In a different strategy, the group of Kutter created highly reticulated materials using a thiol-ene reaction, which possessed residual surface thiols with densities exceeding 135 SH/nm^2.(Lafleur et al., 2013)

The benefits of silicones in a wide variety of applications, notably the ready ability to cast the pre-elastomer mixtures into complex shapes, are widely known. However, there is often a need to selectively tether hydrophilic and functional groups at the silicone interface. Base-catalyzed metathesis proves to be a simple and efficient method to introduce thiols onto silicone elastomer surfaces. When using solvents that do not effectively swell the silicone, the incorporation of thiols could be essentially limited to the external surface of the elastomer body. The process is straightforward and can be used on any precured silicone elastomers of the desired hardness, transparency, roughness, etc. Shore hardness and surface morphologies were not affected during the process,(Demming et al., 2011, Mazutis et al., 2013) although more vigorous conditions (higher base

concentration, longer reactions times) led to more etching, increased crosslinking and undesirable cracking of the surfaces.

Thiol-modified surfaces offer complementary benefits to those of other functional groups including NH_2 or OH. Like HO-surfaces, there are no charges formed. Unlike alkoxides, however, thiolates don't affect the stability of the underlying silicone and, more importantly, undergo radical-based chemistry under mild conditions. These reaction are orthogonal and complementary to ionic reactions of amines and alcohols. The thiol-ene reaction can be trigged in both thermally and photochemically.(Hoyle and Bowman, 2010) The latter route allows selectively modification of different 'photoaddressable' areas of a given surface, a selectivity that is more difficult to achieve with other functional groups.(Jonkheijm et al., 2008, Lafleur et al., 2013) It is also possible to graft polymers the surface during radical polymerization by using the thiols on the surface for chain transfer.(Zhou et al., 2001)

Like other hydrophilically modified silicones, if not immediately treated, hydrophobic recovery of thiolated surfaces started within hours, accompanied by partial migration of a silicone layer over the introduced thiols: even the introduction of cross-linked layers derived from MTS at the external surface did not prevent this rearrangement. However, it was surprisingly easy to recover about 25% of the available thiols simply by soaking in a good solvent for silicones: the thiols remained proximal to the air interface. There was also a significant improvement of stability to hydrophobic reversion when, following introduction of an anhydride, PEG or chitosan were grafted to the surface.

Polymers grafted directly to the surface, or after maleic anhydride coupling, remained at the air interface. This strategy may serve as a useful starting point to creating truly wettable silicone surfaces, functional surfaces (for example, chitosan-modified surfaces have been shown to exhibit antibacterial properties(Tangpasuthadol et al., 2003)) and a starting point for further surface modification of silicone elastomers, for example, in the controlled manipulation of surfaces in microfluidics devices. (Jonkheijm et al., 2008, Lafleur et al., 2013)

2.5 Conclusion

Thiol functional groups were successfully introduced onto the PDMS elastomer surface via base-catalyzed equilibration without significantly affecting the surface morphology. The surface concentration of thiol groups was readily controlled by varying reaction times and temperatures: the total and interfacial concentrations of thiol groups could be titrated by DTDP and iodine methods, respectively. Similar to the hydrophobic recovery, the functionalized thiols became embedded below the surface over time, however, could brought partly back to the interface by changing solvent, and then captured by a thiol-ene reaction. The thiol-functionalized PDMS surface could be modified with hydrophilic molecules containing enes (acrylate and maleic anhydride) via the thiol-ene click reaction: the anhydride-modified surface could be further modified with small molecules and hydrophilic polymers. The modified PDMS surface showed

improvement of hydrophilicity and quite excellent performance on resistance of hydrophobic recovery over a long period.

2.6 Acknowledgements

We gratefully acknowledge the financial support of the Natural Sciences and Engineering Research Council of Canada. We thank Siltech for the gift of surfactant ACR-A008 UP.

2.7 References

ALAUZUN, J. G., FORTUNA, J. N., SHEARDOWN, H., GONZAGA, F. & BROOK, M. A. 2009. Generic, S(N)2 reactive silicone surfaces protected by poly(ethylene glycol) linkers: facile routes to new materials. *Journal of Materials Chemistry,* 19**,** 5033-5038.

BAE, W. S., CONVERTINE, A. J., MCCORMICK, C. L. & URBAN, M. W. 2007. Effect of sequential layer-by-layer surface modifications on the surface energy of plasma-modified poly(dimethylsiloxane). *Langmuir,* 23**,** 667-672.

BERDICHEVSKY, Y., KHANDURINA, J., GUTTMAN, A. & LO, Y. H. 2004. UV/ozone modification of poly(dimethylsiloxane) microfluidic channels. *Sensors and Actuators B-Chemical,* 97**,** 402-408.

BOUNDS, C. O., UPADHYAY, J., TOTARO, N., THAKURI, S., GARBER, L., VINCENT, M., HUANG, Z. Y., HUPERT, M. & POJMAN, J. A. 2013. Fabrication and Characterization of Stable Hydrophilic Microfluidic Devices Prepared via the in Situ Tertiary-Amine Catalyzed Michael Addition of Multifunctional Thiols to Multifunctional Acrylates. *ACS Applied Materials & Interfaces,* 5**,** 1643-1655.

BROOK, M. A., ZHAO, S., LIU, L. & CHEN, Y. 2011. Surface etching of silicone elastomers by depolymerization. *Canadian Journal of Chemistry,* 90**,** 153-160.

CAMPOS, L. M., KILLOPS, K. L., SAKAI, R., PAULUSSE, J. M. J., DAMIRON, D., DROCKENMULLER, E., MESSMORE, B. W. & HAWKER, C. J. 2008. Development of Thermal and Photochemical Strategies for Thiol‚àíEne Click Polymer Functionalization. *Macromolecules,* 41**,** 7063-7070.

CHEN, H., BROOK, M. A., SHEARDOWN, H. D., CHEN, Y. & KLENKLER, B. 2006. Generic bioaffinity silicone surfaces. *Bioconjugate Chemistry,* 17**,** 21-28.

CHEN, H., WANG, L., ZHANG, Y., LI, D., MCCLUNG, W. G., BROOK, M. A., SHEARDOWN, H. & BRASH, J. L. 2008. Fibrinolytic Poly(dimethyl siloxane) Surfaces. *Macromolecular Bioscience,* 8**,** 863-870.

CHEN, H., ZHANG, Z., CHEN, Y., BROOK, M. A. & SHEARDOWN, H. 2005. Protein repellant silicone surfaces by covalent immobilization of poly(ethylene oxide). *Biomaterials,* 26**,** 2391-2399.

CHEN, J. J., STRUK, K. N. & BRENNAN, A. B. 2011. Surface Modification of Silicate Glass Using 3-(Mercaptopropyl)trimethoxysilane for Thiol-Ene Polymerization. *Langmuir,* 27**,** 13754-13761.

CIESIELSKI, W. & ZAKRZEWSKI, R. 2006. Iodimetric titration of sulfur compounds in alkaline medium. *Chemia Analityczna,* 51**,** 653-678.

DEMERS, L. M., MIRKIN, C. A., MUCIC, R. C., REYNOLDS, R. A., LETSINGER, R. L., ELGHANIAN, R. & VISWANADHAM, G. 2000. A Fluorescence-Based Method for Determining the Surface Coverage and Hybridization Efficiency of Thiol-Capped Oligonucleotides Bound to Gold Thin Films and Nanoparticles. *Analytical Chemistry,* 72**,** 5535-5541.

DEMMING, S., LESCHE, C., SCHMOLKE, H., KLAGES, C.-P. & BÜTTGENBACH, S. 2011. Characterization of long-term stability of hydrophilized PEG-grafted PDMS within different media for biotechnological and pharmaceutical applications. *physica status solidi (a),* 208**,** 1301-1307.

DI VIRGILIO, V., BERMEJO, S. & CASTANER, L. 2011. Wettability Increase by "Corona" Ionization. *Langmuir,* 27**,** 9614-9620.

EFIMENKO, K., WALLACE, W. E. & GENZER, J. 2002. Surface modification of Sylgard-184 poly(dimethyl siloxane) networks by ultraviolet and ultraviolet/ozone treatment. *Journal of Colloid and Interface Science,* 254**,** 306-315.

EGWIM, I. O. C. & GRUBER, H. J. 2001. Spectrophotometric measurement of mercaptans with 4,4 '-dithiodipyridine. *Analytical Biochemistry,* 288**,** 188-194.

FRITZ, J. L. & OWEN, M. J. 1995. Hydrophobic recovery of plasma-treated polydimethylsiloxane. *Journal of Adhesion,* 54**,** 33-45.

GANDUBERT, V. J. & LENNOX, R. B. 2005. Assessment of 4-(dimethylamino)pyridine as a capping agent for gold nanoparticles. *Langmuir,* 21**,** 6532-6539.

HARANT, A. W., KHIRE, V. S., THIBODAUX, M. S. & BOWMAN, C. N. 2006. Thiol-ene photopolymer grafts on functionalized glass and silicon surfaces. *Macromolecules,* 39**,** 1461-1466.

HE, Q. G., LIU, Z. C., XIAO, P. F., LIANG, R. Q., HE, N. Y. & LU, Z. H. 2003. Preparation of hydrophilic poly(dimethylsiloxane) stamps by plasma-induced grafting. *Langmuir,* 19**,** 6982-6986.

HILL, H. D. & MIRKIN, C. A. 2006. The bio-barcode assay for the detection of protein and nucleic acid targets using DTT-induced ligand exchange. *Nature Protocols,* 1**,** 324-336.

HILLBORG, H. & GEDDE, U. W. 1998. Hydrophobicity recovery of polydimethylsiloxane after exposure to corona discharges. *Polymer,* 39**,** 1991-1998.

HILLBORG, H., SANDELIN, M. & GEDDE, U. W. 2001. Hydrophobic recovery of polydimethylsiloxane after exposure to partial discharges as a function of crosslink density. *Polymer,* 42**,** 7349-7362.

HILLBORG, H., TOMCZAK, N., OLAH, A., SCHONHERR, H. & VANCSO, G. J. 2004. Nanoscale hydrophobic recovery: A chemical force microscopy study of UV/ozone-treated cross-linked poly(dimethylsiloxane). *Langmuir,* 20**,** 785-794.

HOEK, I., THO, F. & ARNOLD, W. M. 2010. Sodium hydroxide treatment of PDMS based microfluidic devices. *Lab on a Chip,* 10**,** 2283-2285.

HOYLE, C. E. & BOWMAN, C. N. 2010. Thiol-Ene Click Chemistry. *Angewandte Chemie-International Edition,* 49**,** 1540-1573.

HOYLE, C. E., LEE, T. Y. & ROPER, T. 2004. Thiol-enes: Chemistry of the past with promise for the future. *Journal of Polymer Science Part a-Polymer Chemistry,* 42**,** 5301-5338.

HU, S. W., REN, X. Q., BACHMAN, M., SIMS, C. E., LI, G. P. & ALLBRITTON, N. 2002. Surface modification of poly(dimethylsiloxane) microfluidic devices by ultraviolet polymer grafting. *Analytical Chemistry,* 74**,** 4117-4123.

HUI, A. Y. N., WANG, G., LIN, B. C. & CHAN, W. T. 2005. Microwave plasma treatment of polymer surface for irreversible sealing of microfluidic devices. *Lab on a Chip,* 5**,** 1173-1177.

JONKHEIJM, P., WEINRICH, D., KÖHN, M., ENGELKAMP, H., CHRISTIANEN, P. C. M., KUHLMANN, J., MAAN, J. C., NÜSSE, D., SCHROEDER, H., WACKER, R., BREINBAUER, R., NIEMEYER, C. M. & WALDMANN, H. 2008. Photochemical Surface Patterning by the Thiol-Ene Reaction. *Angewandte Chemie,* 120**,** 4493-4496.

KHIRE, V. S., HARANT, A. W., WATKINS, A. W., ANSETH, K. S. & BOWMAN, C. N. 2006. Ultrathin patterned polymer films on surfaces using thiol-ene polymerizations. *Macromolecules,* 39**,** 5081-5086.

KHIRE, V. S., KLOXIN, A. M., COUCH, C. L., ANSETH, K. S. & BOWMAN, C. N. 2008. Synthesis, Characterization and Cleavage of Linear Polymers Attached to Silica Nanoparticles Formed Using Thiol-Acrylate Conjugate Addition Reactions. *Journal of Polymer Science, Part A: Polymer Chemistry,* 46**,** 6896-6906.

KHIRE, V. S., LEE, T. Y. & BOWMAN, C. N. 2007. Surface modification using thiol-acrylate conjugate addition reactions. *Macromolecules,* 40**,** 5669-5677.

KIM, J., CHAUDHURY, M. K. & OWEN, M. J. 2000. Hydrophobic Recovery of Polydimethylsiloxane Elastomer Exposed to Partial Electrical Discharge. *Journal of Colloid and Interface Science,* 226**,** 231-236.

LAFLEUR, J. P., KWAPISZEWSKI, R., JENSEN, T. G. & KUTTER, J. P. 2013. Rapid photochemical surface patterning of proteins in thiol-ene based microfluidic devices. *Analyst,* 138**,** 845-849.

LI, G. Z., RANDEV, R. K., SOERIYADI, A. H., REES, G., BOYER, C., TONG, Z., DAVIS, T. P., BECER, C. R. & HADDLETON, D. M. 2010. Investigation into thiol-(meth)acrylate Michael addition reactions using amine and phosphine catalysts. *Polymer Chemistry,* 1**,** 1196-1204.

MAKAMBA, H., KIM, J. H., LIM, K., PARK, N. & HAHN, J. H. 2003. Surface modification of poly(dimethylsiloxane) microchannels. *Electrophoresis,* 24**,** 3607-3619.

MAZUTIS, L., GILBERT, J., UNG, W. L., WEITZ, D. A., GRIFFITHS, A. D. & HEYMAN, J. A. 2013. Single-cell analysis and sorting using droplet-based microfluidics. *Nat. Protocols,* 8**,** 870-891.

MEINCKEN, M., BERHANE, T. A. & MALLON, P. E. 2005. Tracking the hydrophobicity recovery of PDMS compounds using the adhesive force determined by AFM force distance measurements. *Polymer,* 46**,** 203-208.

MORRA, M., OCCHIELLO, E., MAROLA, R., GARBASSI, F., HUMPHREY, P. & JOHNSON, D. 1990. On the aging of oxygen plasma-treated polydimethylsiloxane surfaces. *Journal of Colloid and Interface Science,* 137**,** 11-24.

RIENER, C. K., KADA, G. & GRUBER, H. J. 2002. Quick measurement of protein sulfhydryls with Ellman's reagent and with 4,4'-dithiodipyridine. *Analytical and Bioanalytical Chemistry,* 373**,** 266-276.

SCOTT, A. F., GRAY-MUNRO, J. E. & SHEPHERD, J. L. 2010. Influence of coating bath chemistry on the deposition of 3-mercaptopropyl trimethoxysilane films deposited on magnesium alloy. *Journal of Colloid and Interface Science,* 343**,** 474-483.

SUI, G. D., WANG, J. Y., LEE, C. C., LU, W. X., LEE, S. P., LEYTON, J. V., WU, A. M. & TSENG, H. R. 2006. Solution-phase surface modification in intact poly(dimethylsiloxane) microfluidic channels. *Analytical Chemistry,* 78**,** 5543-5551.

TANGPASUTHADOL, V., PONGCHAISIRIKUL, N. & HOVEN, V. P. 2003. Surface modification of chitosan films.: Effects of hydrophobicity on protein adsorption. *Carbohydrate Research,* 338**,** 937-942.

VAN DER HEIDE, P. 2011. *X-ray Photoelectron Spectroscopy An Introduction to Principles and Practices,* Wiley, New York.

XIAO, D., ZHANG, H. & WIRTH, M. 2002. Chemical Modification of the Surface of Poly(dimethylsiloxane) by Atom-Transfer Radical Polymerization of Acrylamide. *Langmuir,* 18**,** 9971-9976.

ZHANG, Z., WANG, J., TU, Q., NIE, N., SHA, J., LIU, W., LIU, R., ZHANG, Y. & WANG, J. 2011. Surface modification of PDMS by surface-initiated atom transfer radical polymerization of water-soluble dendronized PEG methacrylate. *Colloids and Surfaces B: Biointerfaces,* 88**,** 85-92.

ZHOU, F., LIU, W., CHEN, M. & SUN, D. C. 2001. A novel way to prepare ultra-thin polymer films through surface radical chain-transfer reaction. *Chemical Communications,* 23**,** 2446-2447.

CHAPTER 3: Reductive degradation of lignin and model compounds by hydrosilanes[§]

3.1 Abstract

The exploitation of lignin, the second most abundant naturally occurring polymer on earth, has been hampered by its network structure, which makes it difficult to process. Hydrosilanes have previously been shown to convert aryl ethers to hydrolyzable silyl ethers in the presence of $B(C_6F_5)_3$. We demonstrate that the process is general and can be used to convert model lignin compounds to both aryl silyl ethers and alkanes. The relative reactivity of functional groups on model lignin compounds was found to be: phenol > primary alcohol > methoxybenzene > alkyl silyl ethers. The process thus leads to cleavage of β-O-4, α-O-4, and methoxybenzene groups with concomitant silylation of phenolic and secondary alcohol groups. At longer time points provided sufficient silane was present, the full reduction of primary and secondary alcohols to alkyl groups was observed. Softwood lignin itself could only be partially solubilized (~ 30%) even using excess hydrosilane and high catalyst loadings: the products were not characterized in

---

[§] This chapter is reproduced from Jianfeng Zhang, Yang Chen, Michael A. Brook, in *ACS Sustainable Chemistry & Engineering*, **2014**, 2, 1983-1991 with permission from American Chemical Society Publications, 2014. Jianfeng Zhang designed the experimental procedure and performed all experiments with suggestion from Dr. Chen. Jianfeng Zhang wrote the majority of the manuscript with additions, edits and guidance provided by Dr. Brook.

detail. The lack of further degradation was attributed to its highly branched network structure containing 5-5, β-5, and 4-O-5 and other linkages derived from coniferyl alcohol monomers that are not susceptible to reductive silylation. By contrast, over 95% of hardwood lignin was efficiently reduced/degraded into organosoluble products by the monofunctional hydrosilane $HMe_2SiOSiMe_3$ over a few hours at 50 °C. The molecular weight of the silylated products was consistent with oligomeric structures comprised of 3-8 linked aryl groups. This process holds promise to increase the accessibility to value-added products using lignin as a starting material.

3.2 Introduction

Lignin is a complex polymeric network that works as a glue to bind and integrate the cellulose and hemicelluloses to form cell walls in plants. The biosynthesis of lignin essentially involves the oxidative polymerization of the three monomers: p-coumaryl alcohol, coniferyl alcohol (G), and sinapyl alcohol (S) (Scheme 3.1).(Adler, 1977, Heitner et al., 2010) A variety of subtle differences exist between the lignins produced by different organisms. For example, the ratio of these basic building units found in lignin depends on its source.(Heitner et al., 2010) The lignin derived from grass and softwood trees contains larger amounts of coniferyl alcohol units resulting in a more highly branched structure (Scheme 3.1). By contrast, hardwood lignin generally consists of approximately equal amounts of coniferyl and sinapyl alcohol units, resulting in a more linear structure.(Heitner et al., 2010, Evtuguin et al., 1998, Zakzeski et al., 2010)

Although lignin is the second most abundant naturally occurring polymer on the earth, with few exceptions it is not effectively used as a resource in industry. In the natural environment, the majority of lignin is degraded, and then recycled as resource for carbon.(Leonowicz et al., 1999) In industry, by contrast, due to the difficulties associated with processing lignin, it is generally used as a comparatively low-value fuel.(Gosselink et al., 2004) In spite of significant efforts, lignin is therefore not a feedstock chemical for the 'biorefinery,' with the exception of vanillin, which may be obtained by extraction from spent sulfite liquors in Kraft pulping plants.(Hocking, 1997, Pearl, 1942, Araújo et al., 2010)

Various methods, including biological, thermochemical, and catalytic reduction/degradation, have been explored to convert lignin into value-added chemicals:(Pandey and Kim, 2011, Zakzeski et al., 2010, Hatakka, 2005) the biodegradation of lignin has been comprehensively reviewed.(Jouanin and Lapierre, 2012, Hisano et al., 2009, Perez et al., 2002) Thermochemical methods for lignin degradation include pyrolysis, hydrogenolysis, hydrolysis, gasification, and thermal oxidation.(Brebu and Vasile, 2010, Pandey and Kim, 2011) These methods usually are associated with harsh temperature and pressure and rather poor efficiencies.

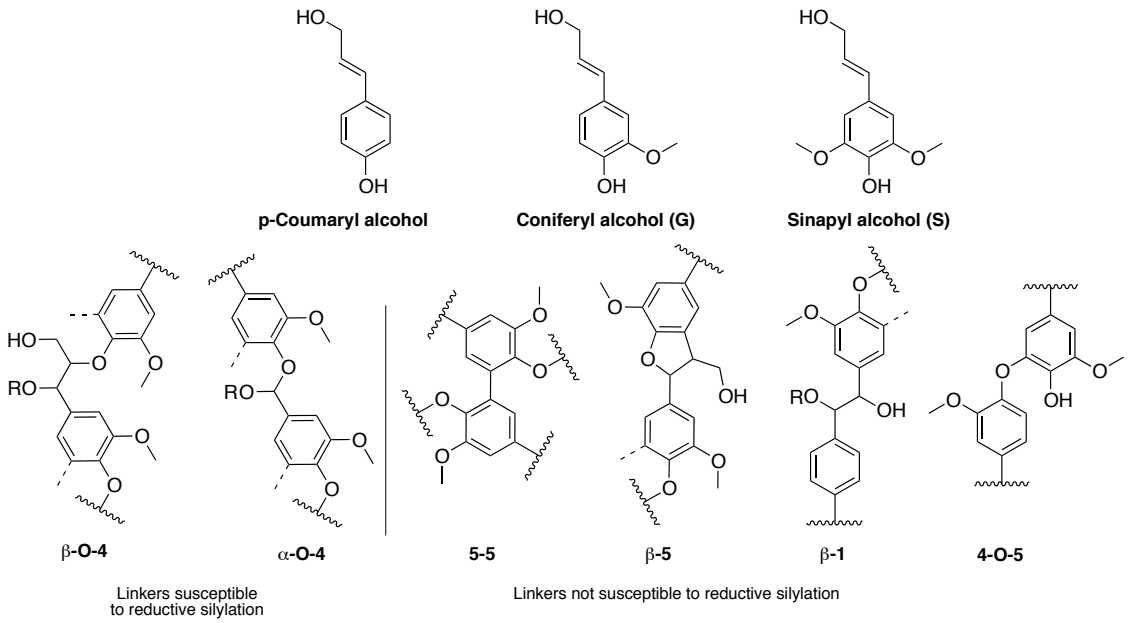

Scheme 3.1 The three basic building units for lignin and some representative linkages found in lignin.

Catalytic processes would be expected to be able to convert lignin efficiently under mild conditions.(Zakzeski et al., 2010) Although many catalysts have been developed and proved to efficiently degrade lignin model compounds,(Zakzeski et al., 2010, Sergeev and Hartwig, 2011) few of them are able to degrade actual lignin with good conversion. Notable exceptions to this include the work of Yan et al., who achieved 42% conversion of lignin using a platinum catalyst.(Yan et al., 2008) Higher conversions were reported by using Ni-Mo (49-71%) or Cu-CrO (70% of lignin)(Harris et al., 1938, Oasmaa et al., 1993) under rather vigorous thermal conditions. More efficient reduction of alkyl aryl and diaryl ethers could be achieved with Ni-catalyzed protocols, which are potentially beneficial in the degradation of softwood lignin, but temperatures in excess of 100 °C and

longer reaction times are required.(Álvarez-Bercedo and Martin, 2010, Cornella et al., 2013, Sergeev and Hartwig, 2011)

$B(C_6F_5)_3$ (tris(pentafluorophenyl)borane), has been widely used as a catalyst for the reduction of organic compounds.(Berkefeld et al., 2010, Piers, 2005) Functional groups including alcohols, aldehydes, ketones, carboxylic acids, and esters are reduced to silyl ethers and then, if sufficient hydrosilane is present, to alkanes, depending the reducing activity of the chosen hydrosilane (Scheme 3.2).(Parks and Piers, 1996, Parks et al., 2000, Gevorgyan et al., 2000, Gevorgyan et al., 2001) Alkoxyphenyl and phenol groups are also converted to aryl silyl ethers.(Cella and Rubinsztajn, 2008, Gretton et al., 2011, Brook et al., 2011) In light of the structural analogy between these phenolic compounds and the functional aromatic rings and aliphatic alcohols found in lignin, we have examined the ability of this reductive silylation reaction to reduce model compounds of lignin and polymeric samples of hardwood and softwood lignin. A study of degradation of selected model lignin compounds was recently published,(Feghali and Cantat, 2014) based on previously described silylation studies,(Fedorov et al., 2013) which showed that many of the functional groups found on lignin are susceptible to these reducing conditions. We describe the reduction of model compounds, relatively reactivity of the functional groups that are found on model lignin compounds and, more importantly, examine the ability of these reducing conditions to convert mostly insoluble hardwood lignin into smaller, silylated, organosoluble oligomers.

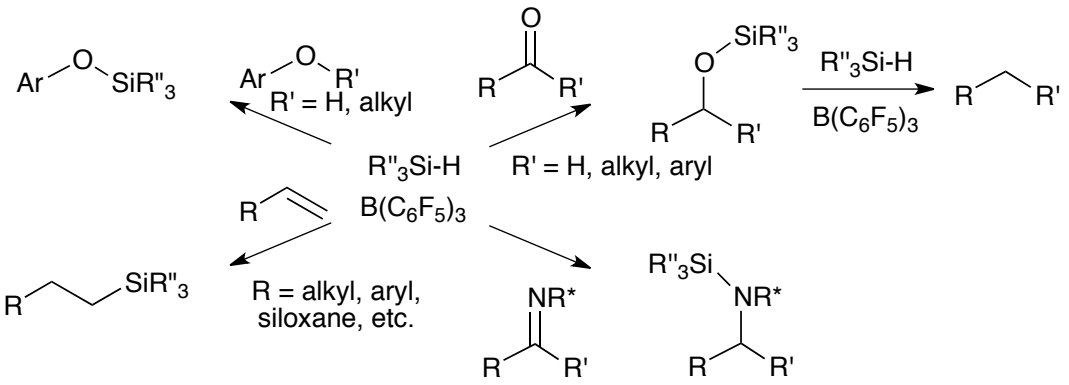

Scheme 3.2 Facile reduction of organofunctional groups using hydrosilanes catalyzed by $B(C_6F_5)_3$.

3.3 Experimental

3.3.1 Materials

Lignin model compounds: 3-hydroxy-4-methoxybenzyl alcohol, 3-phenyl-1-propanol, 1-phenyl-2-propanol, sinapyl alcohol, 2-phenoxy-1-phenylethanol, guaiacylglycerol-beta-guaiacyl ether, diphenyl ether, and benzyl phenyl ether were purchased from Sigma-Aldrich and used as received. Hydrosilanes: pentamethyldisiloxane (PMDS), dimethylphenylsilane (Me_2PhSiH), methyldiphenylsilane ($MePh_2SiH$), triethylsilane (Et_3SiH), and poly(hydromethylsiloxane) ($Me_3Si(OSiMeH)_nOSiMe_3$, PHMS) were purchased from Gelest. Solvents were purchased from Caledon Laboratories and used after drying over activated alumina. The catalyst, $B(C_6F_5)_3$ (Sigma-Aldrich), was dissolved in dry toluene to prepare a stock solution (40 mg/mL, 78.13 mM). Tetra-*n*-butylammonium fluoride (TBAF, Sigma-

Aldrich) was dissolved in THF containing 1% of methanol (TBAF in THF solution, 0.01 mg/ml). Hardwood lignin (Kraft lignin isolated by FPInnovations Lignoforce Technology)(Kouisni et al., 2012) was provided by FPInnovations, Montreal, Canada and softwood lignin was provided by Weyerhaeuser, Tacoma, Washington, USA and used after partial drying in a desiccator under vacuum over Dri-rite.

3.3.2 Methods

NMR spectra were recorded on a Bruker Avance 600 MHz nuclear magnetic resonance spectrometer using chloroform-*d* or DMSO-d_6. The proton impurity of the deuterated solvent was used as a reference for ^{1}H NMR spectra (for chloroform = 7.24ppm, for DMSO = 2.50). For model compounds, 16 scans were sufficient for the ^{1}H NMR, while for lignin samples 128 scans were needed for ^{1}H NMR and 2048 for ^{13}C NMR.

Molecular weights were established by gel permeation chromatograph using a Waters 590 HPLC pump with three Waters Styragel columns (HR2, HR3, and HR4) at 40 °C, and a Waters 410 differential refractometer operating at 35 °C (Table 3.1). The eluent, at a flow rate of 0.5 ml/min, was 50 mM LiBr dissolved in *N,N*-dimethylformamide (DMF) and the system was calibrated with PEG standards (Waters) with molecular weights ranging from 600 to 252,000 g/mol.

Table 3.1 Molecular weight profile[a] of lignin before and after reduction.

	Mn	Mw
Hardwood lignin	3640	30860
Reduced, then desilylated, hardwood lignin fragments[b]	440	465

[a] Solvent: DMF containing 50 mM LiBr determined using poly(ethylene oxide) standards. [b] After reduction, the silyl ethers were removed by treatment with TBAF (see also Appendix, Figure 7.26). Note, these values are below the lowest calibration standard (600 MW) and are thus estimates.

The silylated derivatives of lignin model compounds were additionally characterized by molecules were characterized by GC/MS using an Agilent 6890N GC coupled to an Agilent 5973N Mass Selective Detector (MSD) run in EI mode. The GC flow rate was 1mL/min through a column (DB17-ht 30m length x 0.25mm ID, 0.15um film thickness - a 50/50 mix of methyl/phenyl silicone phase).

Infrared spectroscopy was used to characterize the functional group change during the degradation of hardwood lignin by running under diffuse reflectance infrared Fourier transform mode (DRIFTS, Thermo Nicolet 6700, scan number = 64, resolution = 4 cm^{-1}).

3.3.3 Reduction of lignin model compounds

The reaction conditions for reduction of model lignin compounds are given in Table 3.2. The general experimental procedure is as follows. The model compound was dissolved in an appropriate solvent (dry toluene, hexane or chloroform), to which was added the hydrosilane. Then the catalyst solution was added to initiate the reaction. The mixture was sonicated in a 50 °C water bath for 3 h. After reaction, neutral alumina (~1 g)

was added to facilitate removal of the catalyst. The resultant solution was filtered, purified by silica chromatography, and the appropriate fractions concentrated under reduced pressure. The products were examined using ^{1}H-NMR and GC-MS.

Table 3.2 The reaction conditions and yields of model compounds.

	Model compound (mmol)	PMDS (mmol)	$B(C_6F_5)_3$ (μmol)[a]	mL[b] (solvent)	Yield[c]
3-Phenyl-1-propanol	3.62	11.28	9.77	1 (H)	72 %[d]
1-Phenyl-2-propanol	3.79	12.03	9.77	1 (H)	70 %[e]
Sinapyl alcohol	0.143	10.0	0.98	3 (T)	NA[f]
2-Phenoxy-1-phenylethanol	0.08	1.03	2.73	1 (H)	64 %[e]
3-Hydroxy-4-methoxybenzyl alcohol	3.23	16.33	9.77	3 (T)	86 %[e]
Benzyl phenyl ether	2.72	5.02	15.63	1 (H)	70 %[e]
Guaiacylglycerol-beta-guaiacyl ether	0.006	5.0	0.4	3 (T)	> 90 %[g]
Diphenyl ether	4.25	10.33	11.67	1 (T)	NR[h]

[a] For model compounds, catalyst loadings ranged from about 0.01-0.3mol%. [b] Solvent: (H) = hexane, (T) = toluene. [c] Note: conversion by NMR exceeded 90% in all cases. [d] It was not possible to separate the silicone from the propylbenzene products by silica chromatography. The yield is based on mass recovered and the NMR, which showed only two products (see Appendix Figure 7.14). [e] Yield of the silyl ether. The alkylbenzene was lost during evaporation. [f] A complex mixture of products was isolated including hydrosilylation of the alkene, partial and complete reduction the alkene. [g] Yield estimated from NMR; the outcome was limited by the small scale reaction (~ 2 mg). [h] No reaction was observed when diphenyl ether was treated with PMDS and $B(C_6F_5)_3$.

3.3.4 Reduction of lignins

Softwood and hardwood lignin samples were separately treated using the same protocol. Lignin (low water content <5%, powdered, average particle size = 45 +/- 10 micron) was dispersed in dry toluene and then mixed with the appropriate hydrosilane and $B(C_6F_5)_3$. Extensive experimentation was used to optimize the reduction conditions (Table 3.3). In particular, this involved the catalyst concentration, the concentration of SiH groups in structurally different silanes, and solvents. The suspension was sonicated in a 50 °C water bath for 3 h. The residual undissolved lignin material was washed with toluene and separated by centrifugation (Thermo, Durafuge 100, at 4000 rpm for 20 min). This process was repeated at least three times to completely extract soluble compounds. The supernatants were mixed, and the solvent was removed under reduced pressure. Both the residual and reduced lignin products were examined with ^{1}H-NMR, ^{13}C-NMR, and GPC for hardwood lignin.

Table 3.3 The reaction conditions for degradation of hard- and softwood lignin.

Type of lignin	Starting mass of lignin (mg)	Isolated/ residual products[a] (mg)	Solubilization efficiency[b] (%)	Hydrosilane (mL)	$B(C_6F_5)_3$ vol (μL)	$B(C_6F_5)_3$ wt%[d]	Toluene (mL)
Softwood	87.1	91.4	-[c]	PMDS (6)	108	5	20
	99.3	109.0	-[c]	PMDS (6)	248	10	20
	108	88.6	18.0%	Me_2PhSiH (6)	264	10	20
	49.6	56.7	-[c]	$MePh_2SiH$ (3)	132	10	10
	50.2	97.2	-[c]	PHMS (3)	132	10	10
	53.7	37.8	29.6%	Et_3SiH (3)	132	10	10
Hardwood	122.9	90.2	26.6%	PMDS (8)	30.7	1	50
	163.0	92.4	43.3%	PMDS (10)	200	5	70
	41.1	2.8	93.2%	PMDS (3)	60	6	15
	157.4	6.9	95.5%	PMDS (10)	394	10	70

[a] A decrease in weight of isolated product compared to starting lignin reflects the formation of organosoluble materials. [b] (1 - Final insoluble weight/starting insoluble weight) x 100. [c] Data could not obtained because the mass of silylated isolated product was higher than the mass of starting lignin. [d] Catalyst concentrations (wt%, weight of catalyst/weight of lignin × 100) ranged from 1-10%. Additional experimentation (data not shown) demonstrated there was a large change in efficiency of reduction starting at about 6wt% catalyst.

The efficiency of the reduction/degradation of lignin samples was found to strongly depend on catalyst concentration. A separate suite of experiments was used to probe the

change in reduction with catalyst concentration. Hardwood lignin was exposed to the reduction conditions with catalyst concentrations starting from 2wt% $B(C_6F_5)_3$ (52.5 μL catalyst containing 2.1 mg of $B(C_6F_5)_3$) for 105 mg of lignin in 20 mL toluene with 6 mL PMDS) up to 10.2wt% catalyst. Each batch of lignin was allowed to react for a given period of time, separated from the reaction mixture by centrifugation at 4000 rpm for 20 min (Thermo, Durafuge 100), decanted and washed with toluene. For some samples, following this reaction sequence, the residue was subjected to secondary reduction using additional catalyst ($B(C_6F_5)_3$ 105 μL catalyst,) in toluene (20 mL) and PMDS (6 mL) to first 5.8wt% and, after an additional wash sequence, a third reduction with 10.2wt% catalyst (Appendix, Figure 7.22). For each reaction step, reduction was carried out for 3 h sonication in a 50 °C water bath, the suspension was centrifuged, then washed and recentrifuged (repeated three times). The combined supernatants (from each of the four centrifugations) were combined and purified by removing the solvent by rotary evaporation. Both solid and soluble residues, after evaporation of solvents, were characterized by NMR and FT-IR.

During reduction of hardwood lignin with hydrosilanes, the lignin fragments become partially silylated, typically on phenolic residues. The groups were desilylated by treatment with TBAF solution (dissolved in THF containing 1% methanol) for 48 h. The solvent and siloxane fragments were removed by using a rotary evaporator; and the TBAF was removed by washing the residue with distilled water. After this purification, the sample was dried under vaccum overnight.

3.4 Results and Discussion

A suite of model lignin compounds was chosen, as broadly as possible, to match the functional group patterns found in native lignin. The functional groups present included primary, secondary, allylic, and benzylic alcohols; methoxybenzene and other alkoxybenzenes; and a conjugated alkene. As shown in Scheme 3.3, the ability of $B(C_6F_5)_3$ and Si-H, in the form of PMDS, to reduce these functional groups was explored using a catalyst loading of 0.01-0.3mol%. Each reaction was optimized to use as little catalyst as possible and still have efficient reactions that would be completed within 0.5 h (Table 3.2).(Pandey and Kim, 2011, Owen et al., 2012, Zakzeski et al., 2010) A small amount of organic solvent was added to facilitate the reaction. A large molar excess of PMDS was used both to accelerate the process and because a side reaction leading to silicone polymers competes under these conditions (see below).

Hydrosilanes in the presence of $B(C_6F_5)_3$ efficiently reduced both alcohols and aryl ethers (Scheme 3.3): aliphatic primary, secondary and allylic alcohols were reduced completely to the corresponding alkanes. For example, 3-phenyl-1-propanol was reduced to *n*-propylbenzene, and ethylbenzene was produced from the reduction of 2-phenoxy-1-phenylethanol (Appendix, Figure 7.12). In the case of 1-phenyl-2-propanol, only partial reduction of the alcohol was initially observed under the conditions used (Appendix, Figure 7.13). Secondary silyl ethers are much more resistant to reduction to the alcohol than primary ethers.(Gevorgyan et al., 2000, Gevorgyan et al., 1999) However, the secondary silyl ether could be further reduced to the alkane if a larger excess of

hydrosilane and/or a longer reaction time was used (Appendix, Figure 7.13). The allylic alcohol of sinapyl alcohol was also cleanly reduced to the alkane, a process that was accompanied by partial hydrosilylation of the alkene leading to an inseparable mixture of regioisomeric products (Appendix, Figure 7.18).

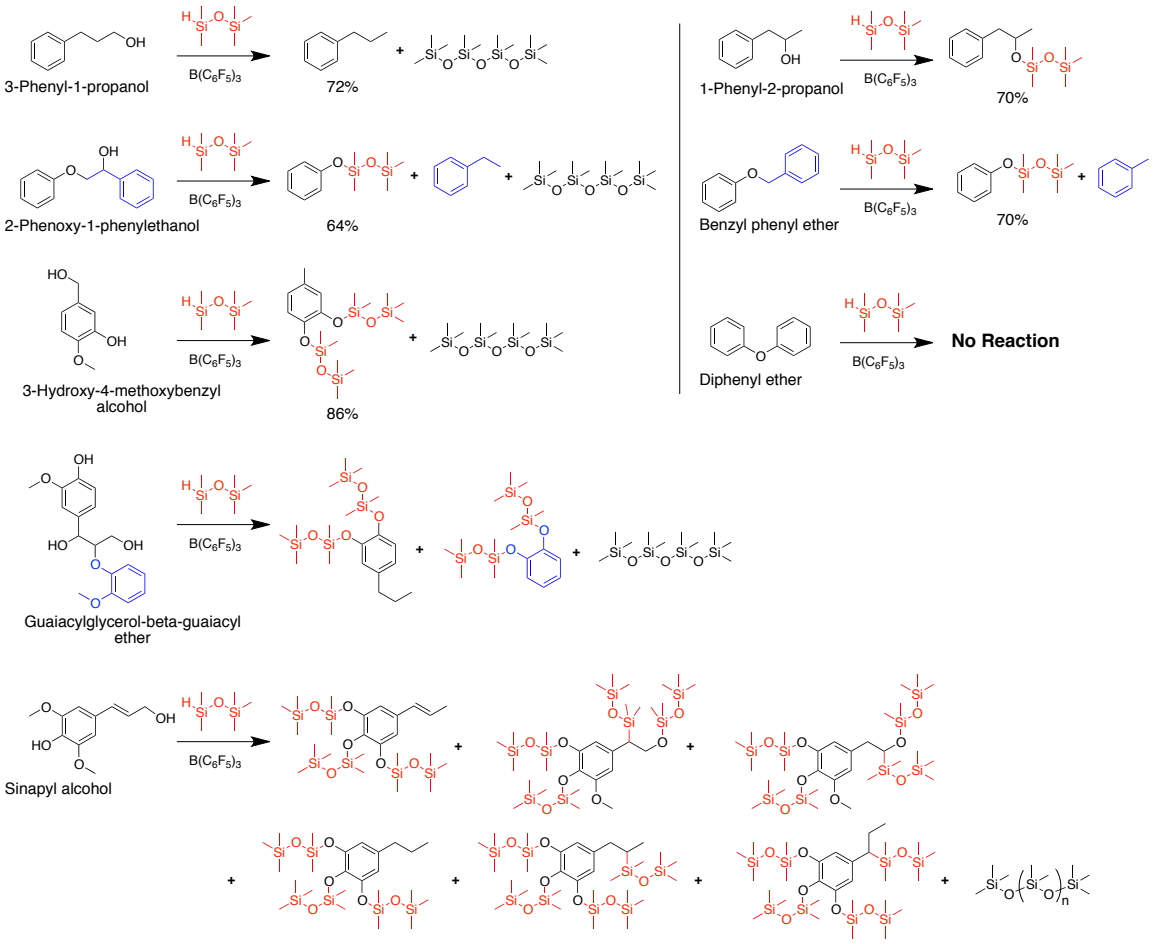

Scheme 3.3 Reaction of model lignin compounds with PMDS in presence of $B(C_6F_5)_3$.

The ether bond between two aromatic rings (corresponding to 4-O-5 linkage in lignin, Scheme 3.1) was not reduced under these conditions: when diphenyl ether was treated with PMDS and $B(C_6F_5)_3$ there was no change in the ^{1}H-NMR and ^{13}C-NMR spectra (Appendix, Figure 7.17). However, aryl alkyl ethers and phenols were cleanly converted into phenyl silyl ethers under the reaction conditions, forming hydrogen or methane byproducts, respectively. This was clearly observed in the reduction of 3-hydroxy-4-methoxybenzyl alcohol (Appendix, Figure 7.16). Most important when developing processes to degrade lignin is the ability to cleave the phenyl/alkyl ethers that bridge aromatic residues. The reduction of benzyl phenyl ether demonstrated that α-O-4 linkages (Scheme 3.1) could be easily cleaved, and the β-O-4 linkage in 2-phenoxy-1-phenylethanol was cleaved even though there was no functional group in the γ position, as previously reported.(Feghali and Cantat, 2014)

The relative reactivity of different groups that present in lignin was determined using the model multifunctional compound 3-hydroxy-4-methoxybenzyl alcohol. Staged reductions were achieved by sequentially adding molar equivalents of the hydrosilane. The phenolic alcohol was found to be more reactive than the other functional groups (Scheme 3.4, and Appendix, Figure 7.16). Additional hydrosilane then led to the stepwise loss of the benzylic alcohol and then the methoxy-benzene group. While the aliphatic ether was finally reduced to the alkane, the aryl silyl ether was stable under these conditions, as has previously been reported.(Gevorgyan et al., 2000)

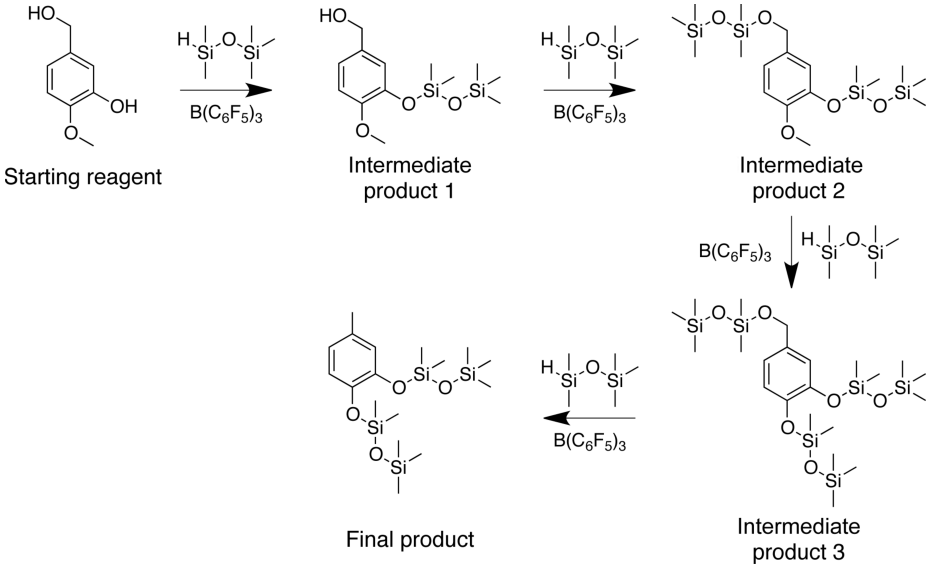

Scheme 3.4 Staged reduction of 3-hydroxy-4-methoxybenzyl alcohol. The relative reactivity order: phenol > primary alcohol > methoxybenzene > aliphatic silyl ether >> aromatic silyl ether.

Guaiacylglycerol-beta-guaiacyl ether is a model compound with a structure that is particularly closely related to lignin polymers, and is therefore widely used as a representative model compound.(Owen et al., 2012, Zakzeski et al., 2010) Compared to guaiacylglycerol-beta-guaiacyl ether, a huge molar excess of PMDS (Table 3.2) was used order in to mimic the conditions that were necessary for actual lignin degradation (see below). The β-O-4 linkage, which is an important primary linkage in lignin, was cleaved efficiently using PMDS in the presence of $B(C_6F_5)_3$. In addition, the methoxybenzene and phenolic groups were converted to aryl silyl ethers, and both the primary aliphatic and benzylic alcohols were reduced to alkanes via the silyl ether (vide infra).

Figure 3.1 shows the ^{1}H-NMR spectra of guaiacylglycerol-beta-guaiacyl ether before and after degradation. The methoxy groups in the starting compound were found at 3.85 ppm; and the peaks for α, β and γ protons (with respect to the aryl ring) were found at 5.57, 4.96, and 3.64 ppm, respectively. After degradation, the methoxy groups had completely disappeared (via methane formation), while the peaks of α, β and γ protons shifted to 2.45, 1.6, and 0.9 ppm, respectively. The two products shown were also identified by GC/MS (Appendix, Figure 7.19). These findings suggested that lignin itself could be reduced into much smaller oligomeric structures under these conditions. To test this hypothesis, we examined the reaction with both softwood and hardwood lignin.

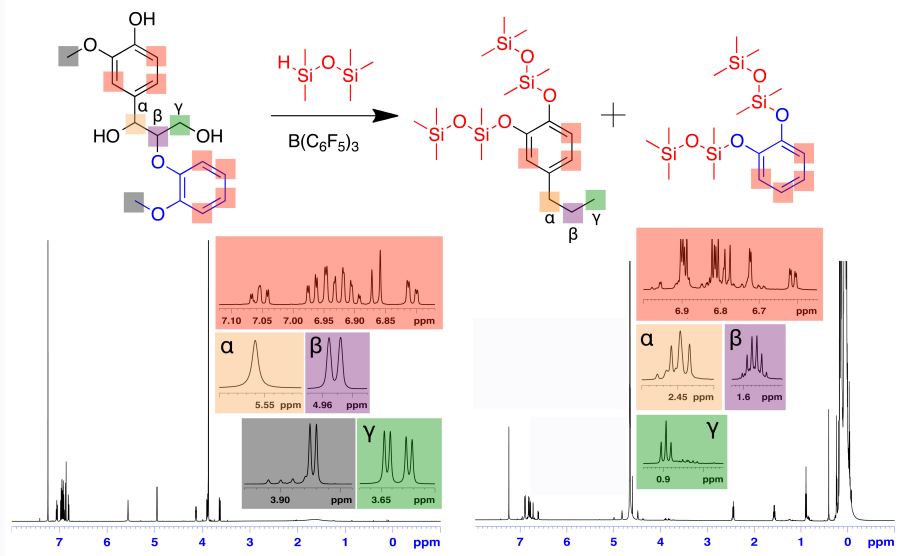

Figure 3.1 ^{1}H-NMR of guaiacylglycerol-beta-guaiacyl ether and its silylated products (solvent $CDCl_3$).

Extensive attempts were made to render softwood lignin organosoluble by reducing/degrading it with hydrosilanes in the presence of $B(C_6F_5)_3$ using the conditions optimized for model compounds. However, after reaction in a 50 °C water bath for 3 hours, with sonication to facilitate both reagent ingress and lignin particle degradation, suspensions of softwood lignin in neat disiloxane PMDS containing $B(C_6F_5)_3$ (up to 10wt%) exhibited no visible changes (Appendix, Figure 7.23). Less than 10% by weight of the lignin was converted to organosoluble materials, as determined by collection and evaporation of the supernatant after centrifugation. Attempts were therefore made to degrade the softwood lignin using hydrosilanes with different chemical structures, such as monomeric $MePh_2SiH$ and Me_2PhSiH (both aromatic, similar to lignin monomers), Et_3SiH (different steric hindrance), and polymeric PHMS (high density of reducing functional groups). Although all the silanes (PMDS, $MePh_2SiH$, and PHMS) led to some reduction (Table 3.3, and Appendix, Figure 7.25), there was only a modest increase in the fraction of organosoluble products. The small organosilanes Me_2PhSiH (~ 13% converted to soluble products) and Et_3SiH (~ 30% converted to soluble products) were only marginally better at breaking down the lignin into organosoluble products than PMDS. This might be associated with improved solubility of these hydrosilanes in lignin. The impact of catalyst concentration on silylation efficiency with the silanes was also studied. However, increasing the catalyst concentration up to 10wt% did not lead to further improvements in conversion (Table 3.2).

The insoluble fraction of all the softwood lignin reduction reactions often exhibited weight gain, consistent with silylation of the surface functional groups but not the required removal of cross-links. Silylation was also qualitatively observed through the enhanced water repellency of the modified surface: the insoluble product would float on, but not disperse in, water.

Given that the desired efficient degradation of softwood lignin was not observed, the product characterization was limited to ensuring that reduction had actually taken place. For the most efficient degradation, performed with Et_3SiH, the organosoluble product mixture was further characterized with ^{1}H-NMR and ^{13}C-NMR (Appendix, Figure 7.25). The chemical shifts for oxygenated aliphatic protons (near 4 ppm) in the ^{1}H-NMR of softwood lignin disappeared, while new peaks associated with aliphatic protons ranging from 0 to 2 ppm were observed. Also, new signals for the reduced carbon were found ranging from 10 to 30 ppm in ^{13}C-NMR.

Thus, reductive silylation and degradation of softwood lignin are occurring, but not nearly as efficiently as would be expected from the model compound studies. The challenge of efficiently degrading softwood lignin by reduction may be attributed to its chemical structure. G units are more abundant than S units in softwood lignin.(Adler, 1977) Many linkages associated with G units exhibit direct carbon chain connectivity or a single oxygen between aryl groups, neither of which is susceptible to reductive silylation. Linkages such as 5-5, β-5, β-1, and 4-O-5 (Scheme 3.1) that are not expected to react under these relatively mild conditions (as shown by the model study with diphenyl ether),

will also impede fragmentation and, simultaneously the ingress of reagents.(Zakzeski et al., 2010, Heitner et al., 2010) In light of the inability to encourage efficient degradation of softwood lignin, the objective of this work, we turned to hardwood lignin.

Hardwood lignin was much more easily reduced/degraded than softwood lignin by hydrosilanes in the presence of $B(C_6F_5)_3$. The process was found to be dependent on the chemical structure of the hydrosilane and the catalyst and hydrosilane concentrations. Using the protocol described above for model compounds, PMDS, a monofunctional low viscosity Si-H bearing disiloxane, was found to be suitable for hardwood reduction/degradation. Unlike the model compounds, a large excess of the reagent was necessary to reduce raw lignin. The reaction productivity was highly dependent on catalyst concentration. When the catalyst was present below 5wt% (weight ratio $B(C_6F_5)_3$ to mass of raw lignin), up to about 43% of the lignin could be reduced/degraded to soluble materials, while at higher catalyst concentrations, starting at 6%, over 90% of the lignin could be converted into organic solvent-soluble materials. These experiments were repeated several times and always showed this dependence of reactivity near 5wt% $B(C_6F_5)_3$. The behavior may be ascribed to a variety of factors. Any Lewis bases present in the medium, including water, competitively complex with $B(C_6F_5)_3$. Any such complexation reduces the effective concentration of active catalyst. The moisture content of the lignin is near 5wt%, which on a molar basis is a large excess compared the concentration of $B(C_6F_5)_3$. In addition, a secondary reaction catalyzed by $B(C_6F_5)_3$ that occurs with the silanes will reduce the available catalyst for the desired reaction. Growth

of linear silicone chains, with concomitant formation of volatile Me_2SiH_2, occurs under these conditions (2 $Me_3SiOSiMe_2H$ → Me_2SiH_2 + $Me_3SiOSiMe_2OSiMe_3$ → longer polymers. For GC/MS, see sinapyl alcohol reduction in the Appendix, Figure 7.18).(Chojnowski et al., 2006)

At the higher catalyst concentrations, the turbid, black suspension typical of the lignin starting materials gave way to a clear light amber colored solution (Appendix, Figure 7.24). The reaction was also much faster than with softwood lignin. For example, a hardwood lignin suspension containing 6% catalyst changed from brown opaque to yellow translucent after only 10 to 20 min of sonication at room temperature, whereas no obvious change in turbidity was observed up to 6 h of treatment of the softwood lignin (Appendix, Figure 7.23).

After reduction/degradation, the hardwood lignin was converted into organosoluble fragments. The starting hardwood lignin, which showed molecular weights ranging up to 3600 g mol^{-1}, was converted, after reduction and then desilylation using TBAF (tetrabutylammonium fluoride),(Ankala and Fenteany, 2002) to fragments of less than 600 g mol^{-1} (DMF with LiBr was used as solvent, Appendix, Figure 7.26). Figure 3.2A shows a model of structural changes of lignin that can occur during the degradation. In the ^{13}C-NMR, as shown in Figure 3.2B (a), signals for the α/β carbons of β-O-4 and methyl carbons of phenyl methyl ethers in the starting lignin could be found in the range from 70-90 and 50-60 ppm.(Hawkes et al., 1993, Wen et al., 2013) However, after reduction by PMDS (Figure 3.2B (b)), the intensity of these signals was reduced with the

concomitant formation of signals ranging from 10-40 ppm (alkyl groups) and near 0 ppm (silyl groups). Thus, the cleavage of β-O-4 linkers, reduction/silylation of α/γ alcohol, and silylation of phenyl methyl ethers occurred.

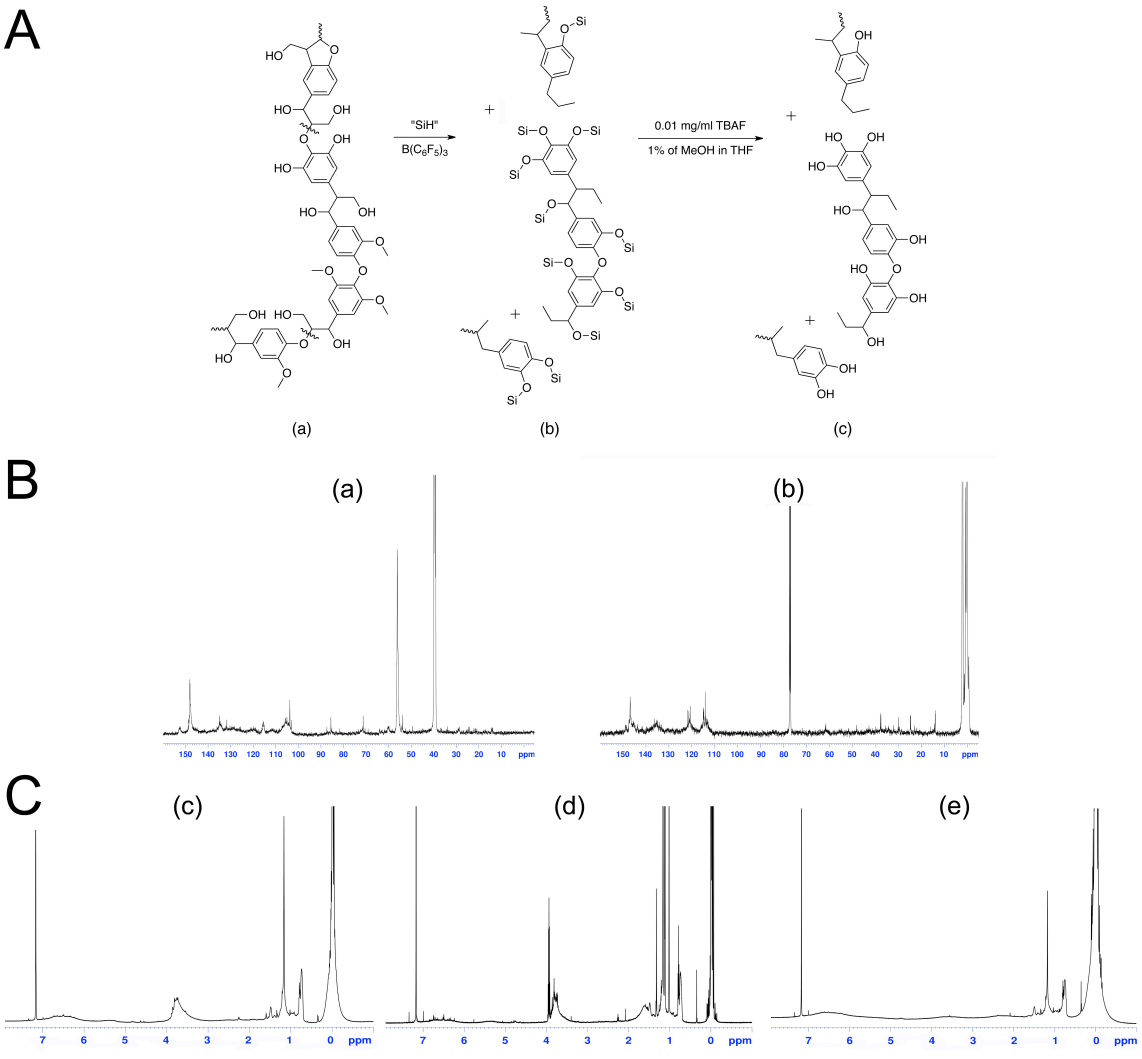

Figure 3.2 (A) Schematic illustration of possible structure changes to lignin during reduction and de-silylation. (B) ^{13}C-NMR of (a) hardwood lignin, (b) reduced and silylated hardwood lignin fragments (in DMSO d_6). (C) Reduction with three different

catalyst concentrations showing increasing reduction/silylation (c 2.0% $B(C_6F_5)_3$, d 5.8%; e 10.2%, samples were run in $CDCl_3$).

^{1}H-NMR spectra of reduced hardwood lignin exhibited new chemical shifts between 0.8 and 1.5 ppm alkyl groups and near 0.0 ppm for methyl siloxane protons (including the isolated/residual products) reflecting, as demonstrated with the lignin model compounds, cleavage of linkages (β-O-4 linkage, alcohol, and alkoxybenzene, etc.) and silylation of alcohols by the hydrosilane PMDS. The changes are most easily observed from the three spectra showing increasing degrees of reduction/silylation produced with increasing catalyst concentrations (Figure 3.2C). The NMR spectral signals attributed to oxygenated aliphatic protons in the range 3 - 4 ppm diminished in intensity or disappeared with increased catalyst loading, while the aliphatic (deoxygenated) signals in the range of 0.6 - 2 ppm increased concomitantly. As with softwood lignin, the 5-5, β-5, β-1, and 4-O-5 linkages in hardwood lignin were not expected to react. However, they have low abundance in this polymer and, therefore, it is possible to break the material into lower molecular weight organosoluble fragments.

FT-IR spectra of soluble products collected from the first, second, and third reductions were also used to track the structural changes of lignin. As shown in Figure 4.3, the exhibited bands of increasing intensity at 1258 cm^{-1}, 1040 cm^{-1}, and 790 cm^{-1} (highlighted by red, blue, and green boxes) are consistent with the presence of Si-O-Si, $Si-CH_3$, $O-Si-CH_3$, and $Si(CH_3)_2$ functional groups, respectively, while the bands at 1214 cm^{-1}, 1324 cm^{-1}, 1378 cm^{-1}, 2850 cm^{-1} due to C-O, $O-CH_3$, groups, etc., either weakened

or disappeared with increasing catalyst loading. A dramatic drop in the intensity of -OH peaks above 3000 cm^{-1} was observed in the IR spectra of soluble products. Note that the Si-O-Si linkages can originate both from silyl ethers ($Ar\text{-}OSiMe_2OSiMe_3$) and the silicone polymers produced in the reaction.

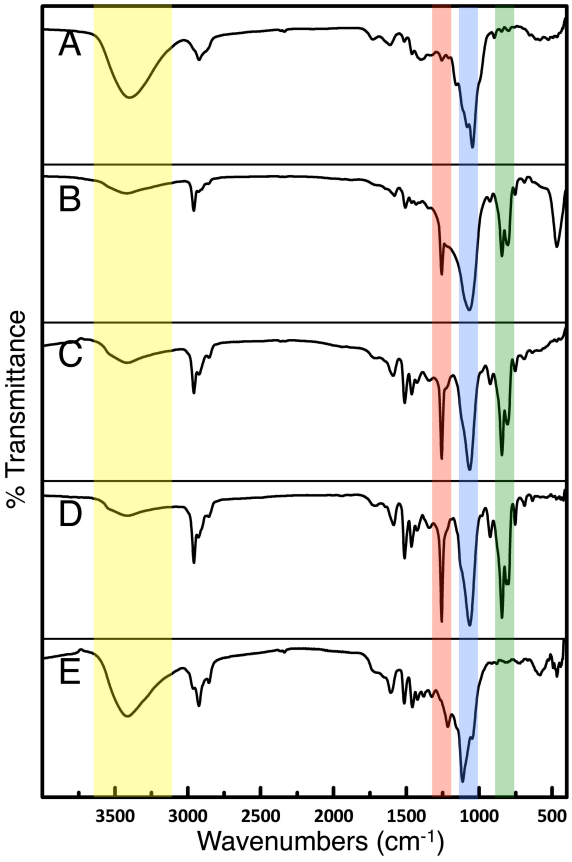

Figure 4.3 The FT-IR spectra of hardwood lignin and its reduced/degraded products: (A) residual/isolated product. Soluble products collected from the (B) third, (C) second, and (D) first reduction processes; and (E) unmodified hardwood lignin (yellow OH groups, red Si-O, blue Ph-O/C-O, green Si-O and Si-CH3).

Lignin is an underexploited resource primarily due to the difficulties in breaking down an aromatic network polymer chains. Reactions with model compounds demonstrate that the combination of hydrosilanes and $B(C_6F_5)_3$ efficiently silylate aryl alkyl ethers and phenols and, in addition, reduce aliphatic alcohols to alkyl groups. Softwood lignin contains a significant fraction of coniferyl alcohol (G) units that are not susceptible to the reductive conditions presented here. As a consequence, while it is possible to surface modify the lignin particles, it is difficult to reduce the network polymer to low molecular weight soluble fragments. Hardwood lignin with low concentrations of coniferyl alcohol (G) units, by contrast, underwent reductive silylation giving over 90wt% of organosoluble products under rather mild conditions. This provides a convenient route to take a readily available thermoset polymer and convert it into low molecular weight materials that are much more amenable for further processing.

3.5 Conclusions

Lignin is a network polymer comprised of linked aromatic rings. Many of the functional groups, including alcohols, phenols, aryl alkyl ethers, are susceptible to reductive silylation by hydrosilanes in the presence of $B(C_6F_5)_3$. Methoxy benzene groups and β-O-4 and α-O-4 linkages in model compounds were cleaved to give phenyl silyl ethers and the corresponding hydrocarbons. Alcohols and phenols were silylated and, in the case of alkyl silyl ethers, reduced to corresponding hydrocarbons. The relative reactivity was found to follow the order of phenol > primary alcohol > methoxy > silyl

ether. Softwood lignin was surface modified with silyl groups, but solubilization was limited to about 30wt% because many of the linkages derived from coniferyl alcohol units are not susceptible to the reaction. By contrast, hardwood lignin, which has a much lower fraction of such groups, was reduced/degraded very efficiently by monofunctional hydrosilanes. The efficiency of the reduction process depended on $B(C_6F_5)_3$ concentration. At higher concentrations, up to 10%, over 95% of hardwood lignin could be rendered soluble in organic solvents.

3.6 Acknowledgements

We thank the Natural Sciences and Engineering Research Council of Canada for financial support, Dr. Angela Dodd of Weyerhaeuser for providing softwood lignin samples, Dr. Michael Paleologou of FPInnovations for providing hardwood lignin samples, and Dr. Prof. John Kadla, Dr. John Grande, and Dr. Vinodh Rajendra for helpful discussions.

3.7 References

ADLER, E. 1977. Lignin chemistry—past, present and future. *Wood Science and Technology,* 11**,** 169-218.

ÁLVAREZ-BERCEDO, P. & MARTIN, R. 2010. Ni-Catalyzed Reduction of Inert C−O Bonds: A New Strategy for Using Aryl Ethers as Easily Removable Directing Groups. *Journal of the American Chemical Society,* 132**,** 17352-17353.

ANKALA, S. V. & FENTEANY, G. 2002. Selective deprotection of either alkyl or aryl silyl ethers from aryl, alkyl bis-silyl ethers. *Tetrahedron Letters,* 43**,** 4729-4732.

ARAÚJO, J. D. P., GRANDE, C. A. & RODRIGUES, A. E. 2010. Vanillin production from lignin oxidation in a batch reactor. *Chemical Engineering Research and Design,* 88**,** 1024-1032.

BERKEFELD, A., PIERS, W. E. & PARVEZ, M. 2010. Tandem Frustrated Lewis Pair/Tris(pentafluorophenyl)borane-Catalyzed Deoxygenative Hydrosilylation of Carbon Dioxide. *Journal of the American Chemical Society,* 132**,** 10660-10661.

BREBU, M. & VASILE, C. 2010. Thermal degradation of lignin - A review. *Cellulose Chemistry & Technology,* 44**,** 353.

BROOK, M. A., GRANDE, J. & GANACHAUD, F. 2011. New Synthetic Strategies for Structured Silicones Using $B(C_6F_5)_3$. *In:* MUZAFAROV, A. M. (ed.) *Silicon Polymers*. Springer Berlin Heidelberg.

CELLA, J. & RUBINSZTAJN, S. 2008. Preparation of Polyaryloxysilanes and Polyaryloxysiloxanes by $B(C_6F_5)_3$ Catalyzed Polyetherification of Dihydrosilanes and Bis-Phenols. *Macromolecules,* 41**,** 6965-6971.

CHOJNOWSKI, J., FORTUNIAK, W., KURJATA, J., RUBINSZTAJN, S. & CELLA, J. A. 2006. Oligomerization of Hydrosiloxanes in the Presence of Tris(pentafluorophenyl)borane. *Macromolecules,* 39**,** 3802-3807.

CORNELLA, J., GÓMEZ-BENGOA, E. & MARTIN, R. 2013. Combined Experimental and Theoretical Study on the Reductive Cleavage of Inert C–O Bonds with Silanes: Ruling out a Classical Ni(0)/Ni(II) Catalytic Couple and Evidence for Ni(I) Intermediates. *Journal of the American Chemical Society,* 135**,** 1997-2009.

EVTUGUIN, D. V., PASCOAL NETO, C., ROCHA, J. & PEDROSA DE JESUS, J. D. 1998. Oxidative delignification in the presence of molybdovanadophosphate heteropolyanions: mechanism and kinetic studies. *Applied Catalysis A: General,* 167**,** 123-139.

FEDOROV, A., TOUTOV, A. A., SWISHER, N. A. & GRUBBS, R. H. 2013. Lewis-base silane activation: from reductive cleavage of aryl ethers to selective ortho-silylation. *Chemical Science,* 4**,** 1640-1645.

FEGHALI, E. & CANTAT, T. 2014. Unprecedented organocatalytic reduction of lignin model compounds to phenols and primary alcohols using hydrosilanes. *Chemical Communications,* 50**,** 862-865.

GEVORGYAN, V., LIU, J. X., RUBIN, M., BENSON, S. & YAMAMOTO, Y. 1999. A novel reduction of alcohols and ethers with a $HSiEt_3$/catalytic $B(C_6F_5)_3$ system. *Tetrahedron Letters,* 40**,** 8919-8922.

GEVORGYAN, V., RUBIN, M., BENSON, S., LIU, J. X. & YAMAMOTO, Y. 2000. A novel $B(C_6F_5)_3$-catalyzed reduction of alcohols and cleavage of aryl and alkyl ethers with hydrosilanes. *Journal of Organic Chemistry,* 65**,** 6179-6186.

GEVORGYAN, V., RUBIN, M., LIU, J. X. & YAMAMOTO, Y. 2001. A direct reduction of aliphatic aldehyde, acyl chloride, ester, and carboxylic functions into a methyl group. *Journal of Organic Chemistry,* 66**,** 1672-1675.

GOSSELINK, R. J. A., DE JONG, E., GURAN, B. & ABACHERLI, A. 2004. Co-ordination network for lignin - standardisation, production and applications adapted to market requirements (EUROLIGNIN). *Industrial Crops and Products,* 20**,** 121-129.

GRETTON, M. J., KAMINO, B. A., BROOK, M. A. & BENDER, T. P. 2011. The Use of Piers-Rubinsztajn Conditions for the Placement of Triarylamines Pendant to Silicone Polymers. *Macromolecules,* 45**,** 723-728.

HARRIS, E. E., D'IANNI, J. & ADKINS, H. 1938. Reaction of Hardwood Lignin with Hydrogen. *Journal of the American Chemical Society,* 60**,** 1467-1470.

HATAKKA, A. 2005. Biodegradation of Lignin. *Biopolymers Online***,** 15 JAN, DOI: 10.1002/3527600035.bpol1005.

HAWKES, G. E., SMITH, C. Z., P., U. J. H., VARGAS, R. R. & VIERTLER, H. 1993. A Comparison of Solution and Solid State ^{13}C NMR Spectra of Lignins and Lignin Model Compounds. *Holzforschung,* 47**,** 302-312.

HEITNER, C., DIMMEL, D. & SCHMIDT, J. A. 2010. *Lignin and Lignans: Advances in Chemistry*, Taylor & Francis.

HISANO, H., NANDAKUMAR, R. & WANG, Z.-Y. 2009. Genetic modification of lignin biosynthesis for improved biofuel production. *In Vitro Cellular & Developmental Biology - Plant,* 45**,** 306-313.

HOCKING, M. B. 1997. Vanillin: Synthetic Flavoring from Spent Sulfite Liquor. *Journal of Chemical Education,* 74**,** 1055.

JOUANIN, L. & LAPIERRE, C. 2012. *Lignins: Biosynthesis, Biodegradation and Bioengineering*, Academic Press.

KOUISNI, L., HOLT-HINDLE, P., MAKI, K. & PALEOLOGLU, M. 2012. The Lignoforce System: A new proces for the production of high-quality lignin from black liquor. *Journal of Science & Technology for Forest Products and Processes,* 2**,** 6-10.

LEONOWICZ, A., MATUSZEWSKA, A., LUTEREK, J., WOJTAŚ-WASILEWSKA, HOFRICHTER, M. & ROGALSKI, J. 1999. Biodegradation of Lignin by White Rot Fungi. *Fungal Genetics and Biology,* 27**,** 175-185.

OASMAA, A., ALEN, R. & MEIER, D. 1993. Catalytic hydrotreatment of some technical lignins. *Bioresource Technology,* 45**,** 189-194.

OWEN, B. C., HAUPERT, L. J., JARRELL, T. M., MARCUM, C. L., PARSELL, T. H., ABU-OMAR, M. M., BOZELL, J. J., BLACK, S. K. & KENTTÄMAA, H. I. 2012. High-Performance Liquid Chromatography/High-Resolution Multiple Stage Tandem Mass Spectrometry Using Negative-Ion-Mode Hydroxide-Doped Electrospray Ionization for the Characterization of Lignin Degradation Products. *Analytical Chemistry,* 84**,** 6000-6007.

PANDEY, M. P. & KIM, C. S. 2011. Lignin Depolymerization and Conversion: A Review of Thermochemical Methods. *Chemical Engineering & Technology,* 34**,** 29-41.

PARKS, D. J., BLACKWELL, J. M. & PIERS, W. E. 2000. Studies on the mechanism of $B(C_6F_5)_3$-catalyzed hydrosilation of carbonyl functions. *Journal of Organic Chemistry,* 65**,** 3090-3098.

PARKS, D. J. & PIERS, W. E. 1996. Tris(pentafluorophenyl)boron-catalyzed hydrosilation of aromatic aldehydes, ketones, and esters. *Journal of the American Chemical Society,* 118**,** 9440-9441.

PEARL, I. A. 1942. Vanillin from Lignin Materials. *Journal of the American Chemical Society,* 64**,** 1429-1431.

PEREZ, J., MUNOZ-DORADO, J., DE LA RUBIA, T. & MARTINEZ, J. 2002. Biodegradation and biological treatments of cellulose, hemicellulose and lignin: an overview. *International Microbiology,* 5**,** 53-63.

PIERS, W. E. 2005. The chemistry of perfluoroaryl boranes. *Advances in Organometallic Chemistry,* 52**,** 1-77.

SERGEEV, A. G. & HARTWIG, J. F. 2011. Selective, Nickel-Catalyzed Hydrogenolysis of Aryl Ethers. *Science,* 332**,** 439-443.

WEN, J.-L., SUN, S.-L., XUE, B.-L. & SUN, R.-C. 2013. Recent advances in characterization of lignin polymer by solution-state nuclear magnetic resonance (NMR) methodology. *Materials,* 6**,** 359-391.

YAN, N., ZHAO, C., DYSON, P. J., WANG, C., LIU, L.-T. & KOU, Y. 2008. Selective Degradation of Wood Lignin over Noble-Metal Catalysts in a Two-Step Process. *ChemSusChem,* 1**,** 626-629.

ZAKZESKI, J., BRUIJNINCX, P. C. A., JONGERIUS, A. L. & WECKHUYSEN, B. M. 2010. The Catalytic Valorization of Lignin for the Production of Renewable Chemicals. *Chemical Reviews,* 110**,** 3552-3599.

CHAPTER 4: Utilization of softwood lignin as both crosslinker and reinforcing agent in silicone elastomers[§]

4.1 Abstract

Lignin, the second most abundant naturally occurring organic polymer on earth, is normally used only as a source of fuel because of the difficulties in processing it for other applications. While the Piers-Rubinsztajn reaction of phenols and alkoxybenzene groups with hydrosilanes can lead to highly degraded hardwood lignin, under different conditions, the process permits partial reduction of surface-presenting groups on softwood lignin. The method requires no pre-modification of the lignin surface, which reacts with silicon-hydride functional groups on silicone polymers in a process catalysed by $B(C_6F_5)_3$. Simultaneously, crosslinking of the silicone occurs to give a reinforced elastomer. Lignin plays dual roles as crosslinker and reinforcing reagent. The mechanical performance of lignin crosslinked/reinforced composites, depending on formulation, is comparable to some commercially available silicone elastomers and can be readily tuned by lignin content and molecular weight of silicones used in the formulation. The composites

---

[§] This chapter is reproduced from Jianfeng Zhang, Yang Chen, Michael A. Brook, in *Green Chemistry*, **2015**, 17, 1811-1819 with permission from Royal Society of Chemistry Publications, 2015. Jianfeng Zhang designed the experimental procedure and performed all experiments with suggestion from Dr. Chen. Jianfeng Zhang also assisted Sewell with DRIFT-IR characterization. Jianfeng Zhang wrote the majority of the manuscript with additions, edits and guidance provided by Dr. Brook.

demonstrated acceptable resistance to solvent extraction and excellent resistance to high temperature aging.

4.2 Introduction

Lignin is one of the most abundant naturally occurring polymers on the earth. However, the majority of lignin that is recovered, typically from kraft pulping processes, is burned as a low value fuel. In one important exception, lignin emerged as a "green" renewable source for vanillin in early 1940s.(Pearl, 1942) In recent decades, several methods have been developed with the aim to convert lignin into value-added products, including biodegradation, thermochemical depolymerization, and catalytic valorization.(Pandey and Kim, 2011, Zakzeski et al., 2010, Hatakka, 2005) However, few successes with depolymerizing actual lignin into monomeric molecules have been achieved with a high conversion yields.(Yan et al., 2008, Harris et al., 1938, Oasmaa et al., 1993, Rahimi et al., 2014)

The low efficiency of lignin depolymerization processes is due to its complex structure and the types of linkages present.(Zakzeski et al., 2010) The building units and polymeric network architecture of lignin vary depending on the species.(Hisano et al., 2009) Typically, the lignin derived from grass and softwood contains more guaiacylpropane (G) units; hardwood lignin consists of approximately equal proportions of guaiacylpropane (G) and syringylpropane (S) units.(Heitner et al., 2010) These units are mostly bridged by β-O-4 linkages;(Chakar and Ragauskas, 2004) complemented with

other linkages such as 5-5, β-5, 4-O-5, β-1, and β-β, known for resistance to chemical degradation (Scheme 4.1).(Zakzeski et al., 2010, Heitner et al., 2010, Boerjan et al., 2003)

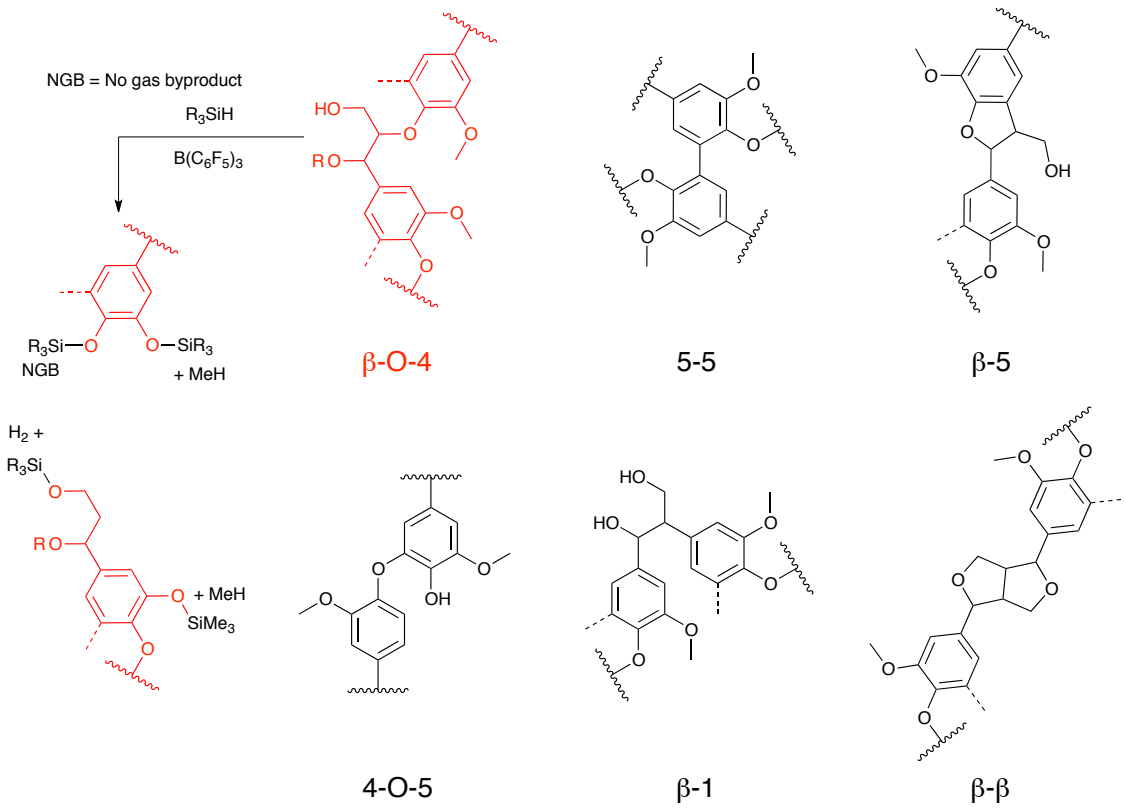

Scheme 4.1 The typical linkages in lignin molecules that are backbone cleavable (red) and partly degradable (black) under Piers-Rubinsztajn conditions

An alternative strategy to utilize lignin for industrial applications would take advantage of its inherent strength.(Qin et al., 2013) Lignin has been examined as a filler/crosslinker in a variety of resins, including phenolic,(Tejado et al., 2007, Donmez Cavdar et al., 2008) epoxy,(Zhao et al., 2001, Hofmann and Glasser, 1993, Qin et al., 2013, Ismail et al., 2010) polylactide,(Chung et al., 2013, Thunga et al., 2014) and

polyurethane resins.(Chung and Washburn, 2012, Feldman et al., 1988, Ciobanu et al., 2004) The hydroxyl groups found on lignin are readily ester functionalized with succinic anhydride leaving residual carboxylic acids that were used as a curing agent for epoxy resins.(Qin et al., 2013) The epoxy resin had excellent properties with a high lignin content (up to 32.3%).(Qin et al., 2013, Ismail et al., 2010) In a separate report, polyurethane (PU) prepared from a hydroxy rich lignin in which methoxy groups had been hydrolyzed demonstrated enhanced mechanical properties compared to the unmodified lignin-base PU.(Chung and Washburn, 2012) More recently, softwood lignin was used as a multifunctional phenolic component to synthesize poly(arylene ether) sulfones.(Argyropoulos et al., 2013) These achievements demonstrate a promising application of lignin, as a phenolic precursor, in polymeric materials.

Although $B(C_6F_5)_3$ (tris(pentafluorophenyl)borane) facilitates reduction by hydrosilanes of functional groups, including alcohols, aldehydes, ketones, carboxylic acids, esters, phenol, and alkoxyphenyl, in presence of silicon hydride,(Parks and Piers, 1996, Parks et al., 2000, Gevorgyan et al., 2000, Gevorgyan et al., 2001, Cella and Rubinsztajn, 2008, Gretton et al., 2011, Brook et al., 2011) it was only recently exploited for the reduction/modification of lignin.(Zhang et al., 2014, Feghali and Cantat, 2014) In the presence of hydrosilanes, $B(C_6F_5)_3$ leads to cleavage of β-O-4 and α-O-4 linkages: silylation of phenols, methoxyl groups, and certain secondary alcohols occurs concomitantly under mild conditions (Scheme 4.1).

Silicone elastomers are used for applications ranging from biomaterials to microcontact printing.(Quist et al., 2005, Zhou et al., 2010) The poor tear resistance of silicones requires the use of filler reinforcements in order to achieve useful performance.(Paul and Mark, 2010) Minerals, particularly silica, are commonly used to reinforce silicone elastomers: reinforcement efficiency depends on loading, filler particle size and chemical nature of filler surface.(Paul and Mark, 2010, Warrick and Lauterbur, 1955) Normally, high surface area fumed silica (nominal particle size ~10nm, aggregate size ~ 50 nm) is prepared by burning $SiCl_4$. As much as 30% or more silica may be included in a silicone elastomer formulation.

Silicone elastomer networks are prepared using the Piers-Rubinsztajn reaction by crosslinking hydrosilicones with alkoxysilanes in the presence of fillers (Scheme 4.2A). Instead of using tetraethyl orthosilicate (TEOS) as a crosslinker,(Fawcett et al., 2013, Grande et al., 2012) we reasoned that is could be possible to obtain reinforced silicone elastomers from the reaction of hydrogen-terminated polydimethylsiloxane (H-PDMS-H) with softwood lignin, catalyzed by $B(C_6F_5)_3$) (Scheme 4.2B). The controlled generation of silicone elastomers formed with the less dense, biodegradable, renewable filler softwood lignin is reported below.

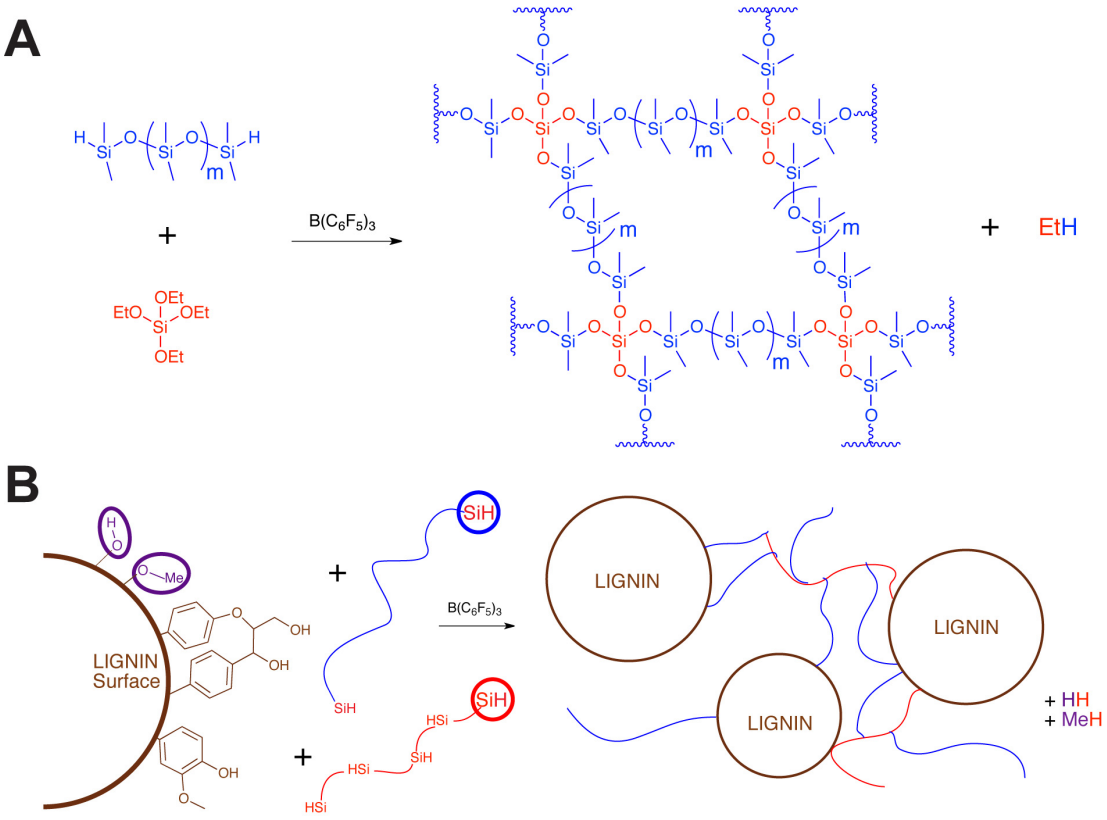

Scheme 4.2 Reaction scheme: A: Piers-Rubinsztajn process for elastomer formation; B: Replacement of alkoxysilane by lignin for both crosslinking and physical reinforcement.

4.3 Experimental Section

4.3.1 Materials

Hydride-functional silicone: pentamethyldisiloxane (PMDS), hydride-terminated PDMS (DMS-H11, H21, H31, and H41, with molecular weights for 1175, 6000, 28000, and 62700 g/mol, respectively), poly(hydromethylsiloxane) (PHMS, Mw = 1800-2100 g/mol), and poly(hydromethylsiloxane)-poly(dimethylsiloxane) (PHMS-PDMS) copolymer (HMS-301, Mw = 1900 ~ 2000 g/mol, and HMS-501, Mw = 900 ~ 1200

g/mol) were purchased from Gelest (Table 4.2). $B(C_6F_5)_3$ (BCF) was purchased from Sigma-Aldrich, and stored as a stock solution (40 mg/ml, 78.13 mM) in dry toluene. With the exception of decamethylcyclopentasiloxane (D_5, $(Me_2SiO)_5$, Gelest), solvents were purchased from Caledon Laboratories and used after drying over activated alumina. Antifoam 2210 was used as received from Dow Corning.

Softwood Kraft lignin (SKL) was provided by Weyerhaeuser (denoted as SKL-W) or purchased from Sigma-Aldrich (SKL-S). Prior to use, the lignin samples were milled into smaller particles sizes (~3 g portion of lignin and 10 steel balls with diameter of 3 mm were placed in a 25 ml PE container; a Flacktek speed mixer served as the ball-mill at a speed of 3500 rpm). The lignin powder was pass through a 75 μm sieve: oversized particles were discarded. The SKLs were stored, with drying, in a desiccator under vacuum and over Drierite. Although we examined two different sources of lignin, there were no significant differences in elastomer properties as a function of SKL origin.

4.3.2 Quantitation of reactive surface functional groups on lignin particles

The concentration of lignin surface functional groups (hydroxyl, methoxyl, β-O-4 and α-O-4) was determined by measuring the volume of gaseous by-products (methane, H_2, etc.) formed during the reaction with hydrosilicones. The generated gas was collected by a water displacement method (Appendix, Figure 7.28). Several different hydride-functional silicones were used in these experiments, but a common procedure was used with each of them. Lignin powder (ranging from 5 to 200 mg) was dispersed in dry toluene (3 ml) to which was added $B(C_6F_5)_3$ (10 μL in toluene, 40mg/ml, 0.8 μmol) with

stirring. After sealing the vessel with a septum, a portion of hydride-functional silicone (PMDS, DMS-H11, HMS-301, 501, or 992, 1 ml) was injected. The suspension was allowed to stir until no further volume changes were observed in the burette (which took from 2 - 8 h). When the reaction was complete, the modified lignin was washed with dry toluene (10 ml x 6 times, followed by centrifugation using a Thermo Durafuge 100 at 4000 rpm for 20 min after each wash cycle) to remove adsorbed (i.e., not covalently bonded) silicone from the lignin. Finally, the lignin was dried at 70 °C under a nitrogen blanket, then characterized using IR diffuse reflectance infrared in Fourier transform mode (DRIFTS, Thermo Nicolet 6700).

4.3.3 Control Experiments

Control experiments were performed to examine the ability of unmodified lignin to reinforce silicone elastomers. Softwood lignin was therefore incorporated into both commercial Pt- and tin-catalyzed silicone elastomer formulations. For the Pt- catalyzed formulation, the vinyl-terminated PDMS (2g, DMS-V35: $(CH_2=CH)Si(CH_3)_2O[Si(CH_3)_2]_nOSi(CH_3)_2(CH_2=CH)$, Mw = 28,000 g/mol, Gelest), PHMS (0.02 g, HMS-992), and lignin (1.5 g to give ~ 40% of lignin in elastomer) were hand mixed to give a homogeneous dispersion, then the platinum catalyst (~ 500 µl of xylenes solution containing 0.5% Pt, ~ 5000 ppm, diluted from Karstedt's catalyst stock solution purchased from Sigma-Aldrich) was added and immediately mixed with the suspension. Finally, the mixture was poured into a Petri dish and allowed to cure at 90 °C.

For the tin catalyst formulation, silanol-terminated PDMS (2g, DMS-S31, HO-$Si(CH_3)_2O[Si(CH_3)_2]_nOSi(CH_3)_2$-OH, Mw = 26,000 g/mol, Gelest), TEOS (0.08 g, tetraethyl orthosilicate, Sigma-Aldrich), and lignin (0.5 g for ~ 20% wt, 1.4 g for ~ 40%, and 3.1 g for ~ 60% of lignin in elastomer) were hand mixed to give a homogeneous dispersion, then, the tin-catalyst (~ 50µl, dibutyltin dilaurate, 95%, Sigma-Aldrich) was mixed and poured into a Petri dish to curing at room temperature.

4.3.4 Fabrication of lignin crosslinked/reinforced silicone elastomers

Lignin could be used directly as both a chemical crosslinking and reinforcing reagent for silicone elastomers (Table 4.1). As an example, a 200 mg portion of lignin was weighed and mixed with 1 g of hydrogen-terminated PDMS (e.g., DMS-H31). Depending on the percentage of lignin and molecular weight of hydride-terminated PDMS in the formula, a solvent (typically D_5 ~ 1 ml per 3.5 g formulation) was required to lower the viscosity. Thus, after hand mixing lignin, hydrogen-terminated PDMS and solvent into a homogeneous dispersion, Antifoam 2210 (1wt% with respect to the weight of elastomer precursor to reduce viscosity building), $B(C_6F_5)_3$ solution, and HMS-992 (acting as co-crosslinker) were added sequentially and mixed immediately. The formula was degassed at vacuum oven (685 mm Hg vacuum, VWR 1415M) at 40 °C for 12 h followed by a post-curing at 90 °C for another 12 h under the same vacuum. The formulations for elastomers with different lignin content are list in Table 4.1.

Table 4.1 Use of lignin as crosslinker/reinforcement in silicone elastomers

Lignin elastomer*	Lignin %	Lignin mg	Hydride-terminated PDMS (mg)	HMS-992 (mg)	D5 (ml)	B(C6F5)3 (ppm)
LE-0.5	0.5	5	DMS-H31 (1000)	21	0	273
LE-05	5	50	DMS-H31 (1000)	41	0	293
LE-09	9	100	DMS-H31 (1000)	50	0	278
LE-16	16	200	DMS-H31 (1000)	83	0.5	312
LE-27	27	400	DMS-H31 (1000)	102	0.8	319
LE-41A	41	800	DMS-H31 (1000)	38.5	1	326
LE-41B	41	800	DMS-H31 (1000)	154	1	307
LE-41C	41	800	DMS-H31 (1000)	308	1	285
LE-46	46	1000	DMS-H31 (1000)	165	1.5	277
LE-50	50	1200	DMS-H31 (1000)	202	1.5	300
LE-57	57	1600	DMS-H31 (1000)	221	2	284
LE-66	66	2400	DMS-H31 (1000)	250	2	274
LE-68	68	2800	DMS-H31 (1000)	298	2.5	293
LE-71	71	3200	DMS-H31 (1000)	310	2.5	266
LE-41D	41	800	DMS-H21 (1000) DMS-H11 (250)	38.5	0	326
LE-41E	41	800	DMS-H21 (550) DMS-H31 (200)	38.5	0	326
LE-41F	41	800	DMS-H41 (1000)	38.5	2	326
LE-41G	41	800	DMS-H31 (842)	HMS-501 (312)	1	307
LE-41H	41	800	DMS-H31 (530)	HMS-301 (623)	1	307

* Nomenclature: the number at the end of the label refers to the wt% lignin in the formula.

4.3.5 Characterization

Infrared spectroscopy was used to characterize the degree of functionalization of Si-H on lignin surface using diffuse reflectance infrared Fourier transform mode (DRIFTS, Thermo Nicolet 6700. Shore A (MFG. Co. Inc., U.S. Patent 2453042) and Shore OO durometers (Rex Gauge Company, Inc. U.S. Patent 2421449) were used to characterize the hardnesses of the elastomers. The modulus and elongation-at-break of lignin/silicone elastomer were determined by a Universal Test System (INSTRON 3366, 50 N load cell). Both ends of the elastomer, cut into dumbbell shape, were clamped with grips, and then stretched using a crosshead speed of 20 mm/min. The dimensions (thickness and width) of tested elastomer specimens were measured with an electronic digital micrometer (Mitutoyo, Japan; 0.001-mm sensitivity) at three random positions. Thermogravimetric analysis (TGA, TA instruments Q50) was performed under air; the temperature range was set from 50 °C to 800 °C with a 10 degrees/min step. The lignin distribution within the elastomer was characterized using a microscope under TV mode (Zeiss, LSCM 510).

4.4 Results and Discussion

The presence of lignin in traditional silicone elastomer formulations led to undesirable outcomes. No elastomer could be obtained from Pt-catalyzed formulation, even when a very large excess of catalyst (5000 ppm) was included. It is inferred that the functional groups found on SKL can act as ligands and poison the Pt-catalyst.(Kilbane Ii and Le Borgne, 2004) Although it was possible to make 20 to 60wt% lignin filled

elastomers using tin-catalyzed room temperature vulcanization, the product elastomers were very brittle and inflexible, showing very low elongation-at-break ratios.

Elastomers can be made using the Piers-Rubinsztajn reaction by combining alkoxysilanes with hydrogen-terminated silicones in the presence of $B(C_6F_5)_3$ (Scheme 4.2A).(Grande et al., 2012, Fawcett et al., 2013) In such a case the stoichiometric ratio of functional groups SiH/SiOR is known from the specific chemical structures of the precursors. When considering the use of the ArOR groups in lignin as a crosslinking centre, however, the calculation is more complex. As a natural polymer with complex and random chemical structures, the functionality of lignin will vary from species to species and from sample to sample.(Hisano et al., 2009) As the lignin will preferentially react at the particle surface, the number of available surface functional groups (hydroxyl, methoxyl, and β-O-4) will also be affected by factors including particle diameter, surface roughness, and aggregation, etc. Therefore, before using the lignin as a crosslinker, it was necessary to establish the concentration of reactive surface functional groups on lignin particles.

One equivalent of hydrogen/methane gas is formed from the silylation of a hydroxyl or methoxyl group, respectively, by $HSiR_3$. By contrast, the cleavage of an ether or silylether yields no hydrogen (or alkane) gas (Scheme 4.1).(Brook et al., 2011, Gevorgyan et al., 2000) Therefore, it is possible to establish approximate concentrations of surface OH, OR, ethers and silyl ethers by titrating the surfaces of a known weight lignin particles with silicones containing a known concentration of SiH groups and

measuring the gas produced (Appendix, Figure 7.29). As shown in Figure 4.1, gas production (from HMS-501 for this model study) depended on the total amount of dispersed lignin.

In a homogenous solution, that is, if SKL was dissolved rather than dispersed, gas production should increase linearly with lignin content. However, it instead followed a power law in this heterogeneous dispersion because of changes in effective surface area over time. The aggregation of lignin particles occurs during the reaction to form aggregates of morphologies that are concentration dependent. The availability of surface functional groups depends on the nature of the aggregate (Figure 4.1). As a consequence, the ratio of active surface area to mass dropped at increased lignin concentrations. At a low solid/liquid ratio, lignin particles were uniformly dispersed (5 mg/g, Figure 4.1A), but formed clusters that gelled at higher solid/liquid ratios (50 mg/g → 200 mg/g). The concentration of reactive surface functional groups on the lignin surfaces was 0.8-11 μmol mg^{-1} (Figure 4.1).

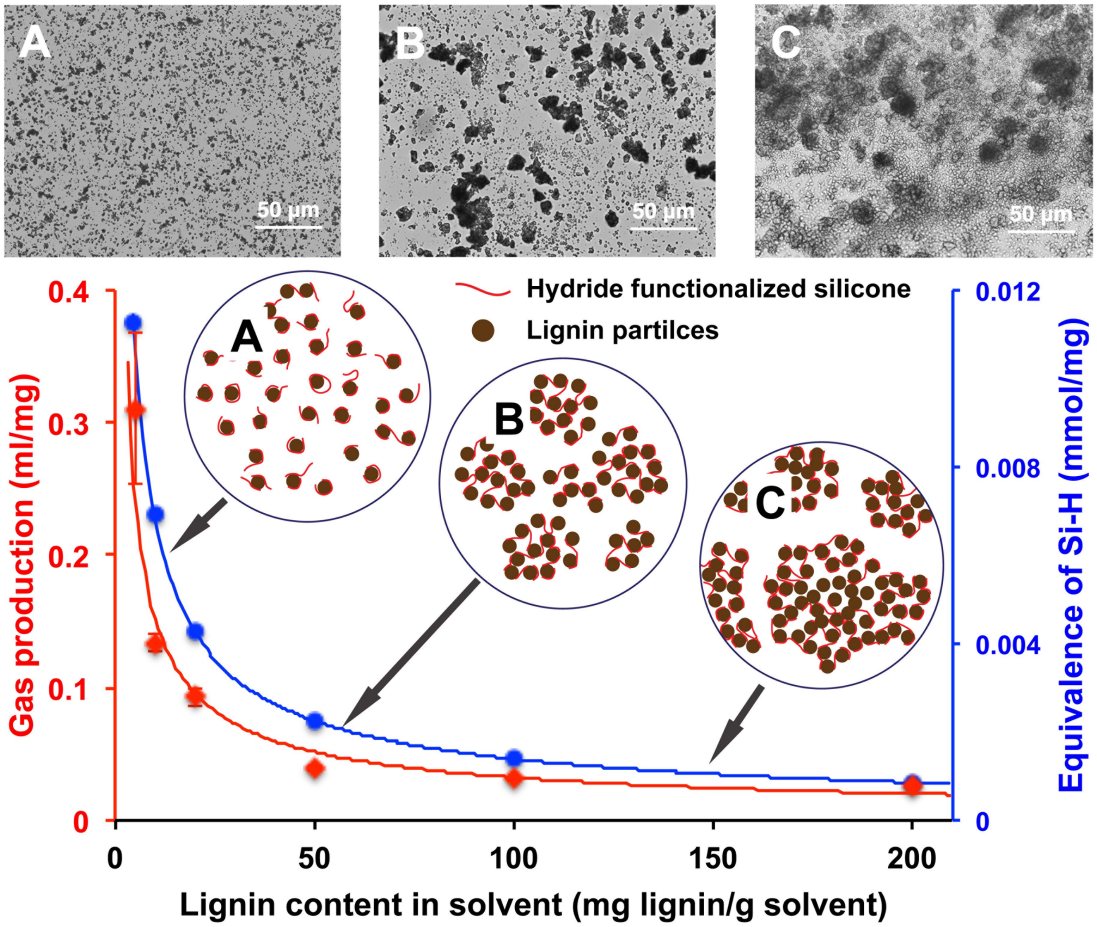

Figure 4.1 Gas production (red) and equivalents of hydride used (blue) as a function of lignin content in the solvent. Images A-C are the microscopic images of lignin dispersions at different solid/liquid ratios: A: dispersion of lignin at low content (5 mg/g), evenly distribution of particles; B dispersion of lignin with higher content (50mg/g), formation of clusters; C highly agglomerated lignin particles at concentrated dispersion (200 mg/g).

These conclusions were supported by DRIFT-IR measurements. The intensity of the Si-H signal on lignin surfaces was found to decrease exponentially with lignin content in

the solvent (Appendix, Figure 7.30). This finding was key to designing formulations for lignin-in-silicone elastomers with different lignin contents: the morphologies of lignin in the silicone, and the resulting elastomeric physical properties depended on surface area, functional group concentrations and amount of fluid present during preparation.

The network structure of the elastomer depends on the lignin as noted above, and also on the nature of the hydrido-silicones. As shown in Table 4.2, several different silicone hydrides, including mono-functional silicone (PMDS), di-functional silicone (DMS-H11), and multi-functional copolymer/polymers (HMS-301, 501, and 992) were doped with lignin. All of the silicone polymers tested reacted efficiently with lignin. The gas production exhibited no significant differences between the silicone hydrides tested (normalized to the same SiH/lignin ratio), and ranged about 4.9 to 5.8 ml (Table 4.2). Thus, the reactivities between lignin surface functional groups and silicone hydrides of different chemical structure are approximately the same under these conditions provided that the surface remains accessible.

Lignin particles reacting with HMS-501 or 992 (Table 4.2) yielded nearly the same volume of gas in spite of their very different SiH concentrations. In the case of HMS-992, the density of functional groups on the silicone backbone may be too high for efficient surface modification. Once initial grafting occurs, the resulting multi-point anchors of a silicone chain block access to reactive groups on lignin. At the other end of the spectrum, DMS-H11 with much lower Si-H density, produced an even lower amount of gas/SiH group. The reason may be attributed to the long polymer chain that, once grafted to the

lignin particle surface, protects it from further reaction. PMDS or HMS-301, either with shorter chain length (PMDS) or lower functional density (HMS-301), consumed more reactive lignin surface functional groups.

Each lignin particle can serve as a multifunctional crosslinking point: the surface functional group density is rather high, 0.8-11 μmol mg^{-1} (Figure 4.1). Note that not every functional group on lignin will lead to a productive crosslink. Phenol and methoxyphenyl groups can undergo silylation, potentially leading to crosslinks.(Parks and Piers, 1996) However, neither can undergo complete reduction to alkanes: such secondary reduction processes(Gevorgyan et al., 2000) consume SiH groups, but do not lead to crosslinks. For example, the reduction of exposed β-O-4 linkages leads both to lignin backbone cleavage and silylether and reduced methylene groups (Scheme 4.1).(Zhang et al., 2014) Ideally, the best network would be formed at functionality ratio of 1:1 between SiH:lignin reducible groups (mainly refer to phenol and aryl ethers), provided that this is the only reaction occurring. However, this ratio must necessarily vary from 1:1 to 3:1 due to these secondary side reactions that consume Si-H.(Macosko and Saam, 1987) The optimal formulations for lignin/silicone composites required a co-crosslinker (HMS-301, 501, or 992) in addition to H-PDMS-H spacers (Appendix, Section 0). Due to the structural complexity of lignin, as well as to facilitate an understanding of the degree to which elastomer properties could be controlled, the SiH:lignin reducible group ratio was tested between 0.5:1 → 4:1.

Table 4.2 The reactivity of lignin particles and silicone hydride with different chemical structures (lignin content = 50 mg/g).

	PMDS	DMS-H11	HMS-301	HMS-501	HMS-992
Gas production (ml)	5.83±0.39	4.89±0.32	5.63±0.16	5.10±0.29	4.96±0.22
Average hydride # per -(Si-O)- unit	0.5	0.07	0.3	0.5	1
Chemical structure	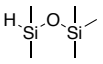	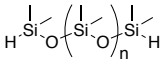	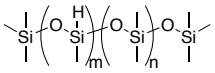		
		n ≈14	m/n = 3/7	m/n = 1/1	n = 0
Mw	148	1000-1100	1900-2100	900-1200	1800-2100

Initial examinations of elastomer formulations were confronted with the presence of bubbles in the products. The elimination of defects, including bubbles and voids within an elastomer body, was an important factor in the composite mechanical performance (see below).(Fawcett et al., 2013, Grande et al., 2012) Depending on the formula, initial structures ranged from porous foams to solid elastomers. Therefore, small amounts of solvent (D_5) were added to facilitate egress of bubbles formed during reaction (Table 4.1). Precursors with higher lignin content required more solvent because not only is the intrinsic viscosity of precursor higher with increased lignin, but the crosslinking density also increases at a rapid rate (Table 4.1, Figure 4.2). Adding an antifoam to control bubble nucleation was found to partly reduce the need for solvent to create a bubble free elastomer. As an example, using an antifoam with the formulation containing 41% lignin (LE-41B), the solvent usage could be reduced from ~ 1.5 ml to 1 ml and still obtain a

bubble free elastomer. Higher concentrations of lower molecular weight H-PDMS-H could also be used to reduce the incidence of bubbles in elastomers: in some cases, bubble free elastomers could be made without solvent (LE-41E,Table 4.1, for cross-section images, see Appendix, Figure 7.31).

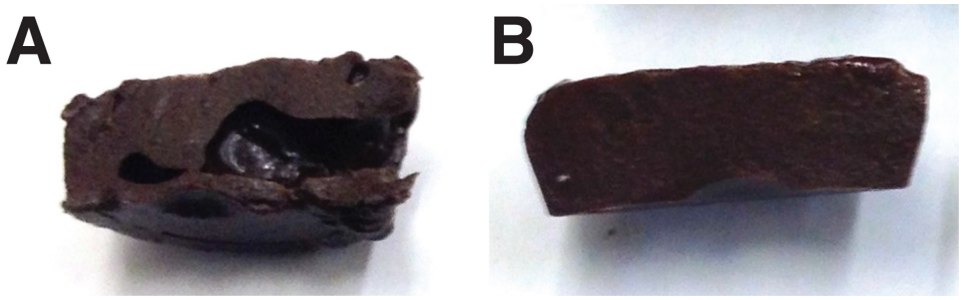

Figure 4.2 Elimination of bubble defects by solvent: A no added solvent, B with D_5

The properties of the lignin-filled elastomers were found to vary with lignin content because lignin plays dual roles as both crosslinker and reinforcing agent. A wide variety of lignin contents were examined, ranging from 0.5 to 71wt% in order to control crosslink density, reinforcement and active surface-to-volume ratio of lignin particles. As shown in Figure 4.3, the optical property change as a function of lignin concentration is very obvious: additional lignin leads to loss of transparency.

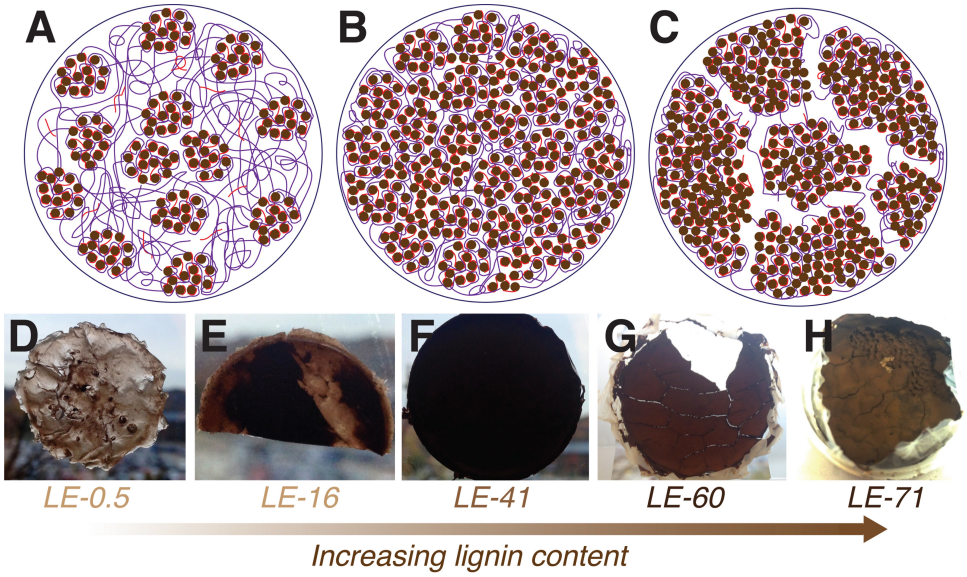

Figure 4.3 A schematic illustration of lignin crosslinked silicone networks at different lignin contents. A: low lignin content (0.5 to 16%); B: optimized content range (27 to 57%); and, C: excess content (60 to 71%). Images D-H show the changes in elastomer appearance with different lignin contents.

Mechanical properties of the elastomer also varied with lignin content. At lower lignin content, the lignin particles were dispersed unevenly in the elastomer (Figure 4.3D). Some of the lignin particles aggregated forming small clusters; moreover, the lignin particles precipitated, forming a bilayered structure (Figure 4.4A and D). As a consequence of lower crosslink density and uneven reinforcement (Figure 4.3A), the resultant elastomer was very soft and weak (Table 4.3). However, with an increase in lignin content, the hardness and modulus of elastomer increased while the elongation-at-break decreased (Table 4.3). These changes could be attributed to the balance of

reinforcing and dilution effects. At the optimized lignin content range, as shown in Figure 5.3B, the lignin clusters merged together because the volumetric fraction was sufficient (Figure 4.4B and E). As one of the best examples, the modulus and elongation-at-break of elastomer were balanced with sample LE-41B, with a lignin content of ~ 41% (Table 4.3). However, with a further increase of lignin content, the elastomer started cracking even without stress, as shown in Figure 4.3G. The amount of silicone was insufficient to hold the particles together (Figure 4.3C) and again an uneven distribution of lignin was observed (Figure 4.4C and F).

Table 4.3 Mechanical performance of lignin/silicone elastomers, the impact of lignin content, co-crosslinker content, and silicone molecular weight.

Lignin elastomer #	Shore OO	Shore A	Modulus (MPa)	Elongation-at-break (%)
LE-0.5	35-45	-[a]	-[c]	-[c]
LE-05	40-50	-[a]	-[c]	-[c]
LE-09	60-65	-[a]	-[c]	-[c]
LE-16	70-75	-[a]	-[c]	-[c]
LE-27	85-90	30-35	0.93 ± 0.22	286 ± 40
LE-41A	85-90	35-40	1.31 ± 0.02	260 ± 14
LE-41B	85-90	45-50	3.28 ± 0.39	146 ± 17
LE-41C	85-90	55-60	5.66 ± 1.01	92 ± 21
LE-41D	85-90	65-70	5.36 ± 0.73	75 ± 15
LE-41E	85-90	65-70	4.40 ± 0.14	53 ± 5
LE-41F	85-90	45-50	1.95 ± 0.49	297 ± 30
LE-41G	70-75	20-25	0.15 ± 0.01	305 ± 21
LE-41H	85-90	55-60[e]	2.88 ± 0.44	71 ± 17
LE-46	85-90	45-50	8.02 ± 1.25	83 ± 14
LE-57	85-90	55-65	16.30 ± 2.97	35 ± 10
LE-66	85-90	75-85	-[d]	-[d]
LE-68	85-90	80-85	-[d]	-[d]
LE-71	85-90	-[b]	-[d]	-[d]

[a] Hardness could not be measured – the elastomer was too soft. [b] Hardness could not be measured because the foam cracked under pressure. [c,d] Modulus and elongation-at-break were not measured due to the inferior mechanical properties of the sample or difficulties in making samples with the required dimensions. [e] The hardness test broke the elastomer.

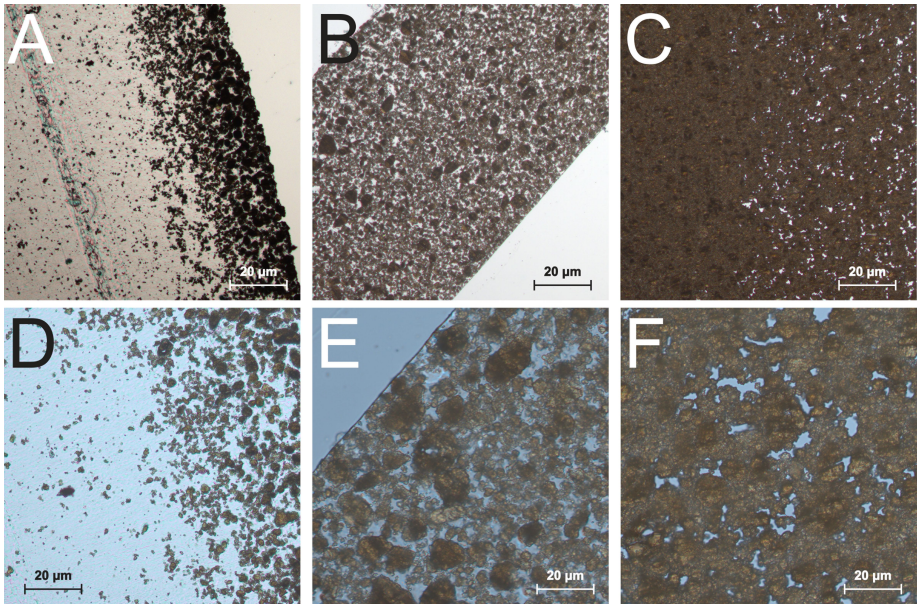

Figure 4.4 Cross-sectional images (D-F are the higher magnification images of A-C) of lignin/silicone elastomers of different lignin content: 16% A, D; 41% B, E; 68% C, F, respectively.

Mechanical performance also varied with the chemical structure and concentration of the silicone co-crosslinker. The elastomer containing 41% of lignin was used as a model formulation to examine the balance between modulus and elongation-at-break as the molar ratios of hydride to reactive surface functional group on lignin were varied from 0.5:1, 2:1 to 4:1, respectively (LE-41 A/B/C, Appendix, Section 0, and Table 7.2). As shown in Table 4.3, the modulus (increasing) and elongation-at-break (decreasing) changed significantly with co-crosslinker content. These changes can be attributed to the differences in interfacial cross-linking density between lignin particles and silicone matrix. Low molar ratios of hydride to reactive surface functional groups lead to low crosslinking

density and, therefore, poor interfacial control between silicone and lignin. However, as the hydride content was increased (e.g., 2:1 and 4:1), increased reinforcement was observed.(Boonstra, 1979)

The influence of the silicone chemical structures on elastomer properties was studied by varying the PHMS-PDMS crosslinking silicone ratio, while holding fixed the ratio of hydride to reactive surface functional groups. As shown in Table 4.3, LE-41G, made using HMS-501 as co-crosslinker, was more elastic due to the spacer siloxane units between the hydride groups; than LE-41H made with HMS-301 as co-crosslinker, which was much more brittle: the elastomer broke during Shore A measurements. Elastomer brittleness resulted from an excess content of low molecular weight HMS-301 in the formulation (more than 50% of silicone was less than 2000 g/mol, Table 4.1) leading to shorter silicone spacers between crosslinkers.

The molecular weight of H-PDMS-H also affects the mechanical performance of lignin/silicone elastomers. As shown in Table 4.3, decreasing the silicone chain length resulted in a consistent drop of elongation-at-break and a concomitant rise of the modulus. The entanglement of silicone chains was expected to be an important contribution for elasticity.(Sivasailam and Cohen, 2000) The elastomer made from higher molecular weight silicone was softer (lower modulus) and tougher (higher elongation-at-break). Note the longer silicone chain will result in a lower crosslinker density (for hydride contents of H-PDMS-H with different Mw, see Appendix, Table 7.3). Thus, the mechanical performances of the lignin/silicone elastomers could be easily tuned by

changing the SKL content, ratio of crosslinker to co-crosslinker, and molecular weight of H-PDMS-H and co-crosslinker.

The ability to control the final composite structure hinges on the competition between covalent bond formation in the developing network developing and gas production. Therefore, the rates for these two processes need to be manipulated in order to obtain elastomers with desirable structures. In addition to the factors just described, the structure of lignin/silicone elastomers varied with the content of lignin and co-crosslinker (Figure 4.5). At low lignin or high co-crosslinker content, undesirable voids in the elastomer could not be avoided even with use of solvent and antifoam (see above). With either an increase of co-crosslinker or decrease of lignin concentration, the network develops too fast for the gas to escape, a problem confounded by the rapid rise of viscosity. Therefore, the content of lignin and co-crosslinker should be in optimized ranges for a defect free elastomer.

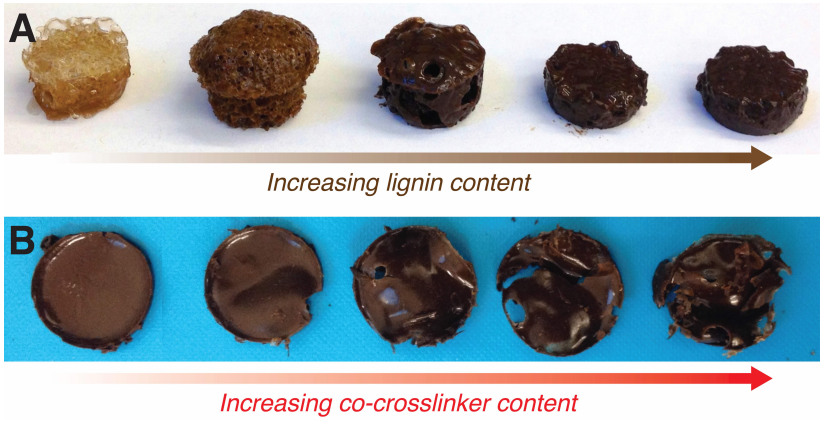

Figure 4.5 Structure evolution of silicone foam/elastomer with: A: increasing lignin content, and, B: co-crosslinker content

Silicone elastomers are known for their resistance to a wide temperature range (up to 300 °C) and extreme environments. How would the presence of lignin affect these thermal properties? The TGA of selected precursor samples were first run to demonstrate the stability of the constituents with increasing temperature. Lignin starts decomposing at 170 °C, while silicone starts to decompose above 350 °C (Appendix, Figure 7.33). The lignin/silicone elastomer, the composite of both materials, also starts to decompose at 170 °C, and from 170 to 300 °C the decomposition occurred at a constant rate.

The mechanical properties of the samples were also tested after aging in air at either 170 and 250 °C. As shown in Table 4.4, the elastomer demonstrated considerable resistance to high temperature without showing significant change on elongation-at-break. It was surprising that the modulus initially dropped with aging at 170 °C, and increased afterwards. However, this behaviour has been attributed to the competition between degradation and repolymerization of lignin at this temperature. After the initial few hours, the repolymerization of lignin occurs, leading a more condensed polymer structure with a concomitant increase of the elastomer modulus.(Li et al., 2007, Wayman and Chua, 1979)

The resistance of the composite to ordinary organic solvents was also tested. Due to the combination of hydrophilic (lignin) and hydrophobic (silicone), the lignin-elastomer was found to undergo swelling: <50% in H_2O, isopropanol, methanol; <100% in acetone, toluene, dimethyl sulfoxide, and; >150% in tetrahydrofuran (Appendix, Section 7.3.3). Significant weight loss (~ 25%) of the elastomer was only found in the presence of tetrahydrofuran, which is a good solvent for both silicone and lignin. The elastomers

extracted in toluene or tetrahydrofuran, respectively, were characterized after extraction. As shown in Table 4.4, both of the elastomers exhibited deceases in modulus and increasing of elongations-at-break, which might be the result of loss of organosoluble integration of PDMS and lignin fragments, or lignin fragments.

Table 4.4 The mechanical performance of lignin/silicone elastomers after treatment at higher temperatures and selected organic solvents

Lignin elastomer #	Condition	Shore OO	Shore A	Modulus (MPa)	Elongation-at-break (%)
LE-41B	Control	85-90	45-50	3.28 ± 0.39	146 ± 17
	170 °C (3 h, air)	85-95	50-55	2.02 ± 0.05	174 ± 20
	170 °C (8 h, air)	~ 95	65-75	4.09 ± 0.50	132 ± 12
	170 °C (96 h, air)	~ 95	75-80	4.92 ± 0.50	123 ± 18
	250 °C (3 h, air)	90-95	55-60	3.01 ± 0.07	146 ± 20
	Toluene (24 h)	85-90	50-55	2.26 ± 0.14	172 ± 24
	THF (24 h)	80-85	35-40	1.62 ± 0.65	198 ± 23

The properties of the composites described above match those of some low consistency silica-reinforced silicone elastomers, with respect to elongation at break, for example. Higher mechanical properties will result from the use of additional lignin as a reinforcing, but not crosslinking filler and/or smaller lignin particle sizes: both options are currently being examined.

Bio-renewable resources have attracted increasing attention from both the academy and industry. Lignin, as one of the most abundant naturally occurring polymers, is rarely

used as a raw material owing to the complexity of lignin structure, and difficulty of processing it. The combination of lignin with silanes using the Piers-Rubinsztajn reaction leads to reinforced silicone elastomers with easily controlled properties that are formed under very mild conditions. Silicone elastomers are widely used in applications ranging from biomedical implants to bathroom sealants. Their properties are unmatched by organic polymers. The utilization of a renewable, recyclable reinforcing agent leads to a new class of silicone elastomers whose properties do not require the user to see 'green' as a compromise; the lignin product compares favorably with its synthetic counterpart.

4.5 Conclusions

The Piers-Rubinsztajn reaction can be used to surface modify softwood lignin particles with silicone groups: the surface density of functional groups was 0.8-11 μmol mg^{-1}. In a one step process, under the same conditions, silicone polymers bearing SiH groups could both surface modify the lignin and undergo crosslinking leading to foams and elastomers. The modulus and elongation-at-break of lignin/silicone elastomers could be readily tuned by lignin content and molecular weight of silicones: products were prepared with properties that are comparable to commercial products. The elastomer exhibited excellent resistance to high temperature aging and acceptable resistance to solvent extraction. This work demonstrates that lignin can serve as efficacious green elastomer fillers.

4.6 Acknowledgements

We thank the Natural Sciences and Engineering Research Council of Canada and Sentinel: NSERC Research Network on Bioactive Paper for financial support, Weyerhaeuser for provision of lignin samples and Siltech Corp. for the gift of hydrosilicones.

4.7 References

ARGYROPOULOS, D. S., SADEGHIFAR, H., CUI, C. & SEN, S. 2013. Synthesis and Characterization of Poly(arylene ether sulfone) Kraft Lignin Heat Stable Copolymers. *ACS Sustainable Chemistry & Engineering,* 2**,** 264-271.

BOERJAN, W., RALPH, J. & BAUCHER, M. 2003. LIGNIN BIOSYNTHESIS. *Annual Review of Plant Biology,* 54**,** 519-546.

BOONSTRA, B. B. 1979. Role of particulate fillers in elastomer reinforcement: a review. *Polymer,* 20**,** 691-704.

BROOK, M., GRANDE, J. & GANACHAUD, F. S. 2011. New Synthetic Strategies for Structured Silicones Using B(C6F5)3. *In:* MUZAFAROV, A. M. (ed.) *Silicon Polymers*. Springer Berlin Heidelberg.

CELLA, J. & RUBINSZTAJN, S. 2008. Preparation of Polyaryloxysilanes and Polyaryloxysiloxanes by $B(C_6F_5)_3$ Catalyzed Polyetherification of Dihydrosilanes and Bis-Phenols. *Macromolecules,* 41**,** 6965-6971.

CHAKAR, F. S. & RAGAUSKAS, A. J. 2004. Review of current and future softwood kraft lignin process chemistry. *Industrial Crops and Products,* 20**,** 131-141.

CHUNG, H. & WASHBURN, N. R. 2012. Improved Lignin Polyurethane Properties with Lewis Acid Treatment. *ACS Applied Materials & Interfaces,* 4**,** 2840-2846.

CHUNG, Y.-L., OLSSON, J. V., LI, R. J., FRANK, C. W., WAYMOUTH, R. M., BILLINGTON, S. L. & SATTELY, E. S. 2013. A Renewable Lignin–Lactide Copolymer and Application in Biobased Composites. *ACS Sustainable Chemistry & Engineering,* 1**,** 1231-1238.

CIOBANU, C., UNGUREANU, M., IGNAT, L., UNGUREANU, D. & POPA, V. I. 2004. Properties of lignin–polyurethane films prepared by casting method. *Industrial Crops and Products,* 20**,** 231-241.

DONMEZ CAVDAR, A., KALAYCIOGLU, H. & HIZIROGLU, S. 2008. Some of the properties of oriented strandboard manufactured using kraft lignin phenolic resin. *Journal of Materials Processing Technology,* 202**,** 559-563.

FAWCETT, A. S., GRANDE, J. B. & BROOK, M. A. 2013. Rapid, metal-free room temperature vulcanization produces silicone elastomers. *Journal of Polymer Science, Part A: Polymer Chemistry,* 51**,** 644-652.

FEGHALI, E. & CANTAT, T. 2014. Unprecedented organocatalytic reduction of lignin model compounds to phenols and primary alcohols using hydrosilanes. *Chemical Communications,* 50**,** 862-865.

FELDMAN, D., LACASSE, M. & ST. J. MANLEY, R. 1988. Polyurethane-based sealants modified by blending with Kraft lignin. *Journal of Applied Polymer Science,* 35**,** 247-257.

GEVORGYAN, V., RUBIN, M., BENSON, S., LIU, J.-X. & YAMAMOTO, Y. 2000. A Novel B(C6F5)3-Catalyzed Reduction of Alcohols and Cleavage of Aryl and Alkyl Ethers with Hydrosilanes,Ä†. *The Journal of Organic Chemistry,* 65**,** 6179-6186.

GEVORGYAN, V., RUBIN, M., LIU, J.-X. & YAMAMOTO, Y. 2001. A Direct Reduction of Aliphatic Aldehyde, Acyl Chloride, Ester, and Carboxylic Functions into a Methyl Group. *The Journal of Organic Chemistry,* 66**,** 1672-1675.

GRANDE, J. B., FAWCETT, A. S., MCLAUGHLIN, A. J., GONZAGA, F., BENDER, T. P. & BROOK, M. A. 2012. Anhydrous formation of foamed silicone elastomers using the Piers–Rubinsztajn reaction. *Polymer,* 53**,** 3135-3142.

GRETTON, M. J., KAMINO, B. A., BROOK, M. A. & BENDER, T. P. 2011. The Use of Piers,ÄìRubinsztajn Conditions for the Placement of Triarylamines Pendant to Silicone Polymers. *Macromolecules,* 45**,** 723-728.

HARRIS, E. E., D'IANNI, J. & ADKINS, H. 1938. Reaction of Hardwood Lignin with Hydrogen. *Journal of the American Chemical Society,* 60**,** 1467-1470.

HATAKKA, A. 2005. Biodegradation of Lignin. *Biopolymers Online.* Wiley-VCH Verlag GmbH & Co. KGaA.

HEITNER, C., DIMMEL, D. & SCHMIDT, J. A. 2010. *Lignin and Lignans: Advances in Chemistry*, Taylor & Francis.

HISANO, H., NANDAKUMAR, R. & WANG, Z.-Y. 2009. Genetic modification of lignin biosynthesis for improved biofuel production. *In Vitro Cellular & Developmental Biology - Plant,* 45**,** 306-313.

HOFMANN, K. & GLASSER, W. G. 1993. Engineering Plastics from Lignin. 21.1Synthesis and Properties of Epoxidized Lignin-Poly (Propylene Oxide) Copolymers. *Journal of Wood Chemistry and Technology,* 13**,** 73-95.

ISMAIL, T. N. M. T., HASSAN, H. A., HIROSE, S., TAGUCHI, Y., HATAKEYAMA, T. & HATAKEYAMA, H. 2010. Synthesis and thermal properties of ester-type crosslinked epoxy resins derived from lignosulfonate and glycerol. *Polymer International,* 59**,** 181-186.

KILBANE II, J. J. & LE BORGNE, S. 2004. Chapter 2 Petroleum biorefining: the selective removal of sulfur, nitrogen, and metals. *In:* RAFAEL, V.-D. & RODOLFO, Q.-R. (eds.) *Studies in Surface Science and Catalysis.* Elsevier.

LI, J., HENRIKSSON, G. & GELLERSTEDT, G. 2007. Lignin depolymerization/repolymerization and its critical role for delignification of aspen wood by steam explosion. *Bioresource Technology,* 98**,** 3061-3068.

MACOSKO, C. W. & SAAM, J. C. 1987. The hydrosilylation cure of polyisobutene. *Polymer Bulletin,* 18**,** 463-471.

OASMAA, A., ALÉN, R. & MEIER, D. 1993. Catalytic hydrotreatment of some technical lignins. *Bioresource Technology,* 45**,** 189-194.

PANDEY, M. P. & KIM, C. S. 2011. Lignin Depolymerization and Conversion: A Review of Thermochemical Methods. *Chemical Engineering & Technology,* 34**,** 29-41.

PARKS, D. J., BLACKWELL, J. M. & PIERS, W. E. 2000. Studies on the Mechanism of B(C6F5)3-Catalyzed Hydrosilation of Carbonyl Functions. *The Journal of Organic Chemistry,* 65**,** 3090-3098.

PARKS, D. J. & PIERS, W. E. 1996. Tris(pentafluorophenyl)boron-Catalyzed Hydrosilation of Aromatic Aldehydes, Ketones, and Esters. *Journal of the American Chemical Society,* 118**,** 9440-9441.

PAUL, D. R. & MARK, J. E. 2010. Fillers for polysiloxane ("silicone") elastomers. *Progress in Polymer Science,* 35**,** 893-901.

PEARL, I. A. 1942. Vanillin from Lignin Materials. *Journal of the American Chemical Society,* 64**,** 1429-1431.

QIN, J., WOLOCTT, M. & ZHANG, J. 2013. Use of Polycarboxylic Acid Derived from Partially Depolymerized Lignin As a Curing Agent for Epoxy Application. *ACS Sustainable Chemistry & Engineering,* 2**,** 188-193.

QUIST, A. P., PAVLOVIC, E. & OSCARSSON, S. 2005. Recent advances in microcontact printing. *Analytical and Bioanalytical Chemistry,* 381**,** 591-600.

RAHIMI, A., ULBRICH, A., COON, J. J. & STAHL, S. S. 2014. Formic-acid-induced depolymerization of oxidized lignin to aromatics. *Nature,* 515**,** 249-252.

SIVASAILAM, K. & COHEN, C. 2000. Scaling behavior: Effect of precursor concentration and precursor molecular weight on the modulus and swelling of polymeric networks. *Journal of Rheology (1978-present),* 44**,** 897-915.

TEJADO, A., PEÑA, C., LABIDI, J., ECHEVERRIA, J. M. & MONDRAGON, I. 2007. Physico-chemical characterization of lignins from different sources for use in phenol–formaldehyde resin synthesis. *Bioresource Technology,* 98**,** 1655-1663.

THUNGA, M., CHEN, K., GREWELL, D. & KESSLER, M. R. 2014. Bio-renewable precursor fibers from lignin/polylactide blends for conversion to carbon fibers. *Carbon,* 68**,** 159-166.

WARRICK, E. L. & LAUTERBUR, P. C. 1955. Filler Phenomena in Silicone Rubber. *Industrial & Engineering Chemistry,* 47**,** 486-491.

WAYMAN, M. & CHUA, M. G. S. 1979. Characterization of autohydrolysis aspen (P. tremuloides) lignins. Part 2. Alkaline nitrobenzene oxidation studies of extracted autohydrolysis lignin. *Canadian Journal of Chemistry,* 57**,** 2599-2602.

YAN, N., ZHAO, C., DYSON, P. J., WANG, C., LIU, L.-T. & KOU, Y. 2008. Selective Degradation of Wood Lignin over Noble-Metal Catalysts in a Two-Step Process. *ChemSusChem,* 1**,** 626-629.

ZAKZESKI, J., BRUIJNINCX, P. C. A., JONGERIUS, A. L. & WECKHUYSEN, B. M. 2010. The Catalytic Valorization of Lignin for the Production of Renewable Chemicals. *Chemical Reviews,* 110**,** 3552-3599.

ZHANG, J., CHEN, Y. & BROOK, M. A. 2014. Reductive Degradation of Lignin and Model Compounds by Hydrosilanes. *ACS Sustainable Chemistry & Engineering,* 2**,** 1983-1991.

ZHAO, B., CHEN, G., LIU, Y., HU, K. & WU, R. 2001. Synthesis of lignin base epoxy resin and its characterization. *Journal of Materials Science Letters,* 20**,** 859-862.

ZHOU, J. W., ELLIS, A. V. & VOELCKER, N. H. 2010. Recent developments in PDMS surface modification for microfluidic devices. *Electrophoresis,* 31**,** 2-16.

CHAPTER 5: Foamed lignin-silicone bio-composites by extrusion then compression molding[§]

5.1 Abstract

The use of lignin, one of the most abundant natural products, has not gained wide use as a feedstock due to the difficulty of processing it. We have developed a simple route to produce lignin-silicone composite foams via first extrusion and then compression molding. The formulation consists of raw lignin particles, suitable mixtures of hydrosilanes, and the catalyst $B(C_6F_5)_3$. In order to balance the reaction rates between extrusion and molding, as well as find other optimized conditions for producing foamed structures, a series of optimizations established that a uniform, closed cell lignin-silicone foam was most effectively made by extrusion at room temperature followed by molding at elevated temperatures under pressure for up to 5 minutes. The morphology and uniformity of the foamed structure depended on many factors, including the quantity of lignin, catalyst, the crosslinking silicone PHMS, the molecular weight of the spacer silicone H-PDMS-H, and the molding temperature. The content of lignin, acting as both reinforcing filler (chemically bonded to the siloxane network) and crosslinker, could be

---

[§] Jianfeng Zhang designed the experimental procedure with the assistant from Dr. Fleury. Jianfeng Zhang performed all experiments and wrote the majority of the manuscript with additions, edits and guidance provided by Dr. Brook. This chapter is currently submitted as a manuscript for *ACS Sustainable Chemistry & Engineering*.

varied over a wide range from 25 to 55%. The mechanical performance of the lignin-silicone foams was characterized using DMA and tensile tests (tensile strength up to 0.42 MPa, break-at-elongation up to 249%). The strength of the foam was improved by post-curing at 140 °C. Although the lignin-silicone foam loses some elasticity after post-curing, it maintains excellent stability even after heating to 140 °C for 12 h. This processing method for lignin-based bio-composites provides new opportunities for better utilization of lignin in silicones and more broadly in organic materials.

5.2 Introduction

There is an increasing trend to the utilization of sustainable and renewable natural resources. Biomass,(Carpenter et al., 2014, Gandini, 2008) particularly cellulose, has been widely used in many fields, such as the food, paper, plastics, and pharmaceutical industries.(Van de Ven and Godbout, 2013, Benhamou et al., 2015, Bendahou et al., 2010) Lignin, the network polymer that glues polysaccharidic moieties together, is far less utilized due to difficulties with its processing.(Gosselink et al., 2004) Unlike cellulose that has well defined structure based on glucose, lignin is a highly crosslinked and branched polymer without well-defined repeating units.(Adler, 1977, Heitner et al., 2010) Lignin makes up about 18 ~ 35% by weight in wood; and the estimated available annual production could be over 20 million tons as the byproduct of paper industry.(Ma et al., 2014, Saito et al., 2012) Currently, lignin is mostly used as a low value fuel; an important

exception is the industrial production of the flavoring agent vanillin.(Araújo et al., 2010, Pearl, 1942)

Lignin has been blended into, or copolymerized with, other polymers to create composites. It acts as a filler in polymers such as in polyurethanes,(Chung and Washburn, 2012, Feldman et al., 1988, Ciobanu et al., 2004, Saito et al., 2013, Nadji et al., 2005, Gandini et al., 2002) epoxies,(Zhao et al., 2001, Hofmann and Glasser, 1993, Qin et al., 2013, Ismail et al., 2010) and phenolics,(Tejado et al., 2007, Donmez Cavdar et al., 2008) among others.(Chung et al., 2013, Thunga et al., 2014, Thielemans et al., 2002, Argyropoulos et al., 2013, Saito et al., 2012, Gandini et al., 2002, Guo et al., 1992) However, most of the methods require the lignin to be pre-modified before use to improve the interfacial interaction between lignin and the polymer matrix. Such additional steps are disadvantageous in industrial processes. Lignin-based polyurethane foams, the best studied lignin-filled composites, have been explored extensively.(Li and Ragauskas, 2012a, Pan and Saddler, 2013, Xue et al., 2014, Cateto et al., 2008, Li and Ragauskas, 2012b, Cinelli et al., 2013, Yoshida et al., 1987, Yoshida et al., 1990, Cateto et al., 2013, Cateto et al., 2011, Cateto et al., 2009) These foams exhibit excellent thermal and mechanical properties, with lignin content of up to 30 weight%. Although the preparation of urethanes using MDI (diphenylmethane diisocyanate) avoids a pre-modification step, the toxicity of this compound is also a drawback.

Extrusion and compression molding are common processing techniques used in the plastics industry to mix polymer formulations and then create objects: these processes

have also been used for biomass processing and modification.(Moad, 2011, Bhandari et al., 2012, Bridson et al., 2013, Carr, 1991) The techniques allow the processing to be performed at a flexible scale without the need for solvents. Various polymers, like PVA (poly(vinyl alcohol)),(Kubo and Kadla, 2003) starch,(Baumberger et al., 1998) and HDPE (high density polyethylene)(Fernandes et al., 2014) have been blended with lignin using reactive extrusion. Lignin has also been extruded together with silicone and silica.(Stiubianu et al., 2009) However, in these cases the lignin was used simply as a non-reinforcing filler with no effort to establish a favorable interfacial interaction between lignin and silicone matrix.

Recently, our group developed a method to efficiently decompose or modify lignin using hydrosilanes, catalyzed by $B(C_6F_5)_3$ (BCF, tris(pentafluorophenyl)borane) – the Piers-Rubinsztajn (PR) reaction.(Brook et al., 2011c, Zhang et al., 2014) The process leads to the conversion of phenol, arylmethoxy groups, and other ethers into alkyl groups or silyl ethers (Scheme 5.1A).(Feghali and Cantat, 2014) As a consequence, the lignin surface becomes siliconized, rendering it much more compatible with hydrophobic polymers. This permitted the use of raw softwood lignin as a reinforcing/crosslinking filler in silicone elastomers in a one step process.(Zhang et al., 2015a) The resulting lignin-silicone elastomer has excellent mechanical properties, even when filled with as much as 40 weight% lignin.

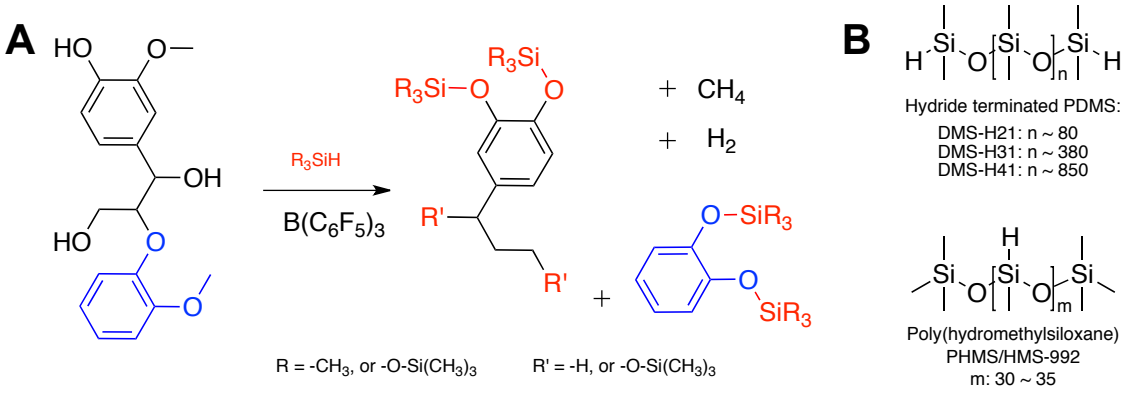

Scheme 5.1 (A) Typical reactions at phenolic linkages in lignin. (B) The chemical structures hydride-terminated PDMS (H-PMDS-H) and poly(hydromethylsiloxane) (PHMS).

The formation of lignin/silicone elastomers required the participation of solvent and reduced pressure in order to remove the gas produced during the reaction.(Gevorgyan et al., 2000, Brook et al., 2011b, Zhang et al., 2015a) While the evolution of gas can cause vacancies/defects in an elastomer, it can be useful for generating foamed materials. We describe a simple and effective method to make foamed lignin-silicone biocomposites via extrusion and compression molding. Although silicone foams are widely used for cushioning, thermal and electrical insulation and protective applications,(Chruściel and Leśniak, 2011) large scale applications are still blocked by the high cost of silicones and challenges in making foams reproducibly when using alcohols/water as co-blowing agents.(Frisch, 1981) In our research, the expensive silicone was diluted and reinforced/filled with raw lignin, which accounted for up to 55 weight% in the composite.

5.3 Experimental Section

5.3.1 Materials

Decamethylcyclopentasiloxane (D_5) and hydride-functional silicones, including hydride-terminated PDMS (H-PDMS-H, DMS-H21, H31, and H41, with molecular weights of 6000, 28000, and 62700 g/mol, respectively) and poly(hydromethylsiloxane) (PHMS, HMS-992, Mw = 1800 ~ 2100 g/mol) were purchased from Gelest (for structures see Scheme 5.1 B). The catalyst $B(C_6F_5)_3$ (Sigma-Aldrich) was dissolved in dry toluene to provide a stock solution (40 mg/ml, 78.13 mM). Anhydrous toluene, cyclohexane, 1-butanol, and KOH (potassium hydroxide) were purchased from Sigma-Aldrich and used without purification. Softwood kraft lignin was obtained from Weyerhaeuser or Sigma Aldrich. The lignins were used as received without further drying or processing.

5.3.2 Lignin-silicone foam fabrication - optimization of conditions and formulations

Preliminary optimizations: a series of preliminary optimization studies were performed in solution to obtain appropriate conditions and formulations that could be used during the extrusion process (Table 7.5). The concentration of Si-H groups (hydrosilane) before and after mixing serves as a surrogate for reactivity (a separate set of experiments measured residual Si-H in the final, cured product, see below). A gas meter was used to measure the volumes of gas released during the reaction (Figure 7.34). The flask and U shaped gas meter were immersed in either an oil or water bath to maintain a constant temperature. The hydrosilanes (DMS-H31 mixed with PHMS) were stored in a 1 ml syringe (*NOTE: The gaseous products can evolve very rapidly and, are comprised of*

flammable constituents including hydrogen, methane and other organic materials. Caution should be exercised. Avoid a closed system and use proper ventilation with *no nearby sources of ignition.*). Other reagents, including lignin, BCF, and D_5, were premixed and heated to the target temperature in the flask; the valve was left open for at least 15 min to avoid a potential gas expansion error caused by heating. The reaction started once the hydrosilanes were injected into the flask. The valve was closed immediately to collect and measure the volume of gas produced. The gas volume was recorded against time. Four parameters including catalyst concentration, hydrosilane concentration, temperature, and the order of feeding were studied. The studies are detailed in Figure 7.36 and show that efficient reactions could be induced at temperatures up to 90 °C with catalyst concentrations ranging from 1000-4000 ppm and lignin content of about 50 weight%.

Extrusion and compression molding of lignin-silicone foam: The lignin-silicone foam mixture was made using a micro-extruder (DMS Micro 15 cc Twin-screw Compounds) and then a compression-molding instrument (TECHMO, clamping force up to 6 tons and heating temperature up to 200 ° C, respectively), as shown in Scheme 5.2. The optimized order of feeding lignin into the injector was determined from preliminary studies. For extrusions, half of the portion of the lignin powder (~ 3 g) was premixed with BCF solution (~ 0.5 ml) to which the H-PDMS-H (~ 7.7 g) was added. The mixture was then added to the upper feeding hopper after the extruder had reached 100 rpm. PHMS (~ 1.2 g, from the upper feeding hopper) mixed with the second half portion of lignin (~ 3 g,

from the side hopper) was added after 15 s. The mixture was allowed to mix in the extruder for 3 min. A mold was placed under the outlet to collect the mixture, which was then immediately transferred to the preheated compression molding (holding at 90 °C for periods ranging from 5 min up to 3 h, under 1 ton pressure). Several conditions and formulations were tested (Table 5.1). For the F-4 formulations, compression molding processes were performed at 60, 90 and 120 °C.

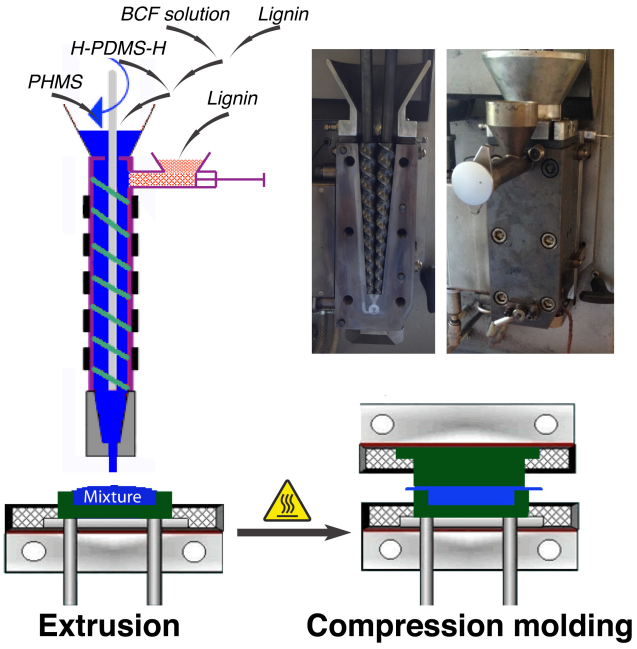

Scheme 5.2 Illustration of the extrusion and compression molding process. The inset images show the cross-section and assembled views of micro-scale twin-extruder.

Table 5.1 Parameters used to optimize extrusion and molding conditions, and formulations for lignin-silicone foam.

No.	Lignin		PHMS		H-PDMS-H		BCF (ppm)	Molding temperature (°C)	Resultant foam structure [a]
	Mass (g)	wt%	Mass (g)	wt%	Type	Mass (g)			
F-1	6.2	41	1.2	8	H31	7.7	300	90	A2
F-2	6.2	41	1.2	8	H31	7.7	1000	90	A1
F-3	6.2	41	1.2	8	H31	7.7	1350	90	A1
F-4 A	6.2	41	1.2	8	H31	7.7	2050	60	A1
F-4 B	6.2	41	1.2	8	H31	7.7	2050	90	B2 [c]
F-4 C	6.2	41	1.2	8	H31	7.7	2050	120	A1
F-5	6.2	41	0.6	4	H31	8.3	2050	90	A1
F-6	6.2	41	2.4	16	H31	6.5	2050	90	C2
F-7	6.2	41	3.6	24	H31	5.3	2050	90	C2
F-8	2.25	15	0.65	4.4	H31	12	2050	90	A1
F-9	3.75	25	0.75	5	H31	10.5	2050	90	B1 [c]
F-10	8.25	55	1.6	10	H31	5.15	2050	90	C1
F-11	6.2	41	1.2	8	H25	7.7	2050	90	A1
F-12	6.2	41	1.2	8	H41	7.7	2050	90	- [d]
F-13	6.2	41	1.2	8	Mix [b]	7.7	2050	90	B1 [c]

[a] The type of foam structures are illustrated in Figure 5.1. [b] Mix = 26% H25, 48% H31, and 26% H41. [c] Foams with homogeneous porous structure and satisfactory mechanical performance. [d] No foam was obtained due to the extreme high intrinsic viscosity of precursor.

Changes in the foam as a function of cure time in the compression mold were determined: ~300 mg samples were cut from molded foam samples after curing for 5, 15,

30, 60, and 180 min, respectively. The samples were characterized using ATR-FTIR, and then extracted in cyclohexane (~ 50 ml) for 12 h. The weight loss of the sample was calculated from the mass before and after extraction. NMR measurements were taken of the extracts from F-3, F-2 (5 min), and F-4 (5 min) (after removal of the solvent by evaporation).

5.3.3 Hydrolysis of Si-H groups remaining after cure

Loss of "Si-H" in solvent was used to show the degree of reaction that could be expected in the extruder (above). The degree of reaction in the second processing step, compression molding, was following by hydrolyzing residual "Si-H" groups in the cured foam (Figure 7.35). The cured lignin-silicone foam (~ 400 mg) was sliced into thin layers (dimension: 0.5 mm × 5 mm × 10 mm) and soaked in 1-butanol (15 ml). The suspension was placed in a 50 ml round-bottomed flask and placed in an oil bath (30 °C) for 20 min, while the valve was kept open. To start the test, 2 ml of a saturated KOH solution in 1-butanol was injected from the syringe; at the same time, the valve was closed and the gas collected. The reaction was allowed to run for at least 30 min until the thin foam layer had had lost its integrity (Table 5.4, Figure 7.35). Theoretically, 37.41 ml of gas would be produced from 1 g of PHMS by this method. Therefore, the conversion of "Si-H" was calculated by using followed equation:

$$Conversion_{Si-H}\ \% = \frac{Volume_{collected\ gas}}{Mass_{foam\ layer} \times wt\%_{PHMS} \times 37.42} \times 100\%$$

where the $Volume_{collected\ gas}$ is read from the experimental setup, the $Mass_{foam\ layer}$ is the weight of sliced thin layer dispersed in 1-butanol: the $wt\%_{PHMS}$ for different formulations may be found in Table 5.1.

5.3.4 Characterization

ATR-FTIR (attenuated total reflectance infrared spectroscopy, Thermo Scientific Nicolet iS10) and ^{1}H NMR spectra (Bruker Avance 400 MHz nuclear magnetic resonance spectrometer with 32 scans for ^{1}H NMR) were also used to characterize Si-H conversion and curing progress during composite fabrication. The modulus and elongation-at-break of lignin-silicone foams were determined using a Universal Test System (INSTRON 3300, 300 N load cell). The foam sheet was cut into a dumbbell shape (according to French Standard NF T51-034, H2) and clamped with grips at both ends. The crosshead speed of stretching was set for 20 mm/min. An electronic digital micrometer (EG100, Onosokki; 0.001-mm sensitivity) was used to measure the average thickness and width of the tested specimens at three random positions. Thermogravimetric analysis (TGA, TA instruments Q500) was run under air from 50 - 800 °C with a 10 °C /min step. Dynamic mechanical analysis (DMA, Triton, Germany) was performed under compression mode with the frequency of 1 Hz and heating rate of 1 °C/min. The tested samples were punched as a disk (dimensions: diameter = 10 mm, and thickness = 3 mm). The glass transition temperature (Tg) was determined from the peak temperature of the damping (tan δ) curve. The morphologies of foam cross-sections were imaged using a digital single-lens reflex camera with macro view mode (Canon T3).

5.4 Results and discussion

5.4.1 Optimal foam structures

Visually, foams are materials containing dispersed voids. They are characterized by overall bubble density, and the homogeneity of bubble size and shape. Preliminary experiments revealed the approximate conditions and formulations necessary to generate foams using mixtures of $B(C_6F_5)_3$, lignin, and silicone hydrides (see Figure 7.36 for details). Two steps were used in the process: formulations were first extruded at room temperature to give a homogenous mixture; in the second stage, the extruded lignin-silicone precursor was compression molded at elevated temperatures to give foamed composite. A few classes of foams produced during model studies are representative of the rest of the foams discussed below. To facilitate that discussion, three typical foams types are presented in Figure 5.1: the "foam" exhibiting large and randomly sized voids (Type A), closed cell foams with uniform morphology (Type B), and solid foams with trapped bubbles and fewer defects (Type C). Foams of Type A1 are generally easy to break, and have domains either very soft or hard. Type C foams are more rigid than the other two types. However, type B foams are of particular interest because of their excellent insulating properties.(Lee et al., 2005) Following a summary of the chemistry used to blow the foams, the ability to control foam structure by varying both processing conditions and formulations will be presented.

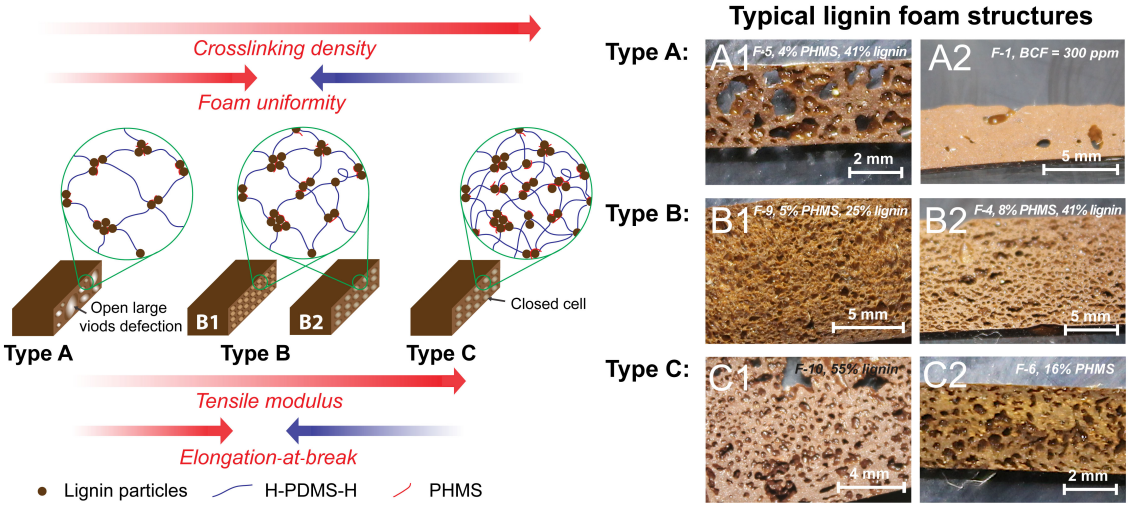

Figure 5.1 Illustrations of lignin-silicone foam structures, and their resultant mechanical properties: tensile modulus increases with crosslinking density, while the elongation-at-break are depended on both crosslinking density and uniformity of foams. Type A structures are foams either with large trapped (A1) or collapsed voids (A2, closer to an elastomer than a foam); Type A1 foams are easy to break with extension of bending due to the large defects. Type B structures are foams with uniform morphology; these foams are flexible with tunable toughness. Types C are foams with excessive crosslinking density and fewer voids; Type C1 foams are tough, while Type C2 were brittle.

5.4.2 Chemistry at the lignin-silicone interface

The reaction between hydrosilanes and lignin in the presence of $B(C_6F_5)_3$ can lead to elastomers and, in the absence of diluents, foams. Two reactions are involved in the process: the reaction between lignin and hydrosilane to 'siliconize' the lignin surface, and crosslinking of the silicone. Both of these reactions produce gas, primarily hydrogen from

OH groups, and methane from ArOMe groups, with other alkanes formed in low concentration (Scheme 5.1, Scheme 5.3). The spontaneously generated gases can act as perfect *in-situ* blowing agents for foam fabrication if molding conditions can be properly managed.

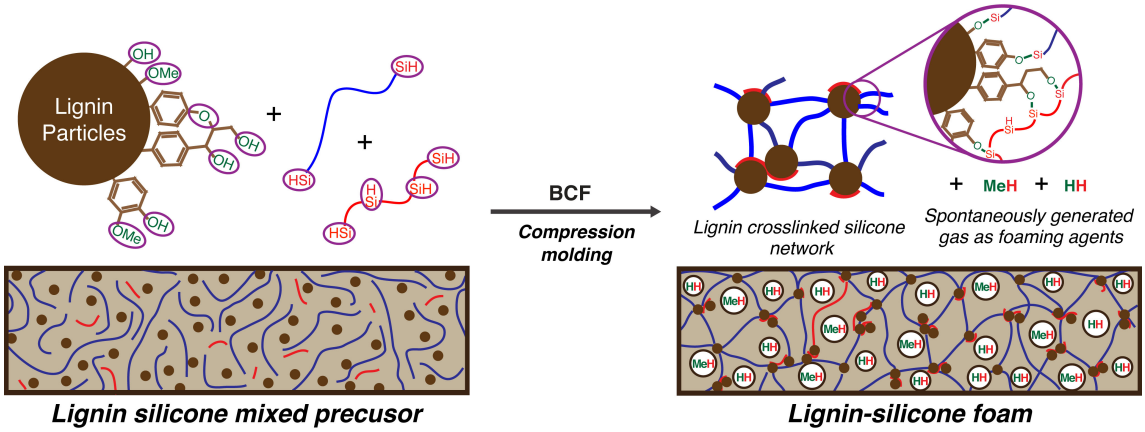

Scheme 5.3 The chemistry at lignin interface: silylation and crosslinking during the compression molding processing.

5.4.3 Optimization of formulations and processing conditions for lignin-silicone foam

One objective of this research was to establish if, while controlling foam structure, the materials could be compression molded into desired shapes after mixing the ingredients in an extruder: mixing rather than chemistry should occur in the extruder. Fortunately, during the extrusion process, the reaction rate for condensation between aryl ether/hydroxyl and hydrosilane is expected to be relatively slow until uniform mixing of the components is achieved, particularly if the materials are not heated. By contrast, during (heated) compression molding the reaction rate is expected to be fast.

During the chemical grafting process (designed to take place during compression molding), the reduction of phenol, alcohol, and methoxy groups at the lignin surface by hydrosilanes results in large volume of gas being produced (Scheme 5.1, Scheme 5.3). Because the gas is trapped in the volume-confined mold, a foamed lignin-silicone composite is produced. The nature of the foamed structure is determined by the competition between crosslinking (and attendant viscosity build) and gas production. Several key process factors were examined, including formulation: catalyst loading; crosslinker (lignin) and co-crosslinker (PHMS) concentrations; and molecular weight of the H-PDMS-H). Reaction conditions including temperature and feeding order of reagents were also investigated during extrusion and compression molding to better understand the relationship between the process and foam structure.

5.4.3.1 Optimization of the formulation

Catalyst loading: The impact of catalyst loading on reaction rate is straightforward: higher reaction rates (of gas generation and crosslinking) were observed with increasing loading. The preliminary studies examined catalyst loading from 300 ppm to 2000 ppm. At higher loadings, e.g., 4000 ppm, the reaction is too fast to control, with induction time less than 30 seconds. In addition, excess catalyst led to scabbing in the channel of extruder (Figure 7.37).

Distinct foam structures were formed as a function of catalyst loading. At lower catalyst loading (300 ppm), the composite presented as a solid elastomer rather than a foam (Type A2 in Figure 5.1). More uniform foams formed at higher catalyst loadings

(BCF = 1000, and 1350 ppm, Figure 7.38). A uniform foam with small, regular and dispersed voids was produced with 2050 ppm BCF (Type B2 in Figure 5.1). In our view, the properties of such closed cell, homogeneous closed cell homogeneous foams are most desirable and optimization methods were developed to lead to such materials

These results are readily understood as a consequence of the competition between curing and gas production. Both rates were low at lower catalyst loadings. Therefore, the gas can escape at a rate comparable with its production during molding process, leaving the upper portion of the mold unfilled and a low porosity product (Figure 7.39). Porous structures required higher catalyst loadings, when both the curing and gas production rates increased.

Lignin (crosslinker) and PHMS (co-crosslinker) content: Lignin, as shown in Scheme 5.3, acts as both polyfunctional crosslinker and filler in the formulation. PHMS, while also acting as flexible crosslinker, is primarily responsible for the formation of hydrogen and alkane by-products and the concomitant crosslinking that occurs during foaming (Scheme 5.3). As a consequence, the lignin and PHMS concentrations controlled the rates of crosslinking.

Lignin: The extrusion/molding optimizations demonstrated that foams with a uniform structure could be made with lignin contents ranged from 25 to 55% (Types B1, B2, and C1 in Figure 5.1), although some defects were found with foams containing 55% lignin: mixtures with higher lignin contents also proved more difficult to extrude.(Zhou et al., 2006) The viscosity of the uncured, mixed precursor increases with direct correlation

to lignin content, simply due to an increase in the solid fraction in the mixture. Formulations with lower lignin content (F-8, 15%) led to foams with Type A1 structure (Figure 5.1, Figure 7.40) due to the slower build in viscosity that facilitated gas escape.

PHMS: Foams with non-uniform and large vacancies resulted when insufficient PHMS was present (4wt%, Figure 7.41), mainly due to the slower rate of gas production. By contrast, foams with uniform pores were obtained within an appropriate range of PHMS content (from 8 to 24wt%). The porous structure of these foams was uniform, but subtle changes in PHMS concentrations led to differences in specific morphologies (e.g., both Types B2 and C2 in Figure 5.1, were made within this PHMS concentration range, Figure 7.41). Foams with the more desirable closed and uniform structure (Type B) were made from formulations with intermediate PHMS content (~8%).

Molecular weight of H-PDMS-H: As noted above, viscosity could be used as an effective tool for tailoring foam morphologies by varying lignin content. H-PDMS-H served as a spacer that reduced crosslink density and an additional way to manipulate viscosity. This ingredient was varied with respect to the chain length of the PDMS spacer. Foams with uniform porous structures (Type B1 and B2 in Figure 5.1) were only obtained when intermediate viscosities were used, either by choosing a spacer of appropriate chain length (F-4B, $Mw_{silicone\ spacer}$ = 28,000 g/mol), or by mixing different H-PDMS-H spacers with a distribution of chain lengths (F-13, $Mw_{silicone\ spacer}$ 6,000 to 62,700 g/mol, Table 5.1, Figure 7.42). By contrast, low viscosities that accompanied the use of 6,000 g/mol H-PDMS-H resulted in a Type A1 structure (F-11, Figure 5.1, Table 5.1, Figure 7.42), and

use of high molecular weight spacers (F-12, Mw 62,700 g/mol) led to mixtures that were too viscous to mix and extrude (Figure 7.43). Therefore, the optimal formulations for Type B foams were F-4B, F-9, and F-13 (Table 5.1).

5.4.3.2 Optimizations with respect to processing

The foam generation process involves two steps: mixing in an extruder, and curing in a compression mold (under different temperatures and holding times). The conditions for each of these steps needed to be optimized in light of the chemical steps taking place. There is normally an induction time for the Piers-Rubinsztajn reaction and the feeding order of reagents impacts the length of that induction time. Substances such as water, alcohol, or other impurities found in lignin can form adducts with $B(C_6F_5)_3$, retarding the rate of the desired reaction:(Brook et al., 2011a, Blackwell et al., 1999) there may be other factors that affect reaction induction. Thus, the timing of the extrusion and holding time/compression steps must be coordinated with these chemical factors.

Mixing order: In preliminary studies, the induction time varied with feed order (Figure 7.36). When BCF was premixed with lignin prior to the addition of the hydrosilanes (Mixing order A), longer induction times and slower initial reaction rates resulted. By contrast, shorter induction times and rapid reaction rates were observed if hydrosilanes were premixed with lignin in prior to adding BCF (Mixing order B). As a slow reaction rate is desired in the first step, “Mixing order A” was adopted as the standard feeding order for preliminary studies, and also for the extrusions.

Temperature: Similar to the impact of catalyst loading, increasing temperature resulted in decreased induction times, while increased reaction rates. In preliminary optimizations using a solution system, not an extruder, a high conversion% of PHMS (more than 50%, as shown by gas evolution) was reached within 300 s at 90 °C (Figure 7.36); by contrast, less than 10% of PHMS was reacted after 1500 s at 30 °C. Therefore, for the extrusion step, lower temperature is desired.

During compression molding, the mixture from extruder developed strength and shape (against the mold surface) while curing, which was also affected by temperature. The properties and performance of resultant materials depended on the curing progress. In our test, incomplete cure was shown by the presence of extractable polymers that had not grafted into the foam network, and which could be removed by cyclohexane extraction. Although cured foams were obtained after holding for 5 minutes over the whole tested temperature range from 60 to 120 °C (see below for other holding times), the quantities of extractable substances were not linear with temperature (Table 5.2). Either higher (120 °C) or lower (60 °C) molding temperatures resulted in higher ratios of extractable substances. This outcome at low temperatures is readily understood: the reaction rate was so slow that unbound hydrosilane remained. By contrast, the fast reaction rate at higher molding temperatures caused immediate gelation, capturing domains of uncured cured materials.

Foam morphology was also affected by molding temperature. Desirable uniform foam structures were observed at intermediate temperatures (90 °C, F-4B, BCF = 2050 ppm, Type B2 in Figure 5.1), whereas non-uniform sized and randomly distributed

bubbles (Type A1 in Figure 5.1, Figure 7.44) were produced at either lower (60 °C) or higher (120 °C) molding temperatures with identical formulations (F-4A and C, BCF = 2050 ppm). As at lower molding temperatures, primary bubbles had time to coalesce at a rate comparable to cure, leading to large and randomly sized bubbles; while at higher temperatures, uncontrolled rapid foaming occurred at the start of reaction, again leading to large voids: as noted above, inhomogeneity led to significant quantities of extractables at this temperature.

Holding time: In general, samples were allowed to cure for 5 minutes during compression molding. Longer holding times were not beneficial as shown using F-3 as an example. The Si-H signal (ATR-IR) was reduced significantly after 5 minutes curing at 90 °C (Figure 7.46), but only a very subtle decrease (~ 5% of peak area) of Si-H signal was observed after additional holding times. Similarly, solvent extraction (Table 5.2, ~ 2% decrease in extractables) and NMR tests (no Si-H was detected after 15 minutes) showed very small changes after this time (Figure 7.47). Thus, there is no benefit to molding for longer times than 5 minutes. Note that a portion of the extractables may have resulted from partially depolymerized fragments from softwood lignin rather than silicones.(Zhang et al., 2014)

Table 5.2 The weight formation (%) of lignin-silicone foams after extraction with cyclohexane

No.	Molding temperature (°C)	BCF (ppm)	Polymer yield (weight% residual foam after extraction) after different holding periods				
			5 min	15 min	30 min	60 min	180 min
F-1	90	300	- [a]	- [a]	- [a]	63	93
F-2	90	1000	81	89	89	90	91
F-3	90	1350	82	90	91	91	92
F-4 A	60	2050	87	88	88	89	91
F-4 B	90	2050	89	90	90	90	92
F-4 C	120	2050	83	84	84	84	86

[a] Extraction failed because the uncured lignin-silicone precursor was a liquid or paste.

Post-curing out of the mold: Si-H groups are susceptible to both oxidation and hydrolysis, leading to the formation of Si-OH groups that, in turn can condense ($R_3SiH \rightarrow R_3SiOH \rightarrow R_3SiOSiR_3$). These processes provide a secondary mechanism for crosslinking once the foam is removed from the mold. As these changes have the potential to impact the mechanical and other properties of resultant lignin-silicone foam (e.g., flammability), it was essential to quantitate the residual Si-H groups and eliminate them as much as possible via an extra post-curing process.

The concentration of residual Si-H groups in cured foams was determined by collecting the gas emitted, hydrolyzing the foam in a KOH/1-butanol solution. The degree of Si-H secondary cure through oxidation/hydrolysis exhibited a dependence on post-

curing temperature (Table 5.4). To test this proposal, a post-curing process was applied to F-4, a foam with good morphological qualities, at a higher temperature than that used during compression. It should be noted that post-curing had no impact on foam morphologies, since the foam structure had been set during compression molding. However, post cure increased the moduli through additional curing. As shown in Table 5.4, the storage modulus increased with samples that had been posted cured near 140 °C for 12 hours (see below). However, compared with post curing at 140 °C, higher post-curing temperatures (> 170 °C) led to degraded mechanical performance. There was no benefit gained at higher temperatures. The conversion % of Si-H was significantly increased, up to 79%, after post-curing beyond 170 °C, which is the critical point for lignin degradation (TGA, Figure 7.48) and repolymerization.(Li et al., 2007) Weight loss and homogenous shrinkage in all dimensions were observed for samples post-cured beyond 170 °C (volume shrinkage: > 8% at 220 °C, and ~ 20 % at 300 °C).

Table 5.3 The conversion ratio of Si-H in lignin-silicone foam after post-curing at higher temperature, and their mechanical performance

Post-curing		Weight	E'	E''
T (°C)	Time (h)	loss (%)	@ T_m + 50 °C (MPa)	@ T_m + 50 °C (MPa)
Control (no post-curing)		0	0.54	0.13
140	12	0	1.2	0.16
220	5	8	1	0.15
	12	16	0.67	0.073
300	12	20	0.52	0.025

5.4.4 Mechanical properties of lignin-silicone foams

The mechanical properties of lignin-silicone foam were measured by tensile tests and dynamical mechanical analysis (DMA, Table 5.1, and Table 7.7). Lignin – in the form of rigid particles – provides reinforcement for the otherwise soft silicone foam, altering the mechanical properties. Also, the morphologies of the foamed structures themselves were shown to strongly impact the mechanical performance of the foams.

DMA: A typical DMA curves for the lignin-silicone foams, including changes of tan δ (tan delta, red), storage (E', blue), and loss (E'', green) modulus with temperature, are shown in Figure 5.2. Similar to other silicone materials: the glass transition (T_g) was found near -112 °C;(Thanawala and Chaudhury, 1999) cold crystallization was observed in a range from -100 to -90 °C;(Chien et al., 2006, Bosq et al., 2014) the melting of silicone (T_m) occurred within the range from -42 to -36 °C.(Kosfeld and Heß, 1979,

Lacoste-Ferré et al., 2006, Bosq et al., 2014) The E' and E" (storage and loss moduli, respectively) in unreinforced silicones decreases continuously in the glassy region.(Darras et al., 2007, Lacoste-Ferré et al., 2006) The storage and loss moduli of the lignin reinforced foam stayed almost constant between -90 to -50 °C in exactly the same way as commercial silica reinforced silicone materials.(Chien et al., 2006, Bosq et al., 2014) More importantly, a significant improvement of the storage modulus in the rubbery region was observed with lignin reinforcement ranging from 0.3 to 17 MPa (Table 7.7), values that are comparable to some silica reinforced silicone materials (usually found in the range from 1 to 10 MPa).(Lacoste-Ferré et al., 2006, Bosq et al., 2014)

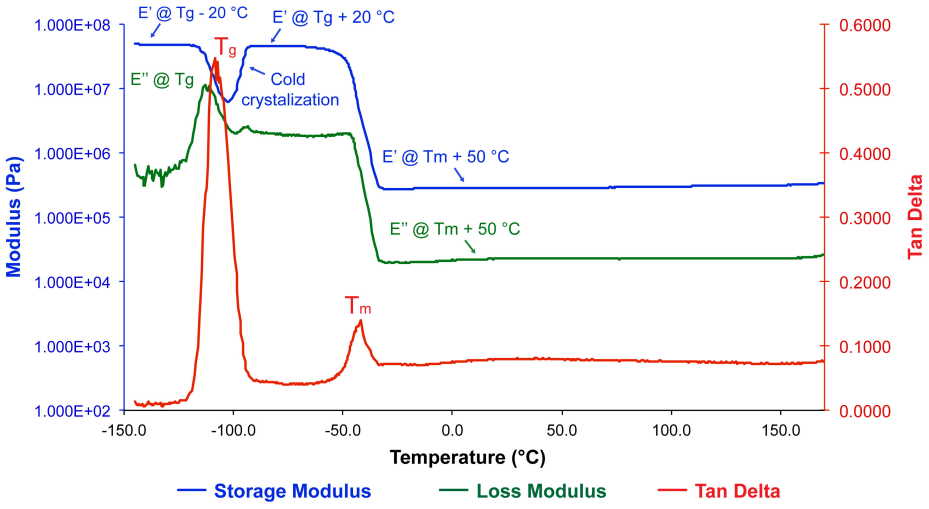

Figure 5.2 The reprehensive DMA curves of lignin-silicone (F-9).

The impact of crosslinking density on mechanical performance (at a molecular level): the storage modulus increases proportionally to crosslinker density ($\rho = E'_{@Tg+50\,°C}/3RT$).(Liu et al., 2014) At the rubbery region, the storage modulus was found to increase

with both lignin and PHMS content (DMA, Table 7.7): as lignin content increased for 25 to 55wt%, E' went from 0.29 to 3 MPa; as the other crosslinker PHMS increased from 8 to 24wt%, E' increased from 0.54 to 17 MPa. The storage modulus of samples with even lower crosslinking density (15% lignin or 4% PHMS) did not follow this rule, however, due to the large voids present.

The impact of polymer network structure on mechanical performance (at a microscopic level): The glass transition temperatures (T_g) of lignin-silicone foam were found to be comparable to the T_g (-119 °C) of an end-linked silicone network (Table 7.7),(Bosq et al., 2014, Schroeder and Roland, 2002) implying the network of which the foam is composed has particles bridged by hydride-terminated silicones. The foams with excess PHMS (F-6 and 7) were found to have higher T_g (Table 7.7), due to the increasing fraction of a secondary crosslinker in the network, and these materials were too brittle to perform tensile tests. The molecular weights of H-PDMS-H also influenced the network structure and mechanical performance. The brittleness of the foam increased as the PDMS chain length was reduced; mixtures of spacer lengths ameliorated the performance (F-4B, F-11, and F-13, Table 5.4).(Schimmel and Heinrich, 1991)

Table 5.4 The tensile test for lignin-silicone foams

No.	Modulus (MPa)	Lignin content (%)	PHMS content (%)	Elongation-at-break (%)
F-4 B	0.30	41	8	139
F-5	0.07	41	4	143
F-6	0.85	41	16	81
F-7	- [a]	41	24	- [a]
F-8	- [b]	15	4.4	- [b]
F-9	0.13	25	5	249
F-11 [c]	0.38	41	8	111
F-13 [d]	0.42	41	8	147

[a] Tensile test failed due to sample brittleness. [b] Tensile test failed due to sample torn at loading. [c] DMS-H25 was used as the spacer. [d] Silicone spacer contains 26% DMS-H25, 48% H31, and 26% H41. The modulus and elongation-at-break were obtained from averaging 3 repetitions of the tensile test.

The impact of morphology on mechanical performance (at macroscopic level): Compared with the factors discussed above, foam morphology plays a much stronger role in determining mechanical performance. The results of DMA and tensile test demonstrated that the homogenous closed cell foams Type B1 and B2 (Figure 5.1) had better performance that balanced strength and elongation-at-break. By contrast, the Type A1 foams (F-5, 8 and 11) were easy to break due to the defects of large voids (Table 5.4); Type A2 was rather described as an elastomer than foam (that was also easy to break due to the distributed large void defects). Type C was much more tough (Type C1) and rigid (Type C2) than type B foams.

Thermal mechanical performance of lignin-silicone foams: Silicone polymers exhibit excellent mechanical performance across a wide temperature range, from -100 to 316 °C. By contrast, the decomposition of lignin usually starts near 170 °C (TGA, Figure 7.48). Therefore, an examination of thermal mechanical performance of lignin-silicone foams at higher temperature was necessary.

As shown in Table 5.3, the mechanical performance of lignin-silicone foams was improved, as shown by increased storage and loss moduli, after post-curing at 140 °C for 12 hours as a consequence of secondary crosslinking through the oxidative/hydrolytic cleavage of Si-H groups. However, the values of storage and loss moduli at T_m + 50 °C dropped if higher temperatures or longer post cures were used (post-curing temperature beyond 170 °C, Table 5.3). Under these conditions, further oxidation and condensation of Si-H to Si-OH and dimerization, or condensation with lignin or repolymerization of lignin, resulted in a significant increase in crosslinking density and, consequently, brittleness.(Zhang et al., 2015b, Li et al., 2007)

The fabrication of lignin-silicone foams via Piers-Rubinsztajn (PR) reaction is beneficial with respect to for its efficiency, simple formulations and processing. Compared to other lignin-based composites, especially lignin-polyurethane foams, no pretreatment on lignin (e.g., removing high molecular weight lignin fractions,(Yoshida et al., 1990) or pre-liquefying lignin with poly(ethylene glycol)(Cinelli et al., 2013) was required to obtain flexible, closed cell, lignin-reinforced foams. The properties of the foam are readily tuned by formulation. The foamed silicone products offer similar

performance in thermal stability to polyurethane, and the materials are far more flexible, even with higher lignin content. The process itself is advantageous because no additional blowing agents are required.(Li and Ragauskas, 2012b)

Softwood is readily incorporated into silicones to make elastomeric bio-composites.[19] A simple extrusion process can be used to efficiently mix ingredients, including lignin in up to 55 weight%. Compression molding at elevated temperatures for a few minutes leads to foams in which the lignin acts as a reinforcing filler and crosslinker. The structures of foam, and their accompanying properties, can be easily tailored by varying formulations and conditions. These facile processes give materials that serve as a more valuable alternative end use for lignin.

5.5 Conclusions

A simple and effective route for the preparation of foamed lignin-silicone composites via extrusion and compression molding was described. The formulation simply consists of hydrosilanes, BCF, and raw lignin particles: no pre-treatment is required. For processing, the reagents, including $B(C_6F_5)_3$, lignin, and silicone hydrides, were first extruded for a homogenous mixture at room temperature, and then molded under compression at elevated temperature. The morphology and uniformity of the foamed structure depends on many factors, including the content of lignin, BCF, or PHMS, the molecular weight of H-PDMS-H, and the molding temperature. The content of lignin, the reinforcing filler and crosslinker, could be varied in a wide range from 25 to

42% to give robust closed cell foams with excellent mechanical performance. The strength of the foam was improved by post-curing. The successful processing method for lignin-based bio-composite could open new pathways to the better utilization of lignin.

5.6 Acknowledgements

We acknowledge with gratitude the financial support of the Natural Sciences and Engineering Research Council of Canada (NSERC) and Sentinel: NSERC Research Network on Bioactive Paper. We thank Weyerhaeuser for the gift of softwood lignin and the FIBRE network for providing a travel grant to JZ to permit collaborative work in France.

5.7 References

ADLER, E. 1977. Lignin chemistry—past, present and future. *Wood Science and Technology,* 11**,** 169-218.

ARAÚJO, J. D. P., GRANDE, C. A. & RODRIGUES, A. E. 2010. Vanillin production from lignin oxidation in a batch reactor. *Chemical Engineering Research and Design,* 88**,** 1024-1032.

ARGYROPOULOS, D. S., SADEGHIFAR, H., CUI, C. & SEN, S. 2013. Synthesis and Characterization of Poly(arylene ether sulfone) Kraft Lignin Heat Stable Copolymers. *ACS Sustainable Chemistry & Engineering,* 2**,** 264-271.

BAUMBERGER, S., LAPIERRE, C., MONTIES, B. & VALLE, G. D. 1998. Use of kraft lignin as filler for starch films. *Polymer Degradation and Stability,* 59**,** 273-277.

BENDAHOU, A., KADDAMI, H. & DUFRESNE, A. 2010. Investigation on the effect of cellulosic nanoparticles' morphology on the properties of natural rubber based nanocomposites. *European Polymer Journal,* 46**,** 609-620.

BENHAMOU, K., KADDAMI, H., MAGNIN, A., DUFRESNE, A. & AHMAD, A. 2015. Bio-based polyurethane reinforced with cellulose nanofibers: A comprehensive investigation on the effect of interface. *Carbohydrate Polymers,* 122**,** 202-211.

BHANDARI, P. N., JONES, D. D. & HANNA, M. A. 2012. Carboxymethylation of cellulose using reactive extrusion. *Carbohydrate Polymers,* 87**,** 2246-2254.

BLACKWELL, J. M., FOSTER, K. L., BECK, V. H. & PIERS, W. E. 1999. B(C6F5)3-Catalyzed Silation of Alcohols: A Mild, General Method for Synthesis of Silyl Ethers. *The Journal of Organic Chemistry,* 64**,** 4887-4892.

BOSQ, N., GUIGO, N., PERSELLO, J. & SBIRRAZZUOLI, N. 2014. Melt and glass crystallization of PDMS and PDMS silica nanocomposites. *Physical Chemistry Chemical Physics,* 16**,** 7830-7840.

BRIDSON, J. H., VAN DE PAS, D. J. & FERNYHOUGH, A. 2013. Succinylation of three different lignins by reactive extrusion. *Journal of Applied Polymer Science,* 128**,** 4355-4360.

BROOK, M., GRANDE, J. & GANACHAUD, F. 2011a. New Synthetic Strategies for Structured Silicones Using B(C6F5)3. *In:* MUZAFAROV, A. M. (ed.) *Silicon Polymers.* Springer Berlin Heidelberg.

BROOK, M., GRANDE, J. & GANACHAUD, F. S. 2011b. New Synthetic Strategies for Structured Silicones Using B(C6F5)3. *In:* MUZAFAROV, A. M. (ed.) *Silicon Polymers.* Springer Berlin Heidelberg.

BROOK, M. A., GRANDE, J. B. & GANACHAUD, F. 2011c. New Synthetic Strategies for Structured Silicones Using $B(C_6F_5)_3$. *Advances in Polymer Science,* 235**,** 161–183.

CARPENTER, D., WESTOVER, T. L., CZERNIK, S. & JABLONSKI, W. 2014. Biomass feedstocks for renewable fuel production: a review of the impacts of feedstock and pretreatment on the yield and product distribution of fast pyrolysis bio-oils and vapors. *Green Chemistry,* 16**,** 384-406.

CARR, M. E. 1991. Starch-derived glycol and glycerol glucosides prepared by reactive extrusion processing. *Journal of Applied Polymer Science,* 42**,** 45-53.

CATETO, C., BARREIRO, F., RODRIGUES, A. & BELGACEM, N. 2008. RIGID POLYURETHANE FOAMS FROM LIGNIN BASED ‐ POLYOLS. *AIP Conference Proceedings,* 1042**,** 243-245.

CATETO, C. A., BARREIRO, M. F., OTTATI, C., LOPRETTI, M., RODRIGUES, A. E. & BELGACEM, M. N. 2013. Lignin-based rigid polyurethane foams with improved biodegradation. *Journal of Cellular Plastics*.

CATETO, C. A., BARREIRO, M. F., RODRIGUES, A. E. & BELGACEM, M. N. 2009. Optimization Study of Lignin Oxypropylation in View of the Preparation of Polyurethane Rigid Foams. *Industrial & Engineering Chemistry Research,* 48**,** 2583-2589.

CATETO, C. A., BARREIRO, M. F., RODRIGUES, A. E. & BELGACEM, M. N. 2011. Kinetic study of the formation of lignin-based polyurethanes in bulk. *Reactive and Functional Polymers,* 71**,** 863-869.

CHIEN, A., MAXWELL, R. S., DETERESA, S., THOMPSON, L., COHENOUR, R. & BALAZS, B. 2006. Effects of filler–polymer interactions on cold-crystallization kinetics in crosslinked, silica-filled polydimethylsiloxane/polydiphenylsiloxane copolymer melts. *Journal of Polymer Science Part B: Polymer Physics,* 44**,** 1898-1906.

CHRUŚCIEL, J. J. & LEŚNIAK, E. 2011. Preparation of flexible, self-extinguishing silicone foams. *Journal of Applied Polymer Science,* 119**,** 1696-1703.

CHUNG, H. & WASHBURN, N. R. 2012. Improved Lignin Polyurethane Properties with Lewis Acid Treatment. *ACS Applied Materials & Interfaces,* 4**,** 2840-2846.

CHUNG, Y.-L., OLSSON, J. V., LI, R. J., FRANK, C. W., WAYMOUTH, R. M., BILLINGTON, S. L. & SATTELY, E. S. 2013. A Renewable Lignin–Lactide Copolymer and Application in Biobased Composites. *ACS Sustainable Chemistry & Engineering,* 1**,** 1231-1238.

CINELLI, P., ANGUILLESI, I. & LAZZERI, A. 2013. Green synthesis of flexible polyurethane foams from liquefied lignin. *European Polymer Journal,* 49**,** 1174-1184.

CIOBANU, C., UNGUREANU, M., IGNAT, L., UNGUREANU, D. & POPA, V. I. 2004. Properties of lignin–polyurethane films prepared by casting method. *Industrial Crops and Products,* 20**,** 231-241.

DARRAS, V., FICHET, O., PERROT, F., BOILEAU, S. & TEYSSIÉ, D. 2007. Polysiloxane–poly(fluorinated acrylate) interpenetrating polymer networks: Synthesis and characterization. *Polymer,* 48**,** 687-695.

DONMEZ CAVDAR, A., KALAYCIOGLU, H. & HIZIROGLU, S. 2008. Some of the properties of oriented strandboard manufactured using kraft lignin phenolic resin. *Journal of Materials Processing Technology,* 202**,** 559-563.

FEGHALI, E. & CANTAT, T. 2014. Unprecedented organocatalytic reduction of lignin model compounds to phenols and primary alcohols using hydrosilanes. *Chemical Communications,* 50**,** 862-865.

FELDMAN, D., LACASSE, M. & ST. J. MANLEY, R. 1988. Polyurethane-based sealants modified by blending with Kraft lignin. *Journal of Applied Polymer Science,* 35**,** 247-257.

FERNANDES, E. M., AROSO, I. M., MANO, J. F., COVAS, J. A. & REIS, R. L. 2014. Functionalized cork-polymer composites (CPC) by reactive extrusion using suberin and lignin from cork as coupling agents. *Composites Part B: Engineering,* 67**,** 371-380.

FRISCH, K. C. 1981. History of Science and Technology of Polymeric Foams. *Journal of Macromolecular Science: Part A - Chemistry,* 15**,** 1089-1112.

GANDINI, A. 2008. Polymers from Renewable Resources: A Challenge for the Future of Macromolecular Materials. *Macromolecules,* 41**,** 9491-9504.

GANDINI, A., BELGACEM, M., GUO, Z.-X. & MONTANARI, S. 2002. Lignins as Macromonomers for Polyesters and Polyurethanes. *In:* HU, T. (ed.) *Chemical Modification, Properties, and Usage of Lignin.* Springer US.

GEVORGYAN, V., RUBIN, M., BENSON, S., LIU, J.-X. & YAMAMOTO, Y. 2000. A Novel B(C6F5)3-Catalyzed Reduction of Alcohols and Cleavage of Aryl and Alkyl Ethers with Hydrosilanes,Ä†. *The Journal of Organic Chemistry,* 65**,** 6179-6186.

GOSSELINK, R. J. A., DE JONG, E., GURAN, B. & ABACHERLI, A. 2004. Co-ordination network for lignin - standardisation, production and applications adapted to market requirements (EUROLIGNIN). *Industrial Crops and Products,* 20**,** 121-129.

GUO, Z.-X., GANDINI, A. & PLA, F. 1992. Polyesters from lignin. 1. The reaction of kraft lignin with dicarboxylic acid chlorides. *Polymer International,* 27**,** 17-22.

HEITNER, C., DIMMEL, D. & SCHMIDT, J. A. 2010. *Lignin and Lignans: Advances in Chemistry*, Taylor & Francis.

HOFMANN, K. & GLASSER, W. G. 1993. Engineering Plastics from Lignin. 21.1Synthesis and Properties of Epoxidized Lignin-Poly (Propylene Oxide) Copolymers. *Journal of Wood Chemistry and Technology,* 13**,** 73-95.

ISMAIL, T. N. M. T., HASSAN, H. A., HIROSE, S., TAGUCHI, Y., HATAKEYAMA, T. & HATAKEYAMA, H. 2010. Synthesis and thermal properties of ester-type crosslinked epoxy resins derived from lignosulfonate and glycerol. *Polymer International,* 59**,** 181-186.

KOSFELD, R. & HES, M. 1979. Dynamisch-mechanische Untersuchungen und Quellungsmessungen an technischen Silicon-Kautschuken. *In:* FISCHER, E. W., MÜLLER, F. H. & BONART, R. (eds.) *Anwendungsbezogene physikalische Charakterisierung von Polymeren, insbesondere im festen Zustand.* Steinkopff.

KUBO, S. & KADLA, J. F. 2003. The Formation of Strong Intermolecular Interactions in Immiscible Blends of Poly(vinyl alcohol) (PVA) and Lignin. *Biomacromolecules,* 4**,** 561-567.

LACOSTE-FERRÉ, M. H., DEMONT, P., DANDURAND, J., DANTRAS, E., BLANDIN, M. & LACABANNE, C. 2006. Thermo-mechanical analysis of dental silicone polymers. *Journal of Materials Science,* 41**,** 7611-7616.

LEE, L. J., ZENG, C., CAO, X., HAN, X., SHEN, J. & XU, G. 2005. Polymer nanocomposite foams. *Composites Science and Technology,* 65**,** 2344-2363.

LI, J., HENRIKSSON, G. & GELLERSTEDT, G. 2007. Lignin depolymerization/repolymerization and its critical role for delignification of aspen wood by steam explosion. *Bioresource Technology,* 98**,** 3061-3068.

LI, Y. & RAGAUSKAS, A. J. 2012a. Ethanol organosolv lignin-based rigid polyurethane foam reinforced with cellulose nanowhiskers. *RSC Advances,* 2**,** 3347-3351.

LI, Y. & RAGAUSKAS, A. J. 2012b. Kraft Lignin-Based Rigid Polyurethane Foam. *Journal of Wood Chemistry and Technology,* 32**,** 210-224.

LIU, W., ZHOU, R., GOH, H. L. S., HUANG, S. & LU, X. 2014. From Waste to Functional Additive: Toughening Epoxy Resin with Lignin. *ACS Applied Materials & Interfaces,* 6**,** 5810-5817.

MA, X., TIAN, Y., HAO, W., MA, R. & LI, Y. 2014. Production of phenols from catalytic conversion of lignin over a tungsten phosphide catalyst. *Applied Catalysis A: General,* 481**,** 64-70.

MOAD, G. 2011. Chemical modification of starch by reactive extrusion. *Progress in Polymer Science,* 36**,** 218-237.

NADJI, H., BRUZZÈSE, C., BELGACEM, M. N., BENABOURA, A. & GANDINI, A. 2005. Oxypropylation of Lignins and Preparation of Rigid Polyurethane Foams from the Ensuing Polyols. *Macromolecular Materials and Engineering,* 290**,** 1009-1016.

PAN, X. & SADDLER, J. 2013. Effect of replacing polyol by organosolv and kraft lignin on the property and structure of rigid polyurethane foam. *Biotechnology for Biofuels,* 6**,** 12.

PEARL, I. A. 1942. Vanillin from Lignin Materials. *Journal of the American Chemical Society,* 64**,** 1429-1431.

QIN, J., WOLOCTT, M. & ZHANG, J. 2013. Use of Polycarboxylic Acid Derived from Partially Depolymerized Lignin As a Curing Agent for Epoxy Application. *ACS Sustainable Chemistry & Engineering,* 2**,** 188-193.

SAITO, T., BROWN, R. H., HUNT, M. A., PICKEL, D. L., PICKEL, J. M., MESSMAN, J. M., BAKER, F. S., KELLER, M. & NASKAR, A. K. 2012. Turning renewable resources into value-added polymer: development of lignin-based thermoplastic. *Green Chemistry,* 14**,** 3295-3303.

SAITO, T., PERKINS, J. H., JACKSON, D. C., TRAMMEL, N. E., HUNT, M. A. & NASKAR, A. K. 2013. Development of lignin-based polyurethane thermoplastics. *RSC Advances,* 3**,** 21832-21840.

SCHIMMEL, K. H. & HEINRICH, G. 1991. The influence of the molecular weight distribution of network chains on the mechanical properties of polymer networks. *Colloid and Polymer Science,* 269**,** 1003-1012.

SCHROEDER, M. J. & ROLAND, C. M. 2002. Segmental Relaxation in End-Linked Poly(dimethylsiloxane) Networks. *Macromolecules,* 35**,** 2676-2681.

STIUBIANU, G., CAZACU, M., CRISTEA, M. & VLAD, A. 2009. Polysiloxane-lignin composites. *Journal of Applied Polymer Science,* 113**,** 2313-2321.

TEJADO, A., PEÑA, C., LABIDI, J., ECHEVERRIA, J. M. & MONDRAGON, I. 2007. Physico-chemical characterization of lignins from different sources for use in phenol–formaldehyde resin synthesis. *Bioresource Technology,* 98**,** 1655-1663.

THANAWALA, S. K. & CHAUDHURY, M. K. 1999. Surface Modification of Silicone Elastomer Using Perfluorinated Ether. *Langmuir,* 16**,** 1256-1260.

THIELEMANS, W., CAN, E., MORYE, S. S. & WOOL, R. P. 2002. Novel applications of lignin in composite materials. *Journal of Applied Polymer Science,* 83**,** 323-331.

THUNGA, M., CHEN, K., GREWELL, D. & KESSLER, M. R. 2014. Bio-renewable precursor fibers from lignin/polylactide blends for conversion to carbon fibers. *Carbon,* 68**,** 159-166.

VAN DE VEN, T. & GODBOUT, L. 2013. *Cellulose - Medical, Pharmaceutical and Electronic Applications*, InTech.

XUE, B.-L., WEN, J.-L. & SUN, R.-C. 2014. Lignin-Based Rigid Polyurethane Foam Reinforced with Pulp Fiber: Synthesis and Characterization. *ACS Sustainable Chemistry & Engineering,* 2**,** 1474-1480.

YOSHIDA, H., MÖRCK, R., KRINGSTAD, K. P. & HATAKEYAMA, H. 1987. Kraft lignin in polyurethanes I. Mechanical properties of polyurethanes from a kraft lignin–polyether triol–polymeric MDI system. *Journal of Applied Polymer Science,* 34**,** 1187-1198.

YOSHIDA, H., MÖRCK, R., KRINGSTAD, K. P. & HATAKEYAMA, H. 1990. Kraft lignin in polyurethanes. II. Effects of the molecular weight of kraft lignin on the properties of polyurethanes from a kraft lignin–polyether triol–polymeric MDI system. *Journal of Applied Polymer Science,* 40**,** 1819-1832.

ZHANG, J., CHEN, Y. & BROOK, M. A. 2014. Reductive Degradation of Lignin and Model Compounds by Hydrosilanes. *ACS Sustainable Chemistry & Engineering,* 2**,** 1983-1991.

ZHANG, J., CHEN, Y., SEWELL, P. & BROOK, M. A. 2015a. Utilization of softwood lignin as both crosslinker and reinforcing agent in silicone elastomers. *Green Chemistry,* 17**,** 1811-1819.

ZHANG, J., CHEN, Y., SEWELL, P. D. & BROOK, M. A. 2015b. Utilization of softwood lignin as both crosslinker and reinforcing agent in silicone elastomers. *Green Chemistry*.

ZHAO, B., CHEN, G., LIU, Y., HU, K. & WU, R. 2001. Synthesis of lignin base epoxy resin and its characterization. *Journal of Materials Science Letters,* 20**,** 859-862.

ZHOU, Y., WANG, S., ZHANG, Y., ZHANG, Y., JIANG, X. & YI, D. 2006. Rheological properties of PDMS filled with CaCo3: The effect of filler particle size and concentration. *Journal of Applied Polymer Science,* 101**,** 3395-3401.

CHAPTER 6: General conclusions

Surfaces and interfaces play important roles in influencing the properties and performance of materials. For certain applications, the modification of a surface or interface, by introducing selected elements or functional groups, is often required in order to improve the original or obtain new functionality for the materials. The focus of this thesis was to develop silane/silicone chemistry to manipulate silicone elastomer interfaces for specific applications.

Silicone elastomers are widely used in our daily life because of their unique properties: flexibility, transparency, and thermal and chemical stability, etc. However, the hydrophobicity of silicone elastomers limits their application in many fields, ranging from biomaterials to microfluidic devices. Various methods have been developed for the modification of silicone elastomers, however, there are still challenges remaining including the ability to overcome "hydrophobic recovery" and surface damages. In addition, there is interest in spatially controlling the behavior of silicone surfaces.

In Chapter 2, the thiol-ene click chemistry was utilized for silicone surface modification to obtain long-term hydrophilicity. The thiols were introduced onto silicone surfaces via base-catalyzed equilibrium silanization of a thiol containing silane coupling agent ($(MeO)_3Si(CH_2)_3SH$). The thiols were demonstrated to be located mainly at interface, however, without significantly affecting the surface morphology. The quantities of thiols at surface were determined using two different but complementary methods:

DTDP (4,4′-dithiodipyridine, titrating thiols only at interface) and iodine titration (titrating thiols throughout the material). The thiol-functionalized PDMS was then modified with maleic anhydride, which enabled the surface to be further modified with variety of polymers or surfactants containing hydroxyl- or amino- groups via a ring-opening esterification/amidation. The modified PDMS surface demonstrated improvement and recovery of hydrophilicity over a long tested period.

From Chapter 3 to 5, controllable modifications on hydrocarbon materials were described. With the increasing pressure on natural resource and energy shortage, more and more attention is paid to biomass application. Lignin is the second most abundant naturally occurring organic polymer on the earth. However, the difficulties of lignin processing have impeded its utilization in the chemical industry. In those three Chapters effective and simple methods for depolymerizing lignin to oligomeric aromatic molecules, and/or for integrating it into silicone as crosslinker/filler of composites were described.

In Chapter 3, the attempts were starting with the depolymerization/modification of lignin model compounds. The linkages and functional groups such as β-O-4, α-O-4, alcohol and methoxybenzene were readily cleaved or silylated by hydrosilanes, catalyzed by $B(C_6F_5)_3$; however, other linkages like 4-O-5 were non-reactive. The chemistry was then pushed to permit depolymerization of actual lignin samples: up to 96% of hardwood lignin was efficiently degraded into organosoluble products by the monofunctional hydrosilane. Due to the high content of non-reactive linkages, only a small portion of

softwood lignin (~30%) was degraded even using excess hydrosilane and high catalyst loadings.

Chapter 4 and 5 of this thesis follows the work of Chapter 3. Although the results for softwood lignin depolymerization were not satisfactory, the results led us to another application – integration of softwood lignin for composites. Catalysed by $B(C_6F_5)_3$, softwood lignin was only partially reduced and preferentially at interface, therefore, it could be integrated into the hydrosilane rich silicone matrix. In this method, the lignin played dual roles as crosslinker and reinforcing reagent; more importantly, no pre-modification was required before processing. In Chapter 4, the lignin was used to crosslink/reinforce silicone elastomers. The resultant lignin-silicone elastomers were demonstrated to have excellent mechanical performance, which is comparable to some commercially available silicone elastomers. The mechanical properties of this elastomer were readily tuned by varying the formulation. Moreover, the composites demonstrated acceptable resistance to solvent extraction and excellent resistance to high temperature aging. In making such lignin-silicone elastomers, significant amounts of solvent were required for eliminating the formation of bubbles, resulting from the gas byproduct. However, the simultaneously generated gas could be used to facilitate the fabrication of foamed material. Therefore, in Chapter 5, a simple and effective method for making foamed lignin-silicone bio-composites via extrusion and compression molding was pursued. The reagents, including $B(C_6F_5)_3$, lignin, and silicone hydrides, were first extruded at room temperature; and then, the mixed precursor was compression molded to

give foamed composites at elevated temperature. The morphology and uniformity of the foamed structures were adjusted over wide ranges by changing lignin content, chemical structure of hydrosilanes, and processing parameters. Remarkably, softwood lignin was integrated in the silicone composite (elastomer and foam) crossed a wide range of content, from 0.5% up to 70%. These successful processing methods for lignin-based bio-composites open a new pathway for better utilization of lignin within silicones and more broadly in organic materials.

CHAPTER 7: Appendix

7.1 Supporting information for Chapter 2: Facile functionalization of PDMS elastomer surfaces using thiol-ene click chemistry

7.1.1 DTDP titration: calibration curve and sample calculation for surface concentration of thiol

DTDP has previously been demonstrated to be an efficient reagent to quantify thiol concentration. Following the literature procedure,(Riener et al., 2002, Egwim and Gruber, 2001) a calibration curve was first developed. MTS (0.0375 g, 0.191 mmol) was dissolved in DMSO (50 ml) to give a stock solution (0.382 mM). Solutions with different MTS concentrations were prepared by mixing 3 ml of media (0.1% Et_3N in DMSO v/v) with 5, 10, 20, 40, 60, 80, 120, and 160 μl, respectively, of the MTS stock solution. Then, DTDP reagent (150 μl of 4 mM in DMSO, 6×10^{-7} mmol) was added to each solution in turn. After 5 min, neat acetic acid (300 μl, 5.24×10^{-3} mmol) was added. Finally, 150 μl of the mixed solutions were placed in a 96 well plate and absorbances were determined at 347 nm.

Disks (diameter 9.5 mm and thickness about 0.5 mm) were punched from the thiol-modified elastomer. The disks were rinsed with methanol (30 ml), and dried under a flow of nitrogen for 5 min. During the titration, each of the disks was soaked separately in 3 ml

of media (0.1% Et_3N in DMSO v/v) containing the DTDP reagent (150 µl of 4 mM in DMSO, 6×10^{-7} mmol). After shaking for 30 min, neat acetic acid was added (300 µl) and the absorbance at 347 nm was recorded.

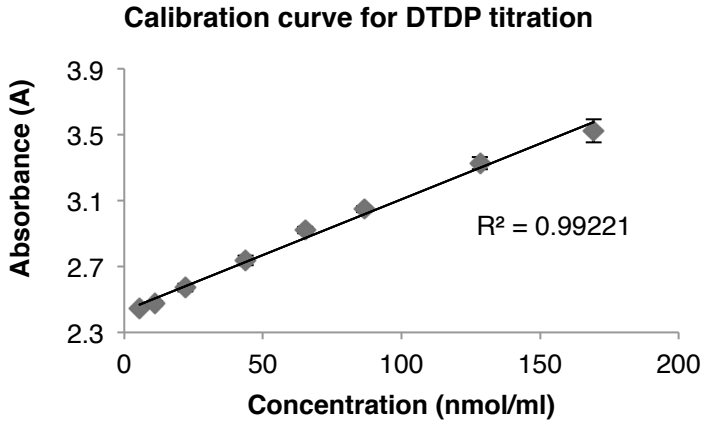

Figure 7.1 Calibration curve for DTDP titration, the eight data points at each concentration were triplicates each from three different DTDP stock solutions. Abs = 0.0068 [SH] + 2.4313.

The surface concentration of thiol could be obtained from following equations:

$[SH]_{surface}$ = ½ ([SH] × Assay Volume / Area)

where the [SH] = (Abs -2.4313)/0.0068

7.1.2 Iodine titration: calibration curve and sample calculation for surface concentration of thiol

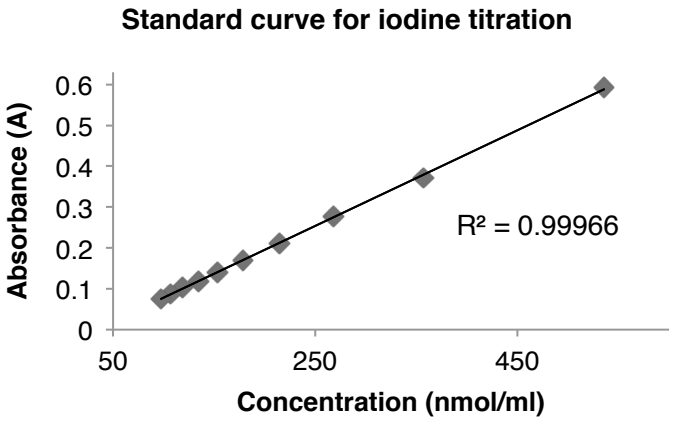

Figure 7.2 Calibration curve for iodine titration, Abs = 0.0012 $[I_2]$(Gandubert and Lennox, 2005) – 0.0387.

The surface concentration of thiol could be obtained from following equations:

$[SH]_{surface} = ½ (Moles_{SH} / Area)$

where the $moles_{SH} = 2 \times moles_{iodine}$

Note that some of the iodine solution remained in the elastomer and was therefore not measured in the UV. A control was used to establish the magnitude of this: the corrected consumption of iodine was:

$Moles_{iodine} = ((Abs_{sample} + 0.0387)/0.0012 - (Abs_{control} + 0.0387)/0.0012) \times$ Assay Volume

Figure 7.3 The sandwich structure of elastomer labeled with rhodamine (PDMS-S-MA-RH)

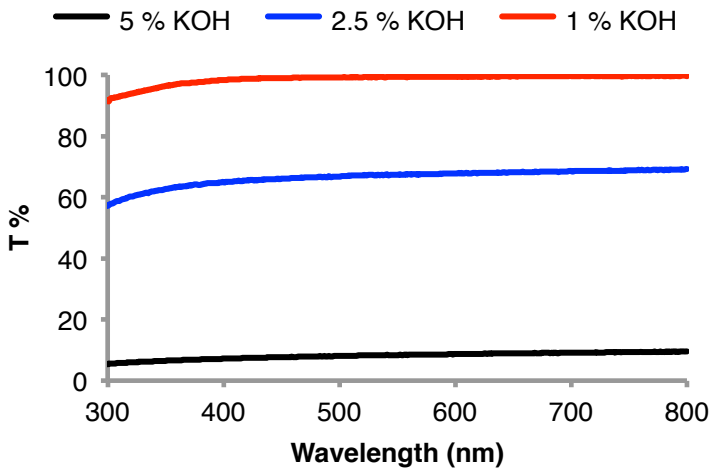

Figure 7.4 Transparency of PDMS elastomer after surface treatment with different base concentrations.

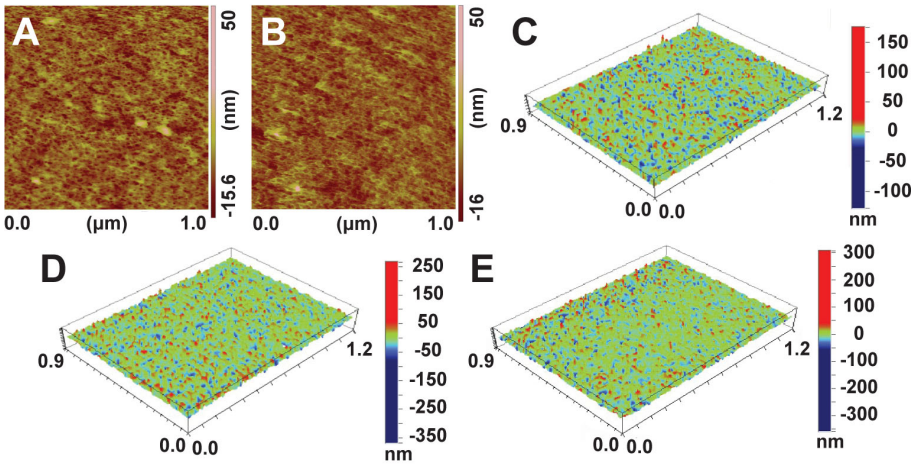

Figure 7.5 AFM and 3D plotted profilometry images for surface roughness characterization. (A) and (C) were measured from unmodified PDMS elastomer surfaces. (B) and (D) are the measurements of PDMS elastomer surfaces treated in 1% of KOH and 10% of MTS at 50 °C for 6 h. (E) 3D plotted profilometry images for surface modified with Silmer ACR. The image Rq for (A) to (E) were 4.09 nm, 4.80nm, 10.92 nm, 27.66 nm, and 20.0 nm, respectively.

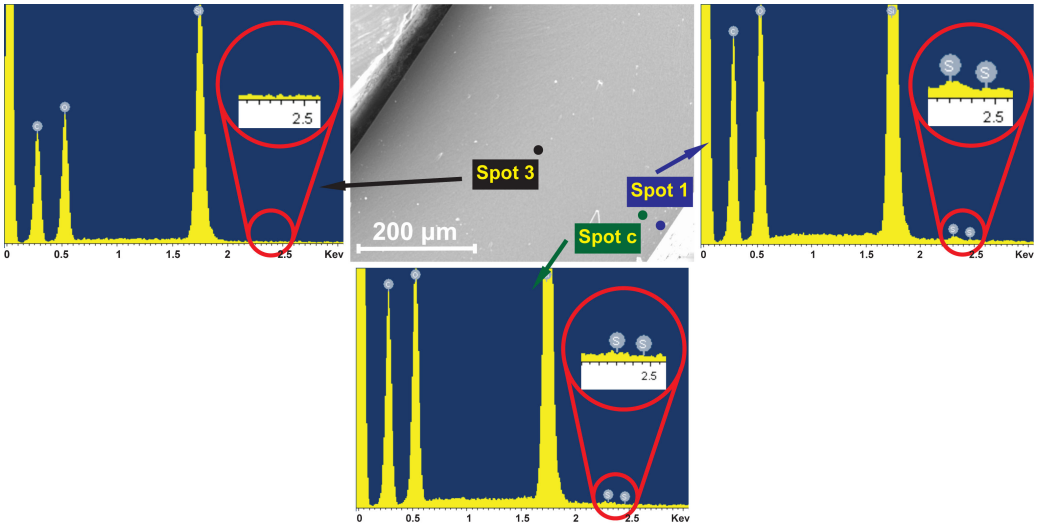

Figure 7.6 The EDX spectra obtained from different regions on the cross-section of the silicone elastomer.

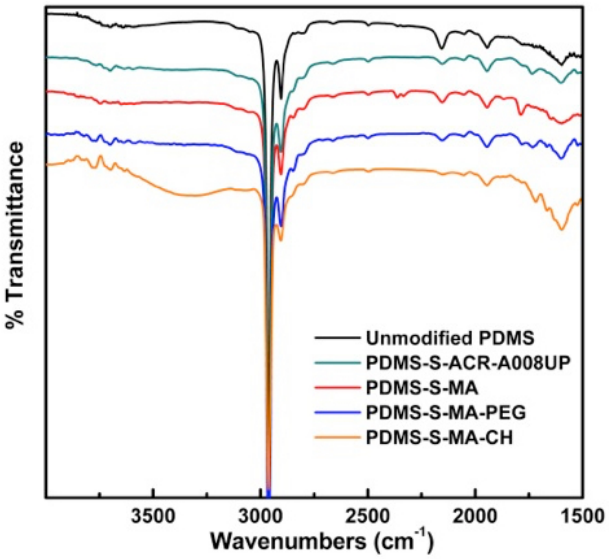

Figure 7.7 The ATR-FTIR spectra for PDMS surfaces modified with ACR-A008 UP (PDMS-S-ACR-A008UP), maleic anhydride (PDMS-S-MA), PEG (PDMS-S-MA-PEG), and chitosan (PEG-S-CH)

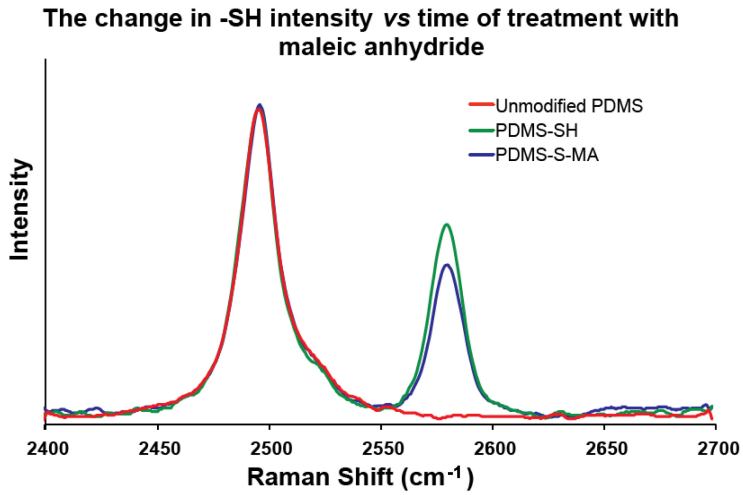

Figure 7.8 The Raman spectra of unmodified **PDMS**, thiol-functionalized **PDMS-SH**, and maleic anhydride modified **PDMS-S-MA**.

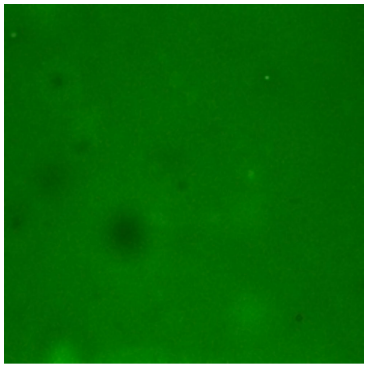

Figure 7.9 Fluorescence microscopy images of the thiol-functionalized PDMS elastomer (stored in ~2 °C refrigerator, sealed and soaked in methanol for more than 4 months), dyed with *N*-(5-fluoresceinyl) maleimide.

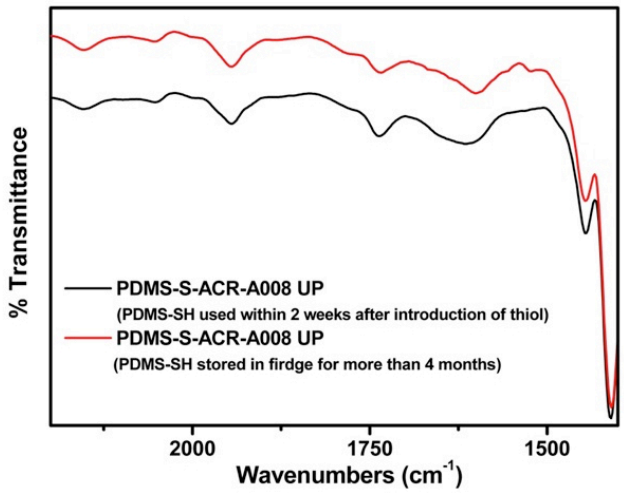

Figure 7.10 The ATR-FTIR spectrum for PDMS-SH surface (used within 2 weeks and over 4 month after base-catalyzed equilibrium treatment) modified with ACR-A008 UP

7.2 Supporting information for

Chapter 3: Reductive degradation of lignin and model compounds by hydrosilanes

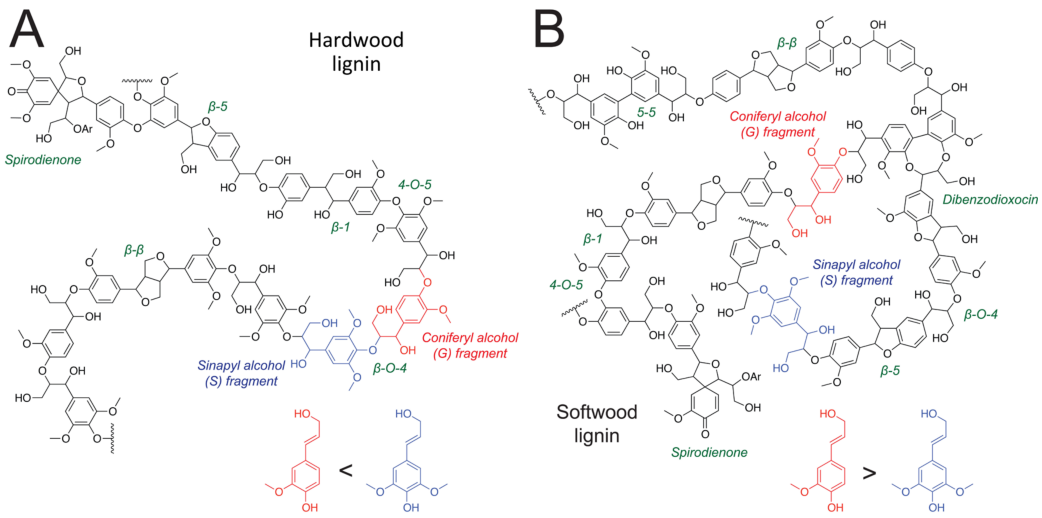

Figure 7.11 Model structures of (A) hardwood lignin, and (B) softwood lignin.

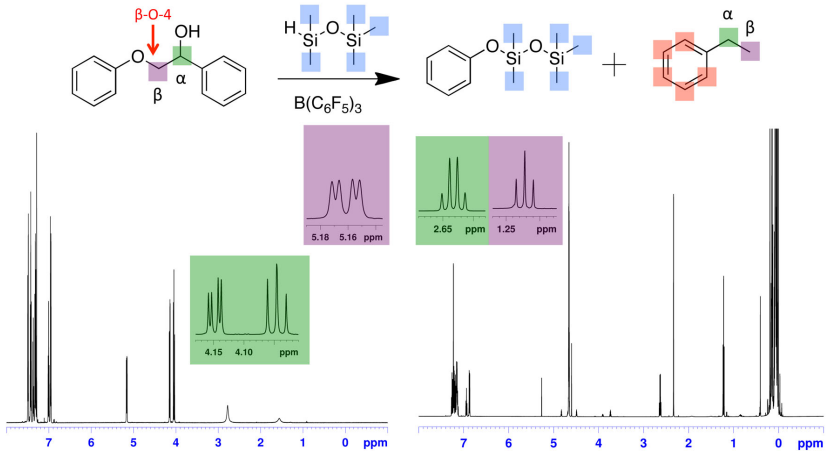

Figure 7.12 ^{1}H-NMR spectrum of 2-phenoxy-1-phenylethanol and its reduced products ($CDCl_3$ solvent).

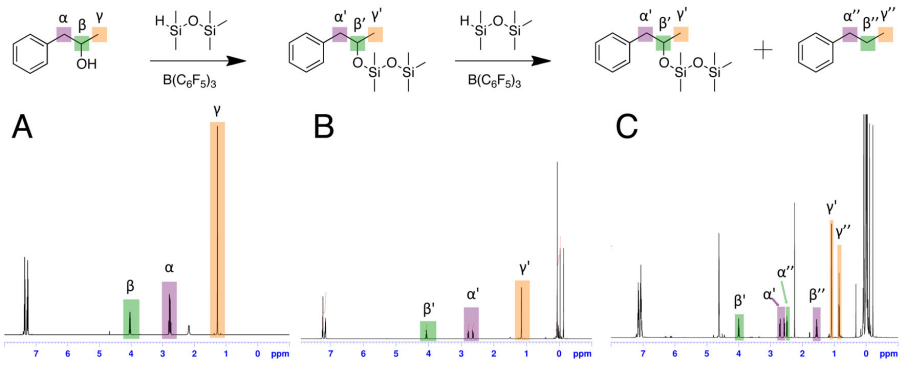

Figure 7.13 ^{1}H-NMR spectrum of 1-phenyl-2-propanol (A), its silylated product (B), and mixture of silylated and fully reduced products (C) ($CDCl_3$ solvent). The silyl ether is a stable intermediate product and rather difficult to completely reduce. The spectra (C) was obtained without removing toluene (solvent) and PMDS (reagent), because the boiling point were very close to the fully reduced product (n-propylbenzene).

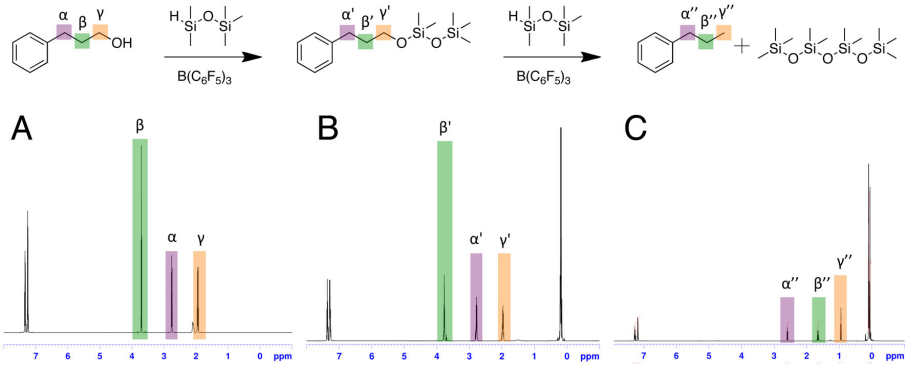

Figure 7.14 ^{1}H-NMR spectrum of 3-phenyl-1-propanol (A), its silylated (B) and fully reduced (C) products ($CDCl_3$ solvent).

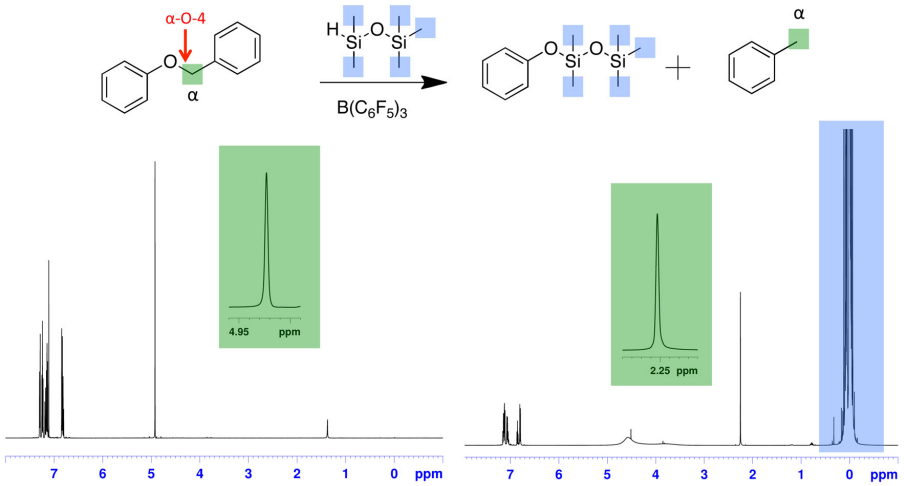

Figure 7.15 1H-NMR spectrum of benzyl phenyl ether and its reduced products ($CDCl_3$ solvent).

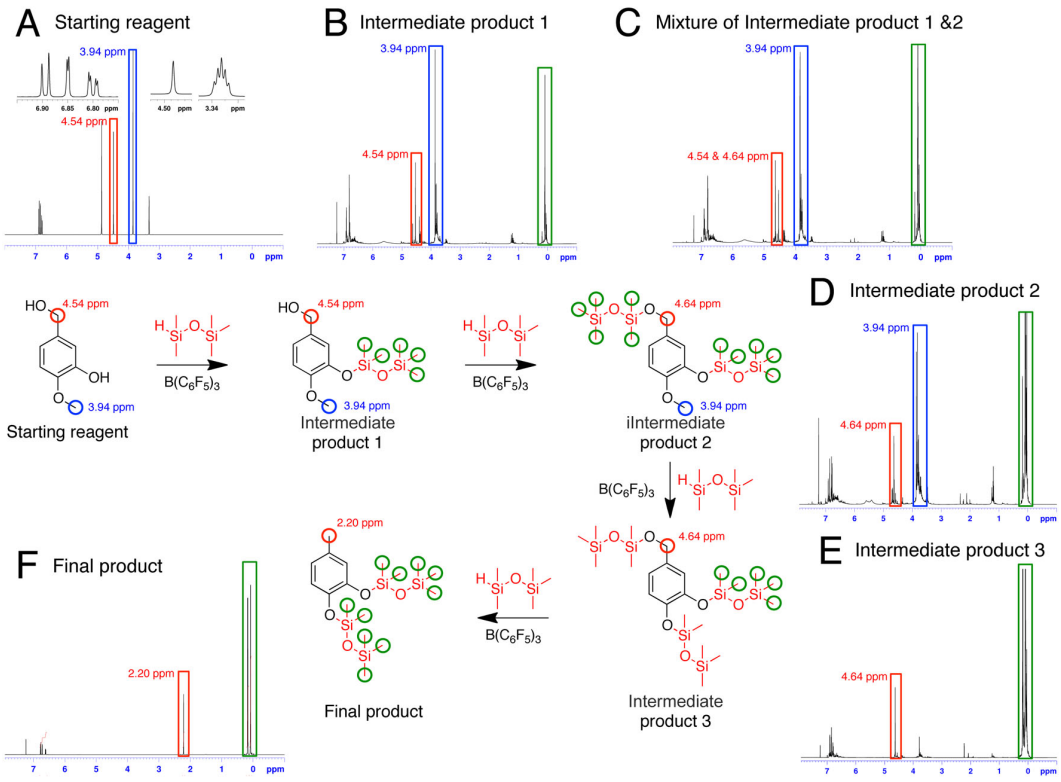

Figure 7.16 ^{1}H-NMR spectrum of intermediate products form staged reduction of 3-hydroxy-4-methoxybenzyl alcohol ($CDCl_3$ solvent). The relative reactivity order was found: phenol > primary alcohol > methoxyl > silylether

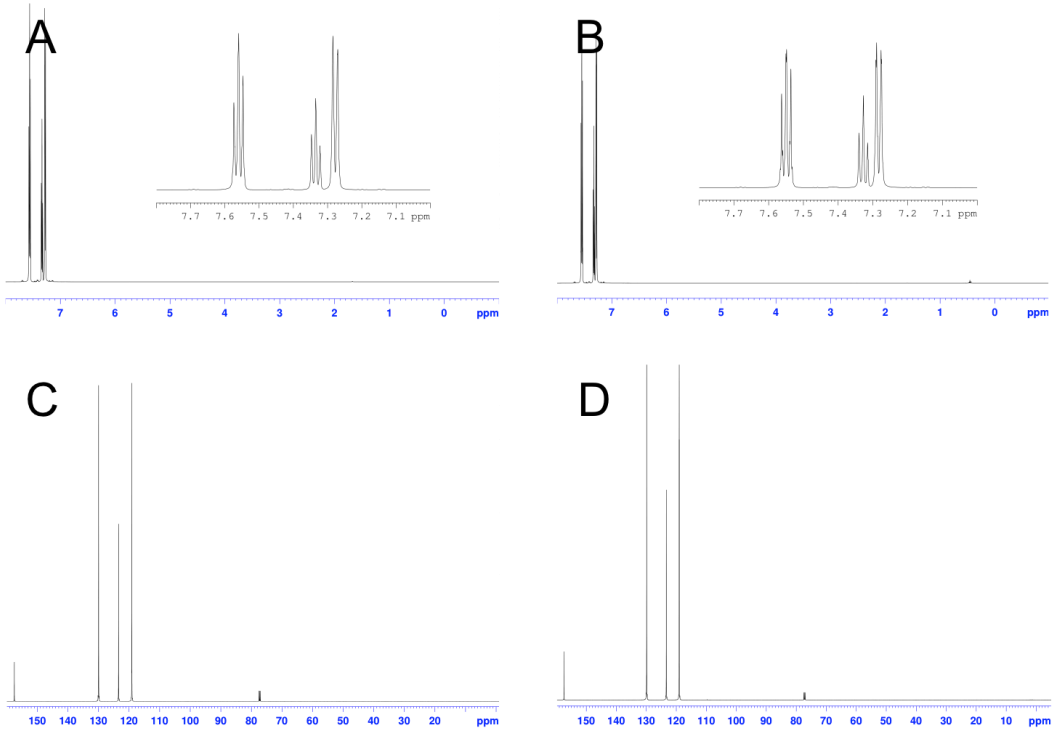

Figure 7.17 ^{1}H-NMR and ^{13}C-NMR spectrum before ((A) and (C)) and after ((B) and (D)) treating diphenyl ether with PMDS and $B(C6F5)_3$. The identical spectra before and after the reaction indicated no reaction occurred during this process.

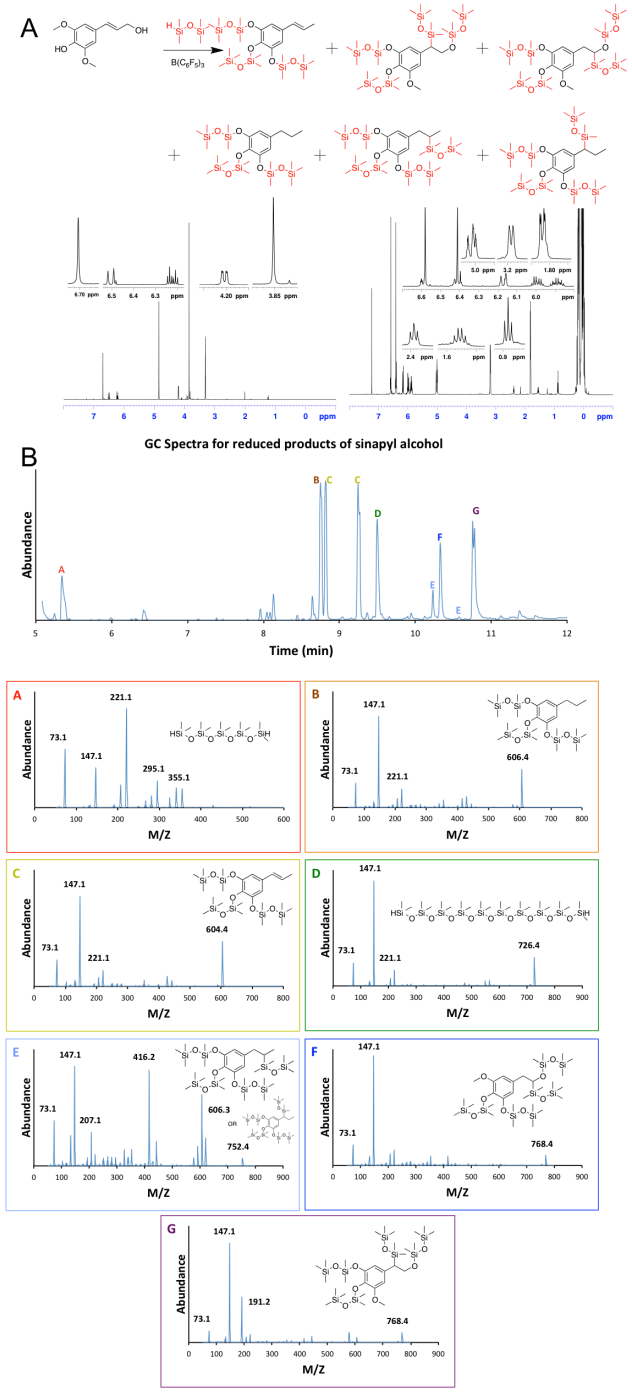

Figure 7.18 (A) ^{1}H-NMR spectrum of sinapyl alcohol and its reduced products ($CDCl_3$ solvent). (B) GC/MS spectrum for reduced products of sinapyl alcohol.

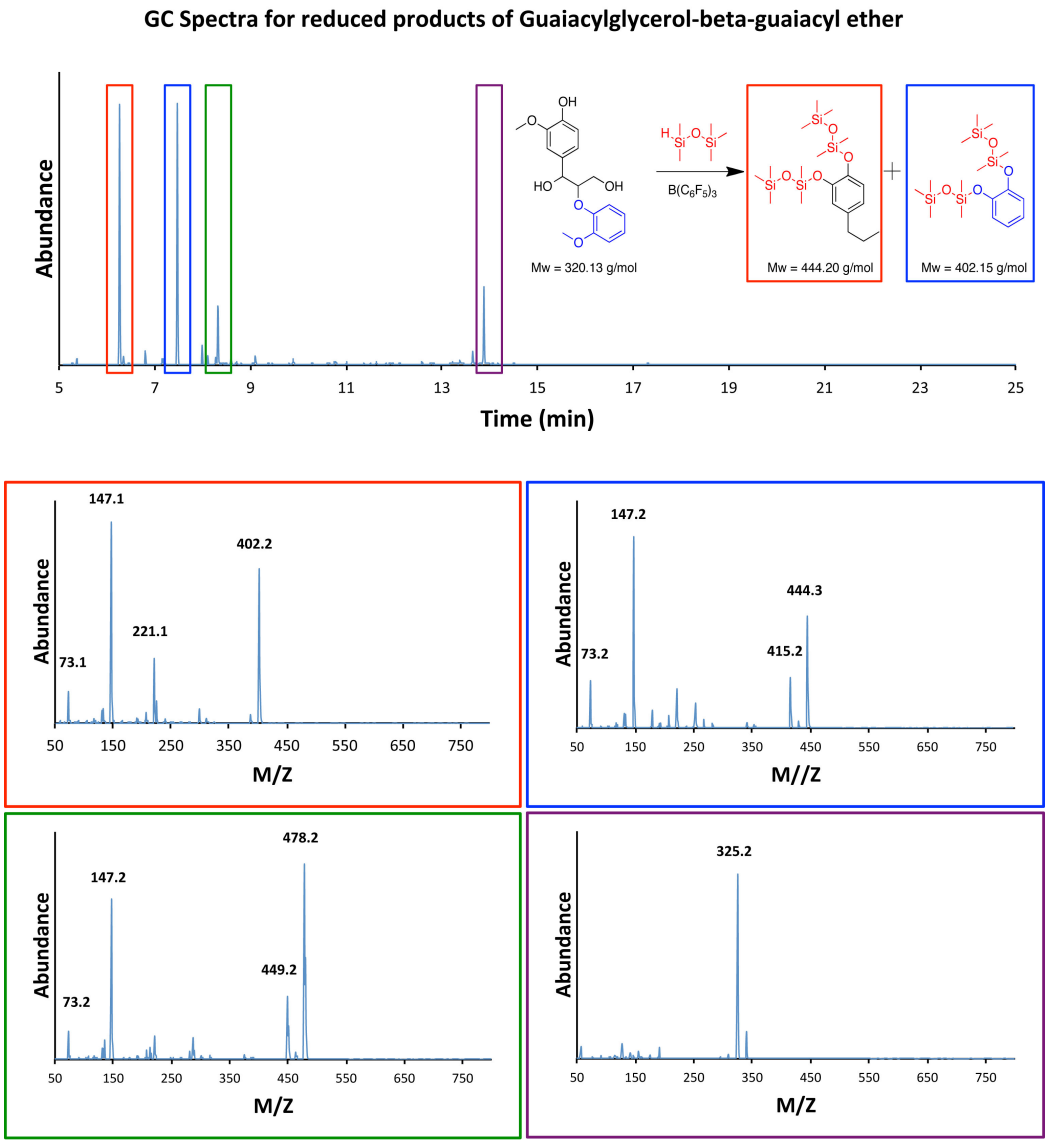

Figure 7.19 GC/MS spectrum for reduced products of guaiacylglycerol-beta-guaiacyl ether. The identified main peaks were highlighted with color masks: peaks highlighted by red and blue masks were the two reduced products. The chemical structures and MS spectra of these two products were also highlighted with corresponding color masks. The

other two peaks do not correspond to structures of guaiacylglycerol-beta-guaiacyl ether or its reduced products.

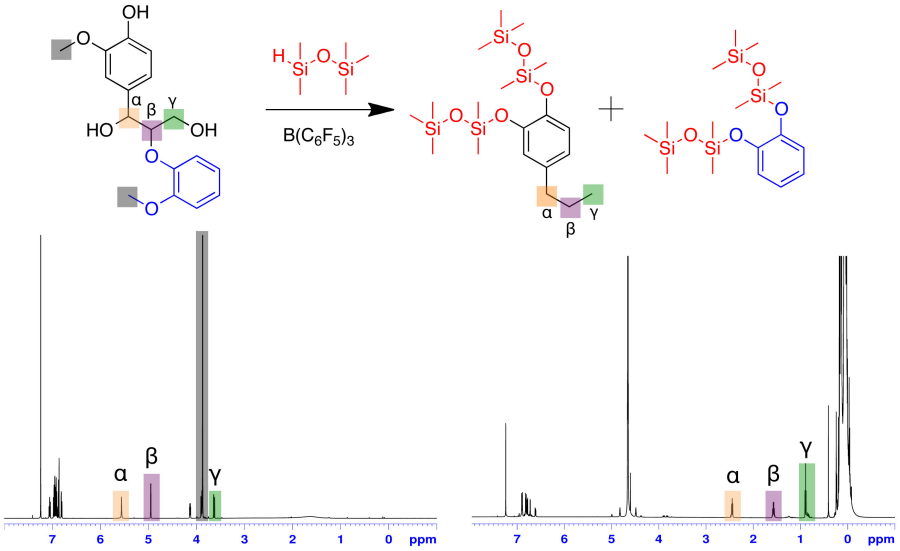

Figure 7.20 ^{1}H-NMR spectrum of guaiacylglycerol-beta-guaiacyl ether and its reduced products ($CDCl_3$ solvent).

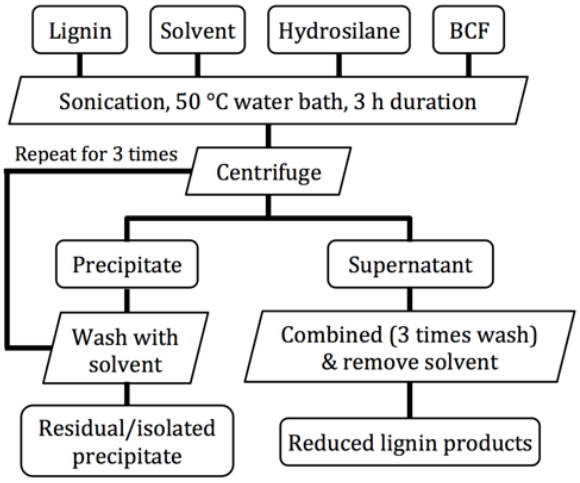

Figure 7.21 General process for the reduction/degradation of softwood/hardwood lignin, and purification of residual/isolated and reduced lignin products.

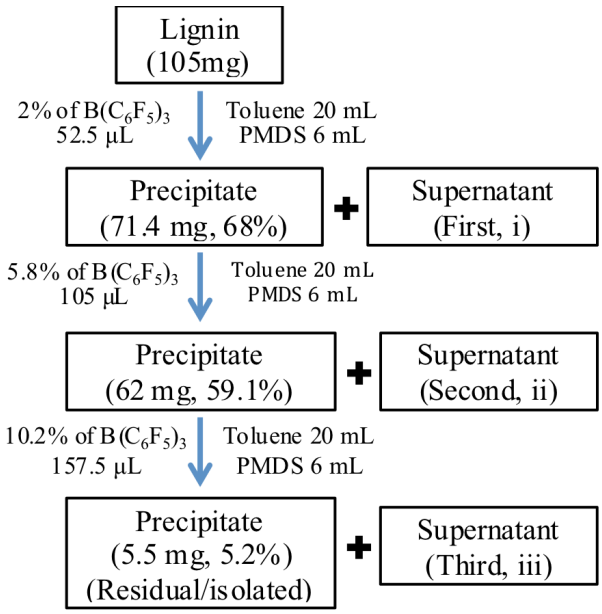

Figure 7.22 Process for degradation of hardwood lignin using increasing amounts of catalyst.

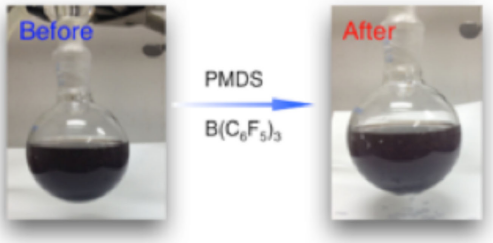

Figure 7.23 Virtually no change in turbidity was noted before and after sonicating softwood lignin with PMDS and $B(C6F5)_3$ in a 50 °C water bath for 3 hours. The percentage of soluble lignin was failed to obtain due to the weight gain of residual.

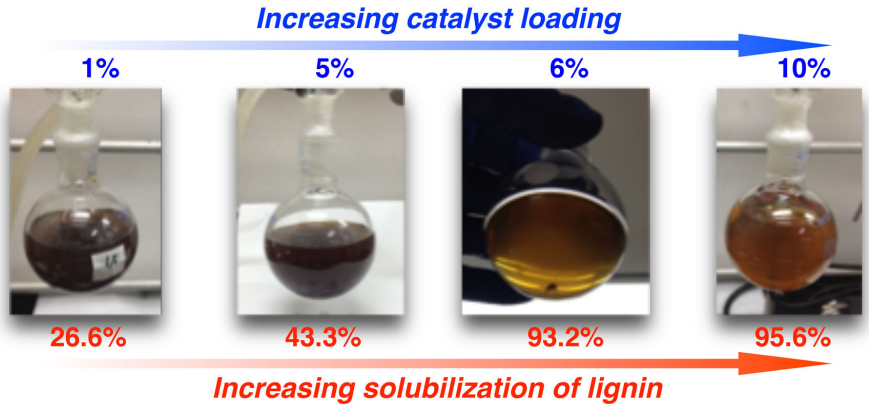

Figure 7.24 The visible difference of hardwood reduction/degradation with different catalyst concentrations. Turbidity decreases dramatically as the residual undissoved lignin drops from 73.4% (26.6% solubilization) to 4.4% (95.6% solubilization).The solubilization percentage is defined as (1 - Final insoluble weight/starting insoluble weight) x 100%.

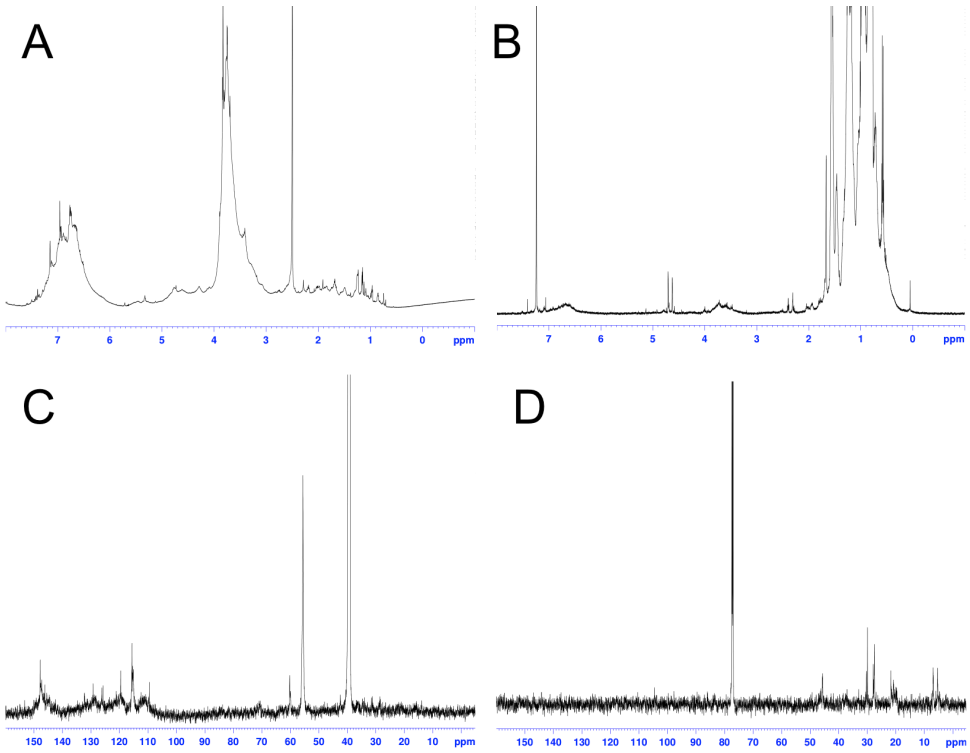

Figure 7.25 The ^{1}H-NMR and ^{13}C-NMR spectra of softwood lignin (A) and (C), and the soluble and products (B) and (D) after reduction by Et_3SiH. The solvent for (A) and (C) was DMSO, and for the more soluble products (B) and (D) was $CDCl_3$.

Table 7.1 Assignments of ^{13}C-NMR signals for lignin (β-O-4 related) (Hawkes et al., 1993, Wen et al., 2013)

Chemical shift (ppm)	Assignments
90-80	G_β or S_β (with α-OH and β-C, β-O-4)
79-70	G_β (with α-OH or/and β-C, β-O-4)
	G_β or S_α (with 1-CO, β-O-4)
	G_α (with α-OH, β-O-4)
65-60	G_γ (with α-OH and γ-OH, β-O-4)
56-52	OMe

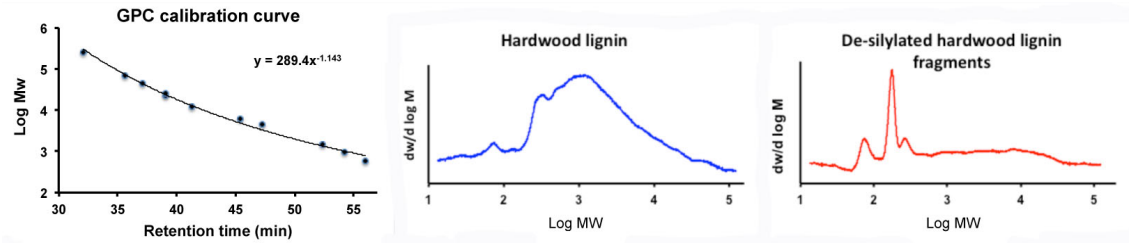

Figure 7.26 A: Calibration curve using PEO standards B: GPC chromatogram of unmodified hardwood lignin in DMF containing 50 mmol LiBr. C: GPC chromatogram of silylated hardwood lignin in DMF containing 50 mmol LiBr, after treatment with TBAF to remove silyl groups.

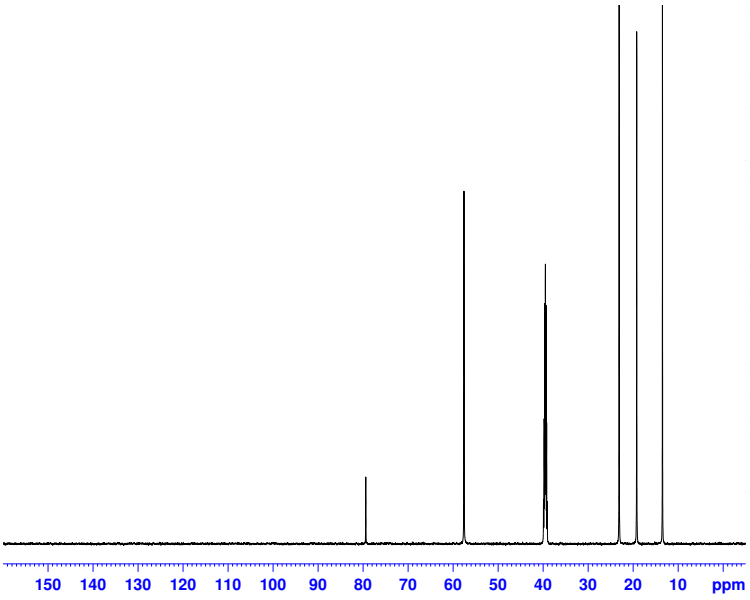

Figure 7.27 ^{13}C-NMR spectra for TBAF (solvent DMSO).

7.3 Supporting information for Chapter 4: Utilization of softwood lignin as both crosslinker and reinforcing agent in silicone elastomers

7.3.1 Equipment associated with titration of the lignin surface

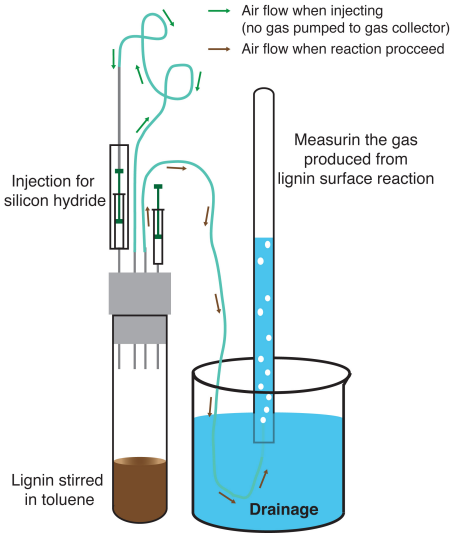

Figure 7.28 The water displacement method for gas production measurement.

7.3.2 Chemistry associated with titration of the lignin surface

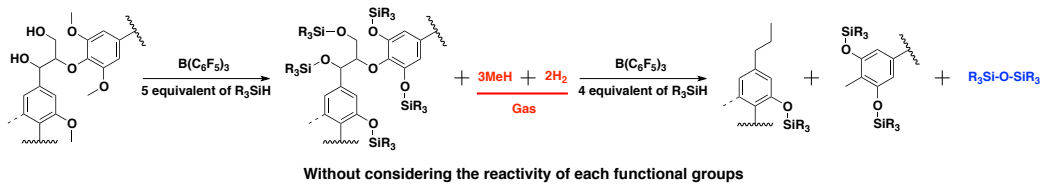

Figure 7.29 The molar ratio of reactive surface functional group to gaseous by-product (5 equiv./4 equiv.).

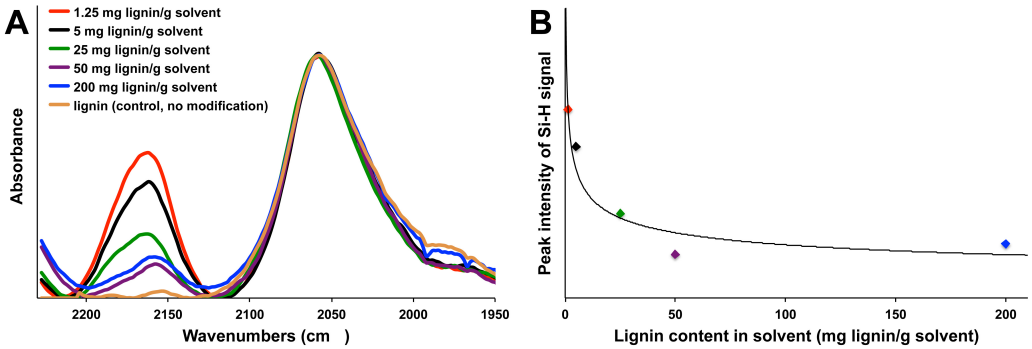

Figure 7.30 The DRIFT-IR spectrum for lignin particles titrated with different concentration in solvent. (A) and (B) The intensity of "Si-H" peak dropped with the increasing of lignin content in solvent (mg lignin/g solvent).

Demonstrated calculation for optimal formulations: balancing available functional group on lignin with [SiH]:

1. The equivalence of hydride:
   - If 800 mg of lignin was require in 1000 mg of DMS-H31 for ~ 40% weight ratio
   - The hydride that lignin could consume: 800 mg × 0.8 μmol/mg × 2 = 1280 μmol (Note, the reason for "× 2" refers to Figure 7.29).
2. The hydride of DMS-H31:
   - If 1000 mg of DMS-H31 was required
   - The hydride content: 1000 mg × 0.07 μmol/mg = 70 μmol

3. The 70 μmol of hydride is not enough for 1280 μmol equivalence hydride required for lignin surface reaction, therefore, a co-crosslinker (HMS-301, 501, or 992) was required.

4. The hydride required to be provide by HMS-992:

- If hydride to reactive surface functional group on lignin was set to 1/2

  The hydride required by HMS-992 = (1280 – 70 × 2)/2 = 570 μmol

  The mass of HMS-992 required = 570 μmol/16.67 μmol/mg = 34.2 mg

- If hydride to reactive surface functional group on lignin was set to 2/1

  The hydride required by HMS-992 = 1280 × 2 - 70 = 2490 μmol

  The mass of HMS-992 required = 2490 μmol/16.67 μmol/mg = 149.4 mg

- If hydride to reactive surface functional group on lignin was set to 4/1

  The hydride required by HMS-992 = 1280 × 4 - 70 = 5050 μmol

  The mass of HMS-992 required = 5050 μmol/16.67 μmol/mg = 302 mg

Table 7.2 Example formulation of lignin (SKL from Weyerhaeuser, 40.9%) as crosslinker/reinforcement in silicone elastomer. a co-crosslinker (HMS-992) was used for keeping the chemical stoichiometry of hydride to surface functional group of lignin close to 1:1.

Lignin (mg)	DMS-H31 (mg)	HMS-992 (mg)
800	1000	34
		150
		302

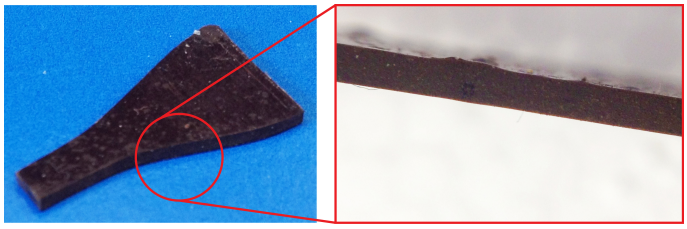

Figure 7.31 Images of bubble lignin/silicone elastomers made without solvent, right image is the cross-section of elastomer.

Table 7.3 The hydride content of hydride functionalized silicone with different chemical structures

	Mw (g/mol)	Chemical structure	Hydride content [Si-H], μmol/mg
DMS-H11	1175	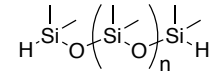	1.70
DMS-H21	6000		0.33
DMS-H31	28000		0.07
DMS-H41	62700		0.03
HMS-301	1900-2100	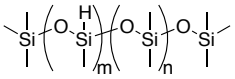	4.36
HMS-501	900-1200		7.46
HMS-992	1800-2100		16.67

7.3.3 Solvent resistance

Table 7.4 Solvent resistance of lignin-C/R-elastomer to organic solvents and water

	DMSO	MeOH	H_2O	Acetone	IPA	THF	THF/DMSO (1:1)	Toluene
Initial (g)	0.0285	0.0244	0.0275	0.0224	0.0218	0.0282	0.0203	0.0270
Swelling (g)	0.0748	0.0396	0.0334	0.0409	0.0315	0.0860	0.0332	0.0466
Swelling ratio (%)	162	62	21	83	44	205	64	73
After extraction (g)	0.0289	0.0237	0.0285	0.0231	0.0249	0.0212	0.0155	0.0257
Weight gain/loss ratio (%)[a]	1	-3	4	3	14	-25	-24	-5

[a] The "-" means a weigh loss percentage (loss weight/original weigh × 100%).

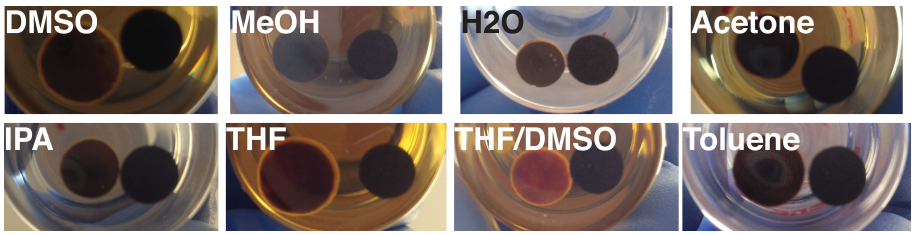

Figure 7.32 Swelling the lignin-C/R-elastomer with different solvent. The diameter ratios before and after swelling are list sequently: 1.32, 1.14, 1.00, 1.12, 1.00, 1.29, 1.41, 1.23, and 1.24 (left is the elastomer swell in solvent, right is control).

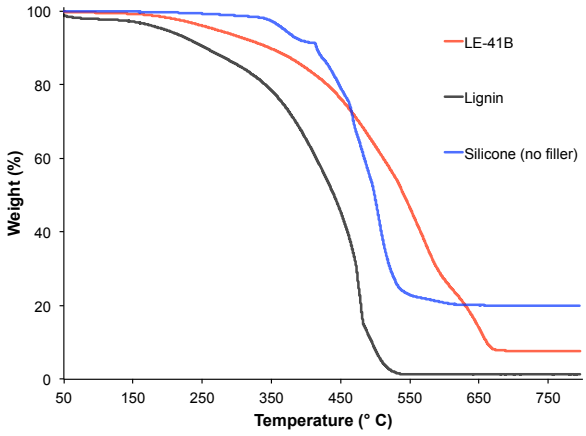

Figure 7.33 TGA thermograms of LE-41B (red), lignin (blue), and silicone (black) under air atmosphere

7.4 Supporting information for Chapter 5: Foamed lignin-silicone bio-composites by extrusion then compression molding

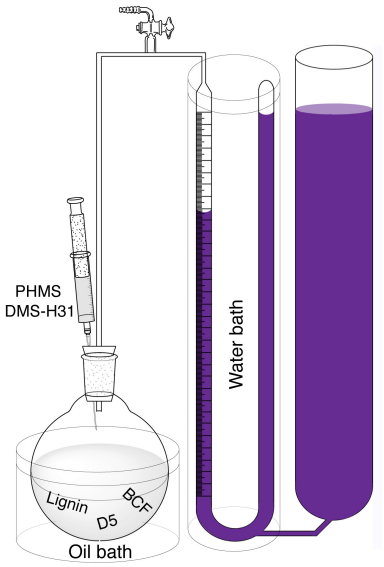

Figure 7.34 A gas volume meter was used to measure volume of gas produced during the reaction in solvent during preliminary optimizations and hydrolysis studies.

Table 7.5 Preliminarily optimizations for extrusion and molding conditions of different formulations.

No.	Lignin		PHMS		H-PDMS-H		D_5	BCF	Reaction temperature
	Mass (g)	wt% [a]	Mass (g)	wt% [b]	Type	Mass (g)	(ml)	(ppm) [a]	(°C)
O-1	0.25	50	0.02	8	H31	0.23	5	1000	30
O-2	0.25	50	0.02	8	H31	0.23	5	1000	40
O-3	0.25	50	0.02	8	H31	0.23	5	1000	50
O-4	0.25	50	0.02	8	H31	0.23	5	1000	90
O-5	0.25	51	0.01	4	H31	0.23	5	1000	50
O-6	0.25	48	0.04	16	H31	0.23	5	1000	50
O-7	0.25	50	0.02	8	H31	0.23	5	2000	30
O-8	0.25	50	0.02	8	H31	0.23	5	4000	30

[a] Weight ratios of lignin and catalyst loading are calculated without considering the solvent (D_5). [b] Weight ratios of PHMS are calculated against lignin weight only.

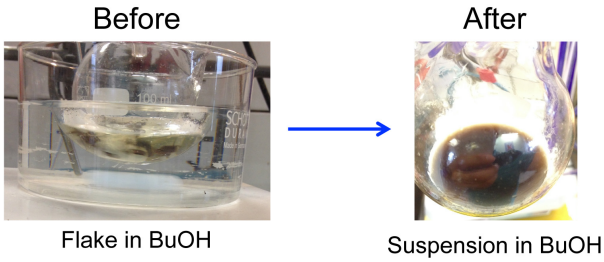

Figure 7.35 Testing the conversion of "Si-H" in lignin-silicone foam. Before reaction, the sliced lignin-silicone foam layers were dispersed in KOH/BuOH; the foam lost its integrity (fell apart to give a suspension) after treatment.

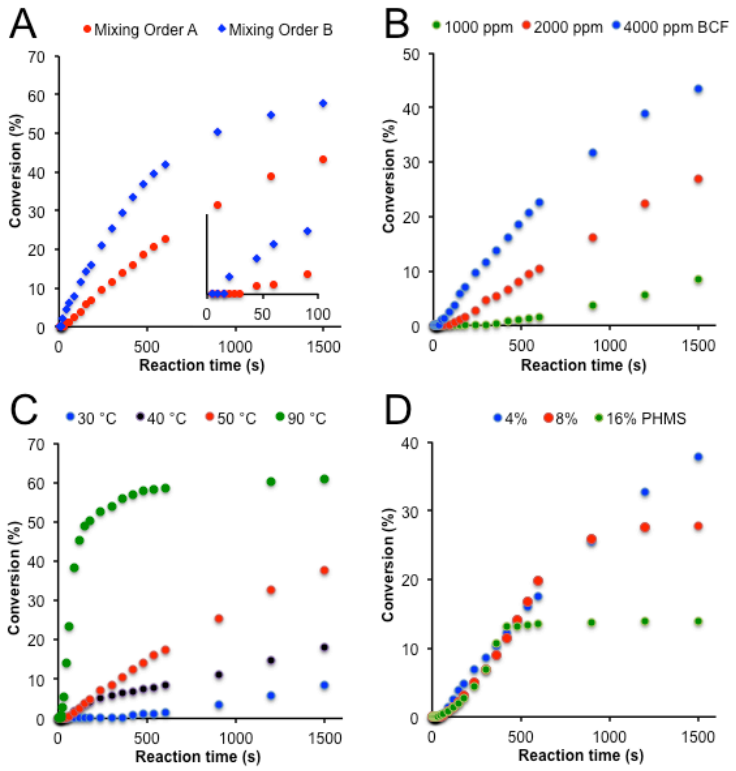

Figure 7.36 Kinetics studies for PHMS conversion % under different conditions and formulations: (A) mixing order: mixing order A led to longer induction times. The inset graph is the expanded range showing different induction times; (B) catalyst loading: conversion% increased, while induction time decreased, with increased catalyst loading; (C) temperature: higher temperature led to faster reaction rates and greater conversion% of PHMS. (D) PHMS content had no impact on induction time.

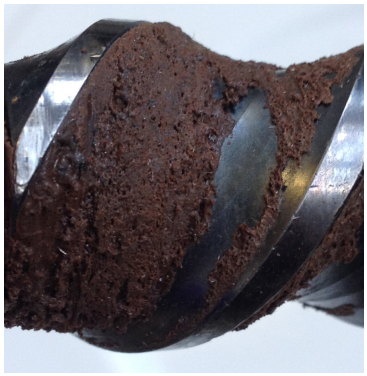

Figure 7.37 Gelation or crosslinking of foam precursors blocked the extruder channels.

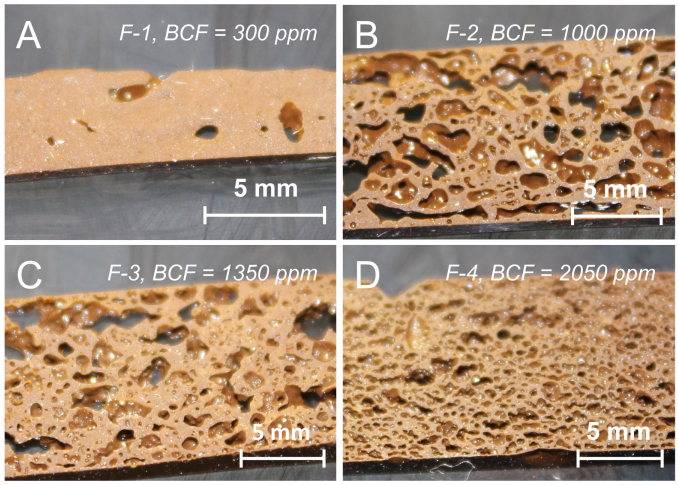

Figure 7.38 Cross-sectional images of lignin-silicone foams prepared from formulations with different catalyst loading: (A) F-1, BCF = 300 ppm, (B) F-2, BCF = 1000 ppm, (C) F-3, BCF = 1350 ppm, and (D) F-4, BCF = 2050 ppm.

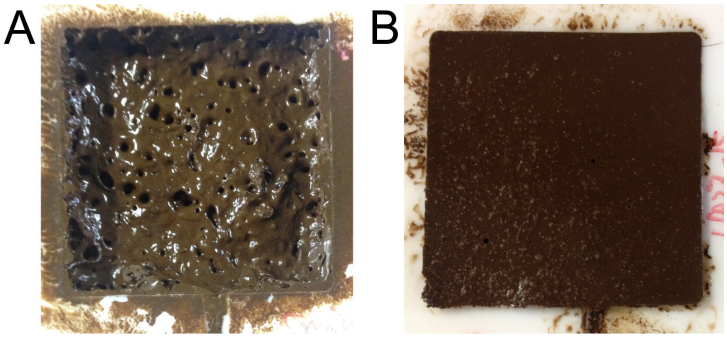

Figure 7.39 Images of lignin-silicone composite foams made with different catalyst content. (A) BCF = 300 ppm, curing for 180 min; (B) BCF = 1000 ppm, curing time = 5 min.

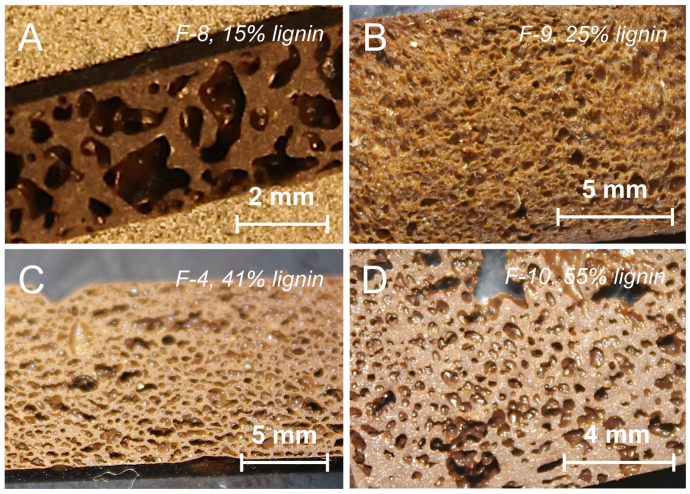

Figure 7.40 Cross-sectional images of lignin-silicone foam sprepared from formulations with varying lignin content: (A) F-8, 15 % of lignin, (B) F-9, 25% lignin, (C) F-4, 41% lignin, and (D) F-10, 55% lignin.

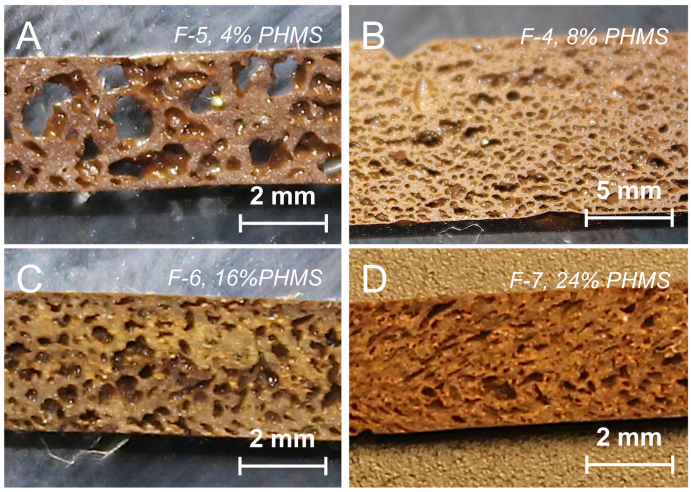

Figure 7.41 Cross-sectional images of lignin-silicone foams prepared from formulations with varying PHMS content: (A) F-5, 4 % of PHMS, (B) F-4, 8 % of PHMS, (C) F-6, 16 % of PHMS, and (D) F-7, 24 % of PHMS.

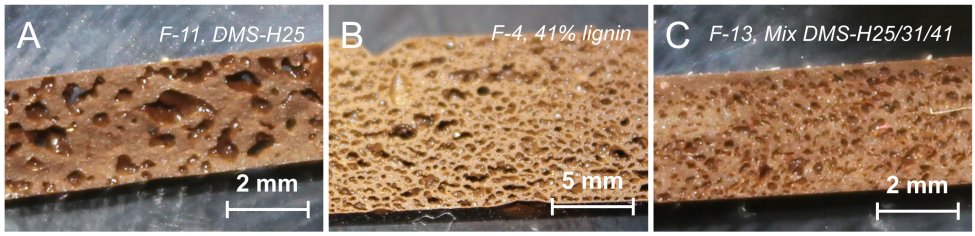

Figure 7.42 Cross-sectional images of lignin-silicone foams prepared from formulations with different molecular weight H-PDMS-H: (A) F-11, DMS-H25 (Mw = 6000 g/mol), (B) F-4, DMS-H31 (Mw = 28000 g/mol), and (C) F-13, Mixture of DMS-H25/31/41 (containing 26% H25, 48% H31, and 26% H41, H-41: Mw = 62700 g/mol).

Figure 7.43 Attempts to make lignin-silicone foams using DMS-H41 (F-12) failed due to the high intrinsic viscosity of DMS-H41. The precursor is semi-cured, and could not be processed in extruder.

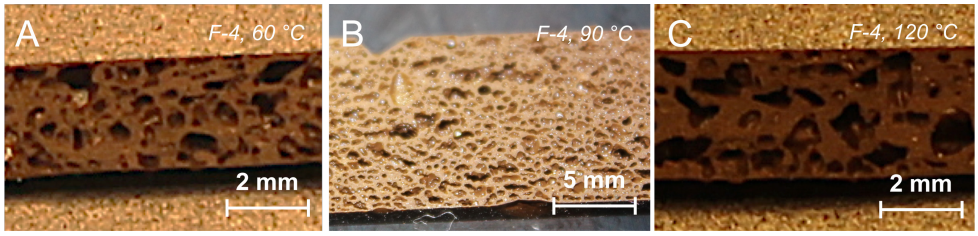

Figure 7.44 Cross-sectional images of lignin-silicone foams (formulation F-4) molded under different temperatures: (A) 60, (B) 90, and (C) 120°C.

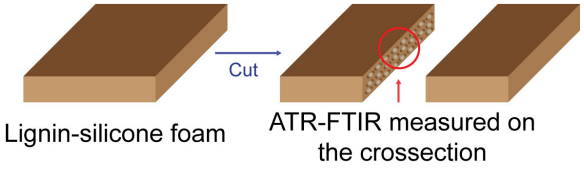

Figure 7.45 Preparation samples for ATR-IR characterization: how signal changes of "Si-H" groups in the foam were tracked.

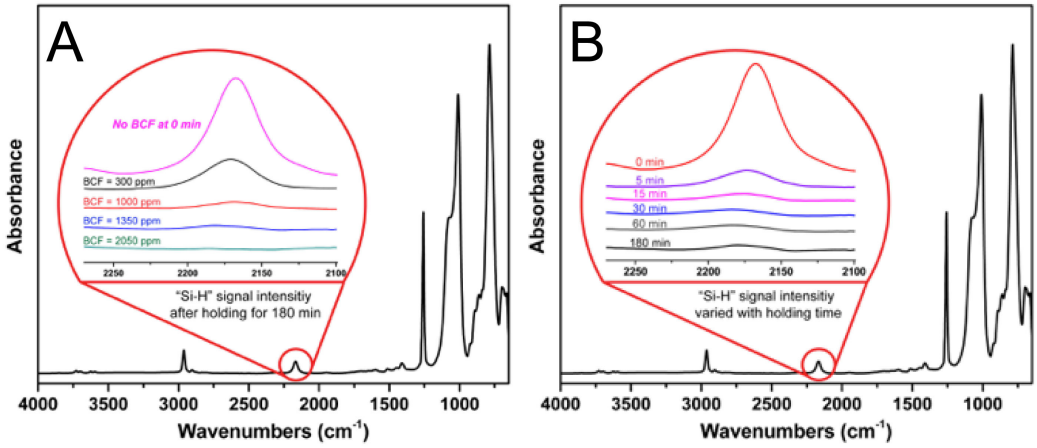

Figure 7.46 ATR-FTIR spectra for lignin-silicone foams made under different conditions and formulations: (A) different catalyst loading (from 300 to 2050 ppm), cured at 90 °C for 180 min, (B) foams in mold with different holding times (from 5 to 180 min), cured with 1350 ppm catalyst at 90 °C. The expanded spectra ranged from 2100 to 2250 cm^{-1} to track the intensity change of the "Si-H" signal.

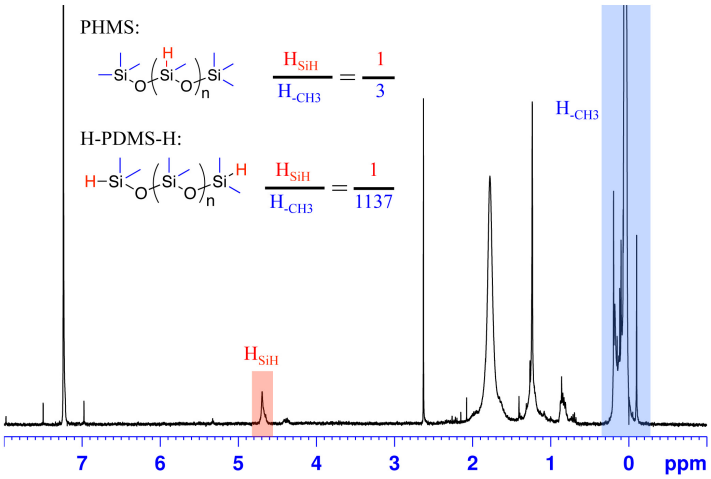

BCF content (ppm)	1000			1340			2050
Curing time (min)	5	5	15	30	60	180	5
Weight loss (%)	19	12	10	9	9	8	11
$\frac{H_{SiH}}{H_{-CH3}}$	1/50	1/67		~ 0			1/142

Figure 7.47 NMR spectrum of the cyclohexane extract from lignin-silicone foam, and the proton ratios ("Si-H"/"Si-CH_3") of samples obtained with different conditions and formulations.

Table 7.6 The degree of conversion of "Si-H" in lignin-silicone foams, tested by hydrolysis in solution

Formulation	Lignin content (%)	PHMS content (%)	H-PDMS-H	Conversion of Si-H (%)[a]
F-4 B	4	8	DMS-H31	43
F-4 B, 140 °C for 12 h	4	8	DMS-H31	44
F-4 B, 220 °C for 5 h	4	8	DMS-H31	69
F-4 B, 220 °C for 12 h	4	8	DMS-H31	77
F-4 B, 300 °C for 12 h	4	8	DMS-H31	79
F-5	41	4	DMS-H31	89
F-6	41	16	DMS-H31	48
F-7	41	24	DMS-H31	35
F-10	55	10	DMS-H31	41
F-11	41	8	DMS-H25	68
F-13	41	8	DMS-H25, H31, and H41	65

[a] The residual "Si-H" = 100% - Conversation of Si-H (%)

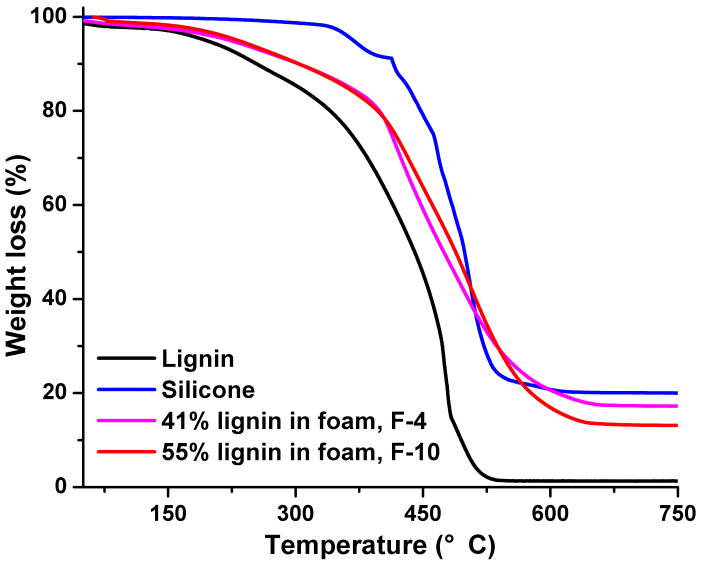

Figure 7.48 TGA of lignin-silicone foams (purple: 41% lignin in foam, red: 55% lignin in foam), lignin (black), and silicone (blue) under an air atmosphere.

Table 7.7 The mechanical properties of lignin-silicone foams characterized using DMA

		Formulation								
		F-4 B	F-5	F-6	F-7	F-8	F-9	F-10	F-11	F-13
T_g (°C)		-116	-110	-110	-111	-115	-109	-116	-111	-113
T_m (°C)		-37	-37	-37	-37	-38	-42	-36	-37	-31
Storage Modulus (E', MPa)	@ T_g - 20 °C	99	51	82	82	95	48	51	71	91
	@ T_g + 20 °C	87	43	58	85	86	46	46	59	81
	@ T_g + 50 °C	0.54	3.5	15	17	0.86	0.29	3	1.3	1.7
Loss Modulus (E", MPa)	@ T_g	7.6	2.1	3.5	7.4	4.7	11	2.5	4	3.5
	@ T_g + 50 °C	0.13	0.58	2.4	2.2	0.16	0.02	0.63	0.2	0.29
Tan Delta	@ T_g	0.09	0.05	0.05	0.09	0.06	0.55	0.05	0.07	0.04
	@ T_m	0.18	0.19	0.13	0.11	0.21	0.14	0.22	0.16	0.2

7.5 References

EGWIM, I. O. C. & GRUBER, H. J. 2001. Spectrophotometric measurement of mercaptans with 4,4 '-dithiodipyridine. *Analytical Biochemistry,* 288**,** 188-194.

GANDUBERT, V. J. & LENNOX, R. B. 2005. Assessment of 4-(dimethylamino)pyridine as a capping agent for gold nanoparticles. *Langmuir,* 21**,** 6532-6539.

HAWKES, G. E., SMITH, C. Z., UTLEY, J. H., VARGAS, R. R. & VIERTLER, H. 1993. A comparison of solution and solid state 13C NMR spectra of lignins and lignin model compounds. *Holzforschung-International Journal of the Biology, Chemistry, Physics and Technology of Wood,* 47**,** 302-312.

RIENER, C. K., KADA, G. & GRUBER, H. J. 2002. Quick measurement of protein sulfhydryls with Ellman's reagent and with 4,4'-dithiodipyridine. *Analytical and Bioanalytical Chemistry,* 373**,** 266-276.

WEN, J.-L., SUN, S.-L., XUE, B.-L. & SUN, R.-C. 2013. Recent advances in characterization of lignin polymer by solution-state nuclear magnetic resonance (NMR) methodology. *Materials,* 6**,** 359-391.